EVALUATING THE EFFECTS OF VARIOUS FACTORS ON MECHANICAL PERFORMANCE OF SC-FRCCs

by

İrem Şanal

M.S., Civil Engineering Boğaziçi University, 2010

Submitted to the Institute for Graduate Studies in
Science and Engineering in partial fulfillment of
the requirements for the degree of
Master of Science

Graduate Program in Civil Engineering
Boğaziçi University
2015

ACKNOWLEDGEMENTS

My greatest appreciation and sincerest gratitude goes to my supervisor, Assoc. Prof. Nilüfer Özyurt Zihnioglu, who has supported me throughout my PhD thesis with her patience, knowledge and motivations. Her flexibility in scheduling, gentle encouragements and friendly demeanor made me have the endeavor to finalize my graduate studies. Without her, this thesis would not have been completed or written. One simply could not wish for a better and friendlier supervisor.

I would like to express my deepest appreciation to Assoc. Prof. Osman Börekçi for acquainting me with academic life and showing me the joy of intellectual pursuit.

It's a pleasure to thank Erhan Karaesmen, for all of his academic and lifetime supports.

I also thank the members of my thesis committee, Prof. Turan Özturan and Assist. Prof. Ahmet Gökçe, for their guidance and suggestions. I am thankful that in the midst of all their activity, they accepted to be members of my thesis committee.

I am grateful to Bogaziçi University Construction Materials Laboratory staff: Ümit Melep and Yener Aydin, who helped me very much with all their efforts during my experiments. I would like to show my gratitude to AKCANSA and BASF-YKS for their supports.

I would never be able to thank enough for all of the support my lovely parents, Handan Sanal and Faruk Şanal, who have given to me all my life. I would like to thank to them for their support, encouragement and especially for the smiles and laughter that they have never hesitated to show me.

I am heartily thankful to my dear, lovely sister, Istem Şanal, for her accompany throughout my graduate studies. I am very lucky to have such a best friend like her,

apart from being the greatest sister forever.

My grandmother, Nimet Söyleyensoy deserves special mention for her endless support and prayers. She was the one who convinced me having a PhD degree. She was always there cheering me up and stood by me through all good times and bad times. Without her and my passed grandfather's encouragement, I would not have finished my PhD degree.

It is a pleasure to thank to my dearest friend Adlen Altunbas, for supporting me in every step I take, motivating me throughout my graduate studies and for many precious memories we shared along the way.

I would like to offer my regards and blessings to Abdullah Akça and Onur Pehlivan, who supported me in any respect during the completion of my thesis, as well as expressing my apology to everyone that I could not mention personally one by one.

Last, but certainly not least, I must acknowledge with deepest thanks, Ardalan Hosseini, being the most supportive long-distance colleague, with his enormous helps in my research. Meeting with him, influenced my research in a number of ways and resulted in a fruitful collaboration, with our conference and journal papers.

I would like to dedicate my PhD thesis to such an inspirational, amazing and perfect person, who has a place of honor deep within my heart; my deceased grandfather Ahmet Söyleyensoy and my foresighted, supportive and loveliest grandmother Nimet Söyleyensoy.

ABSTRACT

EVALUATING THE EFFECTS OF VARIOUS FACTORS ON MECHANICAL PERFORMANCE OF SC-FRCCs

Main objective of this study was to identify the different behaviors of Self Compacting Fiber Reinforced Cementitious Composites (SC-FRCCs) in terms of fresh and hardened state performance by considering the parameters such as specimen thickness/fiber length ratio (t/f_L), specimen width/ fiber length ratio (w/f_L), fiber type (straight or hooked), and fiber aspect ratio. Specimens were cast using same mixes, only fiber length, fiber type, specimen depth and specimen width were varied. Four different fiber lengths, two different fiber types, ten different specimen thickness and two different specimen width values were set. As a result, 14 different groups of specimen were obtained. A series of experiments were performed to examine the fresh and hardened state properties of SC-FRCCs by means of mini-slump flow, mold flow, fiber orientation, flexural strength and toughness, strain localization, crack propagation and crack typology. Results obtained from both traditional measurement methods and Particle Image Velocimetry (PIV) analysis, were combined and used in order to have a detailed understanding on how changing material parameters may affect the material behavior and the parameters used for structural design of fiber-reinforced cement based composites. Current codes for design of fiber reinforced concretes (FRC) were discussed and based on a chosen guideline CNR-DT, constitutive parameters were obtained accordingly, in order to assess and evaluate the effects of one of the studied parameters (t/f_L) on the structural performance, to help further develop the standards for structural design of these materials. Finally, a relationship between the deflection and crack opening of SC-FRCCs were proposed based on t/f_L ratio. The proposed relationships were employed to obtain deflection vs. COD relationships for other researchers' data given in literature and good results were obtained.

ÖZET

ULUSLARARASI MÜTEAHHİT FİRMALAR İÇİN BİR REKABETÇİLİK MODELİNİN GELİŞTİRİLMESİ

Bu çalismadaki asil amaç, numune kalinligi/lif uzunlugu (t/f_L), numune genisligi/lif uzunlugu, lif tipi ve lif narinlik orani gibi parametreler göz önünde bulundurularak, kendiliginden yerlesen lif donatili çimento bazli malzemelerin (SC-FRCC) gerek taze, gerek sertlesmis haldeki farkli davranislarini tanimlamaya yöneliktir. Numuneler sabit karisim degerleriyle dökülmüs olup, sadece lif uzunlugu, lif tipi, numune kalinligi ve numune genisligi degistirilmistir. Dört farkli lif uzunlugu, iki farkli lif tipi, on farkli numune kalinligi ve iki farkli numune genisligi degerleri belirlenmis olup, toplamda 14 farkli numune grubu elde edilmistir.Bu çalisma kapsaminda, SC-FRCC malzemelerinin taze haldeki akis deneyleri, lif yönelmeleri, egilme dayanimlari, egilme tokluklari, bölgesel gerilme yogunluklari, çatlak ilerlemeleri ve çatlak tipolojileri gibi özelliklerini belirlemek amaciyla birçok kapsamli deney yapilmistir. Deney sonuçlari, hem geleneksel ölçüm metodlariyla okunmus, hem de dijital bir görüntü analiz yöntemi olan PIV yöntemiyle analiz edilip, degisen malzeme davranisi üzerinde etkisi olan parametrelerin böylece daha detaylica anlasilmasi amaçlanmistir.Lif donatili malzemelerin tasarim kriterleri için hazirlanmis olan standartlarin genel bir degerlen dirmesi yapilip, bunlar içinden bu çalisma kapsamina en uygun olan CNR-DT seçilmistir. CNR-DT standardi baz alinarak yapisal parametreler hesaplanmis ve lif donatli malzeme lerin tasarim kriterleri için olan standartlarin daha da gelistirilebilmesine yardimci olabilmek adina yapisal performans üzerinde t/f_L etkisi detaylica incelenmistir.Son olarak, SC-FRCC malzemelerde, egilme ve çatlak açilmasi arasinda, t/f_L parametresiyle iliskili bir baginti bulunmustur. Farkli lif tipi ve uzunlugu göz önünde bulundurularak önerilen bu bagintilar, daha önce literatürde yine egilme ve çatlak açilmasi arasinda verilen diger bagintilarla karsilastirilmis ve oldukça iyi sonuçlar verdigi görülmüstür.

TABLE OF CONTENTS

LIST OF FIGURES

LIST OF TABLES

1. INTRODUCTION

It is well known that concrete is much stronger in compression than it is in tension. In many applications of concrete, this is handled by providing steel reinforcing bars to carry the tensile forces once the concrete has cracked. As an alternative to conventional reinforcement, steel fibres can also be mixed into the concrete.

Fibres have been added to cementitious materials in order to improve the characteristics in the hardened state and mostly post-cracking stage. If fibers are compared to ordinary reinforcement, their small diameter with a high surface area can be uniformly dispersed resulting in a randomly distributed arrangement and therefore crack bridging potential. Features of different fibers used in concrete, result in varying material properties, structural behavior and failure modes. Parameters such as fiber type, fiber geometry, fiber dimensions and fiber dispersion features enormously affect the material performance.

Steel fibres, being randomly distributed in the concrete, bridge micro-cracks as they form in the initial stages, as a result reduce the tendency of these micro-cracks to form into larger cracks. After cracking, the fibres transmit tensile forces over the crack into the surrounding concrete. Therefore, fibres bridging over the cracks usually lead to increased flexural toughness, ductility, strain capacity and reduced crack widths.

Recent studies based on extensive experimental investigations highlight the fact that the strength and the ductility of reinforced concrete beams are enhanced by using SFRC instead of ordinary concrete. Therefore, brittle cementitious materials like concrete can significantly benefit from addition of fibres, since fibers will bridge the cracks and retard the propagation of these cracks, ending up with increased energy absorption, toughness and ductility.

Effects of fiber addition on the ductile behavior, bearing capacity and shear strength of concrete have been studied in detail in the literature. Oh, B.H. [1] ex-

amined the increased ductility of beams by the addition of steel fibers. Another study by Campione [2], showed that the addition of fibers increases the bearing capacity of the beams and ensures more ductile behaviour, at the same time reducing degradation effects under cyclic reversal loads. Results of the study of Lim *et al.*, [3] showed that the first crack shear strength increases significantly as fibre content increases and the ultimate shear strength is also improved. Also, the results showed that steel fibres can greatly enhance the tensile properties of concrete and improve resistance to cracking. Increased ductility and flexural behavior of FRC beams were also studied by Chunxiang *et al.*, [4]. The results showed that, the descending Section of the load-displacement curve of the concrete beams without steel fibers is much steeper than that with steel fibers, which shows that the addition of steel fibers makes the high strength concrete beams more ductile.

Self-compacting fiber reinforced cementitious composite (SC-FRCC) further combines the self-compacting, highly flowable and non-segregating performance with the deflection-hardening and multiple cracking behaviour of high performance fiber reinforced cement composites. [5] Therefore, the use of Self-Compacting Fiber Reinforced Cementitious Composites (SC-FRCCs) will continue to increase all around the world due to its many advantages compared to traditional concrete.

Whereas, use of fiber-reinforced cement-based materials for structural and semi-structural applications is hindered due to the lack of well-established codes/standards which define design principles. Efforts are being made for developing new standards to satisfy the needs of academia and industry. These documents are constituted as a result of years of experience of researchers and most of the information and generalized rules are proved by experimental studies. However, more research is needed to quantify the effects of different fiber applications on the material performance. Further research is required for a comprehensive understanding and a more widespread use of SC-FRCC materials.

A comprehensive study was conducted in this thesis to better understand the behavior of FRCs in the fresh and hardened states. The challenges in this thesis were:

- Conduct a comparative study of conventional measurement techniques with an image based non-contact method, both to evaluate fresh and hardened state properties of self-compacting fiber-reinforced cementitious composites (SC-FRCCs).
- Identify the differences in terms of fresh state performance of SC-FRCCs by evaluating the results of mini-slump flow and mold flow test, both by traditional measurement methods and a full field method called particle image velocimetry (PIV), which measures surface displacements and strains using digital image analysis.
- Identify the differences in terms of mechanical performance of SC-FRCC beams by considering the paremeters such as specimen dimensions / geometry, fiber length / specimen thickness ratio, fiber length/ specimen width ratio, fiber type (straight/hooked), fiber aspect ratio.
- Study the influence of the beam size/geometry, fiber orientation and resulting crack propagation behaviour together on the mechanical performance of SC-FRCC beams and for evaluating and characterizing the flexural behavior of the beams.
- Figure out a relationship between the mid-span deflection and crack opening of SC-FRCCs based on t/f_L ratio, to predict deflection data from COD results and vice versa.
- Assess, and evaluate the effects of the studied parameters (mainly t/f_L ratio) on the structural performance by using one of the design rules from guidelines (Italian guide - CNR DT), to help further develop the standards used for structural design of fiber-reinforced composite materials.

Therefore, the main objective of this study was set as to identify the differences of behavior of SC-FRCCs in terms of fresh and hardened state performance by considering the paremeters such as specimen thickness/fiber length ratio (t/f_L), specimen width/ fiber length ratio (w/f_L), fiber type (straight or hooked), and fiber aspect ratio, both by traditional measurement methods and a full field digital image analysis method called particle image velocimetry (PIV) and in the end use the most effective parameter to understand how changing material properties may affect the performance parameters used for structural design of fiber-reinforced cement based composites.

2. LITERATURE REVIEW

2.1. Steel Fiber Reinforced Concrete (SFRC)

Steel fiber reinforced concrete (SFRC) is a heterogeneous structural material comprising of typical concrete elements, with the addition of steel fibers to provide tensile resistance. These fibers are discontinuous discrete entities and are distributed and oriented randomly (nominally uniformly) throughout the concrete matrix. SFRC can be used by itself, or in conjunction with conventional reinforcing bars, depending on the application. [6]

SFRC's are generally characterized by an enhanced post-cracking tensile residual strength due to the fiber reinforcement mechanisms provided by fibers bridging the crack surfaces. [7] This post peak tensile behavior is influenced mainly by the number of fibers effectively crossing a crack, their angle of orientation, and bonding strength properties of the type of fibers used.

SFRCs are supposed to enhance the understanding of the material's behaviour and will provide a basis for experimental research into the aspect of scatter in the post-cracking behaviour. It starts with the rheological properties of SFRC, since the workability can strongly influence several stages of the production process [8], and especially the strongest affect is seen on the post-cracking behavior of the composite material.

The general tensile behavior of concrete is demonstrated in Figure 2.1 [9]. Without any fiber reinforcement, the plain concrete matrix exhibits a strain-softening response with low tensile strength and ductility. Because, due to low fracture toughness of concrete, tensile cracks may easily occur when there is an applied stress. The interfacial bond developed between the fibers and matrix makes use of the strength and stiffness of the fibers in reinforcing the brittle matrix. Once the matrix cracks, load can be still transfered across the crack faces through the steel fibers. As the load on

the composite is increased, the process of fiber pullout affects load carrying capacity and further contributes to energy dissipation. It has also been known that when using a high volume fraction of fibers with a high specific surface area, the crack bridging potential and the strength of the composite are increased [10],[11].

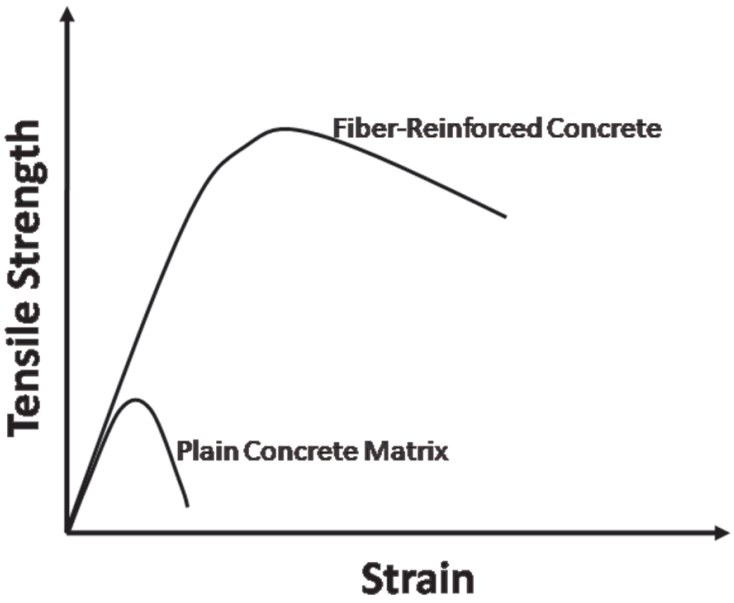

Figure 2.1. General Tensile Behavior of Concrete.

The flexural behavior of SFRC changes substantially compared to plain concrete. Depending on the amount and type of fibers used both the peak load and the ductility can be increased. Explanations will be presented for the fact that the flexural strength can be increased by virtue of fiber addition whereas this is hardly possible with regard to the compressive strength. In bending, the flexural load-bearing capacity can be increased even at low fiber volumes as long as the matrix strength.

Fibre reinforced concrete has found interesting new applications in the past two decades due to its inherent superiority over normal plain and reinforced concrete in the following properties: higher flexural strength, better tensile strength and modulus of rupture, higher shear strength, higher shock resistance, better ductility and fatigue resistance, crack resistance and failure toughness [12].

Fiber-reinforced concrete has received its most increasing interest, especially with

its presence in conventional concrete, improving certain mechanical properties of concrete. Different fiber types, fiber volume fractions and matrix compositions yield very different material behaviors. Even by changing the fiber content alone, the mechanical behavior of the concrete may change from being almost as brittle as plain concrete to even deflection-hardening materials.

In plain concrete, micro cracks develop even before loading, particularly due to drying shrinkage or other causes of volume change. The width of these initial cracks seldom exceeds a few microns. When loaded these micro cracks propagate and open up and due to stress concentration, additional micro cracks are formed. The micro cracks are the main cause for elastic deformation in concrete. Fibre reinforced cement and concrete were developed to overcome these problems. As a result of the incorporation of short discrete fibers cracks propagates into a slow controlled growth. This gives the cement-based materials maximum ductility overcoming its low tensile strength properties.

The crack-bridging effect provided by fibers generates residual tensile strengths that improve both the durability and the toughness of concrete. It is the improvement of toughness and the crack distributing properties that motivate the use of fibers. This fact has been contributing to an increasing number of structural applications of SFRC [13].

The beneficial effects of fiber reinforcement are therefore twofold: not only are mechanical properties such as toughness and strength improved, but there are also new possibilities for optimization of materials for certain structures. Nonetheless, there is still a long way to go on the development of methods and design procedures to improve the reliability of this material.

2.1.1. Various Factors Affecting Performance of SFRCs

SFRC is a composite material, with the ultimate performance being directly affected by the concrete mixture design, material selection and casting quality control

(i.e. fiber type, fiber aspect ratio, volume fraction and uniform distribution). A description of how each of these components plays a role in effecting the material behavior is discussed below.

2.1.1.1. Effect of Fiber Type. Steel fibers intended for reinforcing concrete are defined as short, discrete lengths of steel having an aspect ratio in the range of 20-100, with any cross section and that are sufficiently small to be randomly dispersed in an unhardened concrete mixture using usual mixing procedures [14].

Steel fibers are available in lengths between 6 and 80 mm and with a cross-sectional area between 0.1 and 1.5 mm2. The tensile strength is normally in the range between 300 and 2400 MPa. They are of circular or rectangular cross-sectional shape and are produced by cutting or chopping steel wires or by shearing sheets of flattened metal sheets and steel bars. The fibers are usually crimped or deformed with either a hook at each fiber end or a small head in order to improve the anchorage in the concrete matrix [15].

The fiber volume content V_f can vary up to 2% by volume in normal mixed concrete. For higher volume contents the mix tends to produce fiber balling during the mixing process and workability can not be easily achieved.

Steel fibers are classified based upon the procedure used in the manufacturing (such as cold drawn wire, cut sheet, melt-extracted, etc); based on the cross sectional shapes (such as fibers with square section, fibers with circular sections); based on their geometry (such as straight steel fiber, deformed steel fiber, crimped-end steel fiber, flattened end steel fiber, machine chipped steel fiber, etc).

For fibres to be effective in cementitious matrices, it has been found (by both experiments and analytical studies) that they must/should have the following properties [5]: (i) a tensile strength significantly higher than the matrix (two to three orders of magnitude); (ii) a bond strength with the matrix preferably of the same order as,

or higher, than the tensile strength of the matrix; (iii) an elastic modulus in tension significantly higher than that of the matrix (at least 3 times); and (iv) enough ductility so that the fibre does not fracture due to fibre abrasion or bending.

To improve the bond characteristics, a fibre can be modified along its length by roughening its surface or by including mechanical deformations. Hence, fibres can be smooth, deformed, twisted or with end hooks. Therefore, to maintain high pullout resistance while reducing the aspect ratio, a number of approaches are employed: enlarging or hooking the fiber ends, roughening the surface of the fibers, or crimping to produce a wavy, rather than straight fiber.

2.1.1.2. Effect of Fiber Aspect Ratio. For conventionally mixed fiber reinforced concrete, a higher aspect ratio of fibers results in superior post-peak performance due to the high pullout resistance of the fibers. However, research shows that a high aspect ratio of fibers can lead to a balling effect during mixing, resulting in loss of flexural resistance and consequently an adverse effect. Generally, aspects ratios of steel fibers between 20 and 100 are used in concrete mixtures [14].

2.1.1.3. Effect of Fiber Volume Fraction. The amount of fibers introduced into the mixture (or fiber volumetric fraction), also plays a vital role in the overall material behaviour. Toughness (total area under the load-deflection response) increases with a higher fiber volume dosage. Figure 2.2 shows that the addition of fibers to plain concrete greatly increases the toughness of the material [16].

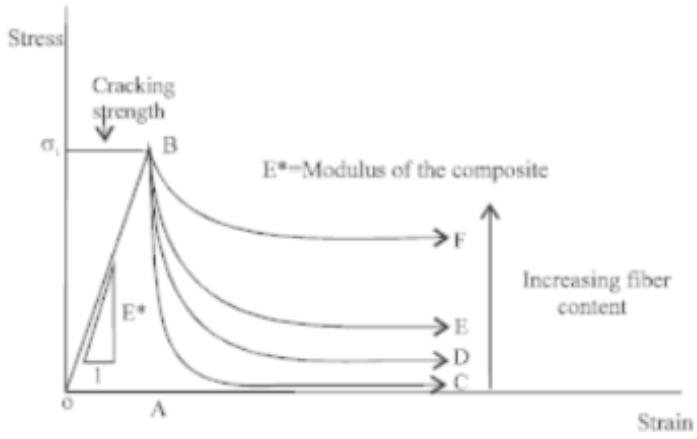

Figure 2.2. Contribution of Fibers to Improvement of Flexural Strength and Toughness [16].

Moreover, increased volume fraction of steel fibers in concrete improves and increases the energy absorption capacity leading to enhanced post-peak ductility. The mechanism associated with increased flexural strength and consequently toughness can be seen in in Figure 2.2, from the results of the previous study of Wegian *et al.*, [16]. Two essential points have been stated in relation to the Figure 2.2. First, the volume of the fibers may influence the peak strength at point B. The strength tends to increase when the fiber volume exceeds the minimum value that would be required to carry the load beyond point B. Second, the slope of the line OB (i.e. elastic modulus, E) would also increase with both the volume of the fibers as well as with the modulus of the fibers them self.

2.1.1.4. Effect of Fiber Distribution. Furthermore, quality control employed during casting is a critical component in achieving the desired material properties. Even with an ideally designed concrete mixture, the structure's overall performance can prove to be inadequate without the presence of proper quality control. The strength of a structure made of fibre reinforced concrete is dependent of the fibre alignment and fibre distribution, which both can be influenced by the properties of fresh concrete.

Effectiveness of fiber reinforcement is highly dependent on fiber dispersion and

orientation. Bentur, (1989) Poor dispersion can cause poor fresh and hardened state properties, affecting the resulting overall performance of the structure. Therefore, fiber dispersion is an important factor that affects both fresh and hardened state properties of cement-based materials.

Previous studies had shown the effect of flow direction on the alignment and distribution of fibers. In these last few years, studies focusing on this subject have shown that the achievement within a structural element of a homogeneous distribution of randomly oriented fibres, is a crucial point in respect of guaranteeing the structural performance with a suitable degree of repeatability. Governing the dispersion and the orientation of fibers in concrete through a suitably balanced set of fresh state properties and a carefully designed casting procedure, if proved effective, would hence be a feasible way to achieve a mechanical performance of the FRC which is optimal to the foreseen structural applications [17].

Akkaya *et al.*, [18] found that, if the fibers were well dispersed, material performance was improved. Therefore, investigating fiber dispersion is very important for both fresh state and hardened state performance of FRC specimens. As a result, comprehensive research is needed so that fiber dispersion can be controlled and monitored.

2.1.2. Limited Use of SFRC

In the recent decades, steel fiber reinforced concrete (SFRC) became a very popular and attractive material in structural engineering because of its good mechanical performance. The most important advantages are preventing macrocracks, delaying microcrack propagation to macroscopic level and the improved ductility after formation of microcracks.

Despite the remarkable advances in the fiber reinforcement technology and the publication of design guidelines, questions continue to arise regarding the performance, the characterization and the modelling of the material [19]. However, their adequacy for certain applications still remains an issue. Moreover, properties such as the fiber

orientation and the probability of fibers crossing along the crack region need to be further considered. These subjects require further research in order to work towards an accurate and efficient design procedure.

While extensive research is being conducted on SFRCs, utilization of them in the construction industry has been very limited due to insufficient details on the design procedures and an absence of a specification/code allowing the use of flexural contribution in SFRC elements. A Section of this research therefore aimed to understand the dependency of structural design models on the changing material parameters.

It was aimed to further help to provide guidance to the designers and code writers for SFRCs on the appropriateness of using steel fibers in different situations. It was also aimed to evaluate one of the existing models with the experimental results and to identify the critical parameters for design of SFRC members. Previous research has shown that fiber volume, fiber aspect ratio, concrete matrix strength and interfacial properties at fiber-matrix interface influence the SFRC tensile properties [20].

2.2. General

During the past four decades, different methods have been proposed and used to characterise the behaviour of fibre-reinforced concrete (FRC): e.g. by measuring the flexural strength or by determining the behaviour in terms of dimensionless toughness indices [21], to determine residual flexural strengths at prescribed deflections [22]. The main test set-ups used are:

- uni-axial tension test or direct tensile test;
- flexural test; and
- panel test or plate test.

SFRC can exhibit either strain-hardening or strain-softening behavior under uni-axial tension, as can be seen in the Figure 2.3 from the previous studies of Naaman and Reinhardt [23]. The discussion following led to suggesting a general classification

of FRC composites such as shown in Figure 2.3 by Naaman and Reinhardt. SFRC displaying strain-softening behavior may either present deflection-hardening or deflection-softening behavior.

Load deflection curves for typical FRC [5] are shown in Figure 2.3. Usually, a linear response is observed up to first cracking (Limit of Proportionality - LOP). Beyond this point, the material can exhibit hardening or softening behaviour. Maximum load after initial cracking can be greater or less than the limit of proportionality.

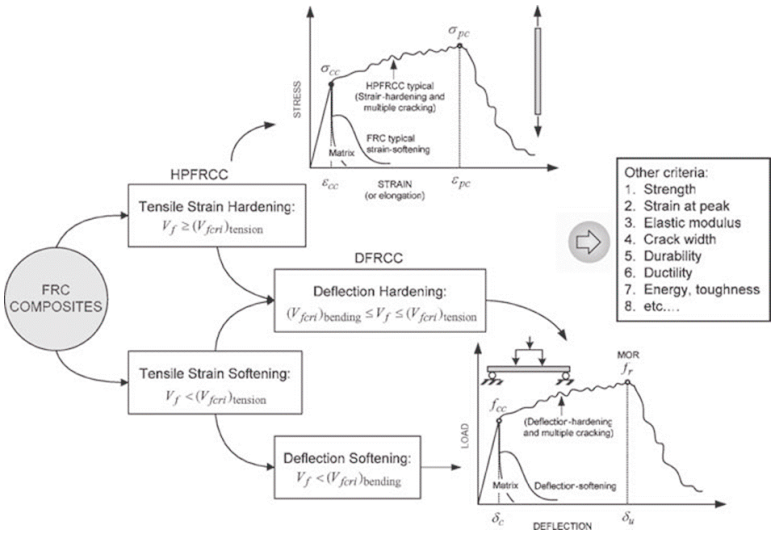

Figure 2.3. Classification of FRC Composites Based on Their Tensile Stress-Strain Response [23].

It was stated by Naaman and Reinhardt [23] that, one key distinguishing material characteristic is whether the response of the composite is strain-hardening or strain-softening in tension, and within this last category, whether it is deflection-hardening or deflection-softening. Practically all fiber reinforced cement composites currently available were stated to be covered by the simple classification of Figure 2.3. It was observed by Naaman and Reinhardt [23] that a strain-hardening composite is considered mechanically more performant than a strain-softening one, while a tension strain-softening material can be deflection-hardening or deflection-softening.

The deflection-hardening behavior in strain-softening SFRC is possible, because in bending tests the linear strain profile along the un-cracked cross section favors a more stable propagation of the cracks. This may induce a significant hardening in bending even if, in uniaxial tension, the material shows a softening behavior after cracking of the concrete matrix. [13] Research has been done on the critical parameters determining whether the material will exhibit deflection-hardening or -softening [5].

Behavior of fresh concrete can also have significant effects on mechanical performance of hardened concrete. Therefore, examining fresh state behavior of concrete and fiber orientation has importance on determining mechanical performance of FRCs. Fibers are added to concrete not only to improve the strength, but primarily to improve the toughness, or energy absorption capacity. Commonly, the flexural toughness is defined as the area under the complete load-deflection curve in flexure; this is sometimes referred to as the total energy to fracture. Alternatively, the toughness may be defined as the area under the load-deflection curve out to some particular deflection, or out to the point at which the load has fallen back to some fixed percentage of the peak load.

Steel fibers are generally found to have much greater effect on the flexural strength of SFRC than on either the compressive or tensile strength, with increases of more than 100% having been reported. The increase in flexural strength is particularly sensitive, not only to the fiber volume, but also to the aspect ratio of the fibers, with higher aspect ratio leading to larger strength increases.

2.2.1. Size Effect on Flexural Performance

The material strength of concrete appears to decrease with increasing structural size. Several comprehensive studies have been carried out to confirm and explain this phenomenon, called size effect. For a long time the size effect was explained statistically as a consequence of the randomness of material strength, based on the fact that it is more likely for a large than a small structure to encounter a material point of lower strength. Later Bazant proposed [24] that the size effect should be explained by

energy release caused by macro crack growth, claiming that the randomness of strength only plays a negligible role. The latter explanation, based on strain energy release due to fracture growth, has gradually been widely accepted and has been thoroughly supported by laboratory evidence [25].

One of the studies done so far to investigate the size effect in SFRC structures is reported in [26]. In this project, an experimental program was carried out at several research laboratories and universities in order to explain and quantify the dependence of the size, and formulate simple rules to achieve a safe design. In addition to specimen depth, the specimen width, the span-to-depth ratio and the influence of additional compression forces was investigated. The σ-σ relationship proposed by RILEM Committee 162 [22] was defined as a basis. The influence of different member depths was investigated by a total amount of 36 specimens with three depths; 100, 400 and 600mm. In general, the calculated loads based on the σ-σ relation were higher than the experimental loads. The ratio of experimental to calculated loads were descending in the range of small to medium depths and maintained at a constant plateau from medium to large depths.

Furthermore, when the fiber content was increased and the conventional reinforcement lowered, the size dependence increased [26]. This is also in accordance with the results of a study by Sener *et al.*, [27], where it was concluded that the bending failure in the steel fiber reinforced beams exhibited a greater size effect than beams cast using plain concrete. In the same manner as for plain concrete, it is evidently practical to include a size factor in the design models for FRC. Moreover, it is useful to carry out more experiments investigating the size effect in FRC structures in order to establish more clearly the dependence of the specimen depths.

2.2.2. Effect of Fiber Orientation on Flexural Performance

It was observed that preferred orientation of fibers results in non-homogenous material properties throughout a specimen. Therefore, it can be concluded that the mechanical performance of composite materials may vary in different Section of the

specimen. Consequently, both fiber dispersion analysis and four-point bending tests should be performed for a clear understanding of the effects of fiber orientation on mechanical performance.

The results obtained from all these studies highlight the need for further investigation of the strong connection existing between fiber distribution/orientation and mechanical properties of fiber reinforced concrete [28]. Carrying out a detailed study on various formwork and fiber dimensions, in terms of both fresh state and hardened state performance was thought to be a remarkable improvement for figuring out this connection between fiber distribution and mechanical properties of SC-FRCC's.

2.3. Measurement of Flexural Performance with 4-point Bending Test

The most common experimental test set up for post-cracking and toughness measurement is the beam bending test carried out on beams with a notch at the tensile side [17]. Recently, the European Committee has proposed a three-point bending test procedure, while the Italian Committee has suggested a four-point bending test configuration. Furthermore, the recent guideline CNR-DT 204 [29] has proposed, for analysis and design of FRC (or HPFRC) structural members, stress- crack opening and stress-strain relationship in uniaxial tension identified by means of four-point and three-point bending tests, respectively.

The highest or maximum flexural stress occurs under the loading head in 3-point bending tests, whereas in 4-point bending tests, the maximum flexural stress is spread over the section of the beam between loading points. Also, a 3-point test best applies where the material is homogeneous, such as plastic materials, whereas a 4-point test tends to be the best choice if the material is not homogeneous, such as composites or wood.

The stress concentration of a 3-point test is small and concentrated under the center of the loading point, whereas the stress concentration of a 4-point test is over a larger region, avoiding premature failure. Therefore, 4-point bending tests are usually

performed to investigate fibers performances and to evaluate their possible use for the design of structural members, by means of the derivation of ductility and tenacity of the material according to standards [30].

The addition of steel fibers significantly improves many of the engineering properties of mortar and concrete, notably impact strength and toughness [31]. The improved fresh state and mechanical performance of fiber-reinforced concrete comes from its increased capacity to absorb energy during fracture. An unreinforced concrete shows a brittle behavior, at the occurrence of cracking stresses during failure. On the other hand, the ductile fibers in fiber-reinforced concrete continue to carry stresses even after the cracking of matrix, which helps providing structural integrity and unity.

Further, if properly designed, fibers undergo a pullout process, and the frictional work needed for pullout leads to a significantly improved energy absorption capability. This energy absorption attribute of SFRC is often termed "Toughness" [32]. The importance of fiber geometry and matrix strength on the toughness characteristics of SFRC has been clearly established by earlier researchers [33, 34].

Performance of fiber-reinforced concrete is affected in different ways by the amount and aspect ratio of fibers in the concrete. As mentioned in ASTM C1609 [35], in some cases, fibers may increase the residual load and toughness capacity at specified deflections while producing a first-peak strength equal to or slightly greater than the flexural strength of the concrete without fibers. In other cases, fibers may significantly increase the first-peak and peak strengths while affecting a relatively small increase in residual load capacity and specimen toughness at specified deflections [35].

The first-cracking stress characterizes the flexural behavior of the fiber-reinforced concrete up to the onset of cracking, while residual strengths at specified deflections characterize the residual capacity after cracking, as can be shown in Figure 2.4[37]:

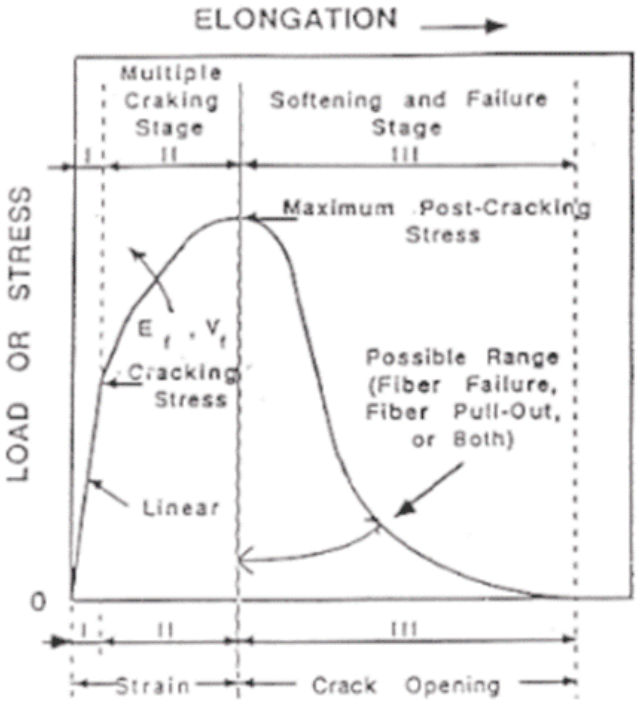

Figure 2.4. Typical Load-Elongation Response in Tension of Fiber Rreinforced Concrete [37].

Boulekbache *et al.*, [36] mentioned that a cracked concrete can continue to support further increases in loading without widening the crack width through fiber crack stitching and through the deformation of the fibres, which causes increased crushing and splitting of the matrix. As a result, at the end of the loading stage, failure is very ductile and soft since most of the energy is absorbed by the deformed fibres. For the fiber reinforced concrete, more than one peak load may occur, one at the end of the cement matrix contribution and others when the fibres reach their ultimate capacity.

Specimen toughness is an important parameter for determining mechanical performance of the specimens, since it measures the energy absorption capacity. The results of toughness test method were used for comparing the performance of various fiber-reinforced concrete mixtures or in research and development work [35]. They may also be used to monitor concrete quality, to verify compliance with construction specifications, obtain flexural strength data on fiber-reinforced concrete members subject to pure bending, or to evaluate the quality of concrete in service.

2.4. Flexural Strength

Compared with tensile and compressive strength, flexural strength is a more representative factor to indicate the influence of steel fibers on brittle matrix. The increase of more than 100% of the flexural strength by the use of steel fibers has been reported in the literature. The increase in flexural strength is particularly sensitive, not only to the fiber volume, but also to the aspect ratio of the fibers, with higher aspect ratios leading to larger strength increases [38]. According to a study carried out by Bencardino [39], the behaviour of the ordinary concrete specimens is almost linear-elastic up to the peak load, followed by a slight descending branch up to failure, then the complete separation of specimens into two Section occurs.

On the contrary, it was stated by Bencardino [39] that SFRC specimen shows a tri-linear variation with an extensive cracking process between first crack load and peak load that clearly differentiated them from the PC specimens. A typical generic curve of the SFRC specimens is characterized by a linear branch up to the first crack followed by non-linear behaviour up to the peak load. In the region near the maximum load there is stable crack propagation due to the crack controlling effect of the fibers located near the ligament surface.

2.5. Flexural Toughness

The addition of steel fibers to concrete not only results in a large increase in flexural strength, but also a considerable increase in toughness. After cracking, the cracks can not extend without stretching and debonding of the fibers. As a result, a large additional energy is absorbed before complete separation of the specimen occurs. Flexural toughness in concrete is related to crack growth. When fibers are present in concrete, after cracking, the cracks can not extend without stretching and debonding of the fibers. As a result, considerable additional energy is absorbed before complete separation of the specimen occurs.

In a load-deflection curve, for most Fiber-Reinforced Concrete (FRC), the pre-

peak response is not expected to be much different from plain concrete. Rather it is actually the post-peak response that is of primary interest. The addition of fibers significantly improves many of the engineering properties of mortar and concrete, notably impact strength and toughness. The enhanced performance of fiber-reinforced concrete compared to its unreinforced counterpart comes from its improved capacity to absorb energy during fracture. While a plain unreinforced matrix fails in a brittle manner at the occurrence of cracking stresses (pre-peak response), the fibers in fiber-reinforced concrete continue to carry stresses successfully beyond matrix cracking, which helps maintain structural integrity and cohesiveness in the material (post-peak response).

Further, if properly designed, fibers undergo pullout processes, and the mechanical and frictional work needed for pullout leads to a significantly improved energy absorption capability. This energy absorption attribute of SFRC is often termed - Toughness.

2.5.1. Flexural Toughness Measurement Methods

There are, however, a number of uncertainties regarding how FRC flexural toughness should be measured, interpreted, or used. Various flexural toughness test methods have been developed in different countries. ASTM-C1018 [21], JSCE-SF4 (JCI) [40], RILEM [22, 41] and EFNARC [42] are the most commonly used test methods.

In general, the guidelines proposed by various standards call for similar testing methodology (third point loading) and to some extent differ in the size of specimen adopted. The real adequacy of any tests method lies entirely in preventing the extraneous deflections which can occur either due to the support settlement, lack of stiffness of the testing machine or rigidity of the deflection measuring device (LVDT). Over decades, toughness measurements have been evaluated using an un-notched concrete beam in flexure either by using a four-point loading (or third point loading) or mid-point loading arrangement. A summary of the various specifications is given in Table 2.1, and these specifications are discussed in the following Section of this work.

Table 2.1. Experimental Test Methods and Toughness Characterization by Various Standards (Sivakumar, 2013).

Name of the standard	Dimensions of the specimen (L*b*h) mm	Rate of loading (mm/min)	Type of loading arrangement	Maximum diflection measured	Toughness measurement
ASTM C-1018[5] (1992)	300*100*100	0.05 to 0.10	Third point loading	Up to point where these is no resistanca on further loading	Determination of toughness indices and residual strength factors
ACI-544 guidelines[6] (1988)	350*100*100	0.05 to 0.10	Third point Midpoint loading	Up to 1.9 mm	Rotion of energy absorbed by a FRC to that of planin concrete
JCI specifications[7] (1984)	300*100*100	L/1500 to L/300	Tpird point loading	Up to L/150	Energy absorbed up to a deflection of L/150 mm
RILEL draft recommendations[8] (1985)	B>50, d>25, L	0.25	Thrid point loading	Up to 3 mm	Energy absorbed up to a deflection of 3 mm
EFNARC specification[9]	450*125*75	0.25±0.05	Thrid point loading	Up to 25 mm	Residual strength factors up to deflection of 1 and 3 mm

2.5.1.1. ASTM C 1018 Standard Test Method. First, it should be mentioned that ASTM C 1018 standard was withdrawn in 1997. However, the method proposed in the standard is still being used for many researchers. The ASTM C 1018 standard test method is based on determining the amount of energy required first to deflect and crack a FRC beam, and then to further deflect the beam out to selected multiples of the first crack deflection, as can be seen in Figure 2.5 and Figure 2.6 [21]. Toughness indices I_5, I_{10}, I_{20}, I_N, etc. are then calculated by taking the ratios of the energy absorbed to a certain multiple of first crack deflection and the energy consumed up to the occurrence of the first crack. The indices give the relative deviation from the response of a perfectly elastic-plastic material. Calculation of toughness indexes requires an accurate assessment of the first-crack energy, which constitutes the denominator in the definition of the various indexes. In addition, it is mentioned by Nataraja *et al.*, [32] that the identification of first-crack deflection is not so simple with ASTM method, due to the substantial non-linearity of load deflection curves even prior to attaining the peak load. Identifying the correct occurrence location of the first crack, which is crucial and one of the main problems with the ASTM method, is not a concern with the JSCE method.

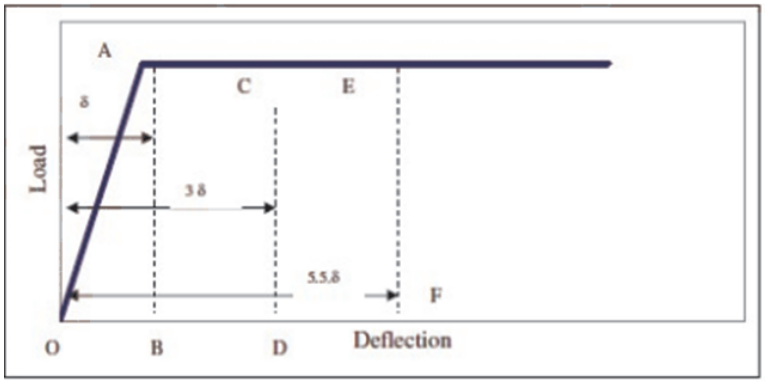

Figure 2.5. Elastic-Brittle and Elastic-Plastic Load-Deflection Curves According to ASTM C 1018 Standard [21].

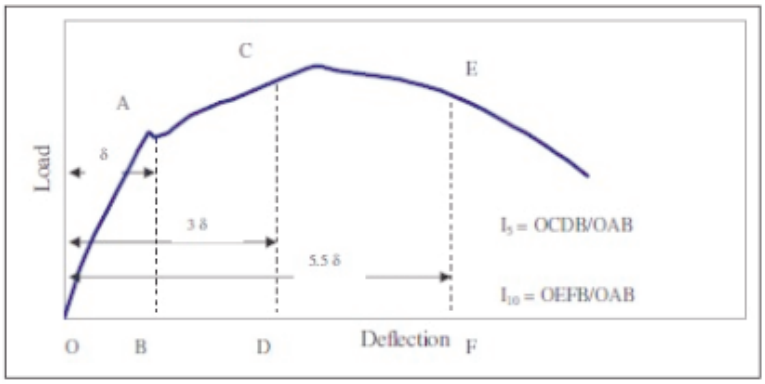

Figure 2.6. Flexural Toughness Values According to ASTM C1018 Standard [21].

Although ASTM C 1018 is a widely used standard test method, there are some problems related to the application of this method like effect of extraneous deformations, decision of location of the first crack point, and stability problems [43].

Evaluating the toughness indices, without excluding the extraneous deformations like support settlements, leads to erroneous results. This is due to the fact that all indices are dependent on the first crack deflection. In order to measure correct deflections some modifications are necessary. The use of so called yoke, which is a frame attached to the beam allowing direct measurement of the net central deflection of the beam, or the use of a top mounted deflection measurement system are possible solutions to this problem [43].

In ASTM C 1018 the first crack point is defined as the point at which the curvature first increases sharply and then slope of the curve exhibits a definite change. This is a subjective definition and often the load-deflection curves lack a distinct point as mentioned in the definition due to micro cracking and subsequent multiple cracks before the peak load is reached. There is a need for an objective definition of first crack so that determination of first crack point is not affected by whom the test is performed and evaluated [43].

If the machine is not sufficiently stiff, the elastic energy stored in the system is released after the peak load and this causes a sudden jump in the curve. Most of these stability problems are reduced if a closed loop system is used. Unfortunately most of the laboratories lack such sophisticated instruments [43].

2.5.1.2. JSCE SF-4 Standard Test Method. In this method the area under the load deflection curve up to a deflection of span/150 is obtained and results obtained from this test method yield an absolute toughness value. A flexural toughness factor is calculated which has a unit of stress. This factor can be considered as the post crack residual strength of the material when loaded to a deflection of (span/150) [40, 43].

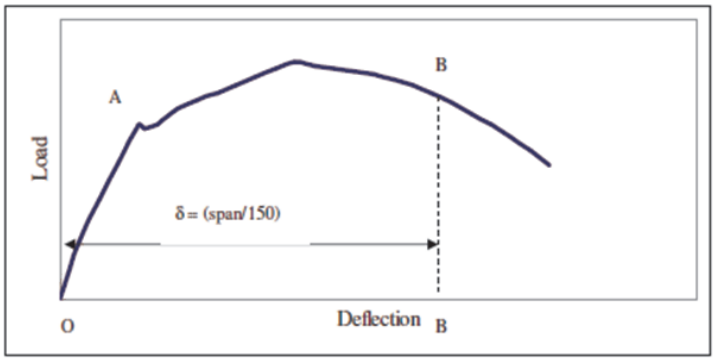

Figure 2.7. Flexural Toughness Values According to JSCE SF-4 Standard [40].

Determination of first crack point is not a concern in this test method. In addition stability problems encountered right after the first crack do not affect the obtained results significantly as beams are deflected too far out from the first crack point. However, results of this test method are highly dependent on specimen size and geometry.

The (span/150) deflection chosen in this test method is often criticized for being much greater than acceptable serviceability limits, as can be seen in Figue 2.7. This test method does not distinguish between the pre and post crack behaviour, which may be very important in some applications [40, 43].

Unlike the ASTM method, the instability in the load-deflection plot right after the first crack is not of major concern in the JSCE method, since the end point deflection of span/150 is too far out in the curve to be affected by the instability in the initial portion [32]. However, as mentioned by Nataraja *et al.*,, JSCE technique is sometimes criticized for the chosen deflection of span/150, as it is considered excessive for many applications. Since this deflection is purely arbitrary, any other suitable limit can be used based on the serviceability requirements, and the method can still be used.

And the main advantages of JSCE are that it is a simple method and flexural toughness can be determined easily by using any deflection measuring technique, without using any sophisticated instrumentation for determining the toughness factor. And in this method, determination of first crack, which is very difficult to identify, is not required. Furthermore, it was suggested by Nataraja *et al.*, that the flexural toughness factor calculated using this approach has good correlation with the fiber-reinforcing index, which is (Vf.L/df), where Vf is volume fraction of fibers, L is fiber length and df is fiber diameter.

Lianrong *et al.*, [44] studied the effects of testing and material variables on both the load-deflection response and the flexural toughness of FRC, investigated the reproducibility of the flexural toughness test methods of FRC, discussed difficulties in toughness evaluation, defined various flexural toughness parameters, assessed relative advantages and disadvantages of different methods of characterizing toughness, and developed recommendations for a more suitable procedure for FRC flexural toughness evaluation. Finally, he stated that the load-deflection response of FRC is an experimental property and so are the flexural toughness parameters derived from the response, and depend not only on material variables but also on testing factors. Out of various testing variables, the deflection measuring system, the loading system, and specimen

size/geometry are the three most important factors; while amongst the various material variables, fibre content and fibre type/profile are the most important. The major difficulties in measuring the load-deflection response, caused by either extraneous deformations, first crack determination, or instability, has much more significant effects on ASTM toughness parameters than on JSCE toughness parameters [40]. As stated by Lianrong [44], ASTM parameters may not be particularly sensitive in distinguishing either amongst different fibre contents for SFRC with similar low fibre contents, whereas JSCE parameters are more sensitive in this regard. Therefore, considering the reliability and efficiency of various toughness parameters, JSCE SF-4 method was used for toughness calculations in this study.

2.6. Cracking Behavior

Concrete is one of the fundamental materials used in civil engineering and has many beneficial features such as high compressive strength, relatively low cost, convenient production and placement, and good durability. However, due to its brittle nature, it tends to crack under tensile loading, resulting in loss of tensile strength in the post-cracking deformation regime.

Cracking results in decrease of the load carrying capacity of concrete and also the aesthetics. The main causes leading to this cracking problem are attributed to the brittle nature of concrete (i.e. weak in tension and flexure) and the shrinkage under the change of temperature and humidity in working environment. A solution of addition of small fibres into concrete to enhance the flexural loading capacity and toughness as well as prevention of cracks for concrete structures has been and being implemented for about 50 years [5, 45-49].

For reinforced concrete, the lack of ductility of concrete has implications on the structural performance as well as long term durability. Internal fiber reinforcement can improve the tensile strength and ductility of concrete beyond the elastic limit. Compared to plain concrete and conventional fiber reinforced cement composites (FRCC), high performance fiber reinforced cement composites (HPFRCC) show a significant

improvement in ductility [50].

HPFRCC are characterized by multiple cracking and pseudo strain hardening under direct tensile loading. Designing for these properties of HPFRCC and prediction of the tensile behavior is essential for structural applications.

Steel fibers in HPFRCC positively modify the macroscopic behavior of the composite and increase its compressive strength, tensile strength, stiffness, fracture toughness and impact resistance. Since a crack often starts at the weakest point of a composite material, the fibres have to be as randomly distributed as possible. The direction in which the fibres are oriented and whether a fibre ruptures or is pulled out determine their effectiveness. This behavior can be achieved by adding a certain proportion of short steel fibers to the matrix mixture, mostly in an amount between 1-3 vol%. Many studies has shown that such an amount of fibers effectively bridge cracks in the matrix and force it to develop many distributed cracks rather than a few widely opened cracks. Therefore, a large amount of energy can be dissipated prior to reaching the peak load or deformation.

It is now generally accepted that the primary effect of fibres is that they improve the post-cracking behaviour and the toughness - i.e. the capacity of transferring stresses after matrix cracking and the tensile strains at rupture - rather than the tensile strength, as it was stated by [51, 52]. In some of the early work on fibre-reinforced concrete, [53] it was thought that the tensile strength could be increased due to an assumption that fibres delay the widening of microcracks (initiated at flaws)- and that the closer the fibres were spaced, the more resistance to cracking.

Previous experimental studies from literature has also indicated that the addition of steel fibers to concrete significantly increased the total energy absorbed prior to complete separation of the specimen [54]. The presence of steel fibers was also found to improve fatigue properties [55], impact strength [56, 57] and shear strength [58]. The improvement of the mechanical properties of SFRC is attributed to the crack controlling mechanism. Bekaert [59] suggested that two mechanisms play a role in

reducing the intensity of stress in the vicinity of a crack. These mechanisms are:

- Steel fibers near the crack tip resist higher loads because of their higher Young's modulus compared to the surrounding concrete.
- Steel fibers bridge the crack and transmit some of the load across the crack.

The ability of the steel fibers to resist crack propagation is primarily dependent on the bond between the concrete and fibers as well as fiber distribution (spacing and orientation). The bond between the concrete and the fiber is the mechanism whereby the stress is transferred from the concrete matrix to the steel fibers. The ability of the steel fibers to develop sufficient bond is dependent on many factors, mainly:

- The steel fiber characteristics (surface texture, end shape and yield strength)
- The orientation of the steel fiber relative to the force direction
- The properties of the concrete

2.6.1. Cracking Mechanism

For most SFRC, the major reinforcing effect of fibres comes about first after matrix cracking. After the cracking of ordinary reinforced concrete members, the steel fibre can transfer tensile stresses across the cracks and so it leads to a reduction of the crack widths. When the residual tensile strength of SFRC is higher than the tensile strength, then strain/deflection hardening post cracking behaviour is achieved. In this case, more cracks will open if the load is still increasing after the cracking. Whereas when the residual tensile strength is lower than the tensile strength of SFRC, then strain/deflection softening behaviour is achieved and no more cracks will open. Depending on stress-strain distribution in the section, the strain hardening is achieved using larger amount of the fibre than for the case of deflection hardening behaviour [60-62].

Examination of fractured steel fibre-reinforced concrete specimens shows that failure takes place primarily due to fibre pull-out and that, for fibres with end-hooks, a

considerable energy dissipation takes place as the fibre is straightened and plastically deformed [63].

Thus, unlike plain concrete, a FRC specimen does not break in such a brittle manner after initiation of the first crack. This has the effect of increasing the work of fracture, which is referred to as toughness or fracture energy and is represented by the area under the stress-crack opening curve Figure 2.8.

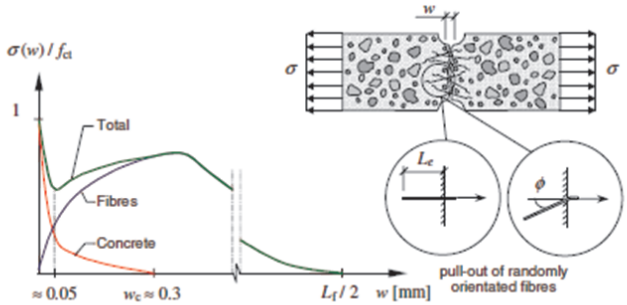

Figure 26. Combined fibre and aggregate bridging for fibre-reinforced concrete loaded in uni-axial tension.

Figure 2.8. Combined Fiber and Aggregate Bridging for Fiber-Reinforced Concrete Loaded in Uni-Axial Tension [63].

The fracture process of fibre-reinforced composites is also a complex phenomenon dependent on a number of parameters. It is generally accepted that when a crack is present in a matrix, and this approaches an isolated fibre, the following mechanisms may be expected to take place and contribute to energy dissipation Figure 2.9:

- matrix fracture and matrix spalling
- fibre-matrix interface debonding;
- post-debonding friction between fibre and matrix (fibre pull-out);
- fibre fracture;
- fibre abrasion and plastic deformation (or yielding) of the fibre.

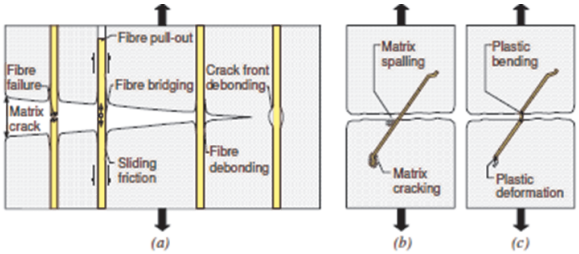

Figure 2.9. (a) A Schematic Illustrating Some of the Toughening Effects and Crack Front Debonding, Debonding and Sliding in the Crack Wake, (b) Matrix Spalling and Matrix Cracking, (c) Plastic Bending (Deformation) of Inclined Fiber During Pull Out- Both at the Crack and at the end-Anchor [63].

To describe the influence of different fibres, [63] distinguish between two levels (see Figure 2.10): the micro-level and the macro-level. The micro-level is initiated after the linear elastic stage is surpassed (A) and small cracks arise within the matrix from initial flaws. At increasing load (A-C), the length of the cracks increases and the microcracks coalesce and finally localise (C). At a given fibre content, microfibres, due to their high number, are more likely to cross these microcracks. In the macro-level stage (C), a crack gradually opens in the direction of the principal tensile stress. Long fibres primarily improve the performance once a macro-crack appears, and their geometry and shape determine at what stage they are active. However, as the microfibres are short, the range for which they are effective is limited and, inevitably, unstable crack growth will dominate the behaviour (C-D) [64-67].

For microfibres to be effective they should have a relatively high aspect ratio and stiffness, so that they can restrain the microcracks as these propagate into the mortar and prevent and postpone the unstable crack growth; see Figure 2.10. Betterman *et al.*, [65] found that the peak-stress increased with increasing fibre volume as well as a decrease in fibre diameter. Lawler *et al.*, [67] observed that if microfibres were present, microcracks were prevented from widening but not from growing in length, but eventually cracks coalesced and transversed the full specimen width, producing a macro-crack where deformation localised. Furthermore, the strain capacity increased with the addition of microfibres, which is indicated in Figure 2.10. Nelson *et al.*, [66]

found in their investigation that some microfibres are capable of effectively postponing the development/growth of microcracks.

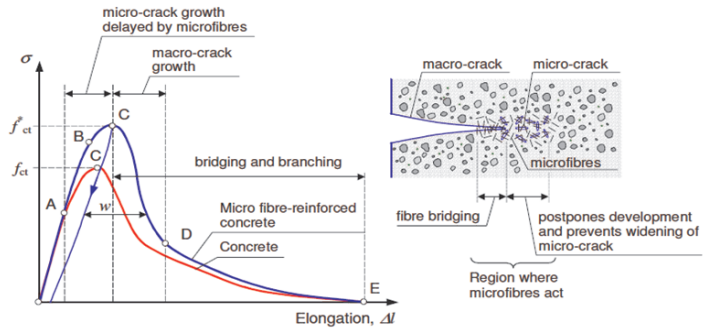

Figure 2.10. Schematic Description of the Effect of Microfibers on the Fracture Process in Uni-axial Tension [63].

Principally, fibers improve the mechanical characteristics of SFRC once the matrix starts cracking. In the initial phase of testing micro-cracks open and localize in macro-cracks later on; the phase at which a fiber starts to transmit a force depends on the fiber type. The performance and the variation of characteristics of SFRC after cracking are directly related to the characteristics, the orientation and the number of fibers in the cracked cross-section. The orientation of the fibres due to the flow, size of the mould and the production method determines their effectiveness, which might be an advantage or a disadvantage dependent on the application and whether it can be controlled. In order to describe the effect of various parameters that affect the alignment of fibres, the orientation number has to be determined.

2.6.2. Strain and Crack Width Measurement Techniques

There are numerous experimental methods available for determining strain distributions and crack-width profiles in flexure [68]. Conventional deformation measurement techniques, such as utilizing an LVDT, a demountable mechanical strain gauge and an electrical strain gauge, despite their vast usage in experimental studies, suffer several disadvantages, including high cost, time-consuming specimen preparation, and the inability to obtain the whole displacement or strain fields. The aforementioned drawbacks on one hand and the importance of deformation measurements in laboratory

tests on the other hand have led researchers to develop other measurement techniques, especially image-based techniques, capable of evaluating whole deformation fields.

Among all of these recently developed methods, particle image velocimetry (PIV) has attracted much interest in all branches of civil engineering experimental investigations; PIV is a powerful image-based technique for evaluating both displacement and strain fields by analyzing successive digital images of a field undergoing deformation. Despite its great potential, however, few studies have been reported that use PIV for obtaining deformations for structural tests, especially for evaluating displacement and strain fields in a conventional bending test.

In order to choose the most appropriate equipment for a particular investigation many factors must first be considered for each method, including: (i) the range of strain (or crack-widths) that can be measured; (ii) the accuracy or sensitivity of the measurements obtained; (iii) the maximum specimen size that can be analysed; (iv) whether the method provides a full-field solution or point by point measurements; and (v) whether the method been used in the past for similar work.

2.6.2.1. LVDTs. Apart from dial gauges, using an LVDT is a simple technique for obtaining deformation in conventional structural tests. Although there are certain advantages to using LVDTs, such as high resolution and accuracy, simple installation, and real-time logging ability, there are also few drawbacks, such as some limitations for monitoring the whole displacement field and relatively time-consuming installations on the specimens if obtaining the full field crack monitoring is the main purpose.

2.6.2.2. Electrical Resistance Strain Gauges. This is probably the most widely used strain analysis technique. Electrical resistance strain gauges offer a simple, quick and relatively cheap method of strain measurement. The method has been used on numerous occasions in the past for obtaining strain measurements from conventional steel bar and steel fibre reinforced concrete specimens in flexure [21-24]. However, strain gauges only measure strain at the point of fixing and in the direction of the gauge

alignment, and therefore they do not provide a full-field analysis. Moreover, the size and geometry of the specimen can limit the number of gauges that can be attached, and strain readings are generally limited to around 2% strain.

2.6.2.3. Grid Methods. The grid method is one of the oldest strain analysis techniques available. The method requires the placement of a well defined grid of spots or lines on the surface of the specimen, which is then photographed before and after loading to determine specimen distortion, and hence strains. Early applications of the grid method were limited by three main problems: it was difficult to apply a well defined grid onto the specimen; the analysis was performed manually by eye, and so the accuracy and precision of the results were poor; and the manual analysis of the deformed grid could be very time consuming.

2.6.2.4. Digital Image Techniques. However, with recent advancements in photographic and computer technology, a new approach has been developed using digital image processing techniques [69, 70]. In these methods, a photo-electronic camera, digitizing (A/D) board and a computer based image-processing system are used to capture a digital image of the grid. This digital image is then analysed, using grey-level threshold techniques and centroid algorithms, in order to determine the positions of the centroids of the grid spots, and hence the grid deformations and strains. The main advantages of the automated grid method include: large strains (greater than 5%) and crack-widths can be measured; the analysis is fully automated; and the method provides a full-field analysis over a large area of the specimen.

2.6.2.5. Photogrammetry. Photogrammetry is the process of obtaining accurate measurements from physical objects using photography [71]. Because of certain advantages of photogrammetry, including the capability of whole field displacement measurements and crack monitoring of RC members during the test process, the technique has been used in some experimental investigations worldwide. Lee and Al-Mahaidi [72] utilized the photogrammetry technique to investigate the torsional and shear behavior of RC beams strengthened with carbon-fiber-reinforced polymer (CFRP). However, despite

certain benefits of photogrammetry, some disadvantages of the technique may be noted, such as the complexity of test setup, the time-consuming specimen preparation, and the incapability of evaluating strain fields. Moreover, because of the required complex test setup, loading of specimens should be paused at several steps to capture the whole field using different cameras.

2.6.2.6. Digital Image Correlation (DIC). Another recently developed method that has the capability of whole-displacement-field measurement is the DIC method. In general, DIC is an image-analysis procedure that uses mathematical correlation functions to analyze successive digital images of a field undergoing deformation. This technique offers the advantage of obtaining continuous measurements of the whole displacement field.

Consequently, the DIC method has been widely accepted in all civil engineering laboratory tests. The method has been successfully utilized in numerous investigations in the field of geomechanics, modeling asphalt aggregate mixtures, analyzing seepage in inhomogeneous geosystems, evaluating shear banding in dilative sand and characterizing viscoelastoplastic damage of asphalt-aggregate mixtures [73-77]. The DIC method has also been utilized in experimental studies in the field of structural engineering for investigating fracture mechanics and strain localization in concrete [78-81]. Furthermore, Huang *et al.*, [82] developed the automatic digital image correlation (ADIC) technique for concrete elasticity modulus determination. However, obtaining precise strain fields with DIC can be challenging in some cases, despite having certain advantages for displacement and strain field measurements [83].

2.6.2.7. PIV Method. Particle image velocimetry (PIV) is another recently developed technique for evaluating the whole displacement and strain fields in common civil engineering tests, which has attracted much interest; PIV is originally a velocity-measuring technique developed in the field of experimental fluid mechanics [84].

This technique is used to determine instantaneous fields of the vector velocity

by measuring the displacements of numerous fine particles that accurately follow the motion of the fluid [84]. The reference image is divided into a grid of square subsets, which are identified by their unique pixel intensity variation signature. The GeoPIV algorithm searches within a specified search zone of a deformed image for a subset which has maximum similarity to the subset's signature in the reference image. The difference, measured in pixels, between the target subset and the reference subset is the displacement vector of the subset's centre. In order to achieve an accurate displacement measurement, the subset must be sufficiently unique from the surrounding search zone. This uniqueness is dependent on the colour variations, or image texture, of the object being observed.

For PIV analysis, the displacement vector of each patch during the interval between the flashes is found by locating the peak of the autocorrelation function of each patch. The peak in the auto-correlation function indicates that the two images of each seeding particle are overlying each other, so the correlation offset is equal to the displacement vector [85]. The technique has been utilized in numerous fluid mechanics studies investigating different fluid parameters. A modified approach was used to implement PIV in geotechnical testing by [85]. Afterwards, it has also been frequently used in granular materials [76, 86].

Nowadays, PIV has been used in the field of concrete/composites also, in order to measure displacement and strain fields [87-91] and monitoring fracture process zones (FPZs) and cracks [91]. Pioneering research done on the subject reveals the potential of this technique for precise and easy measuring of deformation/crack width of concrete specimens [91]. However, the number of studies on the application of this technique for crack monitoring of cement-based materials is still limited.

Consequently, despite other image-based measuring techniques, no embedded markers or painting is necessary for the PIV method for geotechnical tests. According to White's investigations [85], the modified PIV technique offers an order-of-magnitude increase in accuracy, precision, and measurement array size compared with previous image-based methods of displacement measurement.

Therefore, PIV was selected and used in this study to comprehensively analyze cracking of fiber reinforced material and one of the objectives of this study was set to further investigate the ability of PIV for measuring concrete performance in the fresh and hardened states.

2.7. Fiber Orientation

A property that has a direct effect on the efficiency of FRC is fiber orientation, since the structural response depends on how fibers are oriented with respect to the failure plane, since it plays an important role for the mechanical performance of fiber-reinforced composites.

Substantial increase in the tensile strength and toughness are the most acknowledged features of fiber reinforced concrete [51]. Such enhanced properties arise from fiber effectiveness on crack-width control, which depends on the individual performance of all fibers crossing a crack. Modeling the overall fiber bridging force thus requires the actual amount of fibers under each inclination angle and their respective pullout responses.

There are mainly 3 factors affecting fiber efficiency especially for the post-cracking performance: i) fiber dosage, ii) fiber geometry, iii) fiber dispersion. It is known that a higher fiber dosage results in higher postcracking strength [92-96], whereas maximum uniaxial tensile strength is only marginally influenced [97]. Furthermore, fiber geometry (i.e: fiber aspect ratio), is a crucial factor when evaluating postcracking resistance. Similar to the fiber content, a higher fiber aspect ratio generally evokes larger postcracking tensile strength. A third group of crucial impact factors are the fibers' dispersion in the cement matrix and orientation in direction of the applied stress [98].

A perfect fiber alignment in stress direction offers the highest fiber efficiency resulting in higher postcracking strength than for a random orientation, whereas a transverse orientation would theoretically not offer any strength contribution by the fiber at all.

Results on four-point bending tests showing higher bending strength with better fiber alignment are given by [99-102]. Generally larger dimensions (for instance plates) implicate a more three-dimensional (random) fiber orientation compared to small-scale specimens, resulting in lower residual strength values. An extensive experimental study confirming the aforementioned results was performed by [103] on beam elements with different cross-sections. Additionally, the so-called wall effect implicates fiber orientation along the formwork wall as described in [104], presenting higher bending stresses with moulded specimens that for geometrically identical samples previously cut out from a bigger cast block [105].

The post-cracking performance of SFRC is also correlated with the number of fibres crossing the crack [106]. Kooiman [8] and Vandewalle & Dupont [107] reported on counting fibres in the cracked cross-sections of beams tested in bending. The number of fibres was correlated with the toughness. Gettu & Barragán [108] stated that the maximum load was not correlated with the amount of fibres but the toughness was. The high variation (up to 30%) in the peak load and toughness parameters was assigned to the variation of the amount of fibres in the cracked cross-section [109].

Additionally, casting procedures of FRC affect the distribution and orientation of fibers in the concrete matrix [19]. The fibers may not provide a uniform reinforcement with the same efficiency in all directions. In most cases, preferential orientations in the concrete matrix occur as a result of several factors, such as the fresh-state properties, the concrete pouring method, the geometry of the formwork and the type of vibration. This means that, if controlled, fiber orientation may enhance the tensile behavior [110].

Studies on the fresh-state properties (mainly rheological properties) of FRC [99, 100, 105, 109, 111, 112] reported that the flow of concrete affects the fiber orientation and, consequently, the hardened material properties. The study by Martinie and Roussel [111] sets two main reasons for the preferential orientation of the fibers: the wall-effects that depend on the geometry of the formwork and the flow of concrete, which depends on the rheological properties of the material, the geometry of the formwork and the casting procedure.

Fibre distribution and orientation have been found to depend on many factors, including: specimen size, casting and placement technique, fibre size, geometry and fibre content. [99, 101, 109, 113]

2.7.1. Various Effects on Fiber Orientation

2.7.1.1. Effect of Casting Procedure on Fiber Orientation. Several researchers have reported remarkable influences of casting elements and the casting direction on fiber orientation [100-114-115]. These facts lead to the obvious conclusion that the nonuniformity of fiber orientation due to different casting methods has to be considered in the design of structural elements [116]. This explains tremendous differences in structural performances sometimes observed in elements with the same FRC poured in different directions.

The way concrete is poured into the mould has also been recognized to have a major impact on fiber orientation, both due to the casting direction and due to preferential fiber alignment induced by the casting element itself [115]. Indeed, the casting direction was found to have a paramount influence on the mechanical properties of fluid fibrous mixtures, but a significantly smaller effect was observed with more viscous mixtures [117]. The link between the casting method and the rheological properties of fresh concrete is of utmost importance [118].

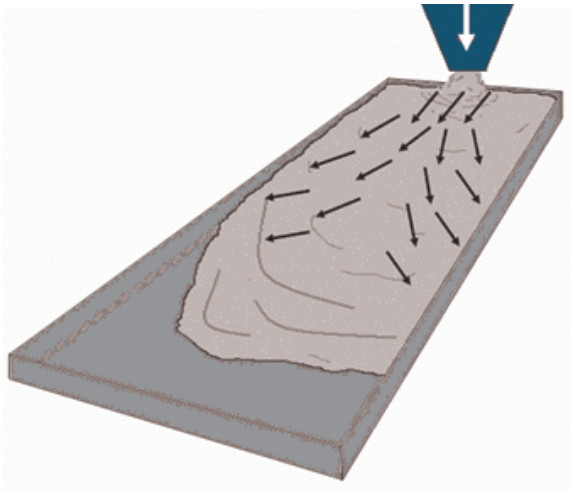

Figure 2.11. Schematic Flow Profile Developing when FRC Flows Along the Formwork.

When FRC flows along the formwork a certain flow profile develops (Figure 2.11), most likely due to frictional restraint with the walls of the formwork [100] and fibers align with the flow of fresh concrete [100 - 109 - 116]. This effect is stronger at higher flow velocity [116] and therefore it may be associated to the material plastic viscosity and casting rate.

Thereby, the influence of flow is inherently related to the casting method and to the geometry of the element itself.

2.7.1.2. Size Effect on Fiber Orientation. In the previous section, the influence of the geometry of the formwork was introduced, focusing on the boundary conditions. Nevertheless, it is also interesting to discuss how a change in the geometry of the cross section (in the width or the thickness) may affect fiber orientation and, consequently, the structural response.

Even though the orientation factor is a step towards a more accurate design, some unresolved issues still remain. Research has provided evidence that, among other factors, the geometry influences the distribution of fibers within the concrete matrix. Bearing that in mind, should the dimensions of the structure be considered when determining the effect of a favorable fiber orientation. For example, focusing on the case of slabs, how are the orientation and its favorable effect affected by increasing the width of the element. Should a different structural response of FRC slabs be expected depending on their size. All these questions must be answered.

The fibre orientation in any structural member (beam, slab, etc.) or materials test specimen is influenced by its boundaries. Analysis has shown that the effect of constrained orientation of fibres is manifested mainly in cases when the dimensions of the member are less than five times the length of the fibres. [8] When the dimensions of the member are greater, the effect of constraint is considerably reduced and the orientation of the fibres approaches those of body-random.

Kooiman [8] conducted an experimental study on the flexural behavior of SFRC beams with the span ranging from 500 to 1500 mm and the width from 150 mm to 450 mm (keeping constant the span to beam depth ratio and the notch depth to beam depth ratio). While the beam depth seemed to have no significant influence, the author reported an increase in the average energy absorption capacity and a reduction of the scatter as the width of the beam increased. The number of fibers in the cross-section indicated that the average number of fibers per cross-sectional area was not significantly influenced by width as long as the casting and compacting procedures were the same.

However, Michels *et al.*, [119] tested large-scale octagonal plates with increasing thickness and observed that the post-cracking residual strength decreased with thickness. Likewise, the analysis revealed that the orientation factor has a small variation in the horizontal plane and a remarkable variation over the thickness of the plate. The author also reported a more pronounced orientation in the horizontal plane in slender plates.

In this regard, it would be interesting to identify if changes in geometry may accentuate the advantageous effect of certain preferential orientations for instance, in slabs, which usually present a preferential fiber orientation perpendicular to the casting direction. For that, further experimental research on the fiber orientation and structural response of elements with different dimensions is required.

2.7.1.3. Effect of Fresh-State Properties on Fiber Orientation. One of the major aspects governing fiber orientation is the fresh state performance and rheology of FRC. Although this influence has been subject of extensive research, standardized equipment and measuring techniques are not yet available and therefore its correlation with the orientation of fibers in fresh concrete is unknown [99]. Hence, given the scarce knowledge about this subject, fiber orientation will be herein approached by simply distinguishing the behavior of conventional and self-compacting FRC in the fresh-state.

The effects of vibration on causing fibers to rotate into planar orientations have

been reported in literature [108] and, in case of self-consolidating concrete, the flow of the fresh concrete has also been identified to play a major role on fiber alignment [28 - 109 - 116].

Several researchers [120-124] have studied the influence of the compaction on the orientation of fibers. Most of these works conclude that external vibration during compaction produces fiber segregation and preferential orientation of the fibers along horizontal planes.

In contrast, a mixture with increased flow-ability in the fresh-state shows a stronger alignment of the fibers than a material with lower flow-ability [100]. SCC requires filling ability for horizontal and vertical flow, thus being prone to induce planar orientation of fibers. The flow can be idealized as taking place in layers that force fibers which are crossing them to align along their borderlines [109].

2.7.2. Fiber Orientation Measurement Techniques

2.7.2.1. Indirect Measuement Techniques. Visual observations during mixing and casting of test specimens can give an idea of the actual fiber orientation in the test specimen. A popular example of a destructive and indirect measurement of fiber orientation is manual counting [108 - 123 - 125], a method which relates the number of fibers in a cross-section with the average orientation of fibers by means of a theoretical expression. Because the average fiber orientation has been found to be proportional to the post-cracking strength of SFRC many investigation have also been evaluating indirectly fiber orientation through mechanical testing [8 - 109].

2.7.2.2. Direct Measurement Techniques. : Direct measurements of single fiber orientation can be obtained through techniques such as the image analysis [109 - 116], X-Ray method [113 - 126] or computerized tomography (CT-scans) [104 - 127].

Apart from the traditional indirect approach based on fiber counting [108], [123

- 125], direct measurements of single fiber orientation can now be obtained through techniques such as the image analysis One of the frequently used methods to determine fiber orientation is the x-ray technique, as was shown by Stroeven [121]. However, the problem with this technique is that it can only provide a two-dimensional representation of reality. Useful x-rays can only be made from thin slices, which causes it to be relatively expensive to carry out, and even then it is quite hard to quantify the effectiveness in efficiency factors.

Another available method on the fiber orientation is to perform photographic analyses of cut sections, as was done by Schönlin [106]. He developed a method to determine the fiber orientation from photographs by calculating the orientation angles of individual fibers from the size of their cross-sections in the cut sections.

Recently, there have been significant advances in the development of non-destructive methods to determine the orientation of steel fibers in large-scale elements. Examples of these methods are the alternating current-impedance spectroscopy (AC-IS) [128 - 112], the open coaxial transmission line, the dielectric waveguide antennas and methods based on electrical resistivity.

These methods allow simple and economical measurements of fiber orientation and have the great advantage that uncertainties that tend to exist between small and large-scale elements can be avoided.

2.8. Image Analysis

Image analysis is one of the most commonly used and well-studied method for fiber dispersion analysis. Two dimensional or three-dimensional micrographs of specimens can be taken and studied using appropriate equipment and image analysis programs. This method is a trusted method when applied appropriately.

Chermant *et al.*, [129], showed that automatic image analysis is a suitable tool to access too many morphological parameters. And, that should allow to establish

a better understanding between morphological parameters and physical properties of civil engineering materials, such as fiber-reinforced concrete. Many illustrations of use of automatic image analysis were given in their paper [129] in order to quantify the morphology of the concrete matrix, microcracks and fibers in FRC. Therefore, it is suggested to be a suitable method for determining fiber dispersion and orientation in FRCs.

It was also shown in the literature [128 - 130], and [131] that, fiber-orientation measurement by two-dimensional (2D) image analysis of polished cross-sections is a rapid and highly efficient method for determining the fiber orientation distribution over large sample areas.

As concluded from previous research, image analysis is a basic method for examining micro-structural characteristics of materials. It can also be used for investigating fiber-dispersion analysis of FRCs. The method is based on obtaining microscopic images of sections to study dispersion of fibers. Either two dimensional or three dimensional microscopic images of specimens can be taken and analyzed using image analysis program.

2.8.1. Fiber Orientation Density Calculations-2D

The measurement of fiber dispersion by 2D image analysis requires the preparation of a cross-section. The method of preparation depends on the technique used to image the specimen, e.g. scanning electron microscopy (SEM) [130]. As a result, the preparation of the concrete specimen for inspection by reflected light microscopy requires high contrast between the steel fibers and concrete matrix, which may not be achieved simply by polishing the specimen, but also grinding with emery paper for several layers.

The orientation of a fiber and the location of its intersection with the section plane are described by the parameters (θ, φ) and (x, y), respectively. These parameters are straightforward to derive from an elliptical fiber cross-section by image analysis. The

parameters that describe an ellipse are its position (xc, yc), axis lengths (a, b) and orientation, φ, as illustrated in Figure 2.12.

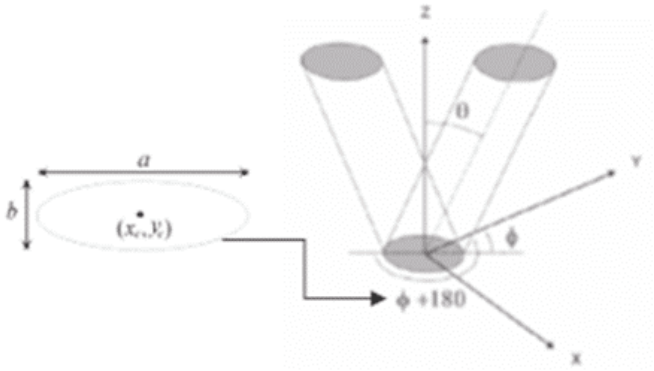

Figure 2.12. The Position and Orientation of a Fiber Can be Determined from the Parameters of its Elliptical Cross Section (a, b, xc, yc, φ). [130].

The calculations of orientation tensors are straightforward, and they give concise information about the fiber orientation density. Orientation tensors are obtained from moments of the orientation distribution function. The orientation of a fiber is derived from the parameters of its elliptical cross-section as follows:

$$\theta = Arccos \tag{2.1}$$

$$\varphi = \varphi \text{or} \varphi + 180 \tag{2.2}$$

The two possible values for f are the result of an ambiguity in determining the orientation of a fiber, due to fibers with orientations φ and φ+180 having identical cross-sections. The diagonal components of the orientation tensor are unaffected by this ambiguity [130].

In this study, a tensor description method was employed for fiber orientation density calculations in the specimen. Data from two dimensional cross-sections were

used for fiber dispersion and orientation analyses and second order orientation tensors were used to calculate fiber orientation, which was adapted from a widely used method for fiber reinforced polymers [130]. This method of Eberhardt *et al.*, was first adopted by Özyurt for cement-based composites for mathematical expression of fiber orientation [132].

A detailed description of the method was given in Section 3.4.5, Experimental Methods, Fiber Dispersion Analysis.

2.8.2. Fiber Orientation Density (FOD) Tensor Description

The state of orientation of a single fiber can be characterized from the angles θ and Φ defined in Figure 2.13. The directions 1, 2, and 3 refer to the flow, width and thickness directions, respectively. The orientation of the fiber can be described by a probability distribution function P(θ, Φ), defined as:

$$P\left(\theta_1 \leq \theta \leq \theta_1 + \delta\theta, \varphi_1 \leq \varphi \leq \varphi_1 + \delta\varphi\right) = \psi_{(\theta,\varphi)} \sin\left(\theta\right) d\theta d\varphi \tag{2.3}$$

An alternative way to describe the orientation of the fiber is by associating a unit vector P to the fiber direction, as shown in Figure 2.13. Thus the distribution function could be written as a function of p, ω (p). The components of the vector p are computed in terms of θ and Φ as:

$$p_1 = cos\theta \tag{2.4}$$

$$p_2 = sin\theta sin\varphi \tag{2.5}$$

$$p_3 = sin\theta cos\varphi \tag{2.6}$$

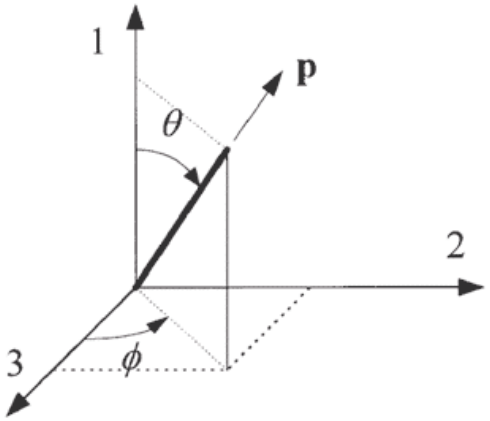

Figure 2.13. Definition of the Co-Ordinate System Used, the in Plane Angle φ, the out of Plane Angle θ and the Unit Vector P.

The directions 1, 2 and 3 refer to flow, transverse flow, and thickness directions, respectively. Experimentally, the second and fourth order tensors can be calculated from the vector components of P as:

$$\langle a_{ij} \rangle = \frac{\sum_n (p_i)\,(p_j) F_n}{\sum_n F_n} \tag{2.7}$$

$$\langle a_{ijkl} \rangle = \frac{\sum_n (p_i)(p_j)(p_k)(p_l) F_n}{\sum_n F_n} \tag{2.8}$$

Moderately aligned orientation states can be modeled by second-order tensors, while highly aligned states require fourth-order tensors [133]. Moreover, higher-order tensors provide complete information about lower-order tensors ($a_{ijkl} = a_{ij}$). From the orientation tensors it is also possible to recover the orientation distribution function [134].

The physical meaning of the terms of the second order tensor of fiber orientation, a 3x3 square matrix, can be readily understood. The sum of the diagonal elements must be the unit, since it equals the length of the unit vector P. The value of each element of the diagonal stands for the relative orientation of the fibers around the axis

(e.g. a_{11} =1 means that all the fibers are aligned in 1-direction, a_{11} =a_{22} =a_{33} =0.333 stands for random in space orientation).

2.9. Structural Design of Fiber-Reinforced Composites

Steel fiber reinforced concrete (SFRC) continues to be used in various applications due to its flexibility and enhanced toughness performance. However, its continued development has been hindered by a general lack of confidence in its design. This is mainly due to a lack of suitable analytical design methods and appropriate material property tests that measure toughness (or strength) parameters. Very different results are seen when the studies given in literature are examined. This is mainly due to the heterogeneity of fiber - reinforced concrete and high number of parameters that affect the performance. It is very hard to evaluate the combined effects of changing specimen size, fiber size, fiber geometry, fiber type and fiber volume ratio and reflect them to the performance. Therefore, further research is needed to further improve and develop the current design guidelines.

2.9.1. Current Codes/Guidelines for the Design of Fiber Reinforced Concretes

The European codes and guidelines for the design of FRC structures that are mentioned in this chapter are, according to the chronological order of publication, the DBV [135], the RILEM recommendations [107], the CNR-DT 204/2006 [29], the EHE-08 [136] and the Model Code 2010 [137].

From the previous study by [19] and [138] an interesting comparative analysis of constitutive models for fiber reinforced concrete was advanced. The authors covered the main features of the most relevant works in Europe, namely: German standards [135] the Italian standards [29] and the Spanish standards [136] as well as the guidelines advanced by the RILEM Committee [22]. From that work, the shape and the parameters defining the proposed constitutive laws as well as their respective test methods could be summarized Table 2.1.

Figure 2.14 presents the constitutive models proposed in the previous documents grouped according to the type of diagram (namely rectangular, bilinear and trilinear or multilinear), indicating the parameters that define each one of the models. Likewise, Figure 2.14 also includes the tests required to obtain the values of these parameters. In Table 2.2, the main criteria considered in each of the constitutive models are presented.

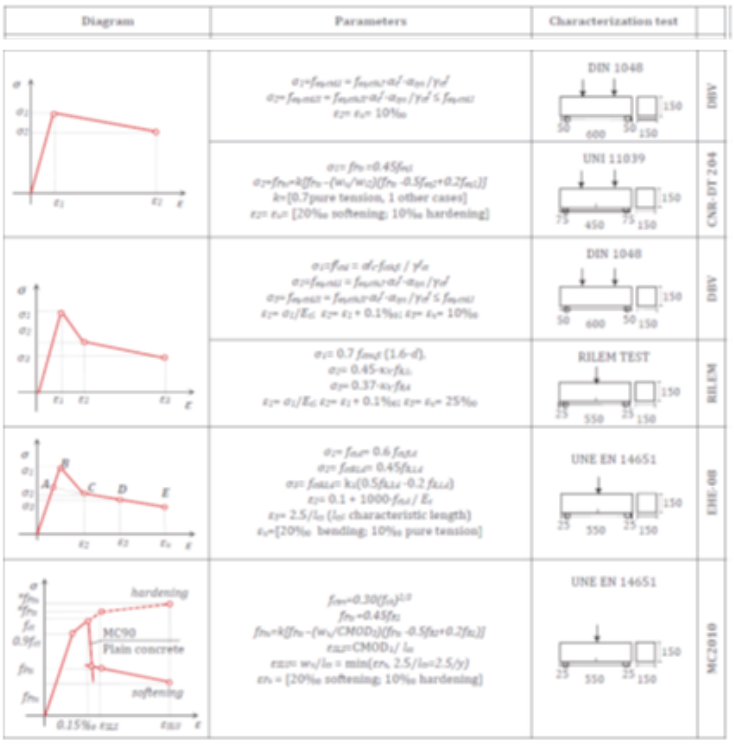

Figure 2.14. Summarized Shape and the Parameters Defining the Proposed Constitutive Laws as Well as their Respective Test Methods (Blanco, PhD Thesis 2013).

Most of them propose stress-strain (σ-ε) curves, even though the CNR-DT 204 [29] and the MC2010 [137] also provide the model in terms of stress-crack width (σ-w). Furthermore, a tendency towards the use of residual flexural strengths (f_R) instead of equivalent flexural strengths (f_{eq}) is observed. Notice that the parameter f_{eq} is related to the energy absorption capacity of the material up to a certain deflection, while the parameter f_R corresponds to the stress associated to the force at a certain deflection.

One of the main differences of the earlier design guidelines (DBV and RILEM)

from the ones published afterwards is that the former only refer to steel fibres whereas the latter distinguish between structural and non-structural fibres. This terminology implies a significant change in the design of FRC since it extends the range of fibres that may be used with structural purposes.

A rather innovative approach is proposed by the MC2010 [137] since it includes an orientation factor in the constitutive model that takes into account favourable or unfavourable orientations.

Table 2.2. Summary of the Characteristics of the Constitutive Models [19].

Assumptions	DBV	RILEM	CNR-DT 204	EHE-08	MC2010
Stress -strain ($\sigma - \varepsilon$) Stress -crack width ($\sigma - w$)	$\sigma - \varepsilon$	$\sigma - \varepsilon$	$\sigma - \varepsilon$ / $\sigma - w$	$\sigma - \varepsilon$	$\sigma - \varepsilon$ / $\sigma - w$
Direct approach (DA)/ Indirect approach (IA)	IA	IA	IA	IA	IA
Continous equation (CE) / Discontinuous equation (DE)	DE	DE	DE	DE	DE
Residual strengths		•		•	•
Equivalent strengths	•		•		
Differentiates the ultimate strain (20 % ; 10%)			•	•	•
Conversion factors regarding the linear-elastic distribution of stresses	•	•		•	
Characteristic length to obtain strain			•	•	•
Safety coefficients	•		•	•	•
Size effect	•	•			
Effect of long-term strength behaviour	•				
Terminology of “structural fiber”			•	•	•
Contribution of fibers in the crack spacing		•	•		•
Effect of fiber orientation					•

It should be noted that all of the standards differ by means of material charac-

terization method they suggest. Some of them suggest using 3 point bending test on notched specimens, while some standards consider 4 point bending tests on unnotched specimens. The standards are also different by means of the methods/equations suggested for structural design. In this study one of the methods suggested in the scope of CNR - DT [29] was adopted for characterization of the material, since material characterization through tests on unnotched beams is recommended in the case of either structural elements in bending less than 150 mm deep or deflection hardening FRCC, which both apply to the present study. Investigation of several design methods for FRC, proposed by different technical committees, indicates that the Italian proposal, CNR-DT [29], is heading in the right direction in several matters. However, Jansson stated that this method, as well as the other investigated methods, is based on rather rough simplifications and is probably better suited for calculations in the ultimate limit state [60].

In the scope of this study, 4 point bending tests on unnothced specimens were employed and constitutive parameters were obtained by using the pathway given in CNR DT. Below related Sections of the CNR DT was given.

The approach of CNR DT for structural design of fiber-reinforced composites was explained here. It should be noted that only a Section of the code was given here (the Section related to the study) for the sake of shortness. This code first defines properties of materials and design basic concepts together with special problems.

Mechanical properties in the hardening state are given under heading 2.5.2 of the CNR DT standard. Tensile behavior of the fiber reinforced concrete matrix is given as follows Figure 2.15:

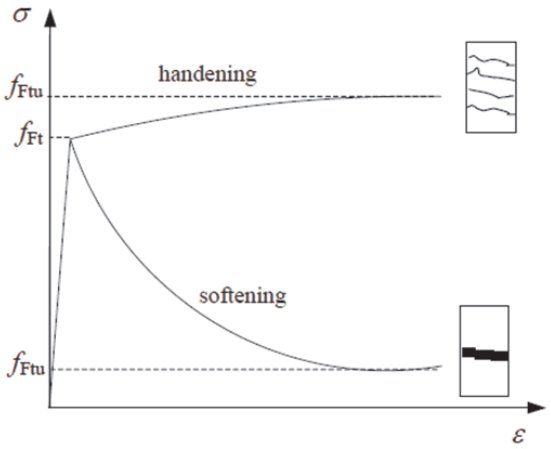

Figure 2.15. Tensile Behaviour of the Fiber Reinforced Concrete Matrix.

Several tatements are made in the code regarding tensile behaviour, some of them are as follows:

- The uniaxial first crack tensile strength of fibre reinforced concrete, f_{Ft}, may be assumed equal to that of the matrix, f_{ct}. For softening behaviour material, the strength, f_{Ft}, may be assumed equal to the maximum stress Figure 2.15.
- The residual uniaxial tensile strength of the material, f_{Ftu} Figure 2.15, is significantly affected by the volume fraction of fibres, V_f, by the aspect ratio, l_f/d_f, as well as the bond between concrete and steel, for both the cases (softening and hardening behaviour).

As a result, the code suggests a performance based approach, able to experimentally identify the constitutive tensile curve by means of appropriate tests and it is mentioned that the nominal stress - crack opening law, σ_N - w, may be determined through uniaxial tension or bending tests.

In this study, bending test is used on un-notched beam specimens since it is suggested for thin walled elements to take into account significant variables such as the casting direction, the mixing technique and the wall effect.

Again based on the code, the post-cracking strength may be defined on the basis

of point values, f_i, corresponding to specified nominal value of crack opening, or on mean values, f_{eqi}, calculated for assigned intervals of crack opening Figure 2.16.

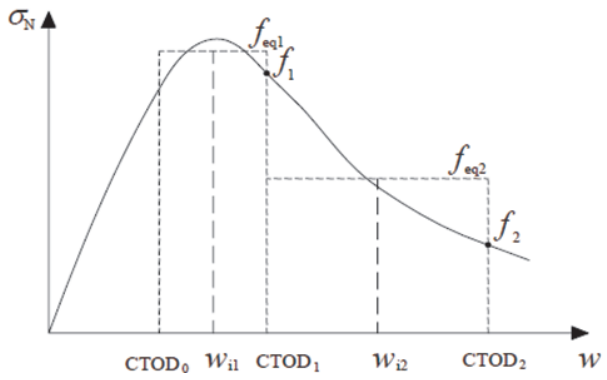

Figure 2.16. Definition of Point and Mean Residual Strength.

Two simplified stress-crack opening constitutive laws may be deduced on the basis of the bending test results: a linear post-cracking behaviour (hardening or softening) or a plastic rigid behaviour, as schematically shown in Figure 2.17.

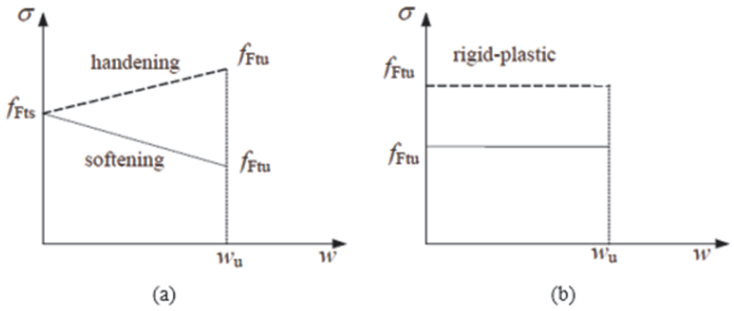

Figure 2.17. Definition of Point and Mean Residual Strength.

The stresses, f_{Fts} and f_{Ftu}, characterizing these two models may be evaluated through the procedure reported in Appendix A (The related Section of the Appendix A will be separately explained).

Following rules are given for stress - strain constitutive law:

- In the case of sections without traditional reinforcement, subjected to bending, combined tensile - flexural and normal compressive - flexural forces with resulting

force external to the section, y = h is assumed);

- When considering a hardening behaviour material, multi-cracking occurs. Thus, a mean strain may be directly obtained from the experimental tests, useful in identifying the constitutive parameters. The ultimate strain value is assumed equal to 1%.

Finally, the tensile stress - strain behaviour may be assumed as shown in Figure 2.18, using the parameters reported in Appendix A.

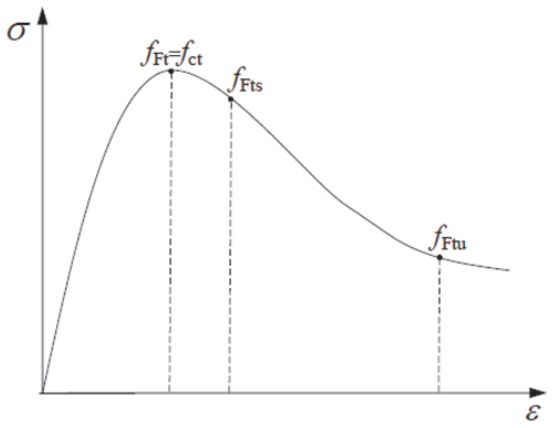

Figure 2.18. Stress-Strain Law.

Simplified models Figure 2.19, corresponding to tension-crack opening laws shown in Figure 2.17, may be used. The first one is based on serviceability and ultimate equivalent residual strengths. The second one, rigid plastic model, is based on an appropriate value of the ultimate residual strength. These laws only concern the residual post-cracking strengths.

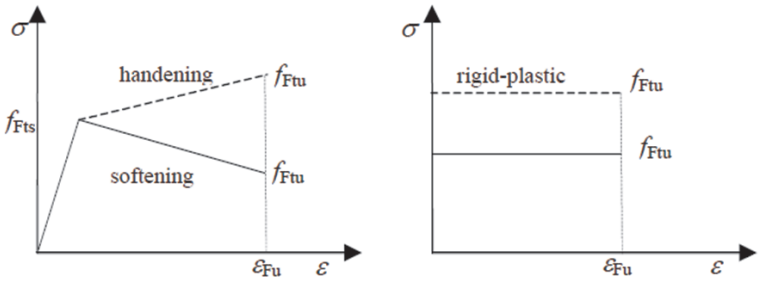

Figure 2.19. Simplified Stress-Strain Constitutive Laws.

In the end a summary of Appendix A of the code should be given to better explain the method used for material characterization and design parameters. Appendix A is on the tensile strength: constitutive parameter identification.

In the 1st Section (9.1 of appendix A of the code) softening behavior (under direct tension) materials subjected to tension identified through bending tests are discussed and following equations are given for f_{Fts} and f_{Ftu} concerning SLS and ULS behavior.

$$f_{Fts} = 0.45 f_{eq1} \tag{2.9}$$

$$f_{Ftu} = k\left[f_{Fts} - \frac{w_u}{w_{i2}}(f_{Fts} - 0.5 f_{eq2} + 0.2 f_{eq1}\right] \geq 0 \tag{2.10}$$

Where, f_{eq1} and f_{eq2} are, respectively, the post-cracking equivalent strength useful for the SLS and ULS (Figure 2.20 (a)); k is a coefficient equal to 0.7 for cross sections fully subjected to tensile stresses and equal to 1 in other cases; w_{i2} is the mean value of the crack opening at the endpoints of the interval where f_{eq2} is evaluated in Figure 2.20.

The last Section that should be given here is the rules defined for unnotched structural specimen (9.1.4 of the code) For structures subjected to bending, having a section depth less than 150 mm, or for hardening bending behaviour, it is better to carry out the identification process of material properties by taking into account the casting direction and the small thickness of the structure without notching the specimens. In this case, the characteristic values of the equivalent strengths, feq1k and feq2k, are evaluated in the intervals $3.w_i$ = w = $5.w_i$ and $0.8.w_u$ = w = $1.2.w_u$, where w_i represents the crack opening corresponding to cracking, calculated where the maximum load is recorded during the test, CNR-DT 204/2006 44 in the interval 0 = w = 0.1 mm. For the ultimate crack opening, w_u, a value equal to 3 mm is assumed. By using the symbology of the standard UNI 11188, it is assumed:

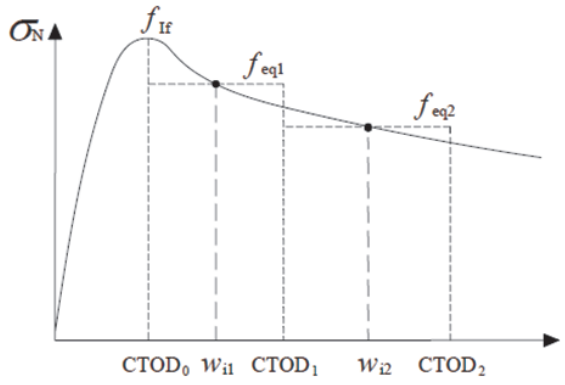

(a)

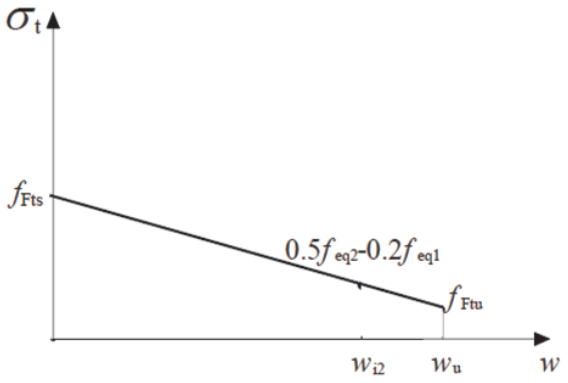

(b)

Figure 2.20. Tensile Strength Determined Through bending test on Softening Materials.

$$f_{eq1k} = f_{1tFk} \tag{2.11}$$

$$f_{eq2k} = f_{Ftfk} \tag{2.12}$$

These equivalent strengths correspond, respectively, to crack opening equal to $w_{i1} = 4.w_i$ and $w_{i2} = w_u$. The value of the tensile strength, f_{Ft} Figure 2.18, may be

calculated based on the first cracking one, f_{ctf}, deduced from the experimental test:

$$f_{Ft} = \frac{f_{ct,\exp}}{\beta(h)} \tag{2.13}$$

$$\beta(h) = \frac{25 + 2.h^{0.7}}{2.h^{0.7}}\,(mm) \tag{2.14}$$

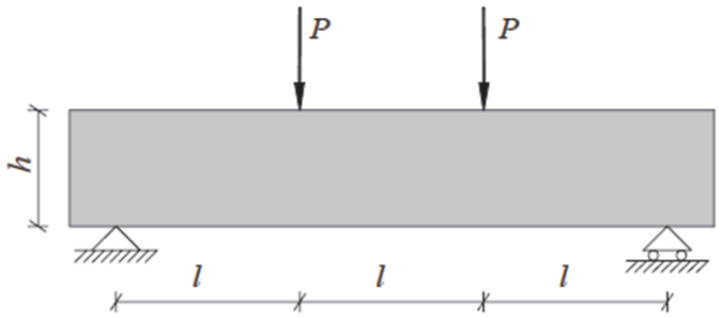

Figure 2.21. Four-Point Bending on Unnotched Specimen.

3. EXPERIMENTAL STUDIES

This chapter provides the results obtained from experimental studies. Experimental studies were carried out for measurement of hardened state performance of SFRC specimens by conducting flexural tests, analyzing of strain localizations and crack propagations using both traditional measurement methods and PIV method, which measures surface displacements and strains using digital image analysis.

For the preliminary experimental program, characterization tests were conducted. This is a four-point bending test for flexural behavior characterization. In addition to the flexural test, crack propagations and fiber orientations of the specimens were also examined in detail with the help of PIV and image analysis results from the monitored high resolution images throughout the experiments.

3.1. Materials and Mix Design

3.1.1. Materials

The mixture used in this study is adapted from previous studies of Şanal and Özyurt [101]. In previous study of Özyurt *et al.*, [99], mix design for a fiber-reinforced cement-based material was optimized for thin section precast elements. Different self-consolidating fiber-reinforced mixes were experimentally examined and mixes which showed the best performance was chosen in that study.

First of all, several trial batches were prepared with the plain mixture and the exact mixture proportions were defined by measuring slump flow diameters. According to these results, trial batches for steel fiber-reinforced mixtures were done by decreasing aggregate (sand) amount gradually. Then, this procedure continued until same mini slump flow diameters were obtained. As a result, both the plain mix and fiber-reinforced mix designs were adjusted in order to keep the same mini slump flow diameter (between 310 mm and 325 mm).

The mix proportions of the SCC used for control mixes without fibers were as follows. Cement: Sand: Slag: Water: Plasticizer: 498 : 1150 : 418 : 220 : 18 kg/m^3. The mix proportions of the SCC used for both straight and hooked end steel fiber-reinforced mixes were as follows. Cement: Sand: Slag: Water: Plasticizer: Fiber: 497 : 1114 : 418 : 220 : 18 : 94.8 kg/m^3.

The mortar mixes were manufactured using a water-cement ratio of 0.44 (w/c=0.44) by weight, water-binder ratio of 0.24 (w/b=0.24) and dosage of superplasticizer was kept 1.7 % for all the mixes.

Three different types of steel fibers were used. Properties of the materials used are given below.

3.1.1.1. Cement. The cement used for concrete specimens was CEM I 42.5 R, which was produced by Akçansa Cement Company. Physical, mechanical and chemical properties of this cement are as follows.

Table 3.1. Physical Properties of Cement.

Physical Properties		
Density	(g/m^3)	3.14
Initial Setting Time	(min.)	139
Final Setting Time	(min.)	194
Le Chatelier	(min.)	0
Specific Surface	(cm^2/g)	3870
Residue on 45μm sieve	(%)	5.9
Residue on 90μm sieve	(%)	0.4

Table 3.2. Mechanical Properties of Cement.

Mechanical Properties		
Mechanical Properties/day	Standards	Test Results
Early Strength 2 day	= 20 MPa	30.5
Early Strength 7 day	-	46.0
Standard Strength 28 day	= 42.5 MPa	59.3
	= 62.5 MPa	

Table 3.3. Chemical Properties of Cement.

Chemical Properties		
SiO2	(%)	19.67
Insoluble Residue	(%)	0.3
Al2O3	(%)	4.45
Fe2O3	(%)	3.43
CaO	(%)	64.31
MgO	(%)	1.12
SO3	(%)	2.99
Loss on Ignition	(%)	2.24
Cl	(%)	0.0412
Na2O/K2O	(%)	0.21-0.76
N/A	(%)	0.78
S.CaO-Free Lime	(%)	1.15
	C3S	64.24
	C2S	8.02
	C3A	6
	C4AF	10.44
LSF		0.99

3.1.1.2. Slag. Chemical and physical properties of the slag used for concrete specimens is as following.

Table 3.4. Chemical Properties of Slag.

Chemical Properties	
CaCO3+MgCO3	-
H2O	0.1
Insoluble	-
SiO2	45.12
Al2O3	10.63
Fe2O3	1.12
CaO	35.12
MgO	6.24
S	0.3
Na2O	0.2
K2O	1.23
Cl	0.0185
Loss on Ignition	0
Total	99.98

Table 3.5. Physical Properties of Slag.

Physical Properties		
Density	(g/m^3)	2.92
Specific Surface	(cm^2/g)	4240
Residue on 45μm sieve	(%)	1
Residue on 90μm sieve	(%)	0
Residue on 200μm sieve	(%)	0
Activity Test Value	(N/mm^2)	12.4

3.1.1.3. Sand. Density of the sand used for concrete mixtures was 2.65 g/cm^3 and grain diameter size less than or equal to 1mm Figure 3.1.

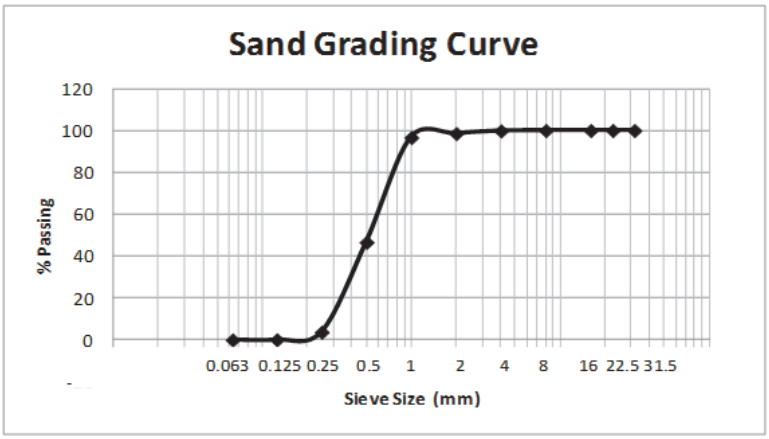

Figure 3.1. Grading Curve of the Sand.

3.1.1.4. Straight Steel Fibers. Density of steel fibers used for concrete mixtures was 7.8 kg/m^3. Two different lengths of these steel fibers were used (6mm and 13mm) and properties of them were given in Table 3.6.

Table 3.6. Properties of Straight Steel Fibers.

	Straight 6	Straight 13
Length	6 mm	13 mm
Diameter	0.16 mm	0.16 mm
Aspect Ratio	37.5	81.3
Tensile Strength	1100 MPa	1100 MPa

3.1.1.5. Hooked End Steel Fibers. : Density of hooked end steel fibers used for concrete mixtures was 7.8 kg/m^3. Two different lengths of these steel fibers were used (35mm and 50mm). Properties of hooked end steel fibers can be seen in Table 3.7.

Table 3.7. Properties of Hooked End Steel Fibers.

	Hooked 35	Hooked 50
Length	35 mm	50 mm
Diameter	0.7 mm	1 mm
Aspect Ratio	50	50
Tensile Strength	1400 MPa	1400 MPa

3.1.1.6. Superplasticizer. Superplasticizer, having 1.075 kg/m^3 density, was used 1.7 % in the concrete mixtures. It is a super-plasticising admixture which is based on chains of modified polycarboxylate ether. It provides flowable concrete with the lowest water/cement ratio without segregation or bleeding.

3.1.2. Mixing Process

For each concrete mix, firstly dry ingredients (sand, cement and slag) were mixed for 1 minute. Then, water and superplasticizer were added during a period of 1 minute and the mixture is mixed for 3 minutes. Finally, fibers were added and mixing process continued for 3 more minutes. This procedure was used for all the mixes in order to have homogenous mixes and decrease the risk of possible inequality between them.

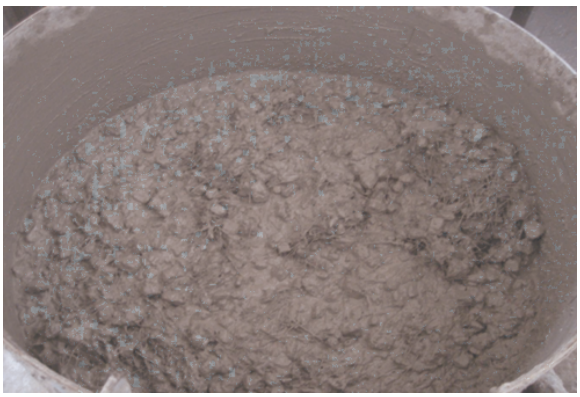

Figure 3.2. Fiber-Reinforced Concrete Mixture.

The mixing process time was about 8 minutes in order to have a uniform composite. Figure 3.2 shows one of the concrete mix obtained.

3.2. Specimens

3.2.1. Formwork Dimensions

First of all, different sizes of moulds have been prepared, in order to obtain various flow behaviors under different constraints. Moulds were designed to have same length (400 mm), but different widths and heights according to the ratio between the smallest specimen dimension and fiber length. Based on this, 15 series, each having 3 control (without fibers) and 3 fiber- reinforced specimens were cast and 90 specimens were obtained in total.

In a previous study [101], it was observed that the ratio of minimum specimen dimension (thickness) to the fiber length (t/f_L) has a significant effect on the resulting flexural behavior of FRC specimens. When this effect was examined further from the load-displacement curves, it was found that when t/f_L ratio was 2, flexural behavior was more likely to be deflection-hardening, when this ratio was 4, flexural behavior was observed to become more deflection-softening and when this ratio was approximately 8, deflection-softening behavior was clearly observed.

It was concluded that there may be a transition from deflection-softening to deflection-hardening behavior in between the 8 and 2 values of t/f_L ratio, so this range should be examined in more detail. Therefore, in this study t/f_L ratios were varied from 2 to 8, and specimen dimensions were chosen accordingly.

Table 3.8. Specimen Dimensions and Related Parameters.

Series No	Number of Specimen		Dimensions			Thickness/ Fiber length	Width/ Fiber length	Fiber Length	Aspect Ratio
	Control	Fib.Reinf	t	w	L	t/f_L	w/f_L	f_L	f_L/d
1	3	3	26	100	400	2	8	13	81.3
2	3	3	26	39	400	2	3	13	81.3
3	3	3	70	100	400	2	3	35	50
4	3	3	100	100	400	2	2	50 (HE)	50
5	3	3	100	150	400	2	3	50 (HE)	50
6	3	3	18	100	400	3	17	6	37.5
7	3	3	39	100	400	3	8	13	81.3
8	3	3	39	39	400	3	3	13	81.3
9	3	3	100	100	400	3	3	35 (HE)	50
10	3	3	24	100	400	4	17	6	37.5
11	3	3	52	100	400	4	8	13	81.3
12	3	3	30	100	400	5	17	6	37.5
13	3	3	65	100	400	5	8	13	81.3
14	3	3	48	100	400	8	17	6	37.5
15	3	3	100	100	400	8	8	13	81.3

Specimens were cast to Specimens were cast to obtain a wide range of t/f_L ratios (between 2 and 8) and different types of fibers were used to examine the effect of different fibers. It was aimed to observe a limit t/f_L value below which, materials show deflection hardening behavior and above which, materials show deflection softening behavior. In the scope of this study, third-point bending experiments were recorded by using a high-resolution camera to examine crack patterns and material behavior with changing t/f_L ratios. obtain a wide range of t/f_L ratios (between 2 and 8) and different types of fibers were used to examine the effect of different fibers. It was aimed to observe a limit t/f_L value below which, materials show deflection hardening behavior and above which, materials show deflection softening behavior. In the scope of this study, third-point bending experiments were recorded by using a high-resolution camera to examine crack patterns and material behavior with changing t/f_L ratios.

3.2.2. Specimen Numbering

The specimens were named according to their thickness, width and fiber lengths. (i.e: S 26/100/13, S representing “Specimen”, the number on the left hand side implying the specimen thickness, the number in the middle implying the width and the number on the right hand side showing the fiber length). Specimens were demoulded the day after casting and cured for 90 days, to see the effect of high amount of slag

used in the mixture.

3.2.3. Curing Process

The specimens were left in molds for 24 hours at a temperature of 20 °C ± 5 °C. Specimens were then de-molded after 24 hours, moved to a water curing tank after de-molding and stored in curing room in water tanks at a temperature of 20 °C ± 2 °C and a relative humidity = 95 % throughout the curing period for 90-days according to the standards [139]. Figure 3.3 shows the specimens in water tank.

Figure 3.3. Curing of the Specimens in Water Tank.

3.2.4. Defined Parameters

Four main parameters, which were pre-defined to be "flow thickness/fiber length" (t/f_L), "flow width/fiber length" (w/f_L), "Fiber Length" (f_L) and "Fiber Type" (fib) varied for different specimens as is seen in Table 3.9. For instance, performances of the mixes 18*100*6, 24*100*6, 30*100*6 and 48*100*6 will be compared by means of varying t/f_L.

Table 3.9. Parameters to be Examined and Compared for Specimens.

Specimen Number	Thickness t/f_L	Width w/f_L	Fiber Length fL	Fiber Type fib
26*100*13 26*39*13	-	Compare	-	-
26*39*13 70*100*35	-	-	Compare	Compare
26*39*13 70*100*35	-	-	Compare	Compare
39*100*13 39*39*13	-	Compare	-	-
39*39*13 100*100*35	-	-	Compare	Compare
26*39*13 39*39*13	Compare	-	-	-
70*100*35 100*100*35	Compare	-	-	-
18*100*6 24*100*6 30*100*6 48*100*6	Compare	-	-	-
26*100*13 39*100*13 52*100*13 64*100*13 100*100*13	Compare	-	-	-

3.3. Measuring Fresh State Performance

3.3.1. Particle Image Velocimetry (PIV)

PIV technique was originally implemented using double-flash photography of a seeded flow and the resulting photographs were divided into a grid of test patches. For PIV analysis, the displacement vector of each patch during the interval between the flashes is found by locating the peak of the auto correlation function of each patch. The peak in the auto correlation function indicates that the two images of each seeding particle overlying each other, so the correlation offset is equal to the displacement vector [85]. A modified approach was used to implement PIV in geotechnical testing by White *et al.*, According to their investigations, the modified PIV technique offers an order-of-magnitude increase in accuracy, precision, and measurement array size compared with previous image-based methods of displacement measurement. [85].

As detailed discussion on PIV technique is beyond the scope of the current study, further details on the PIV technique can be found in the studies of White and Take [33], and White *et al.*, [85]; besides, necessary discussions on the technique are provided in the following sections.

Fresh state performance of the material was evaluated by using mini slump flow and mold flow tests. The flowability and fiber aligning ability as well as dynamic segregation resistance of the material were evaluated by using the data obtained during

measurements. Details are given below.

3.3.2. Mini Slump Flow Test

The mini-slump test is the most common method for quality control in characterizing fresh state performance of pastes and mortars. It measures the consistency of mortar, and its results can be correlated with the yield stress [140-142]. The mini-slump cone, used for the experiments, had a top diameter of 70 mm, a bottom diameter of 100 mm, and a height of 60 mm. The cone is placed in the center of a square piece of glass and filled with mortar. The cone is then lifted up to allow the mortar to flow. After removing the filled truncated mini-cone Figure 3.4, the material flows until reaching a steady state. The resulting final spread diameter, D_f, of the fresh mortar sample is the average value of two measurements (D_1 and D_2) obtained in the two perpendicular directions.

3.3.2.1. Image monitoring for mini-slump flow. Successive digital images at regular time intervals (2 images per second) were taken during the mini slump flow test to evaluate flow behavior of materials using PIV. As shown in Figure 3.4a, mini-slump cone was located on the slump plate, and fresh mortar was poured into the cone.

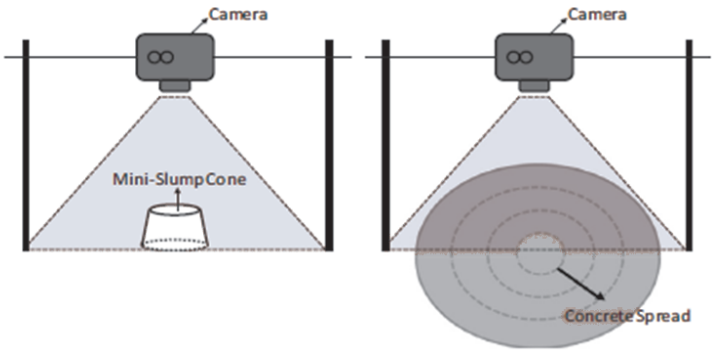

Figure 3.4. Schematic View of the Digital Camera Location and Mini-Slump Test Setup.

The digital camera was placed right above the plate at a distance equal to 500 mm

and the top surface of mortar was leveled. After that, when the slump cone was lifted up, fresh mortar started to flow, and its diameter increased accordingly (Figure 3.4b). In the meanwhile images were automatically taken by using the camera throughout the test. Afterwards, final spread diameters were measured and image recordings were saved to be analyzed by using PIV. Finally, strain field distributions and velocity time graphs were obtained for all mixtures.

3.3.2.2. Dynamic segregation resistance evaluation by using mini-slump flow. Dynamic segregation resistance refers to the ability of mortar matrix to drive fibers during flow. This is important by means of the homogeneity of the cast material. Dynamic segregation resistance of the mortar mixes were studied by using a conventional method (fiber volume measurement at defined regions) and PIV.

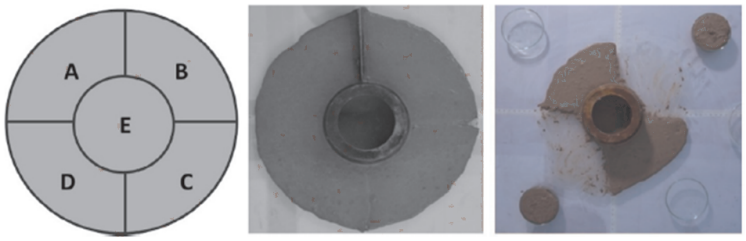

Figure 3.5. Divided Regions of Mini-slump Flow Putty for Fiber Counting.

For measuring material's ability to drive fibers, first mini slump flow test was carried out and fiber volumes in different Sections of the mini-slump flow putty was measured. This was done by dividing the fresh mortar putty into 5 regions, as is seen in Figure 3.5. Then the fresh mortar materials in these volumes were washed and fibers were taken out by a magnet and weighed. The results obtained from fiber weighing tests were evaluated accordingly and compared with the PIV strain field distributions obtained from camera images.

3.3.3. Monitoring of Material Flow by Using PIV

The most important advantages of adopting fibers within SC - FRCC are the improvements of tensile strength and toughness. However, these properties are strongly

influenced by fiber alignment along the direction of tensile loading [100 - 142, 143]. Therefore, the ability of material to align fibers along the direction of flow becomes very important. Previous research show that fibers have a tendency to align in the direction of flow when self-compacting composites are used [17 - 144, 145]. Results of fiber alignment analyses carried out by the authors represent that if a controlled casting procedure is applied (material is cast from the one end of the mold and let the flow to the other end of the member), fiber alignment densities may go up to 0,7 in the direction of flow [101].

Conventionally, time consuming methods (i.e. image analyses) are used to understand the tendency of fiber alignment in the material.

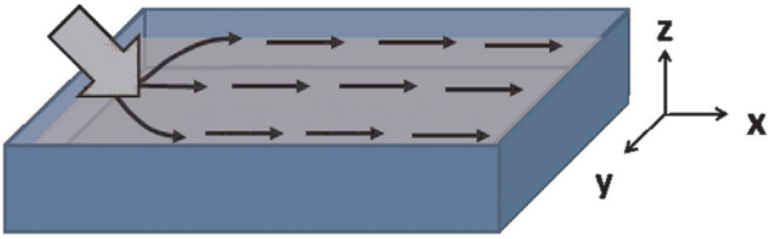

Figure 3.6. Casting Flow Behavior and Alignment of Fibers in the Flow Direction.

In this study, PIV was used (together with image analyses) to roughly evaluate fiber alignment ability of the material by the help of vector field deviation. For this purpose the general procedure used to cast SC-FRCCs in this study was employed. The material was put from one end of the mold and let to flow to the other end (Figure 3.6). Images of flow of a certain material volume were obtained and analyzed by using PIV.

3.4. Measuring Hardened State Performance

3.4.1. Flexural Tests

The beam specimens were tested in four-point bending, according to the test set-up shown in Figure 3.7 by using an MTS Closed-Loop Displacement Controlled Servo Hydraulic Testing Machine with 100 kN capacity. Four Linear Variable Displacement

Transducers (LVDTs) were mounted vertically under the specimen to measure the average deflection and two LVDT's were mounted horizontally just on the opposite sides of loading region of the specimen to measure average crack mouth opening displacement. These LVDTs also provided feedback to the servo-valve for closed-loop control in the test.

For crack monitoring, a camera was placed perpendicular to the beam face at a distance equal to 28 cm. In order to eliminate any probable parasitic lights, the specimen was illuminated using a white light projector. Digital images were taken using a remote control at regular intervals (15 sec.) to follow crack development on the specimens. Test setup and the camera view are shown in Figure 3.7.

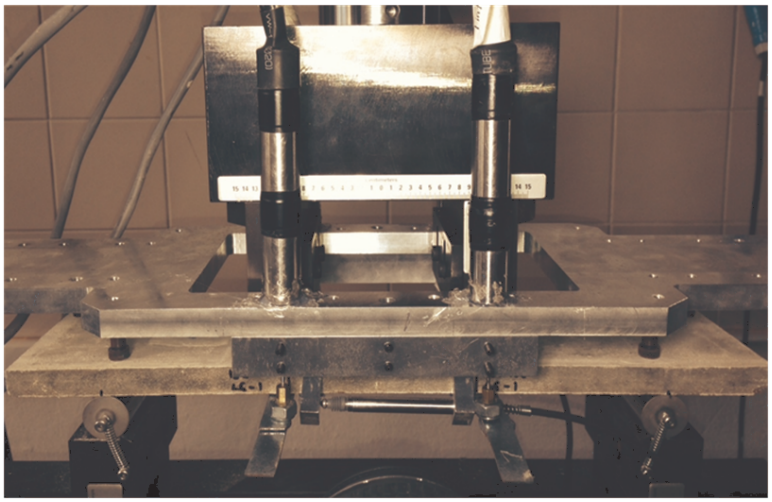

Figure 3.7. View of the Flexural Test Setup.

Span length (L) was 300 mm and gap between the loading heads was 100 mm. Geometry of a 50 mm thick specimen, support and loading position is shown representatively in Figure 3.8.

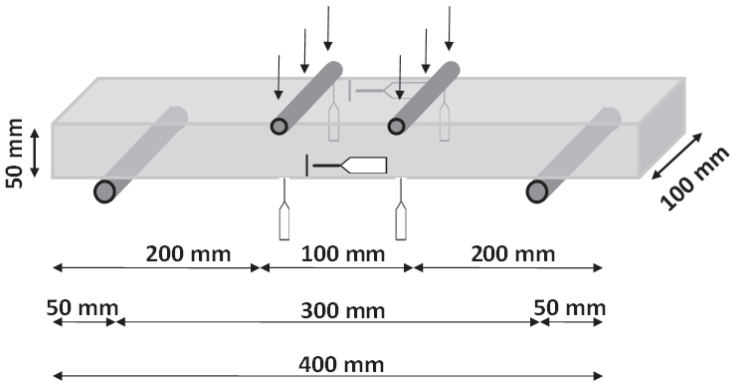

Figure 3.8. Schematic View of the Flexural Test, Support and Loading Positions.

Loading was performed controlling the average LVDT measurement for crack mouth opening, which was applied at a rate of 0.01 mm/min. Testing continued until approximately 3.5 mm crack mouth opening displacement was reached.

3.4.2. Flexural Strength and Strain Calculations

Calculation of the flexural strength σ_f is done by using the following equation:

$$\sigma_f = \frac{3PL}{4bd^2} \tag{3.1}$$

In this equation; σ_f, flexural strength (MPa), P, load at a given point on the load deflection curve (N), L, support span (mm), b, beam width (mm), d, beam depth (mm). Calculation of the flexural strain ε_f is done by using the following equation:

$$\varepsilon_f = \frac{12dD}{3L^2 - 4a^2} \tag{3.2}$$

In this equation; ε_f, flexural strain (mm/mm), d, beam depth (mm), D, maximum deflection of the center of the beam, (mm), L, support span (mm), a, span length between two loading heads (mm).

3.4.3. Flexural Toughness Calculations

Fibers are added to concrete not to solely improve the strength, but primarily to improve the toughness, or energy absorption capacity, since specimen toughness is an important parameter for determining mechanical performance of the specimens. Toughness of FRC can be termed as the energy absorption capacity, which is conventionally characterized by the area under the load-deflection curve. Alternatively, the toughness may be defined as the area under the load-deflection curve out to some particular deflection, or out to the point at which the load has fallen back to some fixed percentage of the peak load.

Although toughness tests can be carried out under different loading conditions like tensile, compressive, and torsional loading, most of the toughness measurements are performed on beams in flexure using four point bending arrangement.

In order to obtain the complete load-deflection curves, the testing system must be equipped with strain or deflection measurement gauges. Obtaining a reliable curve in the post crack zone is very important, thus a closed loop servo controlled rigid testing machine should be used.

There are, however, a number of uncertainties regarding how FRC flexural toughness should be measured, interpreted, or used. Various flexural toughness test methods have been developed in different countries. ASTM-C1018, JSCE-SF4, and NBP No. 7 are three of the most commonly used test methods.

An advantageous approach for quantification of load-deflection curves is using a unitless value termed as the toughness index. The practical application of this approach began with the introduction of ACI 544 toughness index, which is defined as the ratio of the amount of energy required to deflect a FRC beam by a prescribed amount to the energy required to bring the beam to the point of first crack. Similar notions were used in the development of the ASTM C 1018 standard [ASTM C1018].

These test methods give relative toughness values. On the other hand another commonly used method was developed by Japan Society of Civil Engineers, which yields absolute toughness [JSCE SF-4]. The toughness factor suggested in JSCE SF-4 standard is an indicator of the average flexural strength. All these test methods are based on evaluation of the recorded load versus mid-span deflection curve for a four point bending test.

Identifying the correct occurrence location of the first crack, which is crucial and one of the main problems with the ASTM method, is not a concern with the JSCE method. Unlike the ASTM method, the instability in the load-deflection plot right after the first crack is not of major concern in the JSCE method, since the end point deflection of span/150 is too far out in the curve to be affected by the instability in the initial portion.

Therefore, considering the reliability and efficiency of various toughness parameters, JSCE SF-4 method was used for toughness calculations in this study.

The JSCE SF-4 equation used for flexural toughness calculations is as following:

$$FT = \frac{A_{(L/150)}.L}{(L/150)bh^2} \tag{3.3}$$

where, FT is the flexural toughness (MPa), A is the area under Load-Deflection curve (N.mm), L is the distance between supports (mm), b is the width of the beams (mm) and h is the thickness of the beams (mm).

3.4.4. Crack Monitoring

It is well established that one of the important properties of steel fibre reinforced concrete (SFRC) is its superior resistance to cracking and crack propagation. As a result of this ability to arrest cracks, fibre composites possess increased extensibility and tensile strength, both at first crack and at ultimate, particularly under flexural loading; and the fibres are able to hold the matrix together even after extensive cracking. In

order to understand the effectiveness of fibers on bridging cracks, several evaluations were done both using conventional experimental methods and also PIV analyses. Crack evolution along beam depth, relationship between mechanical performance and crack length, width and area, relation between number of cracks (single-multiple) and mechanical performance were observed and crack propagation images at different stages of loading were presented.

Images were captured during four-point flexural tests to evaluate deformations in beams by using PIV method. The test setup for PIV measurements comprised a high-resolution digital camera, i.e. Nikon 8400 EC (24MP), which was applied with the image resolution of 6,016 x 4,000 pixels. The specimen was illuminated using white LED light to provide uniform light intensity across the surface and to eliminate any probable parasitic lights. The camera was placed perpendicular to the specimen surface at a distance equal to 38 cm. Test setup including specimen, camera and projector positions and the testing machine is presented in Figure 3.9.

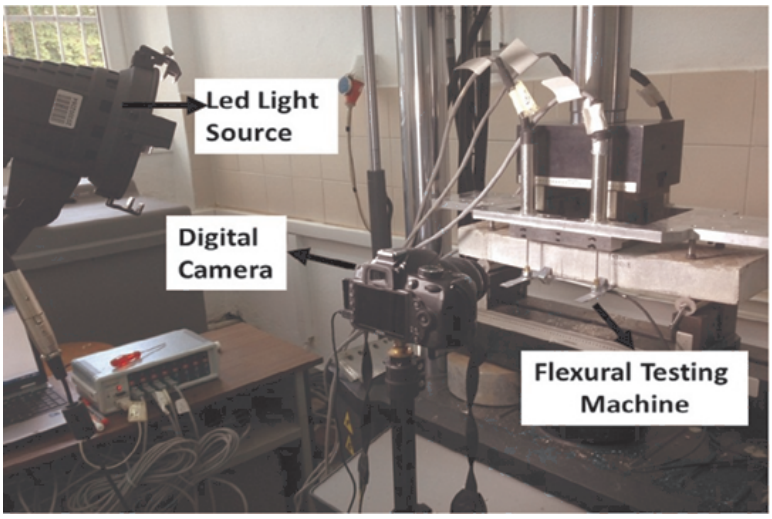

Figure 3.9. Test Setup Including Specimen, Camera and Projector Positions.

Successive digital images were taken from each specimen undergoing deformation during test process. The field of view captured in the digital image was approximately equal to 100 mm x 100 mm. First, a reference image was recorded prior to loading. Then, images were automatically captured, at regular intervals of 15 seconds, throughout the tests. Images were then analyzed using GeoPIV8 software [146]. The

correlation between the deformed images and the unreformed reference image was used to obtain a two-dimensional displacement field on the specimen surface, Figure 3.10.

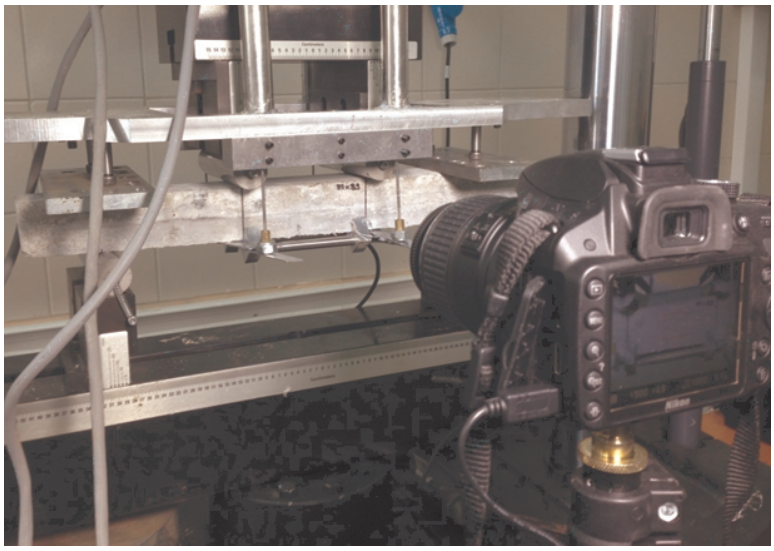

Figure 3.10. View of Crack Monitoring Camera.

The progressive opening of the cracks is studied using PIV, and continuous strain fields during cracking are provided. In addition, PIV technique was used to monitor the cross-sectional flexural strain distributions at midspan. Consequently, the results obtained by conventional methods were compared with the results obtained from PIV analyses.

3.4.5. Fiber Orientations

To quantify the orientation of fibers a tensor description method, which is widely used in the fiber-reinforced polymer composite industry was used. Application of this method to the fiber-reinforced cement-based materials was done by Özyurt *et al.*, [37]. Details of the procedure applied could be found elsewhere [134].

In this study data from two-dimensional cross sections were used for orientation analyses and Image Analysis technique was used for analyzing fiber dispersion and a tensor description method was employed for fiber orientation density calculations in the specimens. A short introduction to the method is given below.

The orientation state of a single fiber can be defined using in-plane (φ) and out of plane angles (θ), as seen in Figure 3.11 and represented by Equation 3.4.

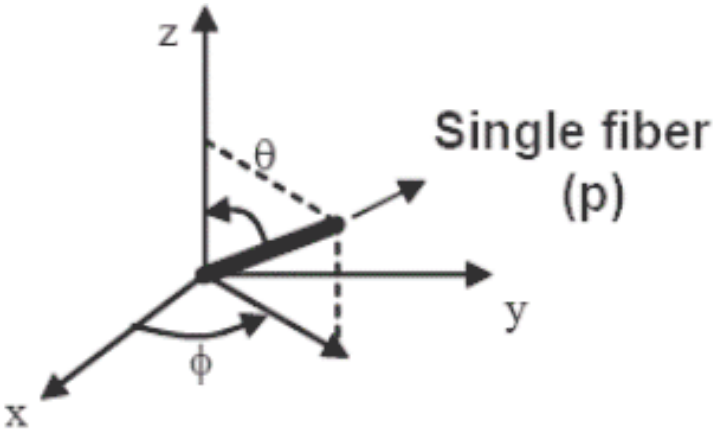

Figure 3.11. Orientation State of a Single Fiber.

$$a_{ij} = \frac{\sum (p_i p_j)_n F_n}{\sum F_n} = \begin{pmatrix} a_{xx} & a_{xy} & a_{xz} \\ a_{yx} & a_{yy} & a_{yz} \\ a_{zx} & a_{zy} & a_{zz} \end{pmatrix} \text{i, j} = \text{x, y, z} \tag{3.4}$$

In Equation 3.4, a_{ij} stands for the components of the orientation tensor; px, py, and pz and give the orientation state of a single fiber in reference directions and are calculated as follows.

$$p_x = Sin\theta Cos\phi, p_y = Sin\theta Sin\phi, p_z = Cos\theta \tag{3.5}$$

In-plane (φ) and out-of-plane (θ) angles for every fiber were measured using an image analysis program. F_n in Equation 3.4 gives the weighing function which is used to account for the effect of fiber orientation on the probability of a fiber being intercepted by the cross section under consideration. The probability of intercepting a fiber that is aligned vertical to the cutting plane is much higher compared to a fiber aligned parallel

to the section. F_n is calculated by using Equation 3.6.

$$F_n = \frac{1}{LCos\theta} \text{for} \theta < \theta_c, F_n = \frac{L}{d} \text{for} \theta > \theta_c \text{and} \theta_c = \arccos\left(\frac{d}{L}\right) \tag{3.6}$$

In this study, the orientation densities in the reference directions were needed. Therefore, only the main diagonal components of the tensor were calculated to obtain the alignments in the X, Y and Z directions, respectively.

4. RESULTS AND DISCUSSIONS- Section I

4.1. Fresh State Performance

4.1.1. Mini-Slump Flow

Conventional measurement of mini-slump flow gives only final spread diameter of the material and final spread diameters alone do not give adequate information to distinguish between different materials. For instance, 3 different materials were compared in the scope of this study (plain, 6 mm fiber-reinforced and 13 mm fiber-reinforced) and final spread diameters of 34.1, 30.5 and 27.8 mm were measured, respectively. This data gives limited information about the fresh state behavior of material. Extra information such as i) evolution of slump flow, ii) velocity-time diagrams, iii) displacement vectors and strain fields of the flow can be retrieved if mini-slump flow tests are recorded and captured images are analyzed by using PIV, giving quite a bit of information for a detailed understanding of the flow behaviors of different materials. These data is especially important when fiber-reinforced mixes are under consideration, since most of the time the rheometers designed for cement paste and mortars are not suitable to be used for fiber-reinforced mixes, since sharp steel fibers damage the instrument container and results in inaccurate data.

More data can be retrieved from mini-slump test if the test is recorded as mentioned above. Several researchers [140, 142] related final spread diameter to yield stress, stating that a higher final spread diameter means lower yield stress. Tregger *et al.*, [142] used camera recordings to obtain spread evolution with time and employed that data to measure the time it takes to reach any particular diameter [140]. They also suggested a procedure similar to the T50 time which is normally used to predict viscosity of self-compacting concretes. T50 time is calculated by using a regular slump cone. When cement paste or mortar is used instead of concrete, mini-slump test is carried out instead of regular slump test and as a result a smaller volume of material is needed. Therefore, they selected 30 cm diameter instead of 50 cm and found the time

needed for the material to reach a spread diameter of 30 cm. An increase in time to reach a selected diameter represents higher viscosity [140]. In the meanwhile, higher viscosity mixes will encounter more resistance during the flow resulting in lower final spread diameter [140].

4.1.1.1. Evolution of slump flow. Mini slump flow diameters were recorded from the captured images, for different time intervals, as can be seen in Figure 4.1. Mini-slump flow diameter over time was plotted, in order to make a comparison between the flowing behaviors of different mortars (plain, 6mm fiber-reinforced and 13mm fiber-reinforced). One of the advantages of plotting spread evolution of different mixes over time is the ability to figure out the time it takes for each mix to reach a selected spread diameter as mentioned above.

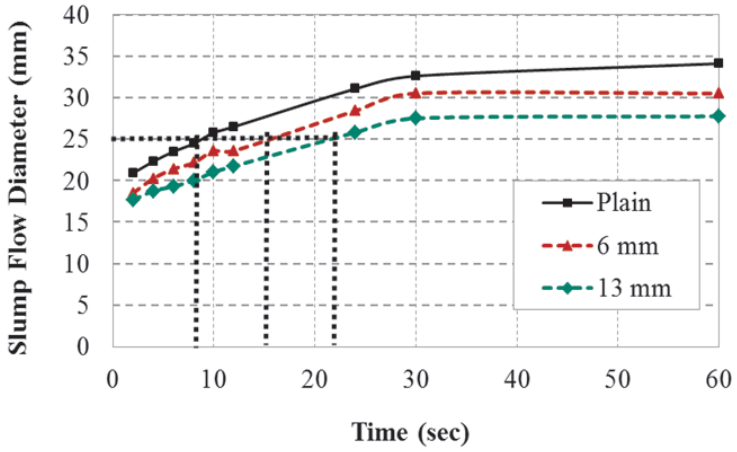

Figure 4.1. Change in Mini-Slump Flow Diameter in Time.

In the current study, final spread diameters for plain, 6mm fiber-reinforced and 13mm fiber-reinforced mixes were found to be 34.1, 30.5 and 27.8 mm (obtained from captured images). A higher final spread diameter means lower yield stress as mentioned above [140, 146]. From this result it can be concluded that plain mix has a lower yield stress when compared to fiber-reinforced mixes as expected. 6mm fiber-reinforced and 13mm fiber-reinforced mixes gave lower final spread diameters probably due to entanglement of fibers.

In the current study, the times required for the mixes to reach a diameter of 25cm are found as suggested by [140]. As is seen in Figure 6, it took 8, 15 and 22 seconds to reach a spread diameter of 25 cm for the plain, 6 mm fiber-reinforced and 13mm fiber reinforced mixes, respectively. These numbers represent that plain mix has lower viscosity when compared to fiber-reinforced mixes as expected. This is also supported by the higher final spread diameter of plain mix since lower viscosity mix will encounter less resistance during flow which will result in higher final spread diameter.

4.1.1.2. Velocity - time diagrams from PIV analyses. Velocity vs. time relation is given in Figure 4.2 for plain, 6 mm fiber-reinforced and 13mm fiber-reinforced mixes, respectively.

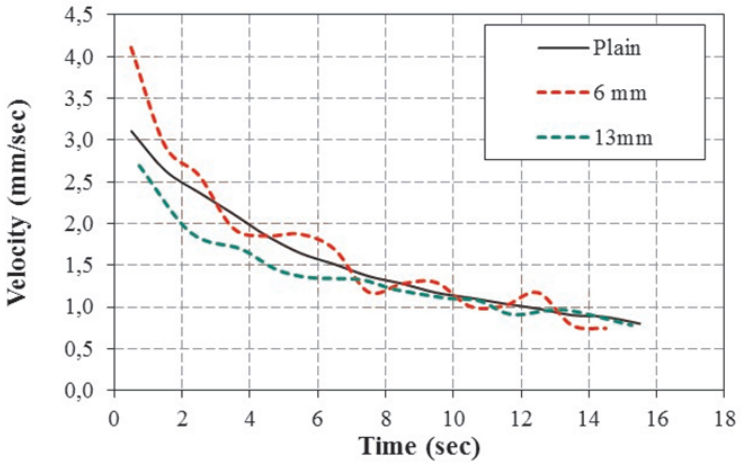

Figure 4.2. Velocity vs. Time Relation of the Mixes.

As is seen from the Figure 4.2 fiber-reinforced mixes represent oscillating velocity curves during the flow whereas plain mix shows a smooth decreasing curve. This represents the resistance of fibers to flow and it is higher when fiber length is increased. Velocities of the mixes are different in the beginning of flow, however after about 8 seconds all the mixes show similar velocities. Initial velocity of 6mm fiber-reinforced mix is higher when compared to plain mix. The possible reason of this behavior will be explained in the next section.

4.1.1.3. Displacement vectors and strain fields. : An informative data which can be obtained from PIV is displacement vectors and strain fields. As is seen from Figure 4.3 suitable meshes were generated on the images of mini-slump and the displacement vector of each patch was calculated for the specified interval (2 images per second) between the captured images.

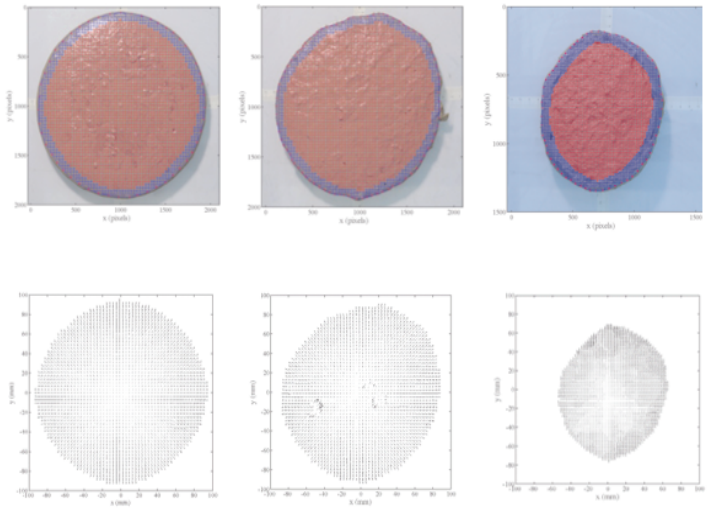

Figure 4.3. Mesh Generation Using 128 x 128 Pixel Patches Spaced at 32 Pixels Center-to-Center (Reference Image at t=0 s) and Displacement Vectors Corresponding to t=1 s.

Then, strain distributions throughout the mini-slump flow were obtained and given for the 1st, 4th and 10th seconds (Figure 4.4).

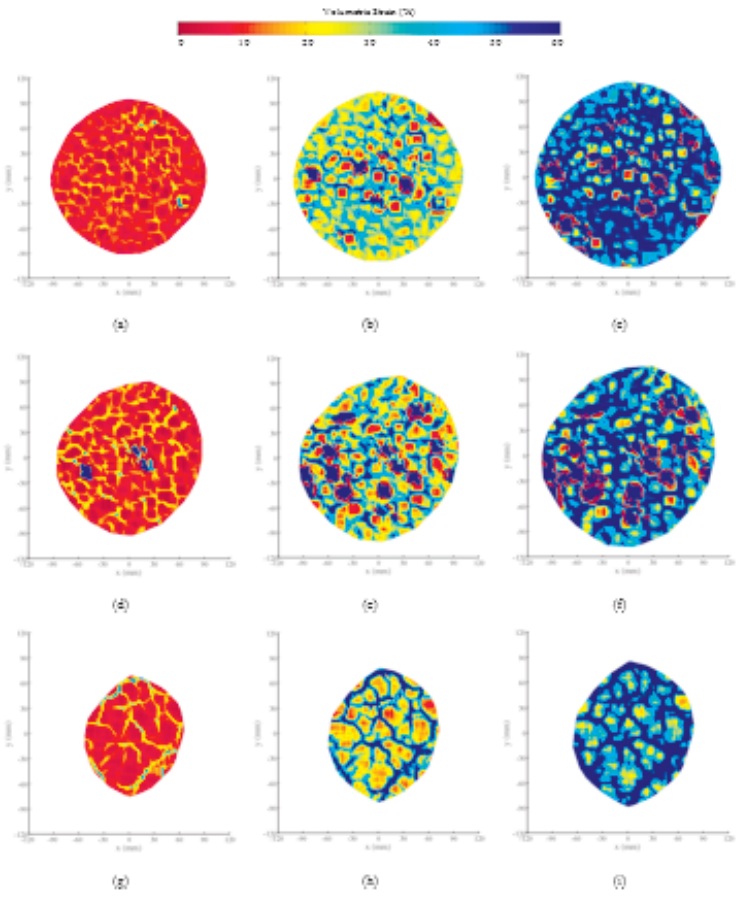

Figure 4.4. Strain Fields for Plain Matrix at (a) t = 1 s, (b) t = 4 s, (c) t = 10 s, 6 mm Fiber- Reinforced Matrix at (d) t = 1 s, (e) t = 4 s, (f) t = 10 s, 13 mm Fiber-Reinforced Matrix at (g)t = 1 s, (h) t = 4 s, (i) t = 10 s.

Strains fields are obtained by calculating the displacements of selected points. Displacement functions in the x and y directions were calculated and normalized by the initial position of the point to obtain strains in both directions. Total strain of a point is calculated as the total sum of the strains in the x and y directions. Figure 4.4 gives strain fields for t= 1, 4, and 10th seconds for 3 different materials (plain, 6 mm fiber-reinforced and 13 mm fiber-reinforced). It is worth mentioning that figures are scaled. First observation from strain distributions is that, plain mix flows in a more symmetrical circular shape, whereas mixes with fibers tend to flow more non-symmetrically with an elliptical shape.

When images obtained at the 1st s of flow are examined, it is seen that plain

matrix represent a large and circular initial spread when compared to fiber-reinforced mixes. Colour intensity of images represents the amount of strains. However, more strains were observed in 6mm fiber-reinforced mix suggesting lower initial viscosity for this mix when compared to plain mix.

This is in conflict with the general opinion saying that adding fibers causes an increase in both yield stress and viscosity. However, this result can be explained based on a previous work of the second author [146]. Kuder *et al.*, [147] used the same 6mm short cut straight steel fibers to understand the effects of fibers on the rheological behavior of mortars (3 different fiber volumes, 1, 2, 4 %). They employed a parallel-plate rheometer to measure yield stress and viscosity of the material and found that both yield stress and viscosity decreased until a critical volume fraction was reached (approximately 2 %) and then increased (w/c was 0.30 and 0.35). They attributed this result to the increased structural breakdown of cementitious matrix occur due to sharp needle-like steel fibers. They stated that small volumes of steel fibers increased structural breakdown; however, this effect was overcome with an increased fiber volume (up to 4%) since the effect created by mechanical interlocking of fibers was more pronounced. This statement is in accordance with the results of this study.

If strain fields are evaluated, it is seen that flow of material is restricted when fibers are used (based on coloured strain legends). Strain fields obtained from the plain mix are more homogenous when compared to the strain fields obtained from fiber-reinforced mixes. On the 4th second, while strain values of plain mix is around 20-35%, varying values of strains are observed for fiber-reinforced mixes at different regions of spread. This may be explained based on blockage of fibers at some regions of spread. Similar observations can be made when the data obtained at the 10th second of flow were examined. To further examine this result dynamic segregation analyses were done and the results were given below. Strain distributions may give information about possible dynamic segregation, homogeneity of fiber distributions in the mix and also fiber clumping (if there exists any).

4.1.2. Dynamic Segregation Resistance

Fiber weight percentages in different Sections of flow area were measured both for the mixes having 6mm and 13mm fibers, after mini-slump test final spread measurements were completed. Fiber percentage calculations were done, in order to observe the dynamic segregation resistance and fiber driving ability of the mixes. Results of the fiber weights and fiber weight per unit area can be seen in Figure 4.5.

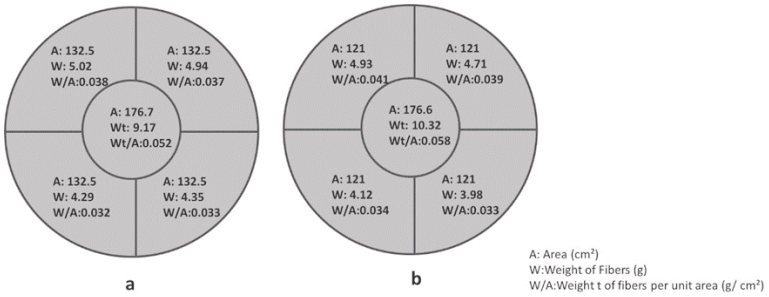

Figure 4.5. Results of Fiber Weights and Fiber Weight per Unit area, a) for 6mm Fibers, b) for 13 mm Fibers.

If all the fibers were to be distributed homogenously, the weight of fibers per unit area would be approximately 0.040. When figures given below (Figure 4.5a and Figure 4.5b) are examined, it is seen that fibers tend to accumulate in the middle region, causing a decrease of the fiber volume in the outer regions and some heterogeneity in distribution of fibers is detected. This result is in accordance with the strain distributions given in Figure 4.4. Varying values of strains representing fiber resistance to material flow is seen for fiber-reinforced mixes.

4.1.3. Monitoring of Material Flow by Using PIV

Increased fiber alignment in the direction perpendicular to loading significantly enhance mechanical performance of materials as explained in Section 3.2.4. Fiber alignment density in cement-based materials can be measured by using time-consuming procedures. Previous studies show that fibers have a tendency to align with flow especially when self-flowing materials are used. In this study PIV was used to roughly

evaluate fiber alignment in the material. It should be noted that the flow of first volume of material put into the mold was followed from one end to the other end of the mold by generating proper patches as is seen in (Figure 4.6).

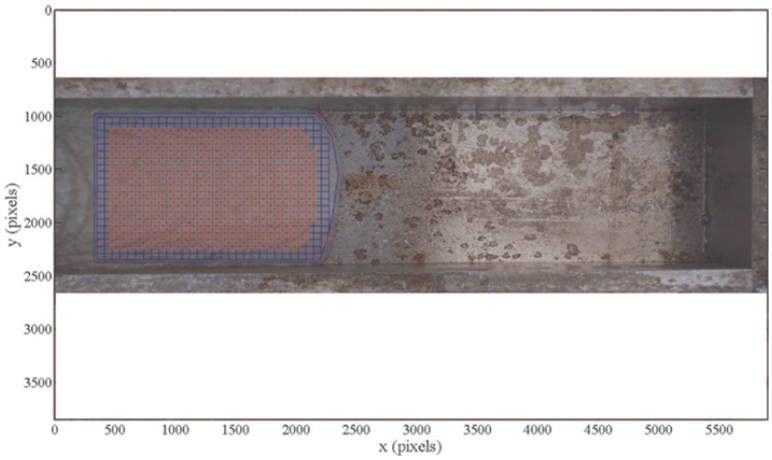

Figure 4.6. Mesh Generation for Mold Flow PIV Analysis Using 256 x 256 Pixel Patches Spaced at 64 Pixels Center-to-Center.

Vector profiles of flow were obtained using PIV and were illustrated in Figure 4.7. It is seen that the material flows in a direction parallel to the casting direction. Previous studies show that material drives the fibers along the flow direction and a fiber alignment density up to 0.7 may be obtained in the casting direction [17,101, 143-145]. It should be noted that increased fiber alignment density in the middle section is especially important if beam elements are used, since the maximum moment occurs in that region.

Considering this fact, flow vectors at the middle section were analyzed (Figure 4.7b). It should be noted that fibers are accepted to align with flow. Deviations of flow vectors from the flow direction were measured and found to vary between 0-25^o. This measurement was evaluated together with the optical microscope images obtained from sections of specimen cut from the middle sections. The results of the detailed fiber orientation analysis will be given in the next Section 5.3, but only some of the selected (Figure 4.8) are used for comparative purposes.

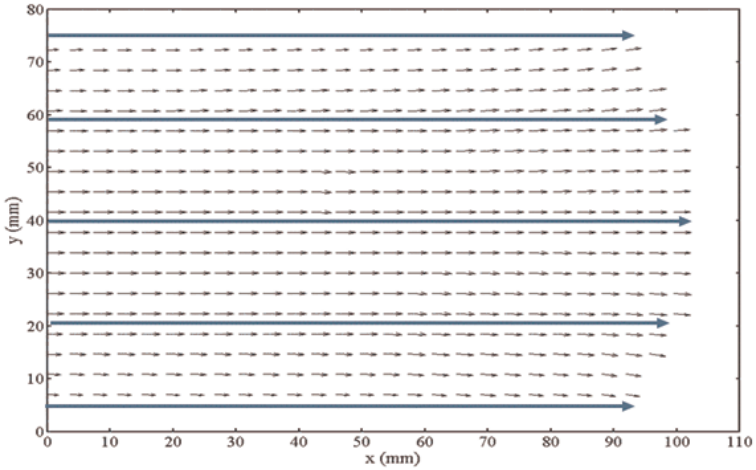

(a)

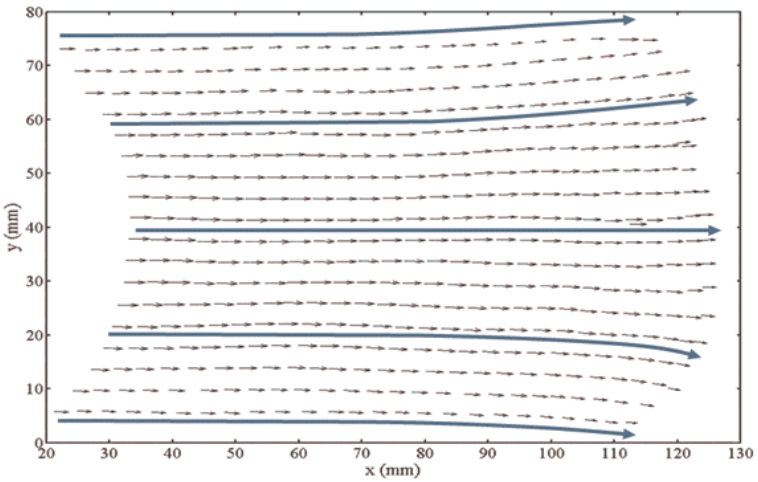

(b)

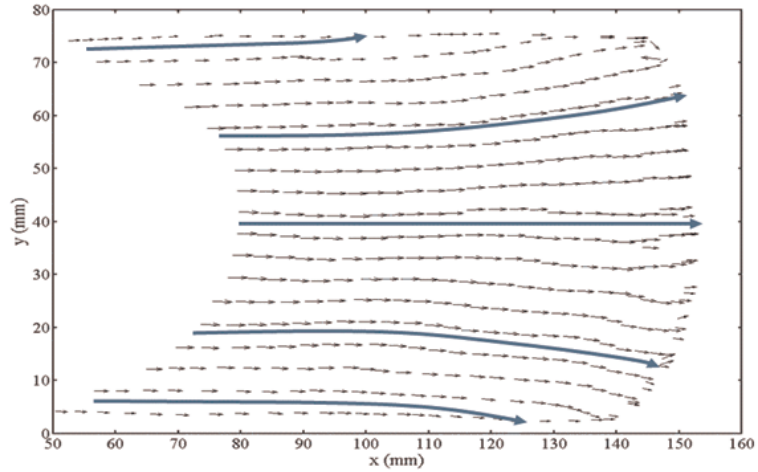

(c)

Figure 4.7. Vector Profiles Representing Material Flow at a) t=2s, b) t=7s, c) t=14s.

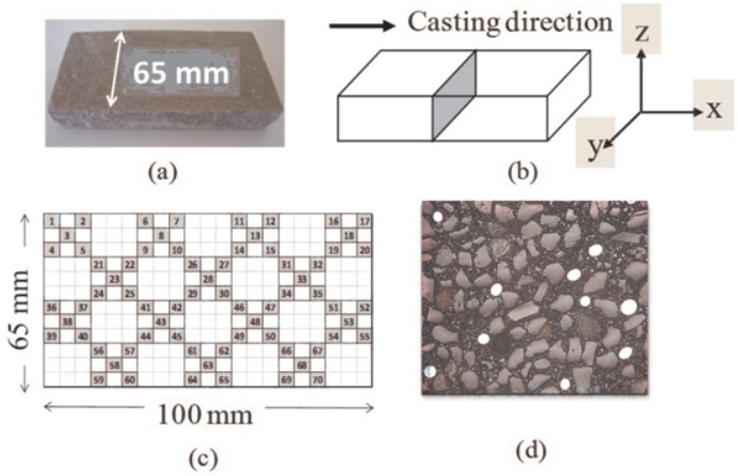

Figure 4.8. a) Cross Section Examined from S 65/100/13 Specimen b) Position of the Section Relative to the Flow Direction (x), c) Chosen Sub-Sections and d) Microscopic Image from one of the Sub-Sections (Bright Circular Shapes are the Cross Sections of Fibers).

As is seen from Figure 4.8d, most of the fibers seen on the cross-section have a circular shape representing that they are aligned in the flow direction (similar to flow vector profiles observations). It should be noted that even if most fibers seem to align in the direction of flow, experimental studies represent that maximum fiber alignment which can be obtained in the direction of flow is around 0.7. Martinie and Roussel [145] made a detailed discussion of the possible reasons of obtaining a lower value (0.7) than the expected value (at around 0.95). For the current study, following reasons may be hypothesized; (i) strong hydrodynamic interactions occur between the fibers during the flow preventing all the fibers aligning in the direction of flow, (ii) fibers do not only align in the plane (xy direction) but also out of plane (z direction), (iii) not all of the fibers may obey our assumption of aligning with the flow.

Based on the discussion given above it can be said that PIV may be used to pre-evaluate fiber alignment state of a material in a qualitative manner.

5. RESULTS AND DISCUSSIONS - Section II

In the scope of this work the correlations between strength, toughness and cracking behavior of SC-FRCCs, as influenced by the formwork dimensions, fiber length and fiber dispersion states have been investigated. Effects of matrix, mode of loading, casting method, span length and support conditions will not be discussed here since they were constant for this study. From the other parameters, fiber length or aspect ratio, fiber orientation and specimen size will be discussed since their effects on strength variations were reported to be more pronounced in the previous research [101].

Therefore, the correlation existing between the (i)"mechanical performance" of the fiber-reinforced composite, as measured through four-point bending tests, (ii) "dispersion of the fibers", as studied through Image Analysis and influenced by the fresh state behavior and (iii) the "crack propagation behavior" of the specimens examined through the detailed PIV analysis, has been comprehensively assessed from both qualitative and quantitative point of view.

5.1. Hardened State Bending Behavior

An interesting possibility to take advantage of SC-FRCC mechanical properties in tension is to use it for thin members in bending without ordinary reinforcement.

The bending behavior of fiber-reinforced composites can generally be classified as either deflection-softening or deflection-hardening, as shown in Figure 5.1 [148]. The material showing deflection- hardening behavior generates a higher load carrying capacity after first cracking compared with normal concrete or deflection softening fiber-reinforced composite material. In this research, the first cracking point is defined as the point where nonlinearity in the load-deflection curve becomes evident.

This difference in the bending behaviour, is due to the fact that after cracking of the matrix, fibres can carry larger tensile forces than the matrix itself. As a

consequence, a large number of cracks develop in the composite and cracking of the matrix is not directly followed by strain localization. This phenomenon, often named multiple-cracking, results in a strain hardening behaviour characterized by a limited or no stress increase with development of large tensile strains, as it can be seen in Figure 5.2a. This phase was named in the study of [149], as pseudo-plastic phaser. Whereas, another phenomenon, often named single cracking or crack localization, results in a strain softening behavior, as it can be seen in Figure 5.2b.

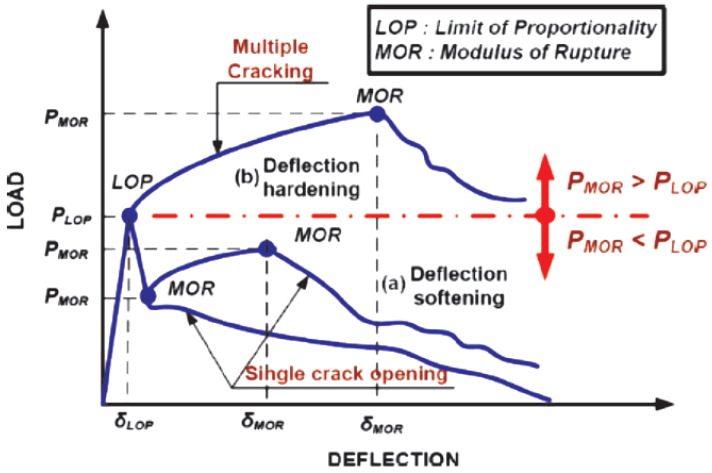

Figure 5.1. Typical Load-Deflection Response Curves of FRCC [148].

As can be seen from Figure 5.2a, composite carries increasing load after the first cracking (F_{LOP}) of the matrix if the pull-out resistance of the fibers at the first crack is greater than the load at first cracking. Because at the cracked section, the matrix does not resist any tension and the fibers carry the entire load taken by the composite. Then, with increasing loads on the composite, the fibers tend to transfer the additional stress to the matrix through bond stresses.

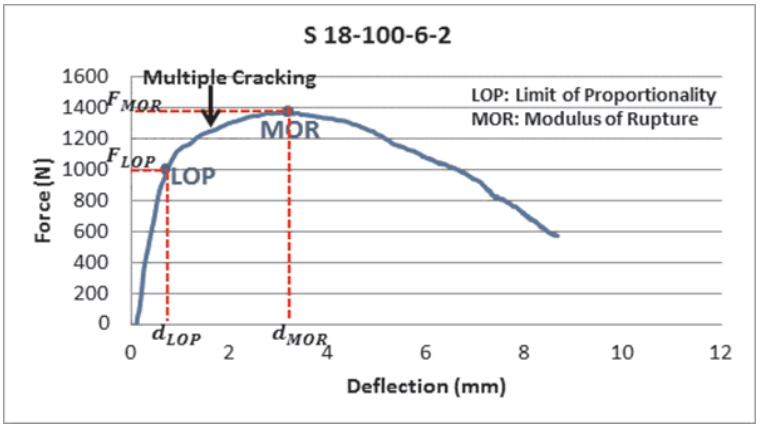

(a)

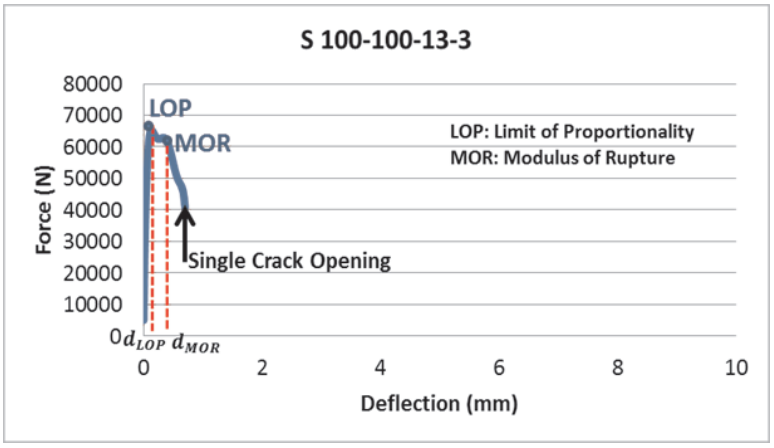

(b)

Figure 5.2. Load-Deflection Response Curves of the two of Experimentally Tested Specimens in the Scope of this Study a) Which Represents Deflection Hardening (t/f_L=2), b) and Deflection Softening (t/f_L=8) Response.

Afterwards, either the process of multiple cracking (Figure 5.2a) or single cracking is observed, depending on the size of the specimen and the effectiveness of fibers. This behavior of multiple cracking or single cracking continues until either fibers fail or the accumulated local de-bonding will lead to fiber pull-out.

From Figure 5.2a it can also be observed that S18-100-6-2 specimen showed a deflection hardening behavior, with a large zone of multiple cracking proceeding, whereas S100-100-13-2 specimen showed a deflection softening behavior with single crack lo-

calization. The linear elastic region, up to LOP, represents the micro cracking stage. The softening stage, after MOR, corresponds to the single failure crack opening and is mainly controlled by the fibre pulling-out process. The presence of fibre also eliminates the sudden fracture of the member, thus easing the fracture energy capturing.

5.2. Specimens without Fiber-Reinforcement (Plain specimens)

Specimens with varying thicknesses were prepared to investigate the effect of beam thickness (t/f_L is not applicable since no fibers are included) on the flexural behavior of SC-FRCCs. Specimens with 10 different thicknesses from 18 mm up to 100 mm were cast and tested. Two specimens were tested for each selected thickness value.

Force-Displacement curves of some of the selected specimens are given in the Figure 5.3 below. In order to compare the curves of plain concrete and fiber reinforced concrete, they are given together in each graph. Force - displacement curves of all the specimens can be found in the Appendix section.

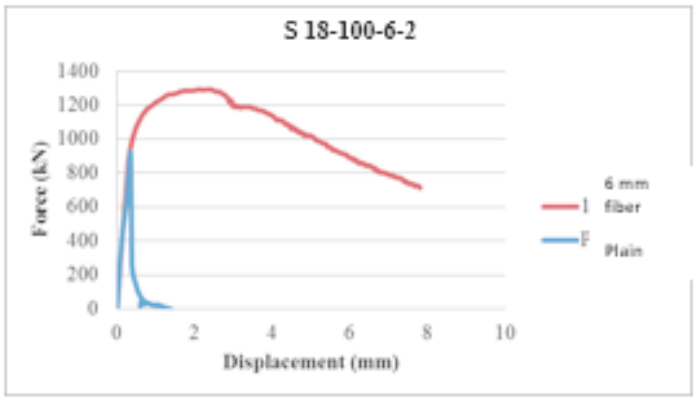

(a)

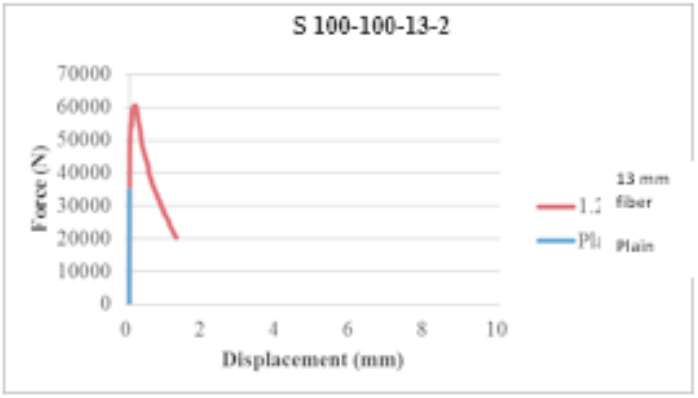

(b)

Figure 5.3. (a), (b) Force-Displacement Curves of Some of the Selected Specimens for Plain and Fiber-Reinforced Specimens.

The effect of fiber-reinforcement on first crack load, ultimate flexural load, mid-span deflection, and load-deflection relationship can be examined using Figure 5.3. As can be seen from the figure, use of fiber-reinforcement significantly increases ultimate flexural load, whereas it does not have an effect on the stiffness of the specimens (slope of the curve in the elastic region).

Considerable reduction in vertical deflection was observed for composite specimens, as fibers resist the cracks and tend to disperse them into multiple fine cracks effectively.

Therefore, it can be concluded that maximum load bearing capacity (peak load) and flexural toughness of unenforced matrix are significantly increased by the addition of fibers. When fiber bridging is introduced, the peak load is shown to be much less dependent on matrix properties. Instead fiber and interface parameters dominate peak load of the SC-FRCC beam.

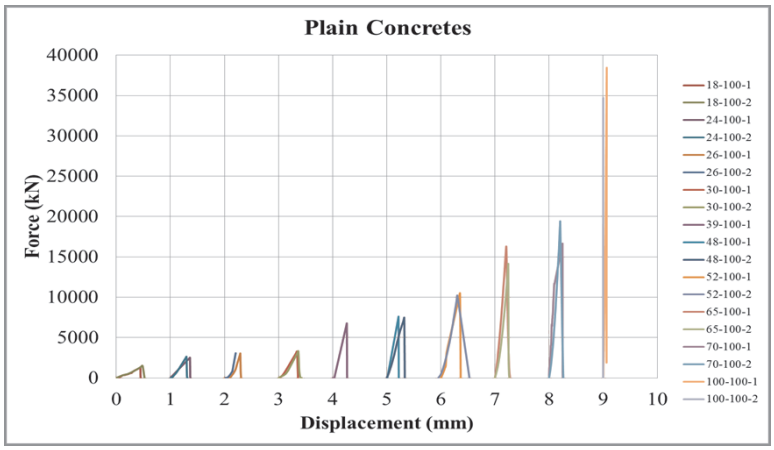

Figure 5.4. Force-Displacement Curves for All Plain Specimens.

Figure 5.4 represents force vs. displacement curves for plain specimens with different thicknesses. Stress vs. strain graphs were also obtained by calculating stress - strain values to be able to compare the behaviors of the specimens with varying sizes (Figure 5.5).

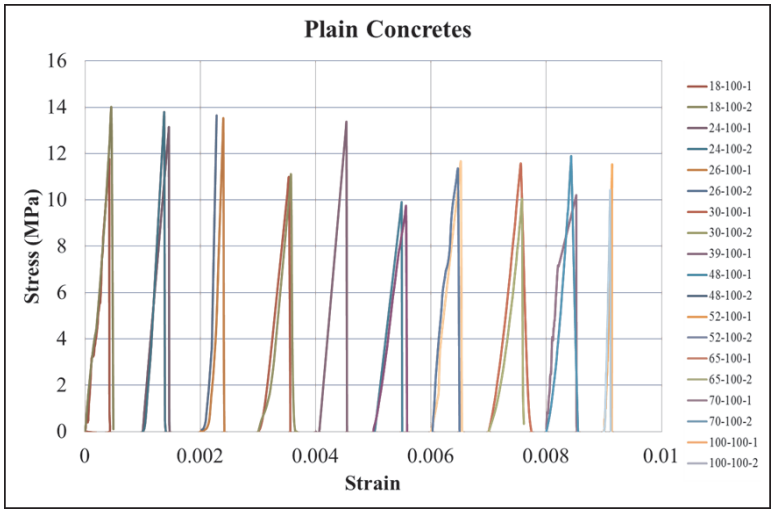

Figure 5.5. Stress vs. Strain Curves of Plain Concretes (Stress and Strain Values Were Calculated Using the Equations Given in Section 3.4.2).

It can be seen from Figure 5 that shallower beams yielded higher values of bending strength (MOR). This was expected since larger specimens are more likely to include critical defects of larger size. However decrease in strength is not as consistent and severe as it was expected (MOR values for the specimens with thicknesses 30mm and 100mm are found to be around 14 MPa). This results supports the findings of Spasojevic [149], who reported that the effect of size on bending strength is much smaller when high performance cement-based composites are used.

Strain capacities of the specimens were found to be similar except for the specimen with a thickness of 100 mm. Data including values of bending strength (peak stress), peak strain and toughness will be given. The results obtained from this section will be evaluated together with the results of fiber-reinforced specimens.

5.3. Specimens with Straight Steel Fiber Reinforcement

It is important to have information about fiber orientation densities before evaluating the results of hardened state tests since it is known that fiber alignment state highly affects the resulting performance for SC-FRCCs. Therefore, results of the optical microscope analyses are given below.

5.3.1. Fiber Orientation Density (FOD) Calculations

To do fiber alignment analyses, beam specimens were cut into 2 pieces following four-point bending tests. Cutting was done near the major crack to obtain a representative information about the fiber dispersion state right next to the major crack, as seen in Figure 5.6.

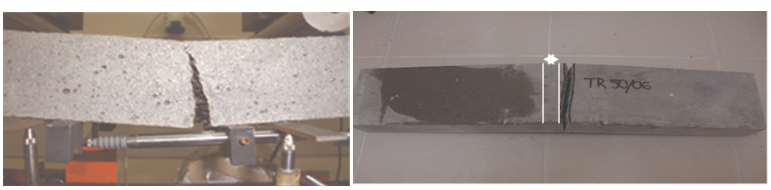

Figure 5.6. Crack Region, where Specimens Cut for Image Analysis.

The preparation procedure includes the cutting of the specimen near the fracture zone. It shoud be noted that although the specimen was cut so as to give a view of the fracture, the actual crack departed from one side of the cross section and did not pass close to the fibers on the opposite side of the cross section.

Obtaining a smooth, clear surface of the specimens is important, since the appearance of their surfaces in the reflecting light microscope is determined by their reflection behaviour or, in other words, their roughness. Therefore, cross section surfaces rubbed by emery paper.

After that, microscopic images were taken from the cross sections by using an optical microscope. Then the fiber cross sections were marked on the image file in Adobe Photoshop, and the center coordinates of each fiber location were found using the "ImageJ" image analysis program. Then these microscopic images were analyzed by using a tensor description method as summarized in Section 2.8. Considering the time, associated with the image processing, it was decided to choose one specimen of each group (not all 3 replicates) and the orientation density analyses were carried out on these subsections.

Schematic of the analyzed specimen position and reference system for fibre orientation density in specimens cut from beams are shown in Figure 5.7 and Figure 5.8.

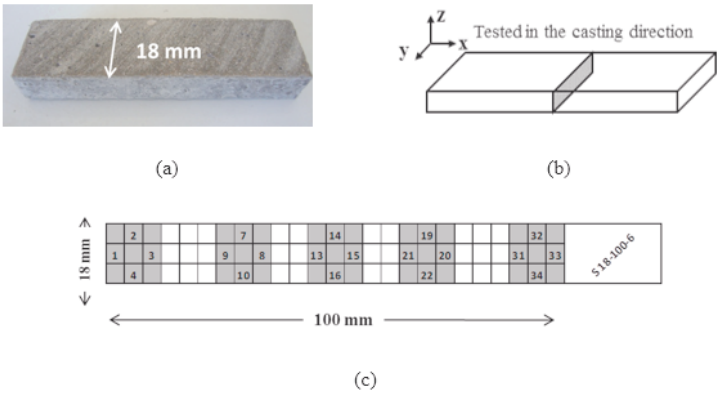

Figure 5.7. Schematic of the Analyzed S 18-100-6 Specimen and Reference System for Fibre Orientation Density in Specimens Cut from Beams.

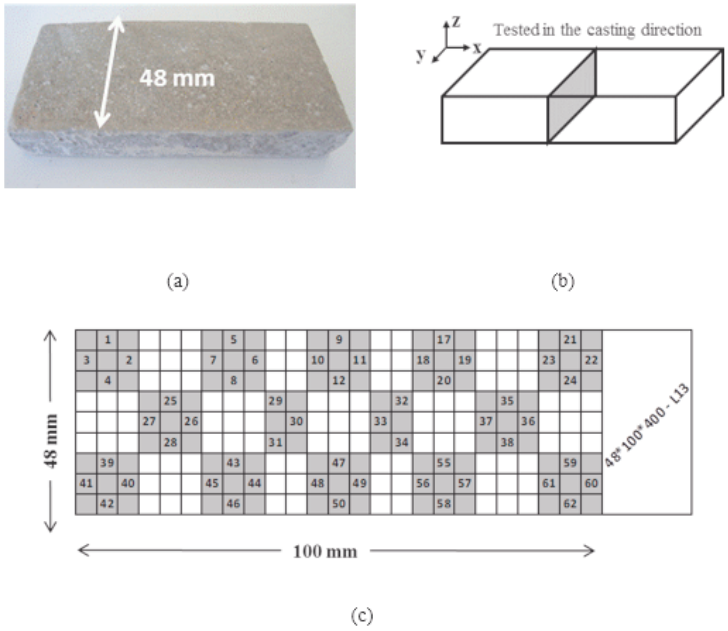

Figure 5.8. Schematic of the Analyzed S 48-100-6 Specimen and Reference System for Fibre Orientation Density in Specimens Cut from Beams.

The schematics in Figure 5.7 and Figure 5.8 detail for each specimen and for each of the examined fracture surface subsections.

5.3.2. Effect of t/f_L Value on Fiber Orientaion

As a result of image analysis, fiber orientations in the (flow) x-directions were obtained for all specimens and given in Table 5.1. As it can be observed from Table 5.1, the results referring to the whole fracture surface provide a strong quantitative evidence to the orientation of the fibres along the direction of the flow (x-direction).

Specimen thickness was expected to be an important parameter, as it was also stated by Özyurt and Şanal [101] since it is a restriction for the fibers that align in the Z direction. Formwork thickness/fiber length (t/f_L) parameter is varied by changing the formwork thickness for the fibers with two different lengths. Similar FODs were obtained in the direction of flow confirming the effectiveness of control of the material flow during casting. A controlled casting procedure for SC-FRCC may provide an

effective alignment of fibers in the direction of casting as it was also mentioned in the previous studies.

Table 5.1. Fiber Orientation Densities (FOD) Calculated for all Specimens.

Specimen	t/f_L	FOD		
		x	y	z
18-100-6-2	3	0.685	0.211	0.104
24-100-6-2	4	0.689	0.196	0.116
30-100-6-2	5	0.679	0.202	0.119
48-100-6-2	8	0.682	0.197	0.121
t fL	t/f_L	FOD		
		x	y	z
26-100-13-2	2	0.669	0.210	0.121
30-100-13-2	3	0.668	0.229	0.103
52-100-13-3	4	0.629	0.230	0.140
65-100-13-3	5	0.667	0.168	0.164
100-100-13-2	8	0.602	0.278	0.151

Figure 5.9 shows variation in the orientation densities in the X (flow) direction with an increase in pre-defined t/f_L parameter. Similar fiber alignments in the X direction can be seen as mentioned above.

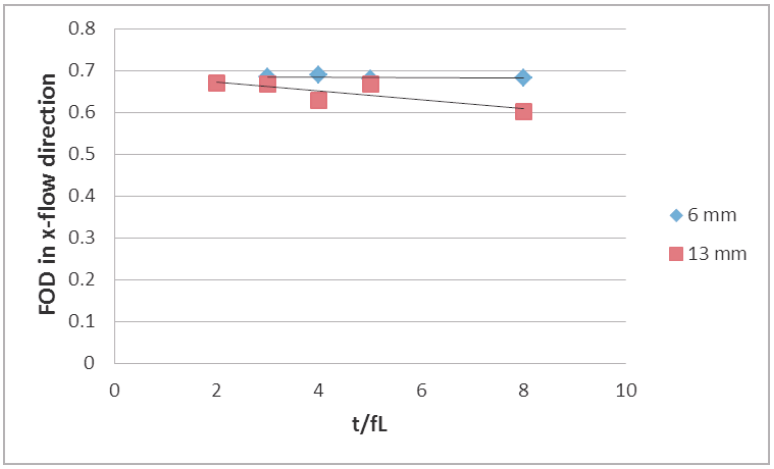

Figure 5.9. Fiber Alignment Densities for 6 mm and 13 mm Fibers in the Casting Direction (X Direction).

5.3.3. Stress vs. Strain and Stress vs. Crack Opening Displacement (COD) Relationships

Stress-strain relationships of specimens including 6 mm and 13 mm fibers are given in Figure 5.10 and Figure 5.11, respectively. Stress-strain relationships will be discussed, considering changes in t/f_L ratio and fiber orientation. Stress vs. strain curves of the selected specimens from each group were given here in this chapter, in order to have a clear understanding and make comparison. Stress-strain curves of all 45 specimens will be given in the Appendices section.

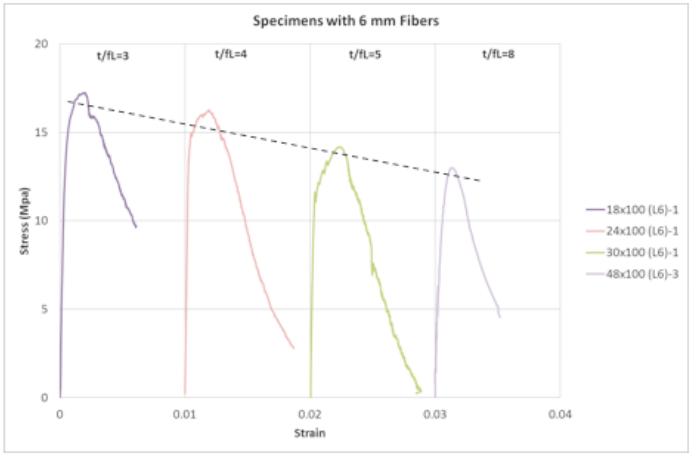

Figure 5.10. Stress-Strain Relationship of Specimens Having 6 mm Fibers.

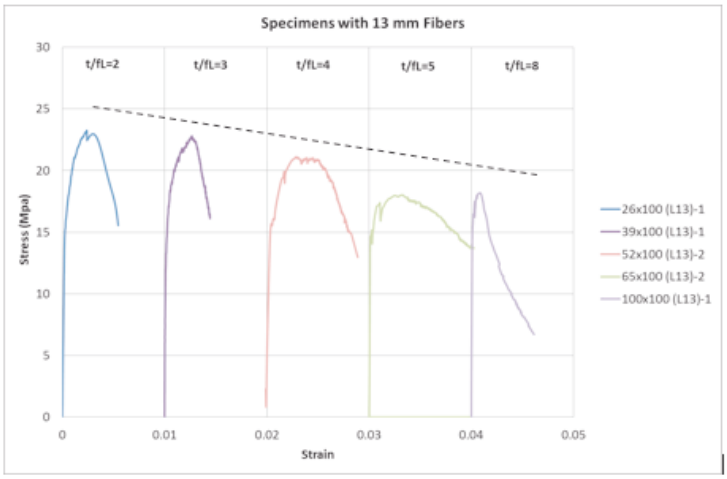

Figure 5.11. Stress-Strain Relationship of Specimens Having 13 mm Fibers.

It can be observed from Figure 5.10 and Figure 5.11 that, stress-strain curves of specimens with 6 mm and 13 mm fibers all showed a decreasing trend with increased t/f_L ratios. All specimens represent an incrase in strength (some multiple cracking) after occurence of the first crack. However, the extent of the region between LOP and MOR is different. This region represents the ability of material to undergo multiple cracking and an increase in strain (even for constant stress values) is observed. The reason for increasing strain is the slow pull out process of "the crack bridging fibers" from matrix with an increasing load.

Variation in the behavior of material may be related to the changing thicknesses of the specimens as it was done by many researchers in the past. However, the differences observed in Figure 5.10 and Figure 5.11 show that more parameters are involved and evaluating them together may be a good approach. Previous experience shows that fiber volume, fiber orientation and fiber aspect ratio are the most effective parameters on bending strength if other properties of the materials are kept constant. It is very well known that increased alignment of the fibers in the direction vertical to the applied load, increases bending strength. Increased fiber aspect ratio also increases bending capacity due to increased efficiency of fibers to bridge the cracks. However, all of this information can not be used to predict or model the bending behavior of high performance cement-based composite materials since behavior changes when size or loading conditions are changed. Therefore, it is important to consider combined effects of several parameters. This is the reason for selecting t/f_L as the parameter to be investigated in this study since it represents the effects of changing size, and fiber length at the same time (fiber volume and loading conditions are kept constant for this study).

If the results given in Figure 5.10 and Figure 5.11 are examined, it is seen that change in material performance is observed when specimen thickness and fiber length are varied. First crack stress and strain, the length of multiple cracking zone, equivalent bending strength and strain are all changed. The main objective of this study was to relate the change observed in the behavior to a single parameter. Previous research (Şanal Özyurt) represented that t/f_L ratio highly effects the performance and a limit

t/f_L value may exist below which the materials show deflection hardening behavior. Therefore, in the present study various specimens were cast to obtain a wide range of t/f_L ratios (between 2 and 8) and different types of fibers were used (results of the hooked end fibers will be given in the next section).

Stress vs. COD curves of these specimens are also given below (Figure 5.12 and Figure 5.13) to better evaluate the behavior. A similar trend is observed when stress vs. COD curves are examined. Average peak COD values were also found to depend on t/f_L ratio.

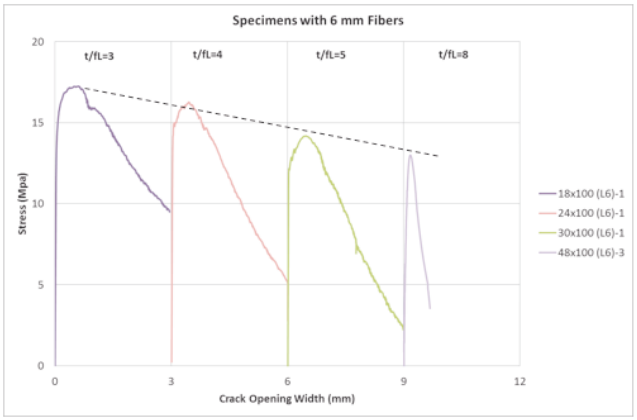

Figure 5.12. Stress-Crack Opening Displacement (COD) Felationship of Specimens having 6 mm Fibers.

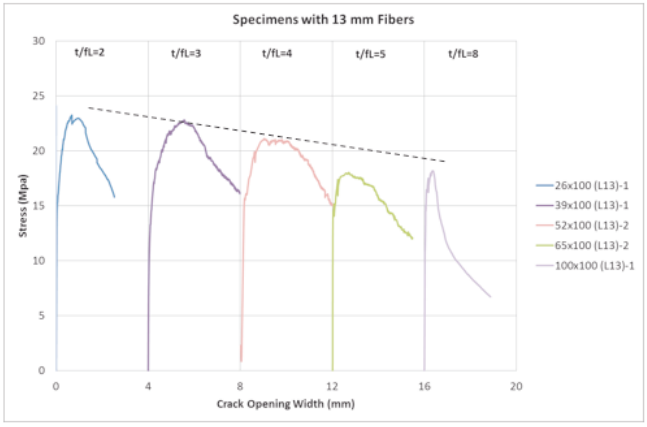

Figure 5.13. Stress-Crack Opening Displacement (COD) Relationship of Specimens having 13 mm Fibers.

Important information which may be retrieved from the curves are separately examined based on the Table 5.2 given below. Table 5.2 represents data for all the specimens.

Table 5.2. Change of Equivalent Stress, Strain and Crack Opening Displacement for Specimens without Fiber - Reinforcement, with Fiber - Reinforcement Having 6mm and 13mm Straight Steel Fibers and with Fiber - Reinforcement having 35mm and 50mm Hooked end Steel Fibers.

	t	f_L	t/f_L	Avg First Crack Stress	Avg First Crack Strain	Avg First Crack COD (mm)	Avg Peak Stress	Avg Peak Strain	Avg Peak COD (mm)	Toughness	Avg Toughness	FOD
Plain Specimens without	18	-	-	12.81	0.00044	0.027	12.81	0.00046	0.027	-	-	-
	24	-	-	13.43	0.00041	0.019	13.43	0.00045	0.019	-	-	-
	26	-	-	13.55	0.00030	0.028	13.55	0.00039	0.028	-	-	-
	30	-	-	10.97	0.00053	0.021	10.97	0.00053	0.021	-	-	-
	39	-	-	13.34	0.00050	0.023	13.34	0.00054	0.023	-	-	-
	48	-	-	9.80	0.00049	0.026	9.80	0.00049	0.026	-	-	-
	52	-	-	11.47	0.00046	0.027	11.47	0.00046	0.027	-	-	-
	65	-	-	10.78	0.00054	0.102	10.78	0.00054	0.102	-	-	-
	70	-	-	11.04	0.00043	0.028	11.04	0.00043	0.028	-	-	-
	100	-	-	10.88	0.00013	0.024	10.88	0.00014	0.024	-	-	-
6 mm Straight Steel Fibers	18	6	3	9.89	0.00028	0.024	18.23	0.0023	0.562	16.6	14.92	0.685
	18	6								14.4		
	18	6								13.7		
	24	6	4	10.39	0.00028	0.021	16.26	0.0018	0.439	13.0	14.31	0.689
	24	6								13.0		
	24	6								17.0		
	30	6	5	9.03	0.00028	0.017	13.93	0.0022	0.389	12.3	12.48	0.679
	30	6								12.4		
	30	6								12.7		
	48	6	8	8.91	0.00040	0.015	13.17	0.0017	0.209	9.7	8.60	0.682
	48	6								9.1		
	48	6								7.0		
13 mm Straight Steel Fibers	26	13	2	10.80	0.00016	0.770	25.24	0.0041	1.523	25.1	21.60	0.669
	26	13								19.6		
	26	13								20.1		
	39	13	3	10.85	0.00027	0.266	23.02	0.0025	0.757	24.6	22.12	0.668
	39	13								24.5		
	39	13								17.3		
	52	13	4	11.25	0.00035	0.267	21.11	0.0044	1.115	16.2	16.10	0.629
	52	13								16.0		
	65	13	5	11.79	0.00017	0.106	18.01	0.0033	0.725	13.8	16.03	0.667
	65	13								18.3		
	100	13	8	11.28	0.00014	0.120	19.63	0.0009	0.488	12.2	15.60	0.602
	100	13								16.8		
	100	13								17.9		
Hooked Fibers	70	35	2	9.32	0.00055	0.107	16.30	0.0035	0.645	14.0	13.80	-
	70	35								13.6		
	100	35	2.8	8.90	0.00028	0.029	16.16	0.0020	0.370	13.7	13.16	-
	100	35								12.6		
	100	50	2	9.78	0.00021	0.015	18.58	0.0060	0.250	15.9	15.61	-
	100	50								15.3		

5.3.4. Examination of first Crack Stress and Equivalent Bending Strength (Peak Stress) Results

Average 1st crack strength and equivalent bending strength values were evaluated based on the data given in Table 5.2. Figure 5.14 and Figure 5.15 represent variation in the first crack stress and equivalent bending strength with an increase in t/f_L ratio for 6 and 13 mm fiber-reinforced specimens, respectively. First crack stress values were found to be similar as expected, since they represent the strength of the cement-based material. Equivalent bending strength values were decreasing with an increase in t/f_L ratio.

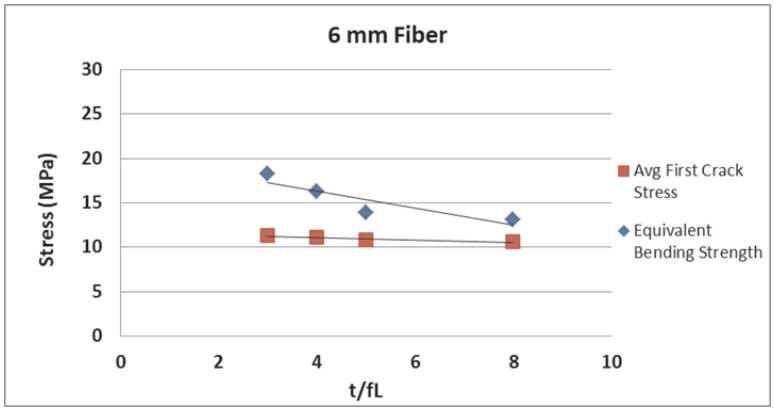

Figure 5.14. Relationship Between t/f_L Ratio and first Crack and Equivalent Bending Strength for Specimens having 6mm Fibers.

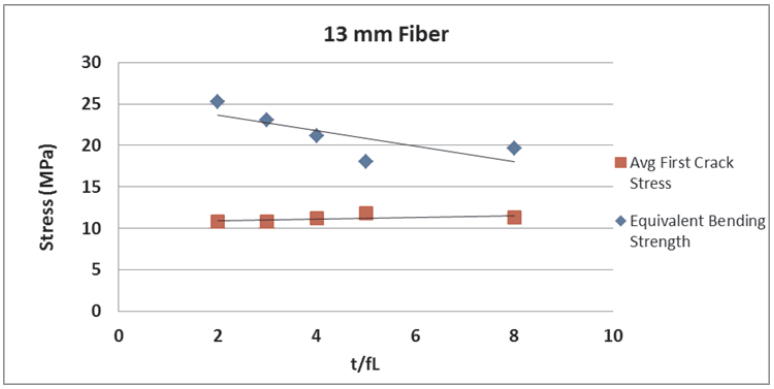

Figure 5.15. Relationship Between t/f_L Ratio and first Crack and Equivalent Bending Strength for Specimens having 13mm Fibers.

Table 5.3 represents average first crack stress data and equivalent bending strength

(peak stress) data for the straigth steel fiber-reinforced specimens studied. From the table (4th column) it is seen that average 1st crack stresses are very close for all the specimens. This was expected since first crack stresses depend on concrete strength. No pronounced change in the first crack stresses was observed with an increase/decrease in the thickness of the specimens. This result is in accordance with the results obtained from the plain specimens. However, when the equivalent bending strengths of the specimens were examined, systematic decrease with an increase in t/f_L ratio was observed for all the specimens. Decrease in peak strength goes up to 28 % with an increase in t/f_L ratio when 6 mm fibers are used, while this value is around 22 % for 13 mm fiber reinforced specimens.

Table 5.3. Average Equivalent Bending Strength Values (From Table 5.2).

	Thickness (mm)	t/f_L	Average first crack stress (MPa)	Av. Equivalent bending strength (MPa)	Increase obtained in equivalent bending strength (%)
6 mm fibers	18	3	11,33	18,23	38
	24	4	11,16	16,26	31
	30	5	10,81	13,93	22
	48	8	10,64	13,17	19
Reduction in av. Equivalent bending strength, %				28	
13 mm fibers	39	3	10,85	23,02	53
	52	4	11,25	21,11	47
	65	5	11,79	18,01	35
	100	8	11,28	19,63	43
Reduction in av. Equivalent bending . strength, %				22	

If the Table 5.3 is used to calculate the increase in strength with respect to first crack stress (last column), average equivalent bending strength of the specimens increased from 19 % to 53 %. For all the specimens this can also be explained in terms of decreasing hardening ability with an increase in t/f_L ratio. Increase obtained in equivalent bending strength was found higher when 13 mm fibers were used as expected.

5.3.5. Examination of Peak Strain and Peak COD Results

The addition of fibers increase strain capacity of materials since they are effective in bridging cracks. Average peak strain values of the specimens with different t/f_L ratios were examined (Table 5.2). This data is important since it also represents the extent of multiple cracking zone. Increased peak strain value means increased strain hardening capacity of the material.

A decreasing trend was observed in peak strains with an increasing t/f_L ratio. Average peak strain values were found to be on the order of 2.5-4.5 x 10^{-3} for 13 mm fiber-reinforced specimens. Only the specimens with a thickness of 100 mm (t/f_L = 8) yielded different results representing much lower peak strain value. A similar result was observed for the plain specimens with a thickness of 100 mm. The peak strains of plain specimens were found to be on the order of 4-5 x 10^{-4}, while the peak strain for 100 mm thick plain specimen was around 1 x 10^{-4}. Peak strains of 6mm fiber reinforced specimens were around 2 x 10^{-3} which was lower than the strain values of 13 mm fiber-reinforced specimens as expected.

Peak COD results are also examined in this Section (Table 5.4). Average peak COD results were found to vary from 0.5 to 1.5 mm for 13mm fiber-reinforced specimens. No tendency was observed with an increase or decrease in t/f_L values. However, with an increase in t/f_L ratio, a decreasing trend of average COD values is observed, which were normalized by dividing the average COD values with the corresponding beam heights. As a result of this, decreased opening of crack in the unit beam length when the t/f_L ratio is increased can be explained by the decrease of multiple cracking behavior as a result of decreased efficiency of crack bridging mechanism, with an increase of the beam height.

Table 5.4. Average and Normalised Average Peak COD Results.

	t	fL	t/f_L	Avg Peak COD (mm)	Normaliz ed Avg COD (COD/t) (mm/mm)
6 mm Straingth Steel Fibers	26	13	2	1.523	0.059
	26	13			
	26	13			
	39	13	3	0.757	0.019
	39	13			
	39	13			
	52	13	4	1.115	0.021
	52	13			
	65	13	5	0.725	0.011
	65	13			
	100	13	8	0.488	0.005
	100	13			
	100	13			
13 mm Straingth Steel Fibers	18	6	3	0.56200	0.031
	18	6			
	18	6			
	24	6	4	0.43900	0.018
	24	6			
	24	6			
	30	6	5	0.38900	0.013
	30	6			
	30	6			
	48	6	8	0.20900	0.004
	48	6			
	48	6			
Hooked Fibers	70	35	2	0,645	0.009
	70	35			
	100	35	2.8	0,370	0.004
	100	35			
	100	50	2	0.250	0.003
	100	50			

5.3.6. Examination of Toughness Factor

In this work, JSCE SF-4 [40] standard technique has been followed, as mentioned and described in the previous sections. According to this method, the area under the load-deflection plot up to a deflection of span/150 is obtained. From this measure of flexural toughness, a flexural toughness factor (FT) is calculated. Additionally, in this study deflection of span/150 leads to low values of deflection and if FT values are only to be calculated up to this limit, they don't not seem to represent the whole energy absorption capacity of the specimens. The specimens tested undergo high deflections, since they are high performance steel fiber reinforced composites. Therefore, JSCE SF-4 standard's FT calculation has been modified in this study, and the calculations based on the area under load-deflection plot were obtained up to deflection values of

span/75.

It may be noted that FT has unit of stress such that its value indicates, in a way, the post matrix cracking residual strength of the material when loaded to a deflection of span/150. Toughness values of specimens were also found to vary depending on t/f_L ratio as expected.

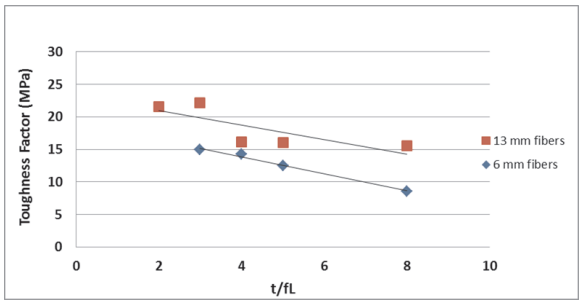

Figure 5.16. Change in Toughness Factor (FT) with t/f_L.

Figure 5.16and Table 5.5 represent change in flexural toughness with an increase in t/f_L ratio for 6 mm and 13 mm fiber-reinforced specimens. Energy absorption capacities of the materials decreased with an increase in t/f_L value. Decrease in toughness was lower when long fibers were used as it was the case for equivalent bending strength. Change in toughness was considered to be due to decreased effectiveness of fiber bridging with an increased t/f_L since FODs in the X direction (fiber alignments) were similar.

Table 5.5. Change in Average Toughness with t/f_L.

	Specimen thickness (mm)	t/f_L	Av. Toughness (Mpa)
6 mm fibers	18	3	14.92
	24	4	14.31
	30	5	12.48
	48	6	8.6
Reduction in av. Toughness, %		42	
13 mm fibers	39	3	21.6
	52	4	22.12
	65	5	16.1
	100	6	16.03
Reduction in av. Toughness, %			26

5.3.6.1. Relationship Between Toughness Factor and Normalized Crack Area. In order to have a detailed understanding of the realtionship between FT and cracking behavior, total projected crack areas were calculated from the crack monitoring images taken during the flexural tests, by using an Image Analysis software (ImageJ). From the crack monitoring images (Figure 5.17a), by the help of Image Analysis software, all of the cracks visible on the examined fracture area were shaded with black and crack patterns are extracted for all specimens and trapezoidal surface areas (2D) were calculated for each of the cracks (considering their length and width) and the sum of all these crack areas were calculated, in order to find the total projected crack area for each specimen.

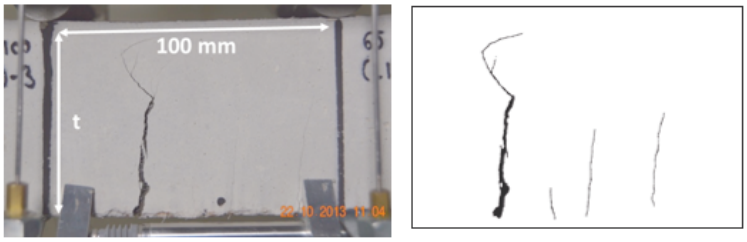

Figure 5.17. a) Crack Monitoring Image from one of the Experimentally Tested Specimen, b) Shaded Visible Cracks of the Same Crack Monitoring Image, by Using an Image Analysis Software.

In order to make a consistent comparison between specimens, the total projected crack areas were normalised over the area of the maximum moment region (thickness of specimen*LVDT measuring range), for obtaining normalised crack area values (crack area/thickness*100). Relationship between FT, normalised crack areas and t/f_L ratios of the specimens were given in Figure 5.18 and Figure 5.19, as following.

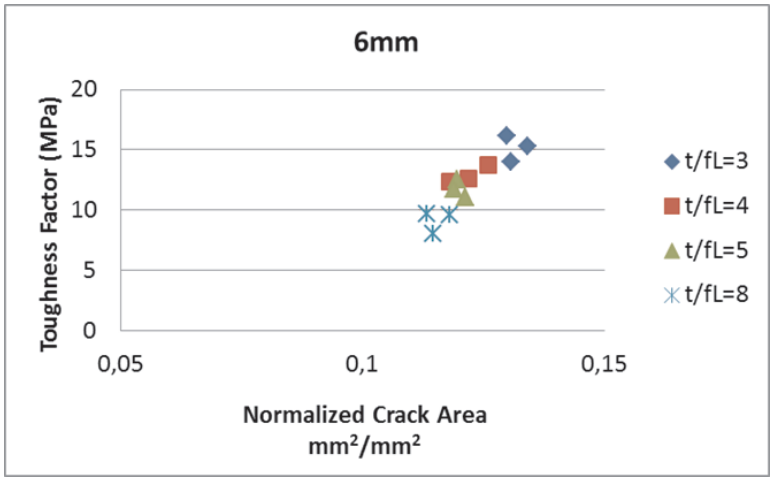

Figure 5.18. Relationship Between FT, Normalised Crack area and t/f_L Uatio of the Mpecimens having 6 mm Fibers.

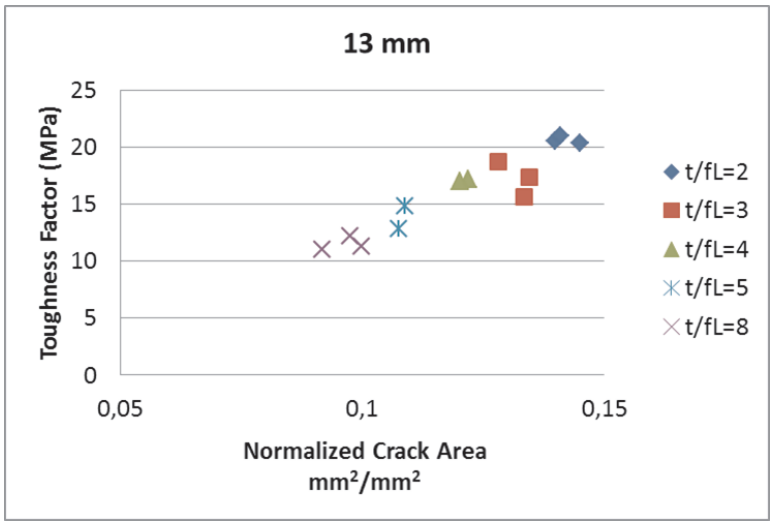

Figure 5.19. Relationship Between FT, Nnormalised Crack area and t/f_L Ratio of the Specimens having 13 mm Fibers.

As it can be seen from Figure 5.18 and Figure 5.19, both normalized crack areas and toughness factor of specimens decreases, when t/f_L ratio increases for both specimen groups having 6mm and 13mm fibers. This result is in accordance with the results of previous sections. Multiple cracking ability of material decreases with an increasing t/f_L value, yielding lower strain capacity and toughness. Figure 5.18 and Figure 5.19 also show that cracking ability of short fibers is limited when compared to 13 mm fibers.

5.4. Specimens with Hooked end Steel Fiber Reinforcement

In this Section of the study, hooked end fibers were used to understand the effect of different fiber types on the hardened-state performance. Force vs. deformation and stress vs. strain relationships of specimens with 70 mm and 100 mm thicknesses, having 35 mm and 50 mm hooked end fibers are given in Figure 5.20 and Figure 5.21.

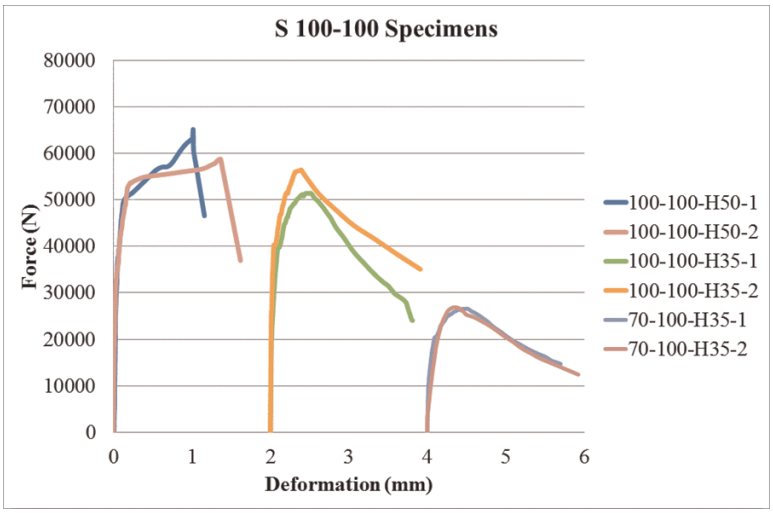

Figure 5.20. Force vs. Deformation Relationships of Specimens with 70 mm and 100 mm Thicknesses, having 35 mm and 50 mm Hooked end Fibers.

As can be seen from the figures, fibers with a length of 50 mm represent different behavior when compared to 35 mm fibers. Their strain capacity was found to be higher in the multiple cracking zone. The specimens cast using 35 mm hooked end fibers yield similar results since their t/f_L values were similar (Figure 5.21). The effect of increased fiber length was seen again when fiber length is increased to 50 mm for the specimens with a t/f_L value of 2.

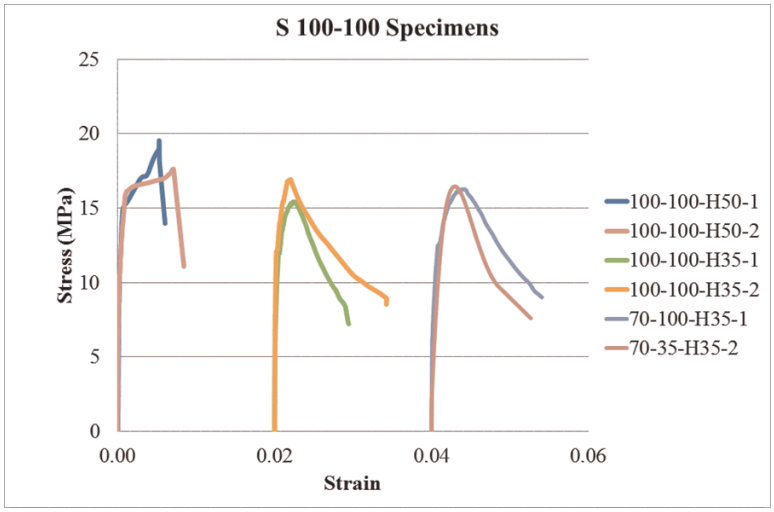

Figure 5.21. Force vs. Deformation Relationships of Specimens with 70 mm and 100 mm Thicknesses, having 35 mm and 50 mm Hooked end Fibers.

When the toughness values of these specimens were examined, the specimens with long fibers (50 mm), represented higher values (15.6 MPa for 50 mm fibers - 13.2 MPa for 35 mm fibers with a t/f_L value of 2.9 and 13.8 MPa for 35 mm fibers a t/f_L value of 2) as it was the case for the straight steel fibers.

5.5. Comparison of Results from Different Types of Fibers

Hooked end steel fibers were also employed in this study to understand the effect of using fibers with different properties. Studying a wide variety of t/f_L ratios was not possible when longer fibers (35 mm and 50 mm) were under consideration since much bigger specimens were needed. Therefore, only 2 t/f_L ratios were studied for 35 mm hooked end fibers and only 1 t/f_L ratio was studied for 50 mm long fibers as explained above. Properties of the fibers were given again in Table 5.6. Fibers were different by means of shape and geometry as is seen in Table.

Table 5.6. Properties of Fibers Used in this Stufy.

	Straight 6	Straight 13	Hooked end 35	Hooked end 50
Length (mm)	6	13	35	50
Diameter (mm)	0.16	0.16	0.7	1
Aspect Ratio	37.5	81.3	50	50
Tensile Strength (MPa)	1100	1100	1400	1400

Figure 5.22 can be used to analyze mechanical performance obtained by using different fibers. As is seen from the figures hooked end fibers represented "equivalent bending strength" and toughness results similar to that of 6 mm straight fibers (for similar t/f_L values). If the performance of fibers for the same t/f_L ratio is compared (Figure 5.22), it is seen that the fibers with highest aspect ratio yield maximum equivalent bending strength, however their efficiency in the post peak stage is relatively lower when compared to longer fibers. If the performances of the 2 hooked end fibers (35 and 50 mm) are compared (for the same aspect ratio and same t/f_L ratio of 2), than it is seen that 50 mm fibers have a better performance in the pre-peak region, while 35 mm fibers have a less steep post peak branch. This result is in accordance with the result obtained for a t/f_L ratio of 3. Based on these experimental results, it can be said that for the same t/f_L ratio, fiber aspect ratio plays a major role in determining the behavior after initial crack, higher aspect ratios yielding higher equivalent bending strength values.

Figure 5.23 and Figure 5.24 also represent that equivalent bending strength and toughness factors calculated for hooked end fiber reinforced specimens are lower than the ones reinforced with high aspect ratio fibers for the same t/f_L ratio.

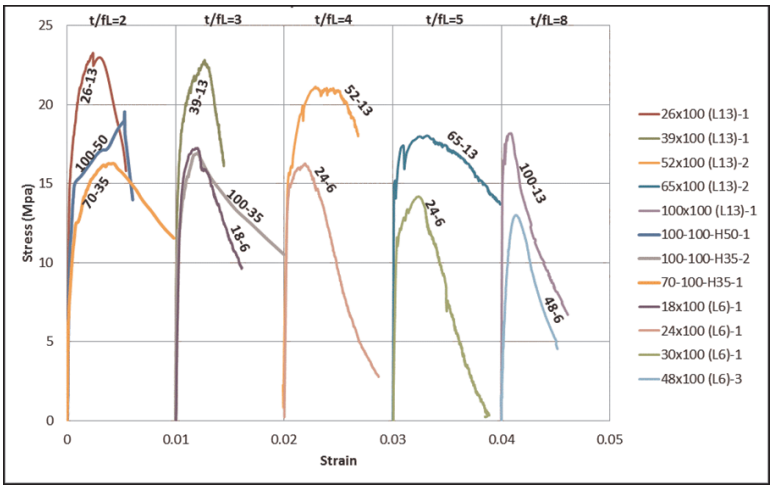

Figure 5.22. Stress-strain relationship of all the specimens, according to change in t/f_L.

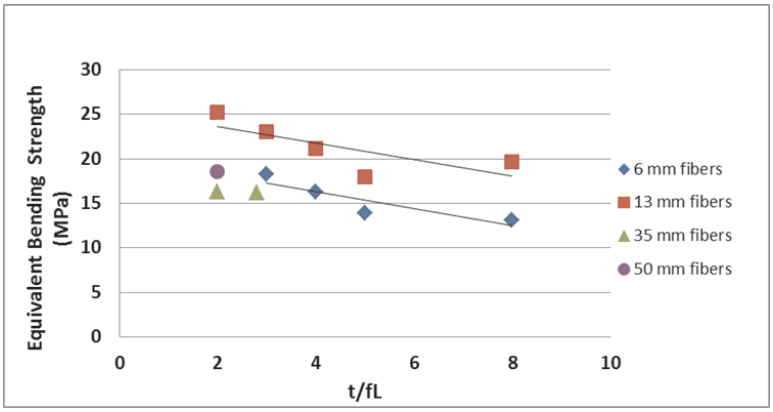

Figure 5.23. . Change in Equivalent Bending Strength for Different t/f_L.

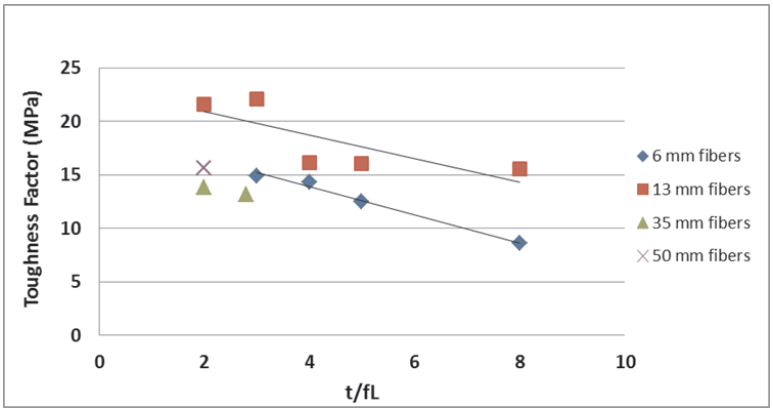

Figure 5.24. Change in Toughness for Different t/f_L.

5.6. Effect of w/f_L on the Hardened State Mechanical Performance

A detailed analysis regarding the effects of varying specimen width on FOD (fiber orientation density) was carried out in a previous study [101]. Results of the previous study represented that increased specimen width (increased flow width) results in decreased FOD in the direction vertical to the crack opening. Figure 5.25 given below represents variation in orientation density (in the X direction) with an increase in flow width. As is seen from the figure FODs decreased from around 0.71 to 0.62 and 0.63 to 0.5 for 6 and 13 mm fiber - reinforced specimens, respectively. That was not a pronounced decrease; however the effect on the mechanical behavior (bending strength and toughness) was important (Figure 5.26). All of the specimens, except the ones with a t/f_L value of 8 represented pronounced decrease with an increase flow width (decreased FOD in the X direction). The authors reported that the effect of w/f_L increased with an increased efficiency of fibers. Efficiency of fibers in bridging the cracks was very limited for the specimens with a t/f_L value of 8. Therefore no effect of varying FOD was seen for those specimens [101].

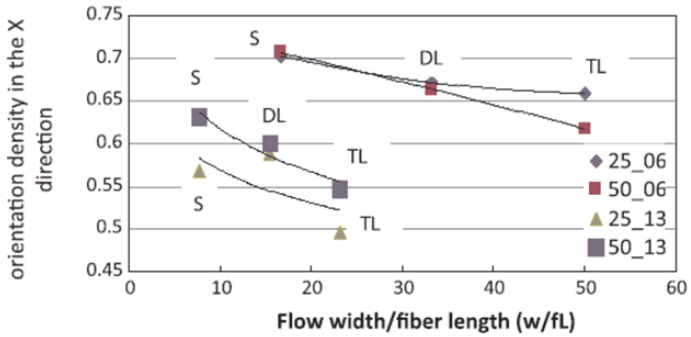

Figure 5.25. Effect of Flow Width/Fiber Length Ratio on the Orientation Density in the x Direction (Şanal, Özyurt [101]).

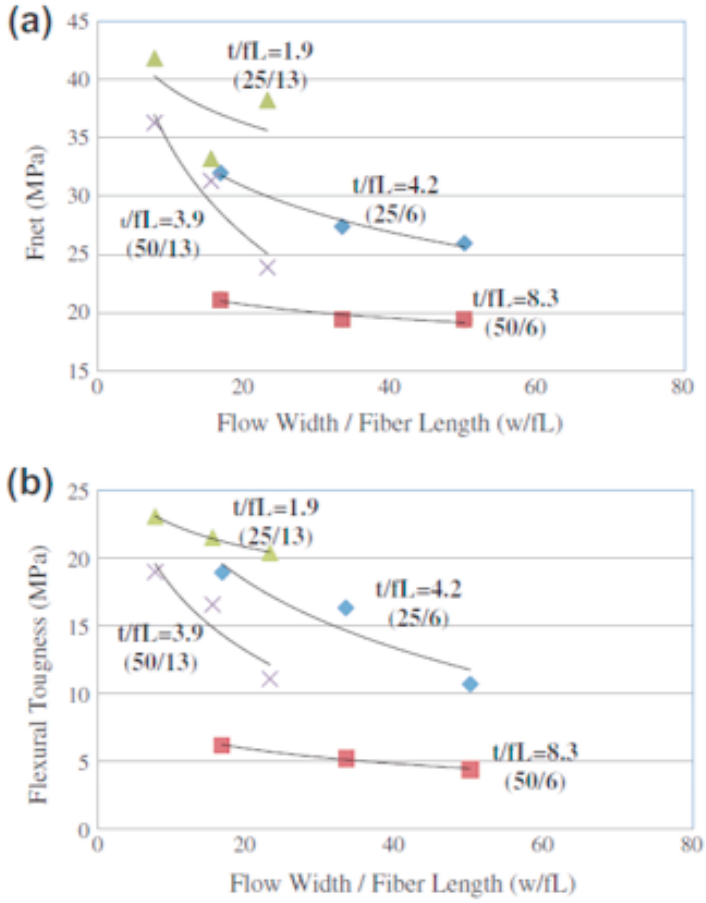

Figure 5.26. Effect of w/f_L and t/f_L on (a) the Flexural Strength and (b) Flexural Toughness of Specimens (Şanal, Özyurt [101]).

The effect of w/f_L was also studied in the scope of this study by using S 26-39-13, S 26-100-13, S 39-39-13 and S 39-100-13 specimens. Figure 5.27a and Figure 5.27b represent that strain capacity of the specimens highly increased when width of the specimens decreased. It was seen that this behavior obtained due to the more effective alignment of fibers in the casting direction (X direction in Figure 5.28), since mould walls cause a restriction and force the material to flow in the direction of casting.

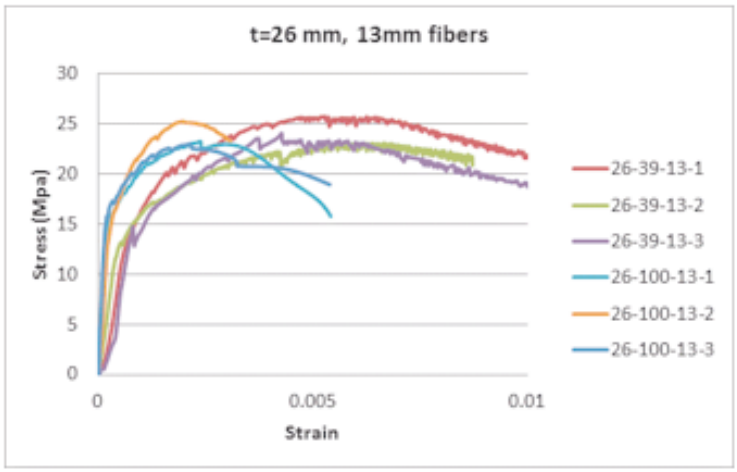

(a)

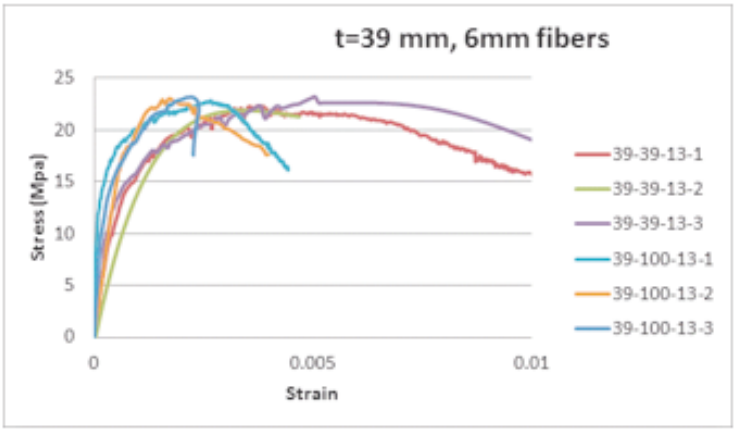

(b)

Figure 5.27. Stress-Strain Relationships of Specimens (a) with 26 mm Thickness and (b) with 39 mm Thickness.

Figure 5.28. Representation of Casting Flow Direction (X-dir).

Table 5.7 represents FODs for the identical specimens cast using moulds with different widths. As is seen in the table FODs (in the X direction) increase with a

decreased mould/flow width and this increase results in the following difference in the stress - strain behavior of the material. Equivalent flexural strengths of these specimens were similar (Figure 5.27), however pronounced difference in the strain values were observed. This is probably because of the increased fiber bridging capacity obtained due to more effective alignment of fibers.

Table 5.7. FODs for the Identical Specimens Cast Using Moulds with Different Widths.

Specimen code	FOD	Equivalent Fluxural strength (Mpa)
S26-39-2	0.818	23.08
S 26-100-2	0.669	25.24
S 39-39-2	0.82	21.88
S 39-100-2	0.668	23.02

5.7. Hardened State Performance Results from PIV Analysis

5.7.1. Comparison of Load-Crack Opening Displacement (COD) Curves from LVDT and PIV

Another parameter which was identified by using PIV was the crack width opening. Four-point flexural tests were done on all specimens and conventional measurement of crack widths were obtained by using 2 horizontally placed LVDTs as explained in the experimental methods section. For PIV analyses images obtained during tests were used. These analyses carried out to measure crack widths, rely on measuring the displacement values near the boundary of the crack. Crack opening displacement (COD) results for selected specimens were measured from experimental data by LVDTs and calculated from PIV analyses are given below, both at first crack and at failure stages:

Table 5.8. Crack Opening Displacement (COD) Values for Selected Specimens, Measured from Experimental Data by LVDTs and Calculated from PIV Analyses.

Specimen				Crack Opening Displacement (COD) (mm)			
				Wfirst crack		Wfinal	
				PIV	Exp.	PIV	Exp.
S	24	100	6	0.25	0.28	2.03	2.64
S	30	100	6	0.17	0.19	3.09	3.12
S	65	100	13	0.1	0.11	3.02	3.62
S	100	100	13	0.01	0.02	2.81	2.98

As it can be observed from Table 5.8, for the first crack, displacements from LVDT and the values calculated from PIV measurements are very similar to each other. But for the final stage COD values, the experimental readings and PIV measurements diverge from each other. In order to investigate this finding in detail, the load-crack opening displacement curves of these selected specimens were drawn together.

Load-crack width diagrams for the selected beam specimens (S 24-100-6, S 30-100-6, S 65-100-13 and S 100-100-13) were obtained from the PIV analyses and are shown in Figure 5.29.

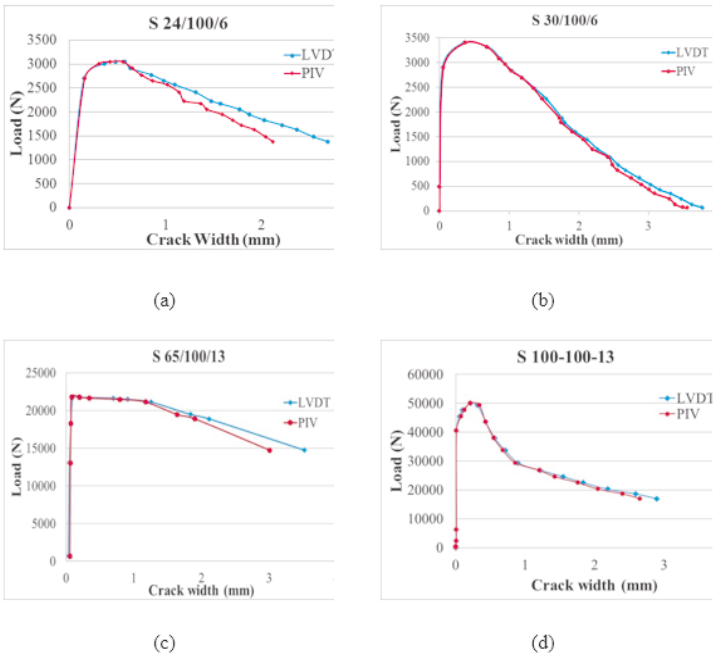

Figure 5.29. Load-crack width Curves Obtained from PIV Analyses and LVDT Measurements.

As it is shown in Figure 5.29, load-crack width curves obtained from PIV analyses and LVDT readings represent good correspondence. However, careful inspection of the figure reveals that there is a systematic difference between the results obtained from the two techniques, especially for the post-crack region of the curves. This can be explained by the rotational movement of LVDTs. Because, as vertical deflection and subsequently the curvature of the beam increases during loading, LVDTs tend to rotate, as is seen in Figure 5.30 and this rotation causes additional readings, resulting in higher values than actual crack width values.

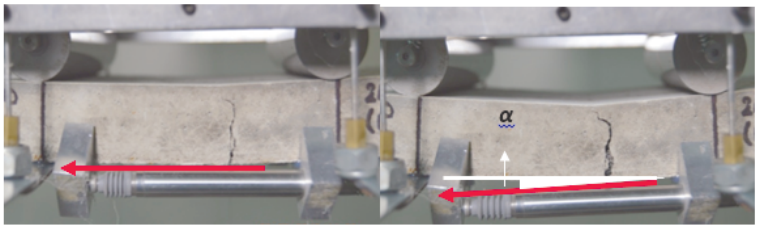

Figure 5.30. Rotational Movement of LVDTs Due to Increased Curvature of the Beam.

The value of LVDT reading is influenced by its location with reference to the axis of rotation. As mentioned before, in this study, 2 LVDTs are placed on both sides and just at the bottom of the beams. Therefore, throughout the flexural test, as the vertical displacement of the beam increases with loading, LVDTs tend to rotate, and give higher values due to this rotated geometry. A representation of this rotated geometry and LVDT measuring distance can be seen in Figure 5.31 with an assumption of all the beam specimens have a major crack in the midspan.

In Figure 5.31a, actual crack opening (w), vertical displacement (δ), beam depth (d), span length (L) are seen. "α" represent both the rotation angle of beam and also LVDTs. Figure 5.31b is the magnified view of the Figure 5.31a, focusing on the crack opening "w" and LVDT measuring distance (r_1+r_2). The values of α, r_1 and r_2 can be obtained as following:

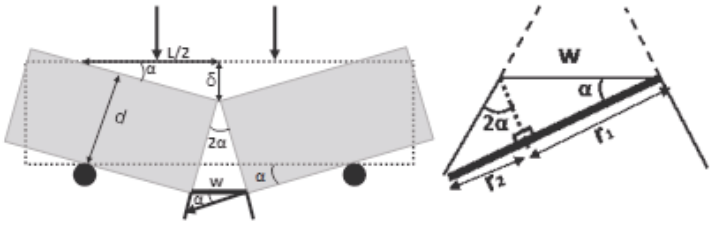

Figure 5.31. a) Idealized Geometry of the Beam Specimen Under Flexural Loading and b) LVDT Measuring Distance.

$$\propto = Arctan\left(\frac{\delta}{L/2}\right) \tag{5.1}$$

$$r_1 = w.\cos(\propto) \tag{5.2}$$

$$r_2 = w.\sin(\propto).\tan(2 \propto) \tag{5.3}$$

$$r_1 + r_2 = w.\cos(\propto)(1 + \tan(\propto).\tan(2 \propto)) \tag{5.4}$$

To take this effect into account, rotation angle (α) of LVDTs for selected data points were calculated and LVDT measurements were corrected according to Equation 5.4. The corrected values are again plotted together with PIV results (Figure 5.32).

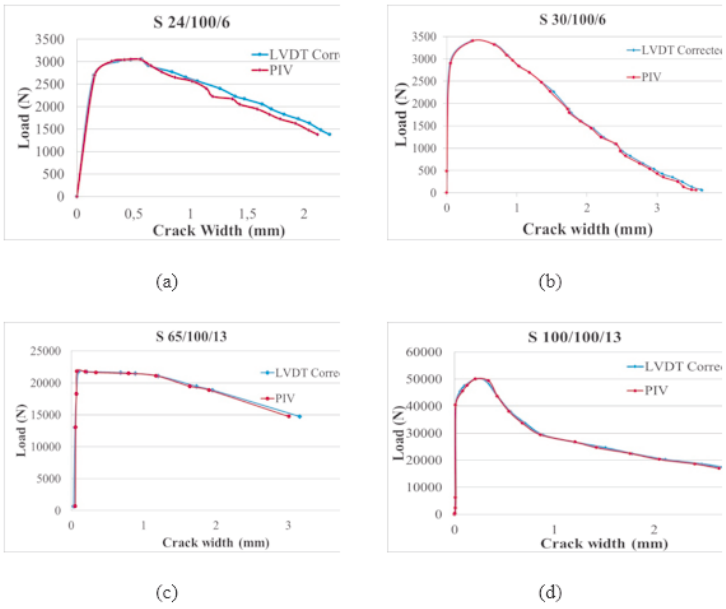

Figure 5.32. Load-crack width Curves for PIV and Corrected LVDT Results.

As it is seen in Figure 5.32, there is almost one-to-one correspondence between the load-crack width curves obtained from PIV and LVDT readings which clearly implies the great ability of PIV, as well as limitations of LVDTs, to measure crack width opening.

5.7.2. Crack Development Monitoring with an Increasing Load Through Strain Field Measurements of PIV

As it was mentioned, the ability of the PIV technique in evaluating precise crack widths of the tested beam specimens was verified. The reason for choosing PIV as one

of the techniques to be used for this study was to comprehensively evaluate cracking behavior of SC-FRCCs.

PIV is capable of measuring the displacement of areas of interest within a series of digital images. It has the potential to be used as an alternative to more traditional linear transducers (LVDTs), and other traditional measuring techniques. But also offers significant advantages over traditional measurement techniques because it can provide full-field surface displacement measurements. It is also advantageous in determining crack movement because a priori knowledge of the crack location is not required. Instead images of the structure can be taken in the general area of where cracks are anticipated and crack measurements can be obtained.

The use of PIV provides the ability to create a two-dimensional displacement or strain field for the entire surface of the crack zone throughout each stage of the test. The contour plots illustrate the movement between the reference image and the image taken at the peak load.

For monitoring crack evolution, the data obtained from images taken during flexural testing of the beam specimens were matched with corresponding force-deformation curves. It is possible to observe progress of cracks and strain distribution all over the maximum moment region during loading by using PIV. Main advantage of this is to understand the state of cracks during a specified level of load.

Obtained strain fields for different load levels are represented below in Figure 5.33 - Figure 5.36. These analyses were carried out for one of the specimens of each series (12 specimens). Four of them are given here and the results for the remaining specimens (load - crack propagation images) can be found in the appendix.

Figure represents the images of specimen S 18-100-6 ($t/f_L = 3$) at different load levels. At the 1st stage (50 % of the peak load), no cracks are visible if examined with naked eye. However, PIV analysis show the most strained regions (where the cracks will begin to form) at around that load and micro cracks then fully develop

to propagate macro cracks. Similar comments can be made for the peak load stage and PIV represents distributed strains (which is a sign of multiple cracking) while only one major crack can be observed by naked eye. This shows the ability of PIV to monitor even very small strains/cracks during loading. The level of strains can also be distinguished by using PIV and the zones which are most susceptible to failure can be detected.

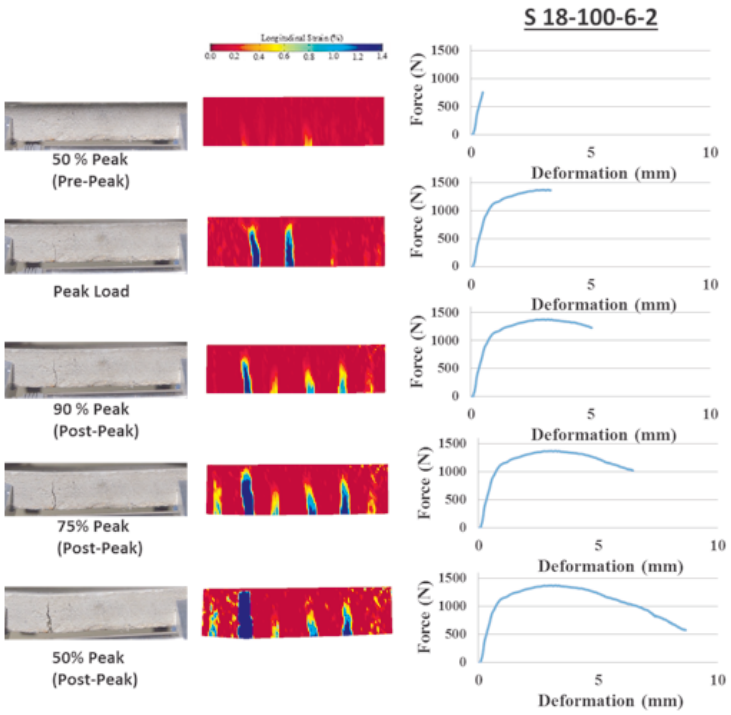

Figure 5.33. Crack Images and Strain Fields for Different load Levels of S 18-100-6-2.

Similar comments can also be made for the following figure for S 39-100-13 specimen again with a $t/f_L = 3$. It is possible to monitor the most strained regions even during the initial stages of loading. The highest level of strains are observed and distributed through the maximum moment region immediately after peak stress and strain localization begins as is represented by dark blue colour. In the end, one major crack is observed together with several other cracks. When the specimen surface was examined for cracks it was seen that four cracks were visible. However PIV represents that probably more cracks form in the specimen. If the strain fields given for specimens (S18-100-6 and S39-100-13) with a same t/f_L ratio (3) but different fiber lengths are compared, it is seen that 13 mm long fibers are relatively more effective in distributing

strains throughout the maximum moment region as is was mentioned before.

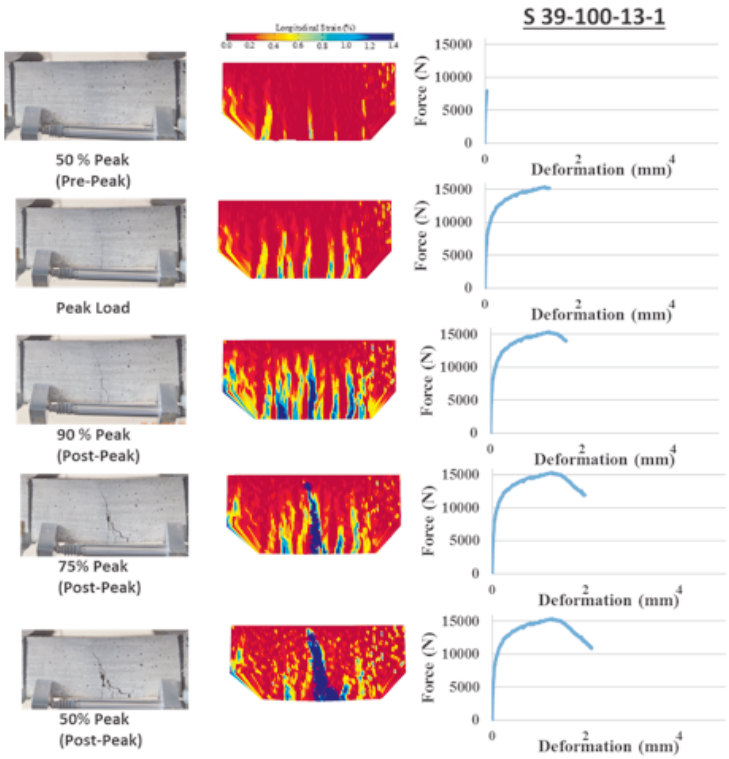

Figure 5.34. Crack Images and Strain Fields for Different Load Levels of S 39-100-13-1.

Figures given below for S 48-100-6 (t/f_L = 8) specimen represent a very good example by means of showing the behavior with an increase in t/f_L. Distribution of strains was very much localized from the beginning of loading. An increaese in load was observed following the 1st cracking, however accompanying strains were limited. While multiple cracking was clearly observed for the previous specimen with a t/f_L value of 3 (Figure 5.39-100-13), 2 single localized cracks were observed for S 48-100-6 (t/f_L = 8). This was also seen when toughness values of the 2 specimens were compared. Toughness of the specimen with a t/f_L value of 3 was calculated to be 24.6 MPa, while the toughness value for the one with a t/f_L value of 8 was 9.1 MPa.

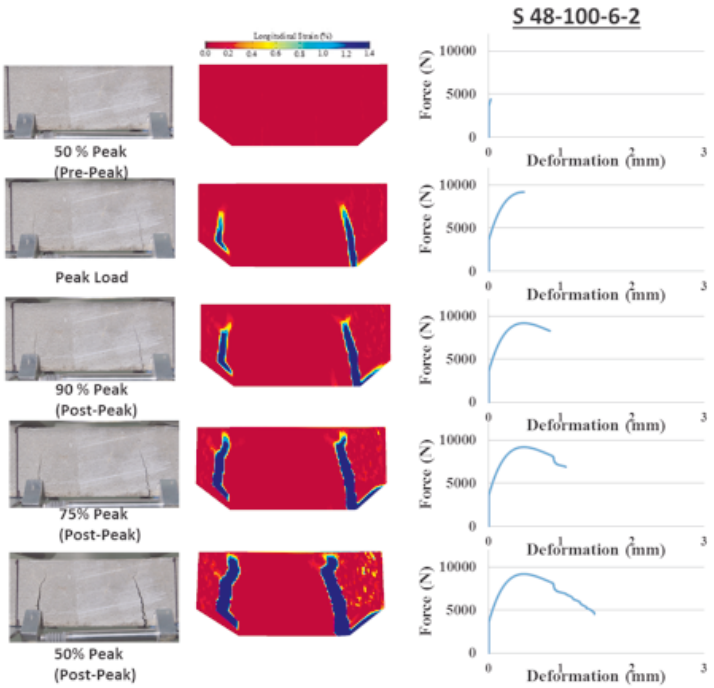

Figure 5.35. Crack Images and Strain Fields for Different Load Levels of S 48-100-6-2.

Figure 5.36 represents another specimen with a $t/f_L = 8$. However, this time fiber length is 13mm. This specimen also shows strain localization from the very beginning of loading. However, distribution of strains are more effective when compared to 6 mm fiber reinforced specimen with a $t/f_L = 8$. Toughness of this specimen is also low as expected (12.2 MPa)

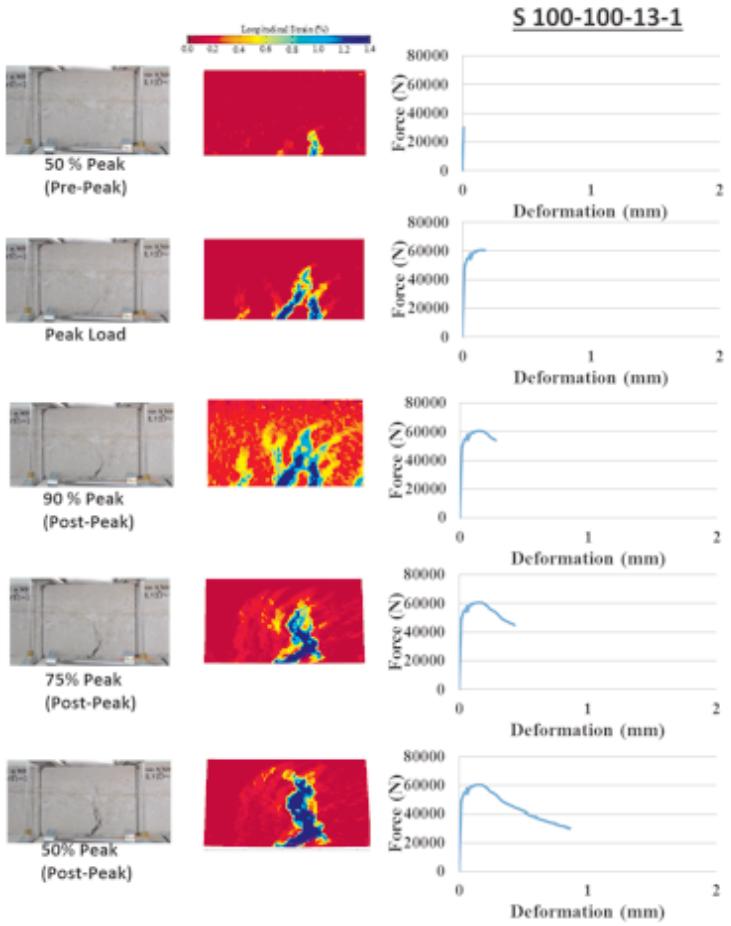

Figure 5.36. Crack Images and Strain Fields for Different Load Levels of S 100-100-13-1.

5.7.3. Crack width Propagations Along the Beam Height

When subjected to bending load, SC-FRCCs are susceptible to cracks originating from tensile stresses. Stress redistribution after crack occurrence leads to the development of stress concentrations where the cracks meet the bridging steel fibers. The fracture usually develops in the form of main crack, with branches, secondary cracks and the micro-cracking zone ahead. Various experimental methods are already employed to detect the fracture process. In this study, PIV analysis is used to measure displacement/strain field in the cracking area. Using displacement field data, crack openings are measured. The progressive opening of the cracks is studied using PIV, and continuous strain fields during cracking are provided as given above. The evolution

of the crack propagation in the maximum moment region, which was followed by PIV analysis are given below.

The total crack width values of the selected specimens were calculated through a summation of all the incremental crack width values from crack initiation until the end of loading, as shown in Figure 5.37-Figure 5.40. Ten images were selected (for each specimen) to obtain propagation of crack widths.

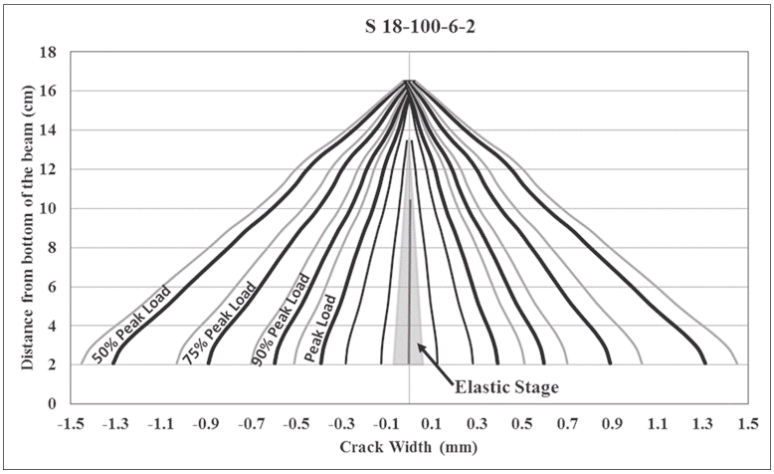

Figure 5.37. Evolution of Crack Opening Profiles During Loading for S 18-100-6 Beam Specimen.

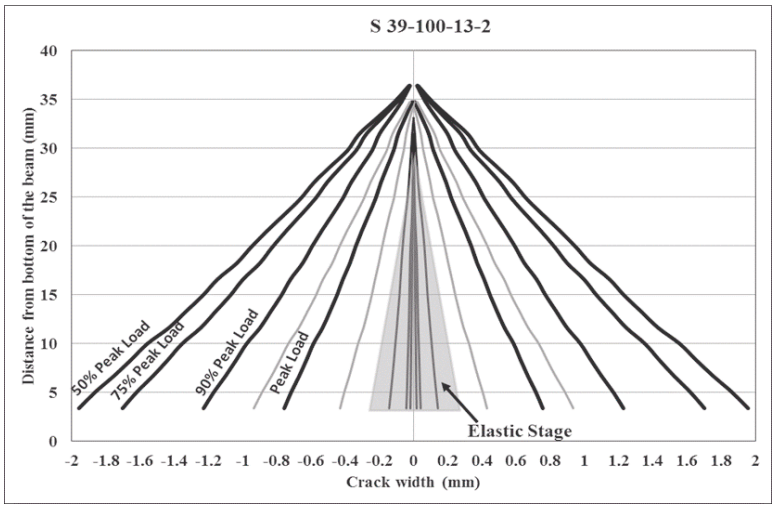

Figure 5.38. Evolution of Crack Opening Profiles During Loading for S 39-100-13 Beam Specimen.

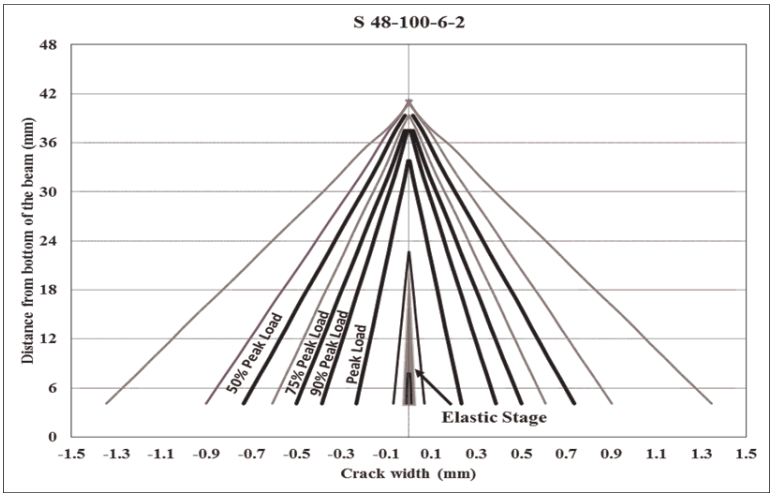

Figure 5.39. Evolution of Crack Opening Profiles During Loading for S 48-100-6 Beam Specimen.

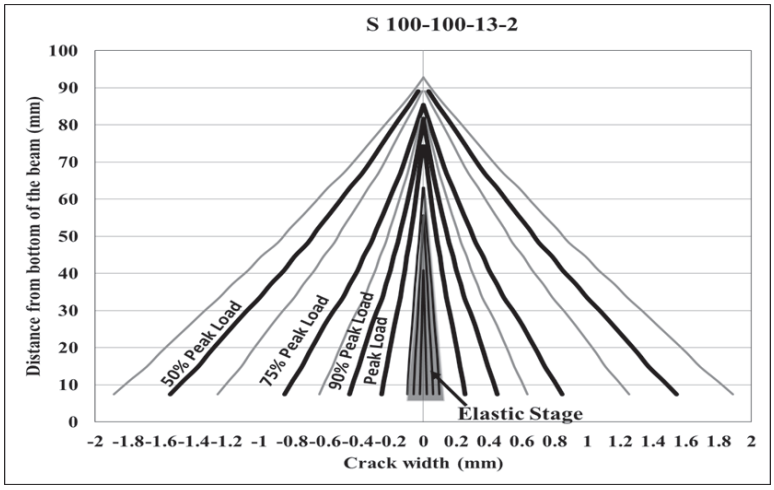

Figure 5.40. Evolution of Crack Opening Profiles During Loading for S 100-100-13 Beam Specimen.

In order to analyze the cracking propagation from crack opening profiles, behaviour of the selected beams was examined by using PIV. The shaded region represents the crack development in the pre-peak region. It can be observed that the crack profiles in the pre-peak region, up to peak-load stage, have very similar slopes and both the crack length and depth are rapidly increasing at each stage of loading. After peak-load stage, slopes of the crack profiles observed to decrease owing to the contribution of fibers. Fibers bridge the cracks following the cracking of matrix delaying the increase in the depth of crack. The increment in the crack length and depth decreases

in the post-peak region, when compared with the crack profiles in pre-peak region. If the specimens given above are compared by means of cracking behavior, the width of the crack sustained for every stage of loading decreases with an increase in t/f_L ratio and decrease in fiber length.

5.8. Cracking and Flexural Behavior Characterization

Table below wass given to compare the cracking behavior of specimens. All the specimens were examined by means of the number of cracks and comments were given below. As can be seen from the Table 5.9 number of cracks increases with an increase in fiber length representing greater multiple cracking capacity and consequently strain hardening behavior. Fiber orientation densities of these specimens in the casting direction (direction vertical to loading) were very similar as can be seen in the table. All specimens, having hooked end fibers observed to have only one major crack, but all these major cracks showed a significant branching behavior, differently from the major cracks formed in the specimens with straight fibers.

Figure 5.41 and Figure 5.42 which were given above in Section 5.3.3 can be seen below. These figures were given again to discuss the change in the behavior with an increased t/f_L and a review based on other studies found in literature was done.

As can be seen from the Figure 5.41 and Figure 5.42, deflection hardening capacity which is represented by increased stress/strain capacity after first cracking decreases with an increase in t/f_L ratio. One of the objectives of this study was to define a limit t/f_L value to represent transition from deflection hardening to deflection softening behavior. The results obtained here show that strain softening is seen for a t/f_L value of 8 for both 6 and 13 mm fibers. Studies given in literature are examined to see if a similar trend was observed.

Table 5.9. Comparison of the Cracking Behavior of Specimens, Examined by Means of the Number of Cracks.

	Specimen	a/d	t/f_L	AR	Toughness Factor (MPa)	FOD	Number of Cracks
	18-6-1	5.6	3	37.5	16.6		2
6 mm Straight Steel Fibers	18-6-2	5.6	3	37.5	14.4	0.685	1
	24-6-1	4.2	4	37.5	13.0		1
	24-6-2	4.2	4	37.5	13.0	0.689	1
	24-6-3	4.2	4	37.5	17.0		1
	30-6-1	3.3	5	37.5	12.3		1
	30-6-2	3.3	5	37.5	12.4	0.679	1
	30-6-3	3.3	5	37.5	12.7		2
	48-6-1	2.1	8	37.5	9.7		2
	48-6-2	2.1	8	37.5	9.1	0.682	2
	48-6-3	2.1	8	37.5	7.0		3
133 mm Straight Steel Fibers	26-13-1	3.8	2	81.3	25.1		2
	26-13-2	3.8	2	81.3	19.6	0.669	2
	26-13-3	3.8	2	81.3	20.1		6
	39-13-1	2.6	3	81.3	24.6		4
	39-13-2	2.6	3	81.3	24.5	0.668	1
	39-13-3	2.6	3	81.3	17.3		2
	52-13-2	1.9	4	81.3	16.2		7
	52-13-3	1.9	4	81.3	16.0	0.629	6
	65-13-2	1.5	5	81.3	13.8		2
	65-13-3	1.5	5	81.3	18.3	0.667	3
	100-13-1	1.0	8	81.3	12.2		2
	100-13-2	1.0	8	81.3	16.8	0.602	2
	100-13-3	1.0	8	81.3	17.9		2
Hooked Fibers	70-35-1		2	50.0	14.0	-	1
	70-35-2		2	50.0	13.6	-	1
	100-35-1		3	50.0	13.7	-	1
	100-35-2		3	50.0	12.6	-	1
	100-35-1		2	50.0	15.9	-	1
	100-35-2		2	50.0	15.3	-	1

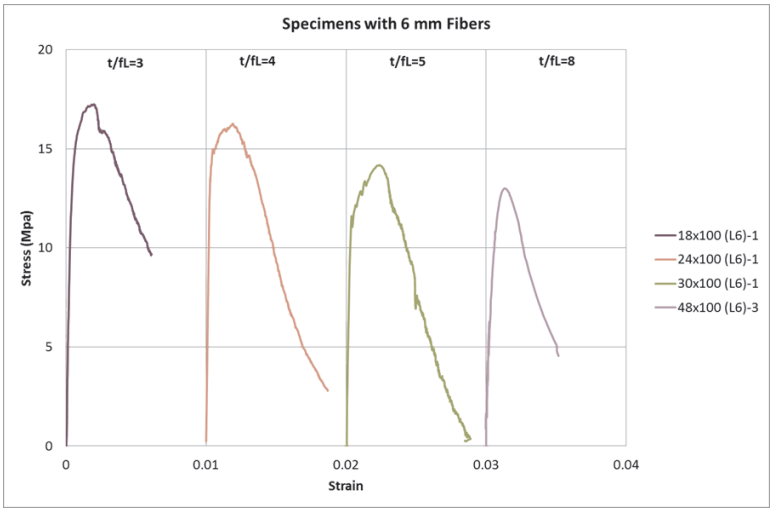

Figure 5.41. Stress-strain Relationship of Specimens having 6 mm Fibers.

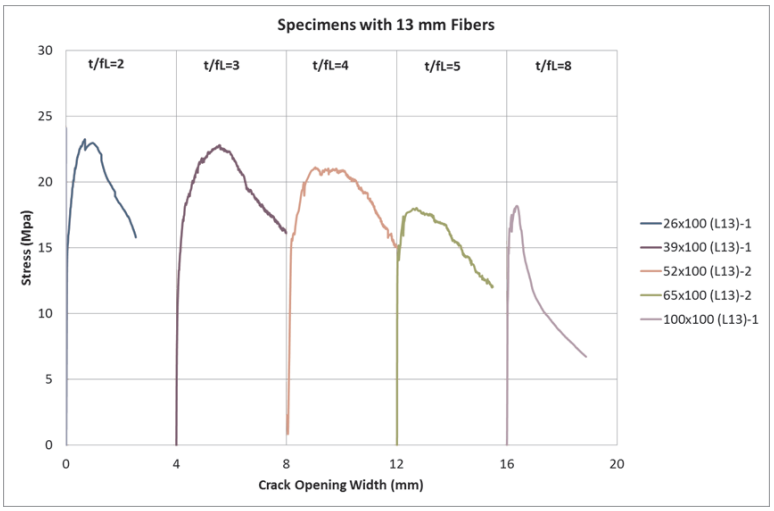

Figure 5.42. Stress-strain Relationship of Specimens having 6 mm Fibers.

In the previous study of Wille and Gustavo [150], effect of beam size, casting method, and support conditions were studied on flexural behavior of UHPFRC's. Considering experimentally tested beam sizes and fiber lengths (13mm straight steel fibers), specimens were calculated to have t/f_L ratios of 7.85 and 11.7 respectively and it was observed that both beam specimens undergo deflection softening behavior.

Again, in a previous study of Spasojevic [149], influence of tensile properties of UHPFRC on size effect in bending were studied in detail. When resulting stress-deflection curves were examined, comparing the peaks of the different curves, it can be noted that for FRC (Figure 5.43) the effect of varying specimen thickness on the bending strength of the member is very significant. The t/f_L ratios were calculated as, 1.3, 2.5, 5, 7.5, 12.5 and 25 respectively for beam thicknesses of, 25, 50, 100, 150, 250 and 500 mm. It can be seen from the Figure 5.43 for FRC specimens, the stress-deflection curve tends to become deflection softening as the beam thickness increases from 25 mm up to 500 mm. First three curves of Figure 5.43, with t/f_L tratios of 1.3, 2.5 and 5 respectively, seem to undergo deflection hardening behavior. But the rest of the specimens, with t/f_L ratios of 7.5, 12.5 and 25 clearly seem to undergo deflection softening behavior.

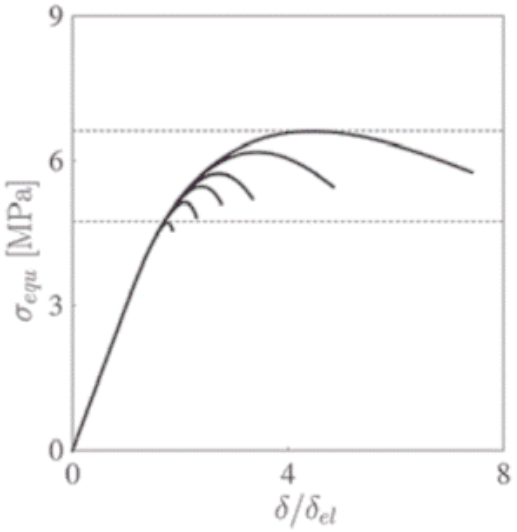

Figure 5.43. Bending Behaviour of Beams Made of FRC. [149].

These results support the finding of current study underlining that after a t/f_L ratio equal or greater than 8, bending behavior tend to become deflection softening, while it is still deflection hardening for a t/f_L value of 5.

5.9. Structural Design of Fiber-Reinforced Composites - Effect of t/f_L on the Constitutive Parameters Used for Material Characterization

The effect of t/f_L ratio on the performance of SC-FRCCs as evaluated through bending tests was represented above. One of the most common uses of these materials is in the area of non-reinforced thin structural elements. The reason for the limited use of these materials is the lack of the established codes and standards required for design as discussed before in the literature review section. There are several standards (RILEM CNR etc.) propose methods for serviceability (SLS) and ultimate limit state (ULS) designs of FRCs. Unfortunately, none of the methods are yet widely accepted and this implies the importance of further developing standards/methods suggested for FRCs. One of the main reasons for delayed adaptation of the suggested design methods by the industry is the problems faced during material characterization. Vast amount of research carried out on fiber-reinforced cement-based materials almost always represent difficulties related to the homogeneity of the material.

Several design methods offered by different codes are summarized in the literature review section. One of the most specific design methods for fiber-reinforced concrete materials is given in the Italian Guideline CNR-DT 204/2006 [29]. Deriving the material properties used in the design methods is an important issue. Bending test is used most of the time, since it is easier to apply when compared to other tests such as direct tension test. However, calculation methods require direct tensile capacities and a translation method is needed [60]. Jansson *et al.*, [60] reviewed the applied translation methods for how the flexural strength can be translated into direct tensile strength and reported that most of them were similar. It was also stated that Italian guideline takes a step forward when compared to other methods, by the introduction of a characteristic length.

In this Section of the study, tensile capacities of the produced specimens (with different thickness and as a result different t/f$_L$ ratio) were calculated as described by the Italian Guideline and performance parameters (for SLS and ULS) calculated for tension were compared for different t/f$_L$ ratios.

5.9.1. Characterization of Flexural Behavior According to CNR-DT Guideline and Constitutive Parameters

In 2006, the Italian National Research Committe published the Guide CNR- DT 204 for the Design, and Construction of Fibre Reinforced concrete structures. This document proposes two different relations for the tensile behaviour of FRC: the linear elastic model and the plastic rigid model, both expressed in terms of σv s.ε and σv s.w diagrams.

Coherently, with a straightforward application of current CNR-DT guideline on the design of SFRC structures [29], from the nominal stress versus COD curves, direct the equivalent post-cracking strengths can be calculated as indicators of the material mechanical performance. The linear elastic model of CNR-DT identifies two reference values, f$_{Fts}$ and fFtu, concerning SLS and ULS behaviour respectively.

Details of the standard were given in the literature review section. f_{Fts} and f_{Ftu} were calculated by using the following equations for linear elastic model.

$$f_{Fts} = 0.45 f_{eq1} \tag{5.5}$$

$$f_{Ftu} = k\left[f_{Fts} - \frac{w_u}{w_{i2}}(f_{Fts} - 0.5 f_{eq2} + 0.2 f_{eq1}\right] \geq 0 \tag{5.6}$$

feq1 and feq2 are, respectively, post-cracking equivalent strength useful for the SLS and ULS. feq1 and feq2 were evaluated in the following intervals; 3.wI = w = 5.wI and 0.8.w_u = w = 1.2.w_u, where wI represents the crack opening corresponding to cracking, calculated where the maximum load is recorded during the test, CNR-DT 204/2006 in the interval 0 = w = 0.1 mm. For the ultimate crack opening, w_u, a value equal to 2,5 mm is assumed (since that was the minimum crack opening value which was possible to obtain for all the specimens) . Therefore, feq1 and feq2 correspond to crack opening equal to wi1 = 4.wI and wi2 = w_u, respectively. k is a coefficient equal to 0,7 for cross sections fully subjected to tensile stresses and equal to 1 for other cases. wi2 is the mean value of the crack opening at the endpoints of the interval where feq_2 is evaluated in (Figure 5.44).

Table 5.10 gives the values of f_{Fts} and f_{Ftu} respectively, calculated by following the procedure defined in the guideline as summarized above.

As is seen from the table, f_{Fts} data which represents performance for SLS, is similar for all of the specimens since it considers a very small range of w values in the initial stages of the test when 0 = w = 0.1 mm. Greater differences are observed for f_{Ftu} since it represents the ultimate limit state residual strength (for an assumed ultimate crack opening, w_u = 2,5 mm). As is seen from the table f_{Ftu} is almost equal or smaller than "0" for high values of t/f_L for all of the fiber lengths, which means no residual strength in the ultimate state.

Table 5.10. Calculated f_{Fts} and f_{Ftu} data which represents performance for SLS and ULS.

Specimen	t/f_L	SLS (fFts) (MPA)	ULS (fFtu) (MPA)
S 26-13-2	2	9.8	3.2
S 39-13-2	3	8.3	3
S 53-13-3	4	8	3.1
S 65-13-2	5	7.9	2.8
S 100-13-2	8	8.7	0.6
S 18-6-1	3	7.4	1.3
S 24-6-2	4	7.1	1
S 30-6-3	5	6.1	0.6
S 48-6-1	8	5.8	-

Calculated f_{Fts} and f_{Ftu} data can be used for structural design of SC-FRSCs as outlined in the code. Basic requirements must be satisfied for structural use of fiber reinforced materials based on the applied load and the boundary conditions of the element. According to the guideline (CNR DT) the material discussed here can't be used for structural applications without conventional reinforcement since following requirement is not satisfied.

$$(f_{Ftu}/f_{Fts}) \geq 1,05 \tag{5.7}$$

For this requirement to be satisfied, the SC-FRCC material should yield strain hardening behavior (under direct tension), as well as it represents deflection hardening behavior. Therefore, this material can be used with certain amount of conventional reinforcement or for semi-structural applications.

5.10. Relationship Between Deflection and COD

5.10.1. Importance of Determination of a Relationship Between Deflection and CMOD

Determination of toughness parameters of materials is necessary for structural design of fiber reinforced materials as explained above. Toughness parameters can be obtained by using stress - deflection or stress - crack opening relationship. Studies to relate COD results to deflection values has been conducted in the past since it may not be possible to carry out both tests at the same time. Ding [151] stated the importance of finding a relationship among deflection and CMOD value of FRCs considering the need for predicting the possible maximum crack width for a given deflection because the crack width is an important parameter both for the structural safety, for the serviceability and the durability of SFRC elements. He also mentioned observed difficulties in selecting the fiber length correctly if crack width of the loaded beam elements can't be defined, especially where a large deformation or wide cracking may occur. It is therefore important to investigate the crack development under a given deflection [151] and efforts were made to relate deflection and COD results for cement-based materials.

5.10.2. Relationship Between COD and Deflection from Previous Studies

This section gives simple correlations between the mid-span deflection and the crack opening displacement (COD) from the previous studies in literature and guidelines. In order to investigate the relationship between the deflection behavior and the crack width developing, the crack mouth opening process has been measured simultaneously with the beam deflection. Vandewalle and Dupont [152], determined an average relationship between CMOD and midspan deflection, which is only applicable in the post-peak region, as following :

$$\delta = 0.85CMOD + 0.042 \tag{5.8}$$

where δ is the deflection (mm); CMOD is the crack mouth opening (CMOD) value (mm).

Vikram and Sivakumar [153] studied the linearity between deflection and CMOD in hybrid fiber reinforced concrete and figured out the below relationship as in Equation 5.9 for plain concrete specimens:

$$\delta = 0.96CMOD + 0.004 \tag{5.9}$$

In the study of Farhad [154], the proposed equivalences between CMOD and deflection for SCC beams were given as in equations below: For plain concrete beams:

$$PlainConcrete(N - SCC) : \delta = 0.70CMOD + 0.12 \tag{5.10}$$

For steel fiber reinforced beams:

$$FRC\,(D - SCC) : \delta = 0.88CMOD + 0.19 \tag{5.11}$$

All of the proposed linear equations relate deflection and COD in slope - intercept format (y = mx + n) and slope values are similar to each other. Other researchers also mentioned the linearity of the relationship between deflection and COD values [155].

In this study variation of deflection vs. COD relationship based on varying t/f_L values were investigated, since slope values were observed to change with an increase in t/f_L ratio. Results are given below.

5.10.3. Relating Deflection and COD Based on t/f_L Ratio

A series of bending beam tests on SC-FRC, with different fiber lengths, fiber types, beam dimensions and consequently different fiber orientations and t/f_L ratios

have been carried out, as it was mentioned in the previous chapters. Based on the experimental results, relationship between the deflection and COD of SC-FRCC was aimed to be established. This relationship relies on the load-deflection and the load-COD behaviors of the beams tested under bending. Ultimate values of mid-span deflection and COD were determined for each of the specimens from the results of flexural tests and slope of the deflection/COD curves were measured in order to understand the effect of t/f_L on the deflection/COD relationship (detailed linear curve fittings in the y=Ax+B format will be given in the following chapter). It was decided to use only 2 duplicates of specimens having the same geometry and including the same fibers, for the sake of time.

It can be seen from the Table 5.11 that t/f_L ratio influences mid-span deflection, whereas the ultimate COD value is kept constant (2.5 mm). 2.5 mm value of maximum COD was determined according to the specimen undergoing the lowest COD value, and it was set as a maximum limit for all of the specimens, in order to make consistent comparisons. It is seen that, as the t/f_L ratio increases, deflection/COD (d/c) ratio decreases, both for 6mm and 13mm fiber reinforced specimens.

The decrease in the deflection/COD ratio goes further down even to 1 for the higher t/f_L ratios of 8, which is implying that the deflection and crack opening values are becoming nearly the same for the increased values of t/f_L. For constant fiber lengths (when 6mm and 13 mm fiber reinforced specimens are considered separately) this can be explained by the decreased effectiveness of the fibers for bridging the cracks, due to the increased beam thickness. For lower beam thickness values (and lower t/f_L values for constant fiber length), it is seen that deflection and COD values diverge from each other, and deflection even goes further up to 3 times of COD values. This can be explained as, for the beams with small thickness, crack opening values are very low compared to deflection values, which indicate that the fibers play more effective role to resist the crack openings, even though undergoing high amount of deflections.

Table 5.11. Results of Mid-span Deflection/COD (d/c), Obtained from Load-Deflection and Load-Crack Opening Displacement Curves.

			*From F-d and F-COD curves			
t	fL	t/f_L	Mid-Span Deflection (d) (max) (mm)	COD (c) (max) (mm)	Deflct./COD (d/c)	AVG d/c
18	6	3	6.2	2.5	2.5	2.8
18	6	3	7.6	2.5	3.0	
24	6	4	4.6	2.5	1.8	2.0
24	6	4	5.2	2.5	2.1	
30	6	5	4.0	2.5	1.6	1.6
30	6	5	4.1	2.5	1.6	
48	6	8	2.6	2.5	1.0	1.0
26	13	2	4.5	2.5	1.8	1.9
26	13	2	5.0	2.5	2.0	
39	13	3	3.6	2.5	1.4	1.7
39	13	3	4.8	2.5	1.9	
52	13	4	2.9	2.5	1.2	1.1
52	13	4	2.4	2.5	1.0	
65	13	5	2.5	2.5	1.0	0.9
65	13	5	2.2	2.5	0.9	
100	13	8	1.2	2.5	0.5	0.5
100	13	8	1.5	2.5	0.6	
70	35	2	1.7	2.7	0.6	0.7
70	35	2	1.9	2.4	0.8	
100	35	3	1.8	2.4	0.8	0.7
100	35	3	1.3	2.3	0.6	
100	50	2	1.6	2.7	0.6	0.6

Considering the specimen groups of different fiber lengths separately, for the same t/f_L value of 3, the deflection/COD ratio is 2.8 for 18 mm thick beams having 6 mm fibers and it is 1.7 for 39 mm thick beams having 13 mm fibers.

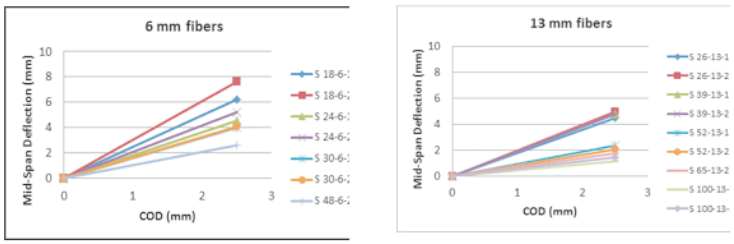

(a) (b)

Figure 5.44. Relationship Between t/f_L and Deflection vs. COD Curves for Specimens having a) 6mm and b) 13 mm Fibers.

Figure 5.44 gives the relationship between deflection vs. COD curves and t/f_L ratios for all of the specimens. For specimens having different length of fibers, it can be seen from Figure 5.44 (a) and (b), short fiber (6 mm) reinforced specimens, represented higher COD values for the same mid-span deflections when compared to long fiber (13 mm) reinforced specimens (for a constant t/f_L value). This can be explained again by the effectiveness of fibers, since the ability of bridging cracks decreases with decreased fiber lengths, resulting in less resistance to crack opening.

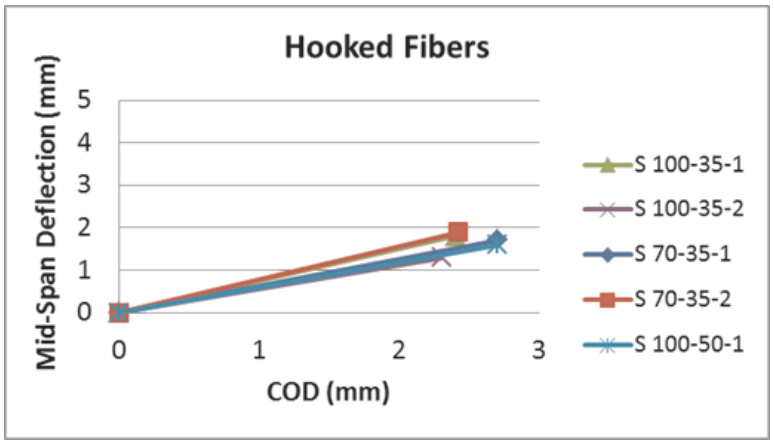

Figure 5.45. Relationship Between Deflection and COD Curves for Specimens having Hooked Fibers.

For the specimens with hooked fibers, it can be observed from Figure 5.45 that, very small amount of mid-span deflections, correspond to very high crack opening values. This can be explained by the decreased ability of bridging cracks, due to decreased amount of fibers and their inability to arrest micro-cracks, which causes a sudden opening of one major crack.

$$y = A.x + B \tag{5.12}$$

$$\delta = A.COD + B \tag{5.13}$$

First the relationship between the deflection and COD of each specimen was

determined from the experimental results of force vs. deflection and force vs. COD curves. After plotting deflection-COD curves of each specimen, trend-lines were fitted on each curve and the constants of A and B of every specimen were determined separately for this linear relationship, as given in table:

Linear trend-line fitting on the curves taken from the results of flexural tests (Load-deflection and Load-COD curves) giving the relation between the deflection and COD for 4 selected specimens can be seen in the Figure 5.44, as follows:

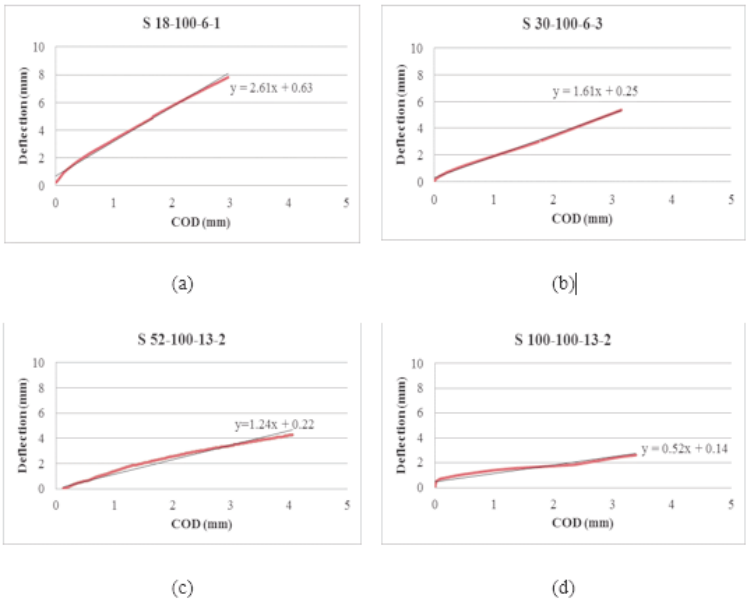

Figure 5.46. (a-d) Fitting Linear Trendlines and Determining Equations for Deflection-COD Relationships of Some Selected Specimens.

Table 5.12. Slope (A) and Constant (B) values Calculated form Thefitted Linear Trendlines for all Specimens.

t	fL	A (slope)	B (constant)
26	13	2.5	0.3
26	13	2.4	0.2
39	13	1.3	0.1
39	13	2.1	0.4
52	13	1.2	0.2
52	13	1.6	0.1
65	13	1.1	0.1
65	13	0.9	0.3
100	13	0.5	0.1
100	13	0.8	0.4
18	6	2.6	0.6
18	6	3.0	0.9
24	6	1.7	0.5
24	6	1.9	0.6
30	6	1.7	0.5
30	6	1.6	0.3
48	6	1.1	0.3

Afterwards, the slope (A) is plotted against t/f_L to evaluate the variation of slope with an increased t/f_L, for all the specimens (Figure 5.47).

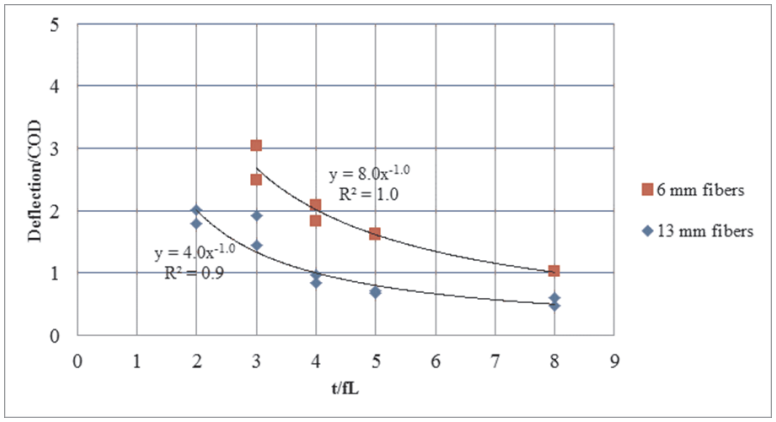

Figure 5.47. Relationship Between Slope (A) and t/f_L.

In the Figure 5.47 the relationship between t/f_L and deflection/COD ratios can be seen. There is a decreasing trend of deflection/COD ratio with increased t/f_L for both groups of the specimens. And, considering the same t/f_L values, the difference between the deflection/COD ratio (of 6mm and 13mm specimens) observed to diminish as the t/f_L value increases. Therefore, for the very high values of t/f_L ratio, the effect of fiber length on crack opening disappears (d/c = 1 for both fiber lengths) since the beam thickness increases and effectiveness of fibers resisting cracks decreases.

If the slope values of deflection vs. COD curves and t/f_L values were plotted against each other, a curve may be fitted to data to predict slope (A) by means of varying t/f_L.

$$For specimens having 6mm fibers : A = 8(t/f_L)^{-1} \tag{5.14}$$

$$For specimens having 13mm fibers : A = 4(t/f_L)^{-1} \tag{5.15}$$

This indicates that with an increase in beam thickness or t/f_L ratio, the slope of deflection vs. COD relation decreases. Therefore, it can be concluded that as the beam thickness or t/f_L ratio increases, COD values tend to decrease for the same mid-span

deflection.

Therefore a simple equation which predicts deflection by means of COD and t/f_L can be given as follows:

$$For specimens having 6mm fibers : d = \frac{8}{t/f_L}.COD \tag{5.16}$$

$$For specimens having 6mm fibers : d = \frac{4}{t/f_L}.COD \tag{5.17}$$

$$For specimens having 6mm fibers : d = \frac{1}{t/f_L}.COD \tag{5.18}$$

5.10.4. Use of the Proposed Equations for Predicting Deflection vs. COD Behavior for Different Materials Reported in Literature

In the scope of this study, for determining simple relationship between deflection and crack opening displacement (COD) based on t/f_L value, results of the specimens having below properties were tested experimentally.

Table 5.13. Properties of the Tested Specimens for this Study.

Şanal PhD Thesis (2015)	
Straight	Hooked
t=18 to100 mm	t=70 -100 mm
fL=6-13mm Straight	fL=35-50 Hooked
t/f_L= 2 to 8	t/f_L= 2 and 3
AR: 37.5-81.3	AR: 50
Vf=1.2%	Vf=1.2%
4-pt (Unnotched)	4-pt (Unnotched)

Determined relationships 5.16 - 5.18 were used to see their ability to predict deflection when different materials used. Data found in literature was used. Table 5.14 represent data from previous study of the researchers for straight steel fibers.

Table 5.14. Properties of the Tested Specimens with Straight Steel Fibers [17] and [101].

Ferrara *et al.*, (2011)		Şanal MSc Thesis (2010)		
Beam L1	Beam L2	25-13	50-06	50-13
t=30 mm	t=30 mm	t=25 mm	t=50 mm	t=50 mm
fL=13mm Straight	fL=13mm Straight	fL=13mm Straight	fL= 6mm Straight	fL= 13mm Straight
t/f_L= 2.3	t/f_L= 2.3	t/f_L= 2	t/f_L=8	t/f_L= 4
AR: 81.3	AR: 81.3	AR: 81.3	AR: 37.5	AR: 81.3
Vf=1.27%	Vf=1.27%	Vf=1.2%	Vf=1.2%	Vf=1.2%
4-pt (Unnotched)	4-pt (Unnotched)	4-pt (Unnotched)	4-pt (Unnotched)	4-pt (Unnotched)

Figure 5.49 represent that proposed equation predicts deflection vs. COD relation with a close proximity for different specimens.

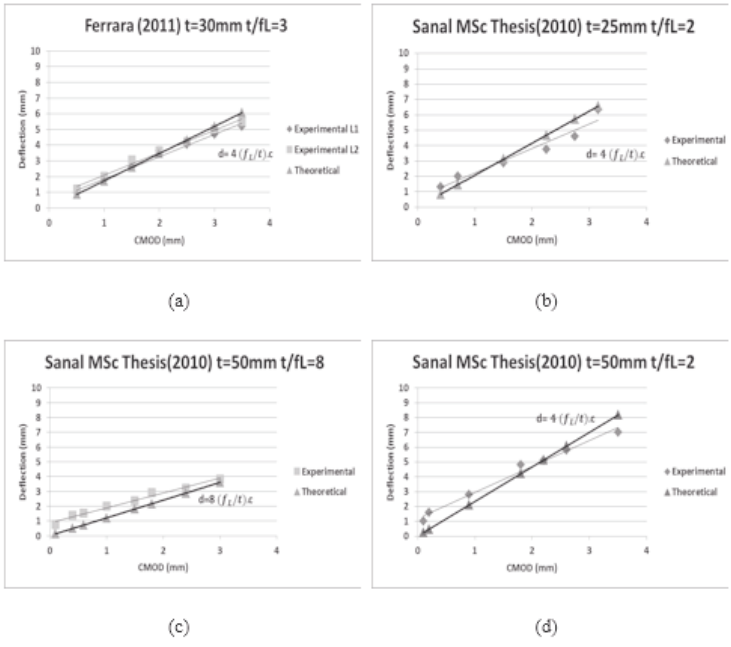

Figure 5.48. Deflection -COD Curves of the Tested Specimens with Straight Steel Fibers [17] and [101].

Table 5.15 shows data found in literature which represent experimental studies carried out by using hooked en fibers. Studies are different by means of their experimental set up, matrix properties and fiber volume ratios as can be seen in Table

5.15.

Table 5.15. Properties of the Tested Specimens with Longer Hooked-end steel Fibers [151], [156], [157], [158].

Robins (2001)			Lameiras (2015)	Gopalaratnam (1995)	Ding (2010)
1	2	3			
t=50 mm	t=75 mm	t=100 mm	t=150 mm	t=90 mm	t=150 mm
fL=30mm Hooked	fL=30mm Hooked	fL=30mm Hooked	fL=35 mm Hooked	fL=30 mm Hooked	fL=60mm Hooked
t/f_L=1.7	t/f_L=2.5	t/f_L=3	t/f_L=4	t/f_L=3	t/f_L=2.5
AR: 60	AR: 60	AR: 60	AR:63.6	AR: 60	AR: 66.7
Vf=1.7%	Vf=1.7%	Vf=1.7%	-	Vf=0.5-1%	-
4-pt (Unnotched)	4-pt (Unnotched)	4-pt (Unnotched)	3-pt (Notched)	4-pt (Unnotched)	3-pt (Notched)

Figure 5.49 shows the data obtained by using the proposed equation together with experimental data reported by researchers (Table 5.15). As can be seen from the figure proposed equation predict the behavior to some extent. The extent to which the behavior was predicted was considered to be good since not only t/f_L but many other parameters (matrix, experimental set - up fiber volume, fiber properties, etc.) were also different for these studies.

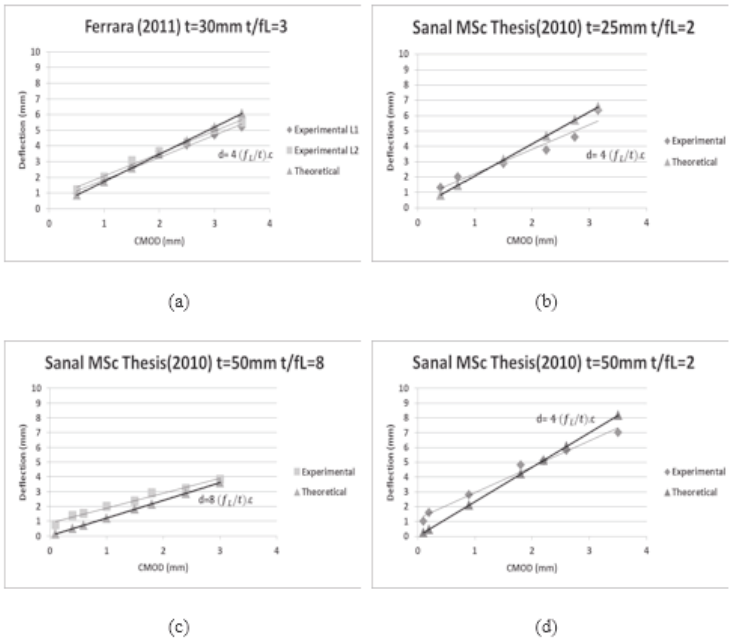

Figure 5.49. Deflection -COD Curves of the Tested Specimens with Longer Hooked-end Steel Fibers.

6. CONCLUSIONS

Main objective of this study was to identify the different behaviors of SC-FRCCs in terms of fresh and hardened state performance by considering the parameters such as specimen thickness/fiber length ratio (t/f_L), specimen width/ fiber length ratio (w/f_L), fiber type (straight or hooked), and fiber aspect ratio. Specimens were cast using same mix designs, only fiber length, fiber type, specimen depth and specimen width were varied.

A series of experiments were performed to examine the fresh and hardened state properties of SC-FRCCs by means of mini-slump flow, mold flow, fiber orientation, flexural strength and toughness, strain localization, crack propagation and crack typology.

6.1. Fresh State Performance

6.1.1. Evolution of Flow From Mini Slump Flow

Mini slump flow diameters were recorded from the captured images, for different time intervals.

Comparison of the flowing behaviors between different mortars (plain, 6mm fiber-reinforced and 13mm fiber-reinforced) was done. Spread evolution over time for reaching a selected diameter, velocities over time of different mixes were plotted, and PIV displacement vectors and strain fields were calculated in order to figure out a more detailed understanding of the mini-slump flow behavior.

- It was observed that plain mix has a lower yield stress when compared to fiber-reinforced mixes as expected.
- 6mm fiber-reinforced and 13mm fiber-reinforced mixes gave lower final spread diameters probably due to entanglement of fibers.

- Fiber-reinforced mixes represent oscillating velocity curves during the flow whereas plain mix shows a smooth decreasing curve, due to the resistance of fibers to flow and this resistance further increases for higher fiber lengths.
- First observation from strain distributions was that, plain mix flows in a more symmetrical circular shape, whereas mixes with fibers tend to flow more non-symmetrically with an elliptical shape.
- It was seen that plain matrix represent a large and circular initial spread when compared to fiber-reinforced mixes.
- It was seen that strain fields obtained from the plain mix are more homogenous when compared to the strain fields obtained from fiber-reinforced mixes. Therefore, when strain fields are evaluated, it is seen that flow of material is restricted when fibers are used (based on coloured strain legends).

These results show that PIV can give detailed information (when compared to conventional methods) about the fresh state behavior of cement-based materials, especially when distinguishing between similar materials are needed.

6.1.2. Dynamic Segregation Resistance

Fiber weight percentages in different Sections of flow area were measured for all mixes, in order to observe the dynamic segregation resistance and fiber driving ability of the mixes.

- It was seen that fibers tend to accumulate in the middle region, causing a decrease of the fiber volume in the outer regions and some heterogeneity in distribution of fibers was detected. This result was in accordance with the strain distributions, since varying values of strains representing fiber resistance to material flow was seen for fiber-reinforced mixes. However, the extent of dynamic segregation was not severe, and it was considered to be in the acceptable limits.

Comparison of fiber weighing and PIV strain fields (obtained by analyzing images obtained during mini-slump flow test) represent that PIV can be employed to evaluate

material flow and dynamic segregation resistance of fibers.

6.1.3. Monitoring of Material Flow Using PIV

Vector profiles of flow of material throughout casting into the mould were obtained using PIV and were illustrated in order to roughly evaluate fiber alignment in the material.

- It was seen that the material flows in a direction parallel to the casting direction. Deviations of flow vectors from the flow direction were measured and found to vary between 0-25^o.
- It was concluded that PIV may be used to evaluate fiber alignment state of a material in a qualitative manner.
- This measurement was further evaluated together with the optical microscope images obtained from sections of specimen cut from the middle sections. Image analyses results represented fiber alignment (orientation) densities going up to 0,7 in the flow direction (direction of casting). This result is in accordance with the observation made using PIV.
- It was observed that use of fiber-reinforcement significantly increases ultimate flexural load, whereas it does not have an effect on the stiffness of the specimens (slope of the curve in the elastic region).
- Considerable reduction in vertical deflection was observed for composite specimens, as fibers resist the cracks and tend to disperse them into multiple fine cracks effectively.
- It can be concluded that maximum load bearing capacity (peak load) and flexural toughness of unreinforced matrix are significantly increased by the addition of fibers.
- When fiber bridging is introduced, the peak load is shown to be much less dependent on matrix properties. Instead fiber and interface parameters dominate peak load of the SC-FRCC beam.

Stress vs. strain graphs were also obtained to be able to compare the behaviors of the plain specimens with varying sizes.

- It was observed that shallower beams yielded higher values of bending strength (MOR). This was expected since larger specimens are more likely to include critical defects of larger size. However decrease in strength was not as consistent and severe as it was expected (MOR values for the specimens with different thicknesses are found to be similar). This result supports the findings of one of the previous studies reported in literature [146] which mentions limited effect of size on bending strength when high performance specimens were used.

6.1.4. Specimens with Straight Steel Fiber Reinforcement

6.1.4.1. Fiber orientation density (FOD) calculations. In order to do fiber alignment analyses, beam specimens were cut into 2 pieces following four-point bending tests, microscopic images were taken from the cross sections by using an optical microscope. Then the fiber cross sections were marked on the image file in Adobe Photoshop, and the center coordinates of each fiber location were found using the "ImageJ" image analysis program. Then these microscopic images were analyzed by using a tensor description method as summarized in Section 2.8.

- Effect of t/f_L on Fiber Orientaion

- Similar FODs were obtained in the direction of flow confirming the effectiveness of control of the material flow during casting. A controlled casting procedure for SC-FRCC may provide an effective alignment of fibers in the direction of casting as it was also mentioned in the previous studies [101].

This result is important by means of evaluating hardened state mechanical performance since most of the time differences in bending behavior is related to the differences in fiber orientation density. This finding represent that fiber orientation itself is not responsible for variation in mechanical performance.

6.1.4.2. Stress-strain relationships. Stress-strain relationships of specimens including 6 mm and 13 mm fibers were plotted and discussed, considering changes in t/f_L ratio and fiber orientation.

- Change in material performance was observed when specimen thickness and fiber length are varied. First crack stress and strain, the length of multiple cracking zone, equivalent bending strength and strain are all changed.
- With decreased t/f_L ratios, specimens represented an increase in strength (some multiple cracking) after occurence of the first crack. However, the extent of the region between LOP and MOR was observed to be different, where this region represents the ability of material to undergo multiple cracking.
- With decreased t/f_L ratios, an increase in strain (even for constant stress values) was also observed. The reason for increasing strain was considered to be the slow pull out process of "the crack bridging fibers" from matrix with an increasing load.

6.1.4.3. Stress-COD relationships. A similar trend is observed when stress-COD curves are examined. Average peak COD values were also found to depend on t/f_L ratio.

6.1.4.4. Examination of first crack stress and equivalent bending strength results. Average 1st crack strength and equivalent bending strength values were evaluated.

- No pronounced change in the first crack stresses was observed with an increase/decrease in the thickness of the specimens. This result was expected since the 1st crack stress is assumed to be a representation of matrix performance.
- When the equivalent bending strengths of the specimens were examined, systematic decrease with an increase in t/f_L ratio was observed for all the specimens. It should again be noted that, fiber alignment densities were found to be very similar for these specimens, emphasizing that decrease obtained must be mainly due to changing t/f_L ratio.
- Strength increase from first crack stress to equivalent bending stress was found

to be higher when 13 mm fibers were used as expected representing increased multiple cracking ability with an increase in fiber length.

6.1.4.5. Examination of peak strain and peak COD results. Average peak strain values of the specimens with different t/f_L ratios were also examined, since it represents the extent of multiple cracking zone. Increased peak strain value means increased strain hardening capacity of the material.

- A decreasing trend was observed in peak strains with an increasing t/f_L ratio. Only the specimens with a thickness of 100 mm ($t/f_L = 8$) yielded different results representing much lower peak strain value. A similar result was observed for the plain specimens with a thickness of 100 mm.
- With an increase in t/f_L ratio, a decreasing trend of average COD values was observed, which were normalized by dividing the average COD values with the corresponding beam heights. As a result of this, decreased COD in the unit beam length when the t/f_L ratio is increased. This can be explained by the decrease of multiple cracking behavior as a result of decreased efficiency of crack bridging mechanism, with an increase of the beam height.

6.1.4.6. Flexural toughness. In this work, JSCE SF-4 [40] standard technique has been followed, as mentioned and described in the previous sections. The area under the load-deflection plot up to a deflection of span/150 is obtained and a flexural toughness factor (FT) is calculated, according to this method.

- It was observed that energy absorption capacities (toughness) of the materials decreased with an increase in t/f_L value.
- Decrease in toughness was seemed to be lower when long fibers were used as it was the case for equivalent bending strength also.

In order to have a detailed understanding of the realtionship between FT and cracking behavior, total projected crack areas were calculated from the crack monitoring images

taken during the flexural tests. The total projected crack areas were normalised over the area of the maximum moment region (thickness of specimen*LVDT measuring range), for obtaining normalised crack area values.

- It was seen that both normalized crack areas and toughness factor of specimens decreases, when t/f_L ratio increases for all specimens. This was due to the decrease in multiple cracking ability of material with an increasing t/f_L value, yielding lower strain capacity and toughness. It was also observed that cracking ability of short fibers (6mm) is limited when compared to 13 mm fibers.

6.1.4.7. Effect of w/f_L on the hardened state mechanical performance. The effect of w/f_L was also studied in the scope of this study, in addition to detailed examination of effect of t/f_L.

- It was observed that strain capacity of the specimens highly increase when width of the specimens decrease (w/f_L decreases). It was seen that this behavior obtained due to the more effective alignment of fibers in the casting direction (the X direction), since mould walls cause a restriction and force the material to flow in the direction of casting. This result was confirmed by image analyses which represented decreased fiber alignment with an increased w/f_L.
- Change in w/f_L, observed to have no effect on equivalent flexural strengths of these specimens. However, pronounced difference in the strain values were observed. This is probably because of the increased fiber bridging capacity obtained due to more effective alignment of fibers.

If the effect of t/f_L and w/f_L parameters are evaluated together (for straight fiber reinforced specimens), it can be said that changing width of the specimen mostly effects fiber alignment state resulting in a change in the strain capacity and toughness of the material. On the other hand the extent to which changing t/f_L effects fiber alignment is much smaller, however equivalent bending strength and toughness is still affected.

6.1.5. Specimens with Hooked-end Steel Fiber Reinforcement

Hooked end fibers were used to understand the effect of different fiber types on the hardened-state performance. Following results were found.

- For the same t/f_L ratio, fiber aspect ratio was found to a major role in determining the behavior after initial crack, higher aspect ratios yielding higher equivalent bending strength values (when different types of fibers were compared). Fiber length was also effective in increasing equivalent bending strength, however its effect was less significant (specimens reinforced with 2 different lengths of hooked end fibers were compared (t/f_L =2)).
- It was not possible to clearly observe the effect of decreasing t/f_L for long fibers since the range of t/f_L values were limited by the size of the specimens which would fit into the equipment used in the lab. Only two different t/f_L ratios were obtained by using the same hooked end fiber and changing the specimen thickness. Similar results as obtained from the straight fibers (decreased multiple cracking ability with an increase in thickness) was observed.

6.1.6. Hardened State Performance Results from PIV Analysis

The reason for choosing PIV as one of the techniques to be used for this study was to comprehensively evaluate cracking behavior of SC-FRCCs. The ability of the PIV technique in evaluating precise crack widths of the tested beam specimens was verified. Also, the progressive opening of the cracks was studied using PIV.

- Very similar (almost one-to-one) results were found when the load-crack width curves obtained from PIV and LVDT readings were compared. This result clearly implied the great ability of PIV to measure crack width opening, as well as some limitations of LVDTs.
- It was observed that, displacements from LVDT and the values calculated from PIV measurements were more similar to each other for the first crack, when compared to the post-crack region of the curves. This was explained by the

rotational movement of horizontal LVDTs during the test.

- Continuous strain fields during cracking were provided by PIV analysis and the specimens were compared by means of cracking behavior. The results obtained by using stress vs. strain graphs were better understood when strain fields were examined. PIV clearly represented strain distributions throughout the experiment with incremental loading. Changes occurred in specimens (cracking behavior) with an increased specimen thickness were clearly observed. It was seen that distributions of strains (represents multiple cracking ability) were localized for greater values of t/f_L, while they were distributed throughout the specimens for smaller values.
- Crack developments through the section depth were also monitored by using PIV and it was found that the width of the crack sustained for every stage of loading decreases with an increase in t/f_L ratio and decrease in fiber length.

Finally, it can be concluded that, PIV has the potential to be used as an alternative to more traditional linear transducers (LVDTs). And, also offers significant advantages over traditional measurement techniques because it can provide full-field surface displacement measurements, be advantageous in determining crack movement because a priori knowledge of the crack location is not required and most importantly PIV has the ability to monitor even very small strains/cracks during loading.

6.1.7. Cracking and Flexural Behavior Characterization

All the specimens were examined by means of the number of cracks, both from the images of crack monitoring and strain field results of PIV analysis. It was observed that number of cracks increases with an increase in fiber length representing greater multiple cracking capacity and consequently strain hardening behavior.

- It was observed that, all specimens having hooked end fibers have only one major crack, but all these major cracks showed a significant branching behavior, differently from the major cracks formed in the specimens with straight fibers.
- Deflection hardening capacity which is represented by increased stress/strain ca-

pacity after first cracking observed to decrease with an increase in t/f_L ratio.

- One of the objectives of this study was to define a limit t/f_L value to represent transition from deflection hardening to deflection softening behavior. The results showed that strain softening is observed when t/f_L values going up to 8 was under consideration. Other previous studies from the literature were also examined in order to verify this finding and it was found that these results support the finding of current study underlining that after a t/f_L ratio equal or greater than 8, bending behavior tend to become deflection softening, while it is still deflection hardening for a t/f_L value of 5.

6.1.8. Structural Design of Fiber-reinforced Composites - Effect of Varying t/f_L

In this Section of the study, tensile capacities of the specimens (with different t/f_L ratio) were calculated as described by the Italian Guideline (CNR DT 204) and performance parameters (for SLS and ULS) calculated for tension were compared for different t/f_L ratios. Therefore, effect of t/f_L on the constitutive parameters used for material characterization were examined.

- It was observed that, f_{Fts} data which represents performance for serviceability limit states (SLS), is similar for all of the specimens since it considers a very small range of crack opening values in the initial (elastic) stages of the test.
- Greater differences were observed for f_{Ftu} since it represents the ultimate limit state (ULS) residual strength (for an assumed ultimate crack opening, w_u = 2,5 mm) and f_{Ftu} is almost equal to or smaller than "0" for high values of t/f_L for all of the fiber lengths. This represents that material performance very much depend on specimen properties (such as specimen size, geometry, fiber length and fiber volume ratio).
- According to the guideline (CNR DT) the material discussed here can't be used for structural applications without conventional reinforcement since following requirement (fFtu/fFts) $\geq$ 1,05 is not satisfied. Therefore, this material can be used with certain amount of conventional reinforcement for structural applications or

for semi-structural applications.

6.1.9. Relationship Between Mid-Span Deflection (δ) and COD

Correlations between the mid-span deflection and the crack opening displacement (COD) from the previous studies in literature were given and a relationship between the mid-span deflection and COD of SC-FRCCs were proposed based on specimen t/f_L ratio.

- It was observed that, as the t/f_L ratio increases, deflection/COD (d/c) ratio decreases for all specimens. This decrease in the deflection/COD ratio goes further down even to 1 for the higher t/f_L ratios of 8, since the beam thickness increases and effectiveness of fibers resisting cracks decreases.
- It was also observed that, for the beams having small t/f_L ratios, crack opening values are very low compared to deflection values, which indicate that the fibers play more effective role to resist the crack openings, even though undergoing high amount of deflections.
- Proposed relationships based on the experimental findings, were verified with the results of the previous studies from the literature. It was found that, proposed equations for both straight fibers and hooked fibers, predict the behavior with good approximation even for different matrixes/materials.

APPENDIX A: FORCE-DEFORMATION CURVES FOR ALL SPECIMENS

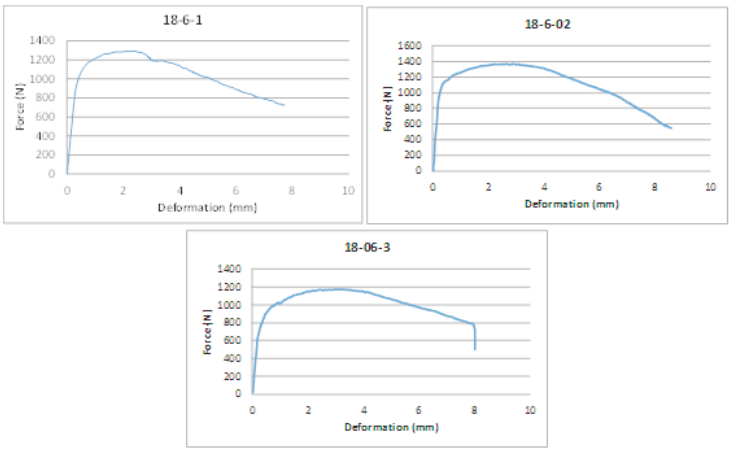

Figure A.1. Force-Deformation Curves of 18mm Thick Beams.

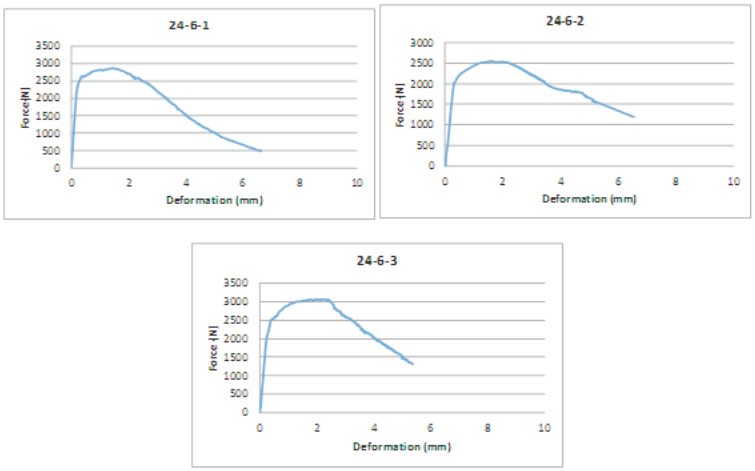

Figure A.2. Force-Deformation Curves of 24mm Thick Beams.

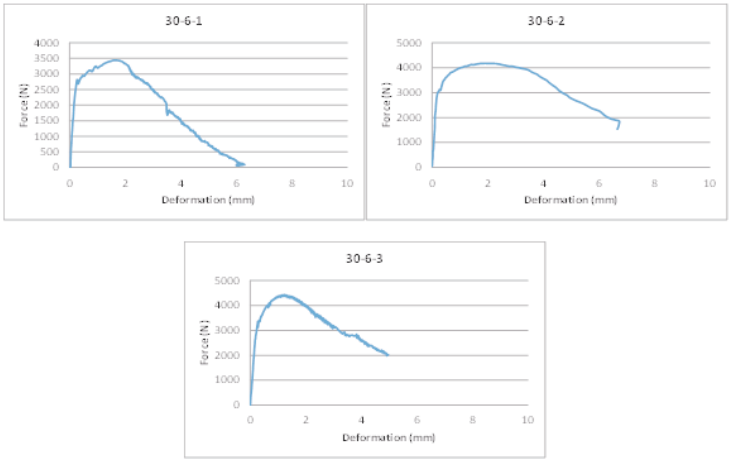

Figure A.3. Force-Deformation Curves of 30mm Thick Beams.

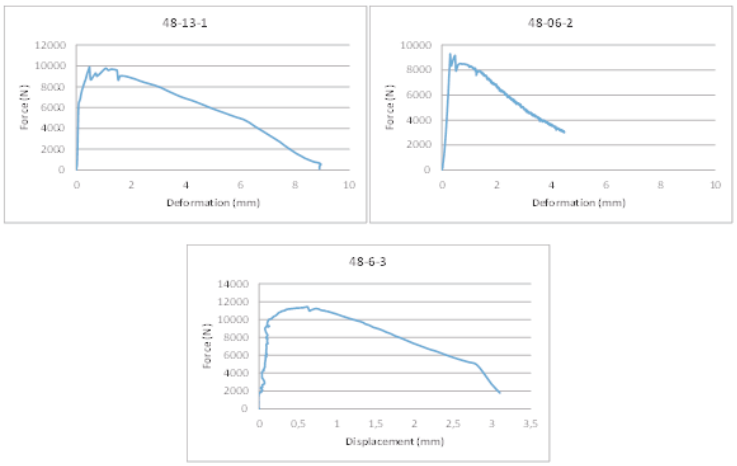

Figure A.4. Force-Deformation Curves of 48mm Thick Beams.

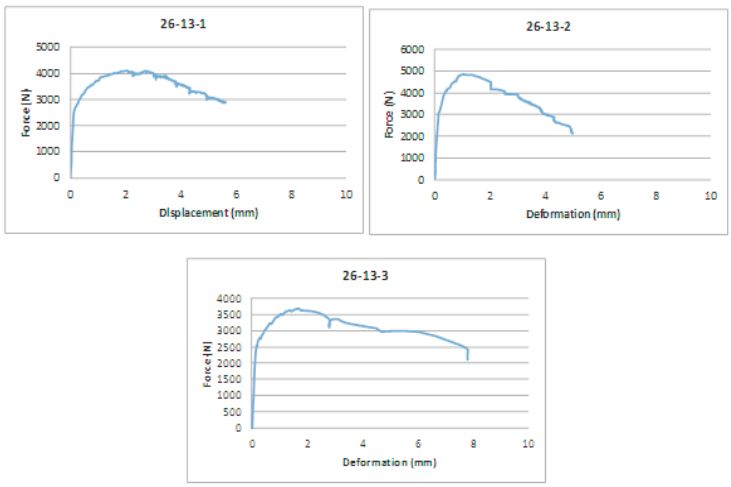

Figure A.5. Force-Deformation Curves of 26mm Thick Beams.

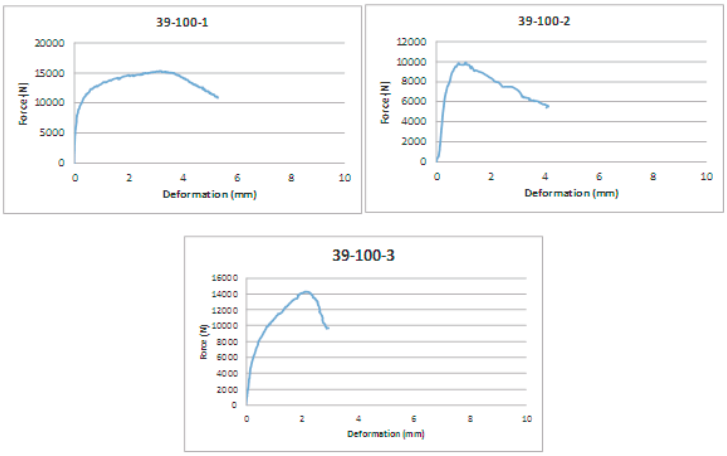

Figure A.6. Force-Deformation Curves of 39mm Thick Beams.

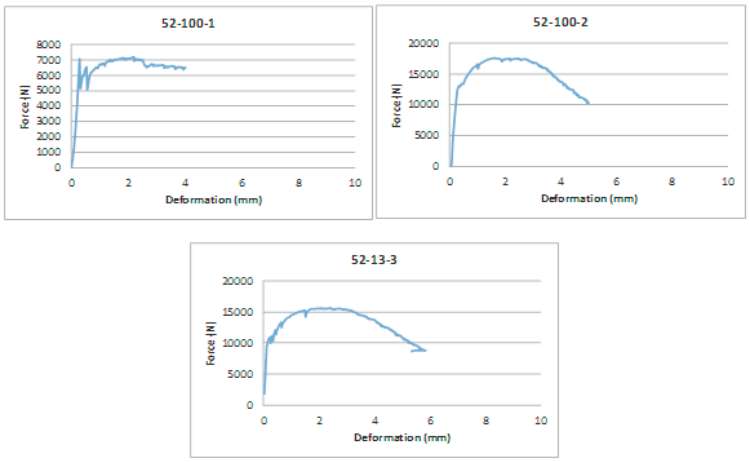

Figure A.7. Force-Deformation Curves of 52mm Thick Beams.

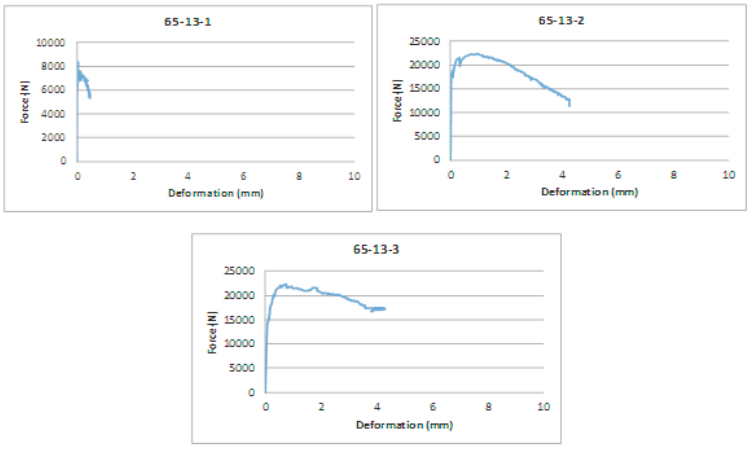

Figure A.8. Force-Deformation Curves of 65mm Thick Beams.

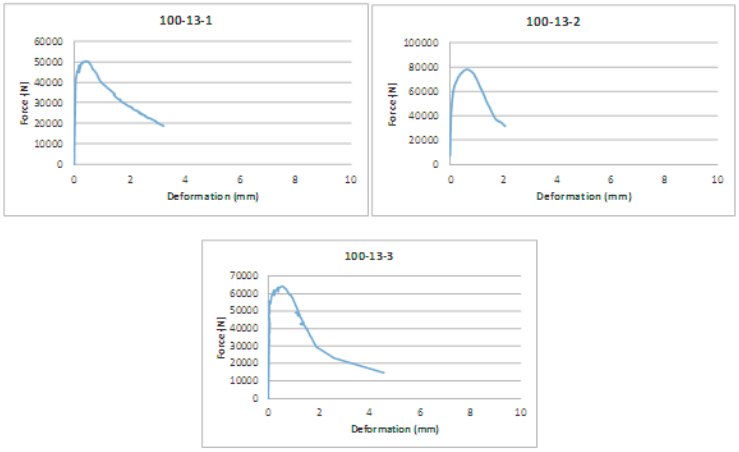

Figure A.9. Force-Deformation Curves of 100mm Thick Beams.

APPENDIX B: FORCE-DEFORMATION CURVES FOR ALL SPECIMENS

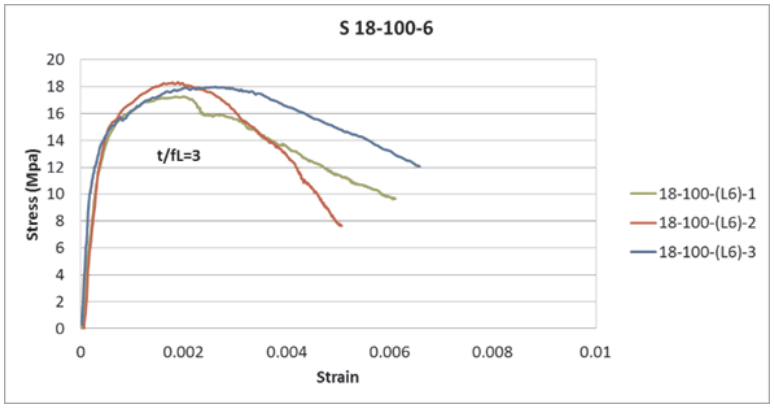

Figure B.1. Stress-Strain Curves of 18mm Thick Beams.

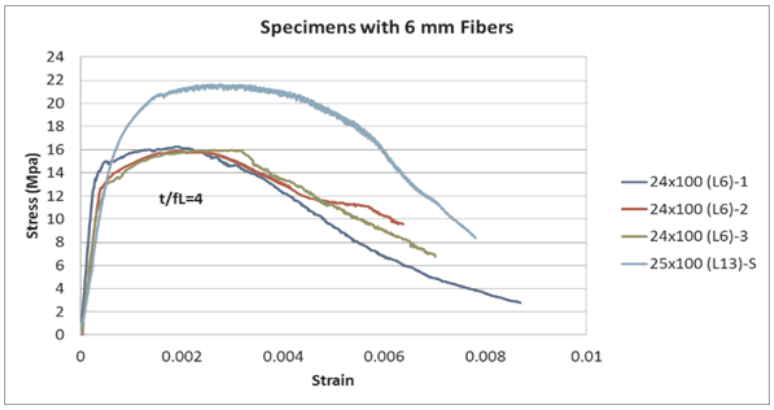

Figure B.2. Stress-Strain Curves of 24mm Thick Beams.

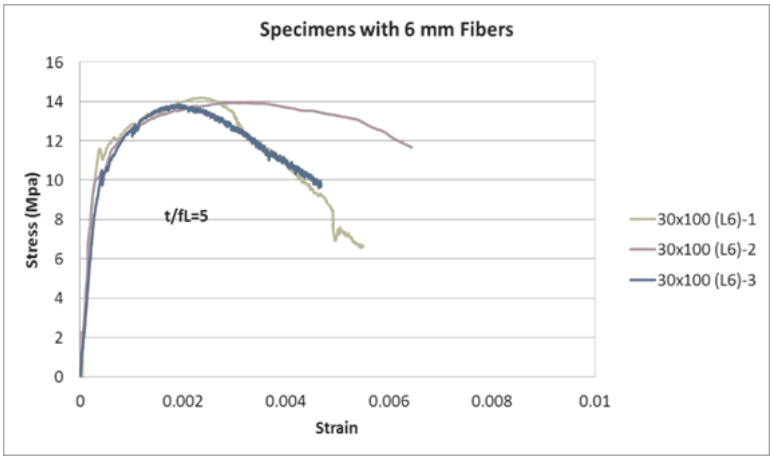

Figure B.3. Stress-Strain Curves of 30mm Thick Beams.

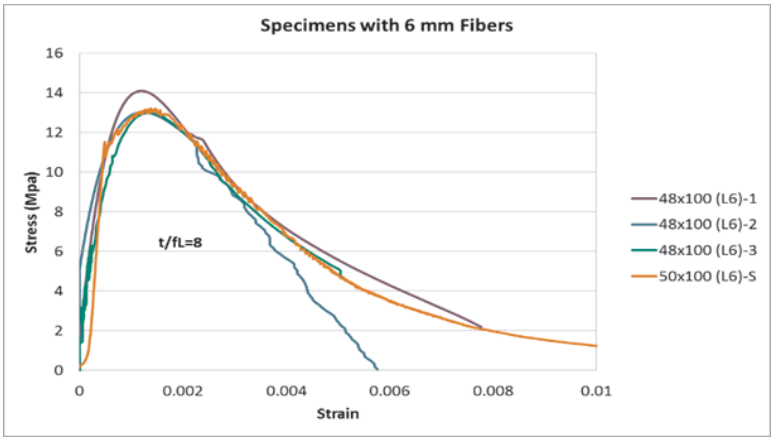

Figure B.4. Stress-Strain Curves of 48mm Thick Beams.

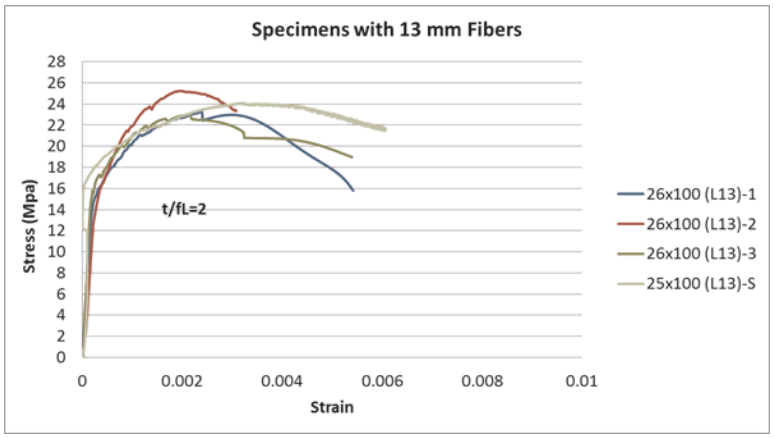

Figure B.5. Stress-Strain Curves of 26mm Thick Beams.

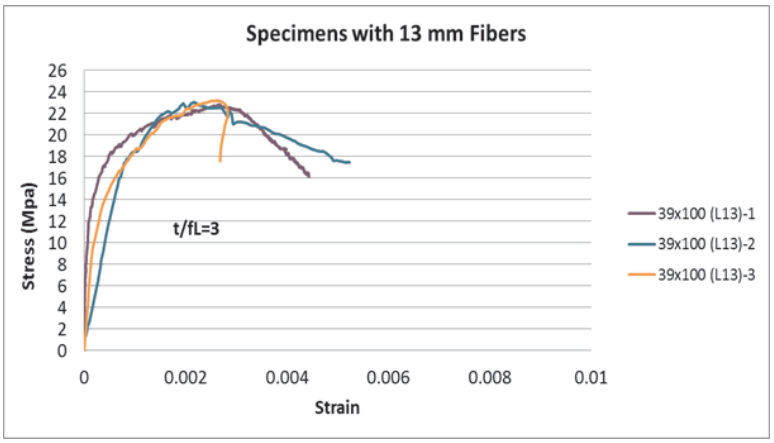

Figure B.6. Stress-Strain Curves of 39mm Thick Beams.

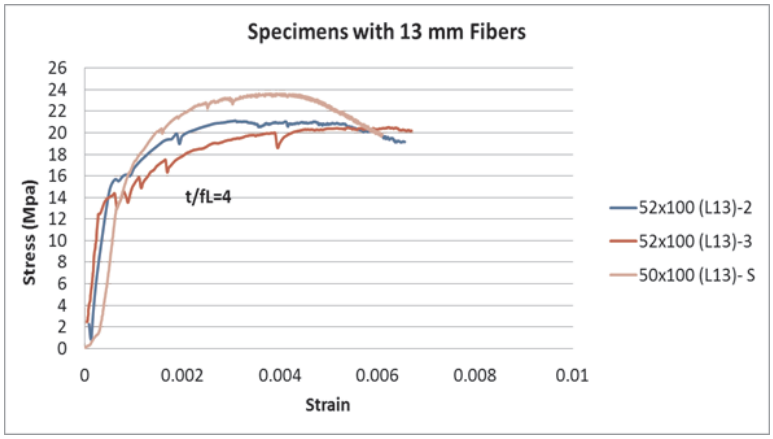

Figure B.7. Stress-Strain Curves of 52mm Thick Beams.

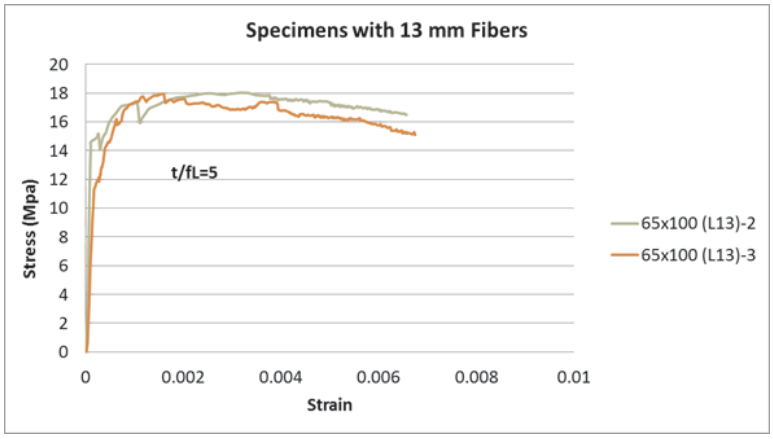

Figure B.8. Stress-Strain Curves of 65mm Thick Beams.

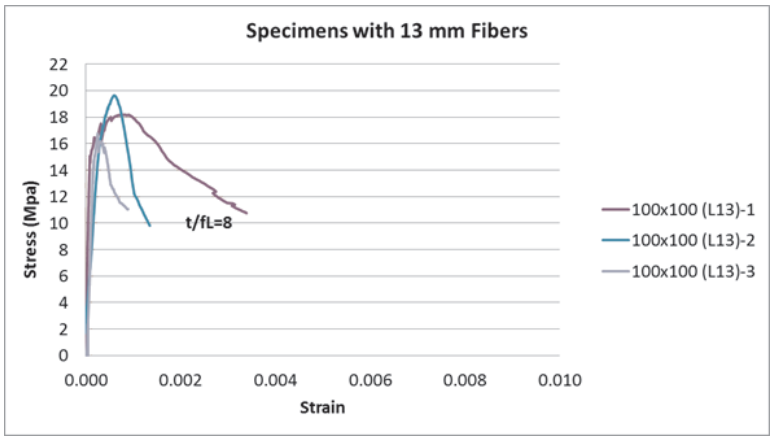

Figure B.9. Stress-Strain Curves of 100mm Thick Beams.

B.1. PIV Strain Fields

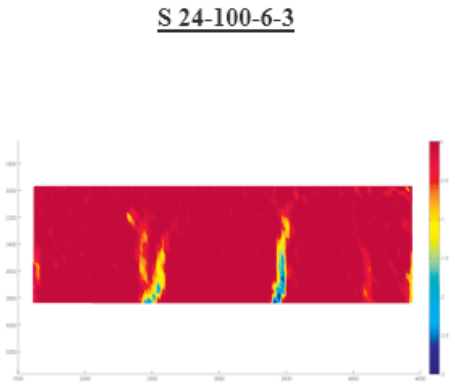

Figure B.10. Longitudinal Strain Field (ε_{xx}) Corresponding to Image 2 of the Series (Image 0402), Strain Legend is in %. (Comment: There are Signs of Some Other Cracks which are Not Visible in the Captured Images).

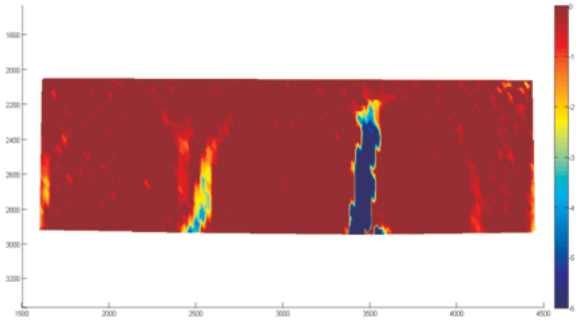

Figure B.11. Longitudinal Strain Field (ε_{xx}) Corresponding to Image 7 (Strain Legend is in %). (Comment: The Maximum Strain in the Legend was Increased to 6.0 %).

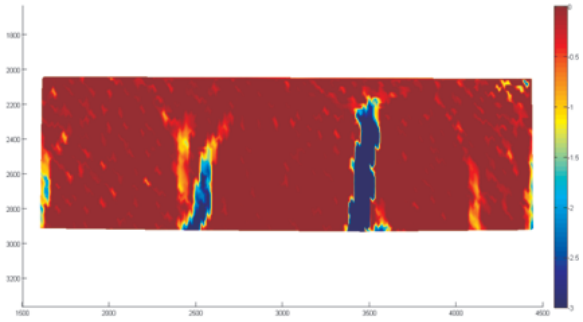

Figure B.12. Longitudinal Strain Field (ε_{xx}) Corresponding to Image 6 (Strain Legend is in %).

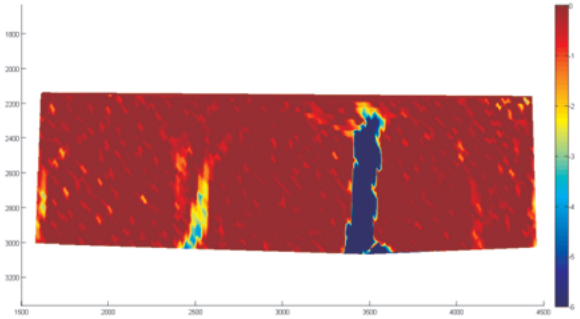

Figure B.13. Longitudinal Strain Field (ε_{xx}) Corresponding to Image 15 (Strain Legend is in %).

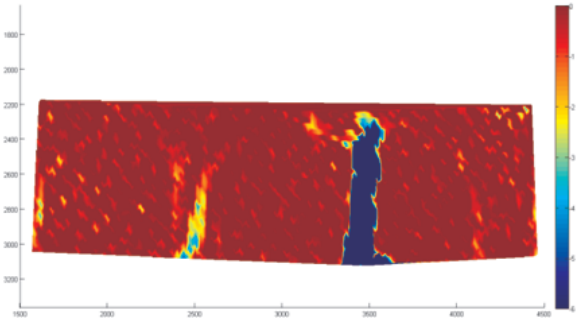

Figure B.14. Longitudinal Strain Field (ε_{xx}) Corresponding to Image 19 (Strain Legend is in %).

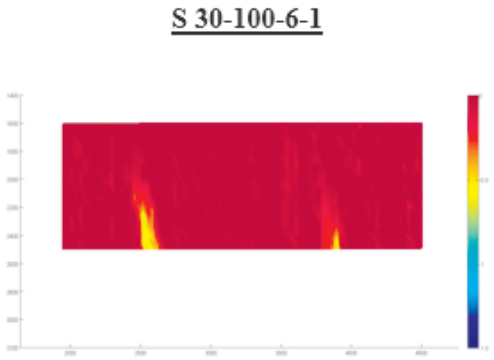

Figure B.15. Longitudinal Strain Field (ε_{xx}) Corresponding to Image 2 (Strain Legend is in %).

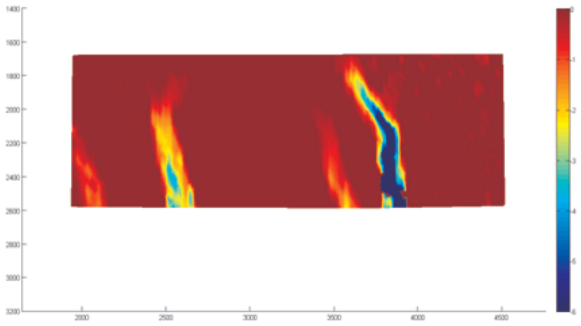

Figure B.16. Longitudinal Strain Field (ε_{xx}) Corresponding to Image 4 (Strain Legend is in %). (Comment: The Maximum Strain in the Legend).

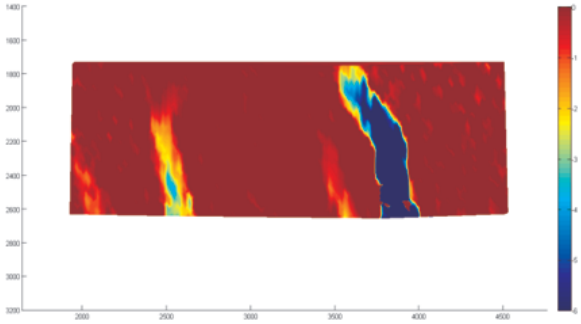

Figure B.17. Longitudinal Strain Field (ε_{xx}) Corresponding to Image 9 (Strain Legend is in %).

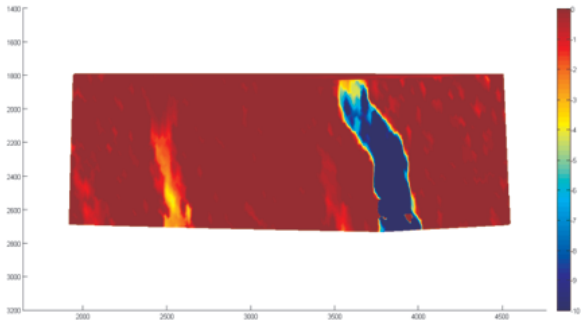

Figure B.18. Longitudinal Strain Field (ε_{xx}) Corresponding to Image 15 (Strain Legend is in %).

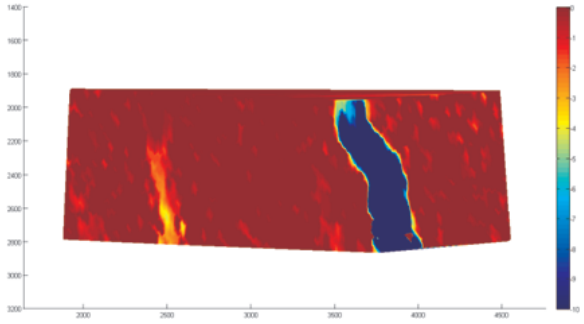

Figure B.19. Longitudinal Strain Field (ε_{xx}) Corresponding to Image 26 (Strain Legend is in %).

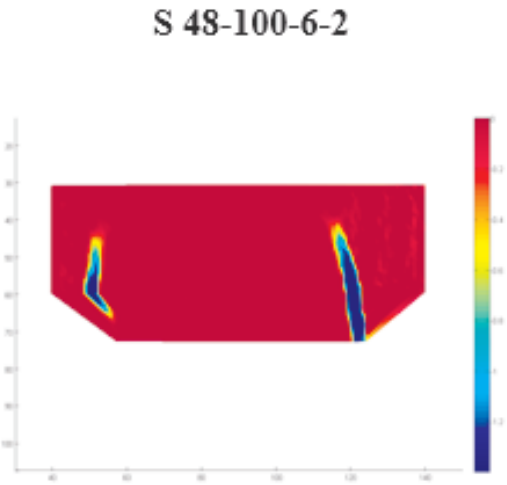

Figure B.20. Longitudinal Strain Field (ε_{xx}) Corresponding to Image 97 (Strain Legend is in %; Axes are in mm; Comment: Obviously the Edges of the Strain Field are not Valid!).

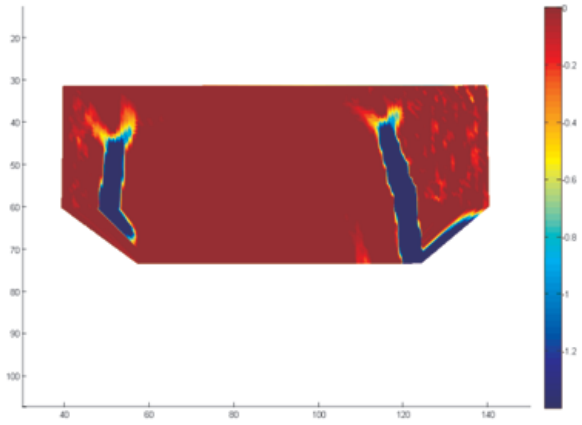

Figure B.21. Longitudinal Strain Field (ε_{xx}) Corresponding to Image 100 (Strain Legend is in %; Axes are in mm).

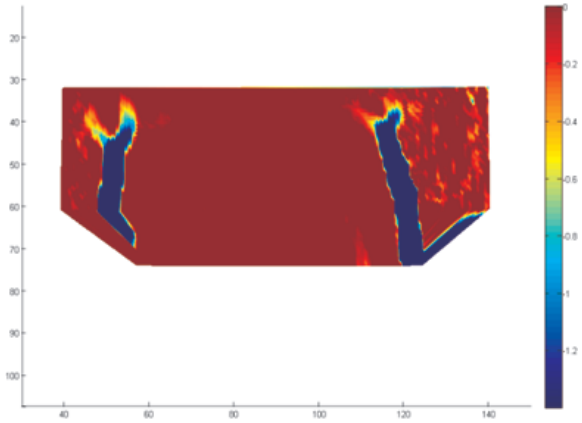

Figure B.22. Longitudinal Strain Field (ε_{xx}) Corresponding to Image 103 (Strain Legend is in %; Axes are in mm).

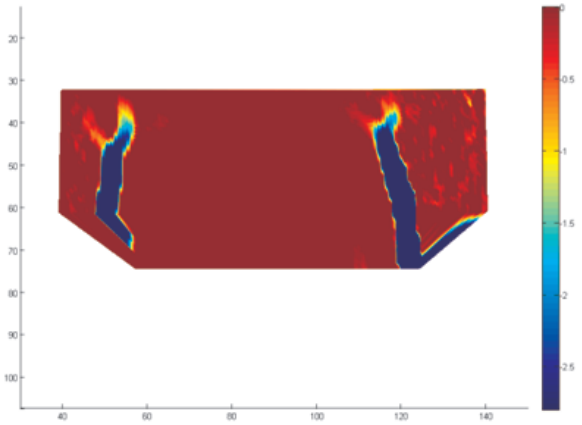

Figure B.23. Longitudinal Strain Field (ε_{xx}) Corresponding to Image 105 (Strain Legend is in %; Axes are in mm; the Upper Bound in the Legend is Increased to 2.8%).

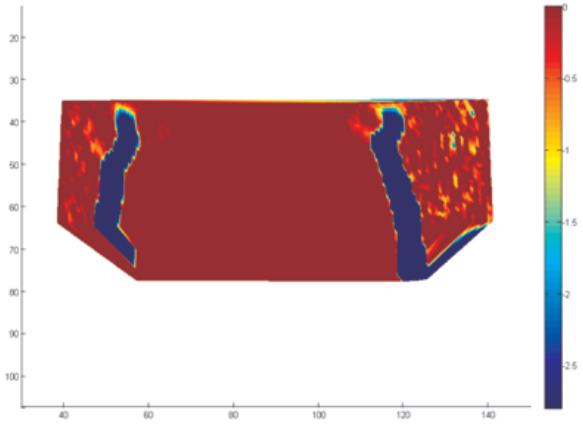

Figure B.24. Strain Field (ε_{xx}) Corresponding to Image 120 (Strain Legend is in %; Axes are in mm).

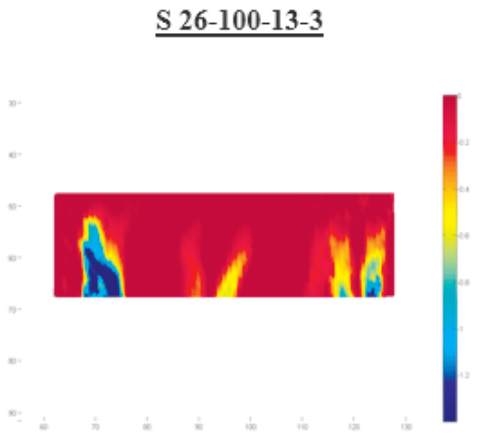

Figure B.25. Displacement Vectors Corresponding to the Last Image, Magnification Factor = 0.2.

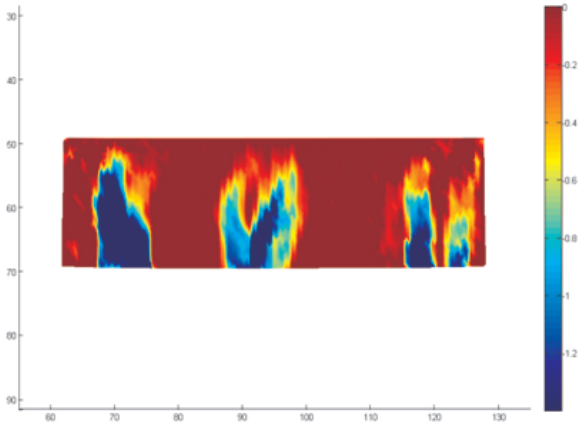

Figure B.26. Longitudinal Strain Field (ε_{xx}) Corresponding to Image 9 (Strain Legend is in %; Axes are in mm).

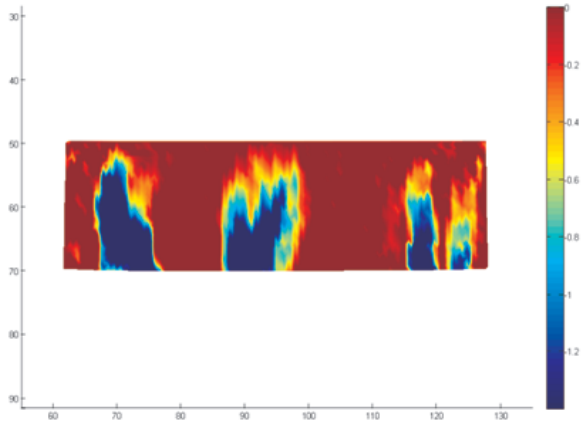

Figure B.27. Longitudinal Strain Field (ε_{xx}) Corresponding to Image 11 (Strain Legend is in %; Axes are in mm).

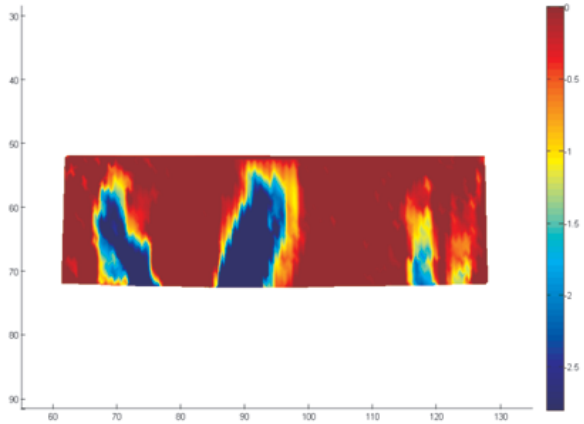

Figure B.28. Longitudinal Strain Field (ε_{xx}) Corresponding to Image 14 (Strain Legend is in %; Axes are in mm).

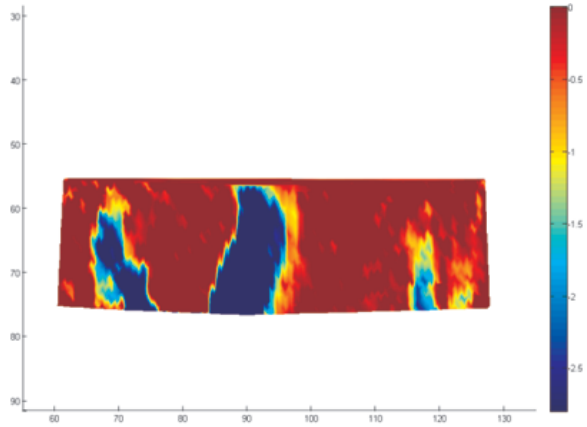

Figure B.29. Longitudinal Strain Field (ε_{xx}) Corresponding to Image 21 (Strain Legend is in %; Axes are in mm).

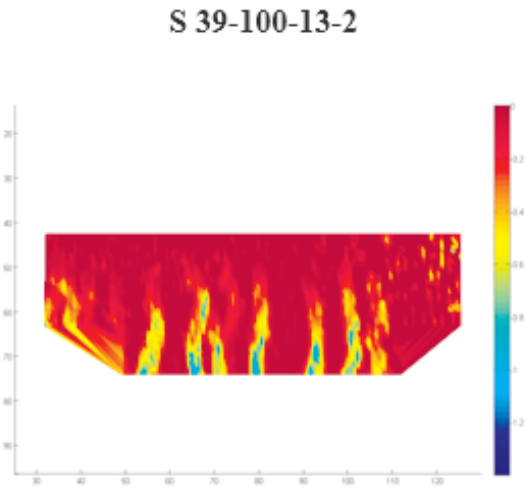

Figure B.30. Longitudinal Strain Field (ε_{xx}) Corresponding to Image 322 (Strain Legend is in %); Axes are in mm; Comment: Obviously the Edges of the Strain Field are Not Valid!).

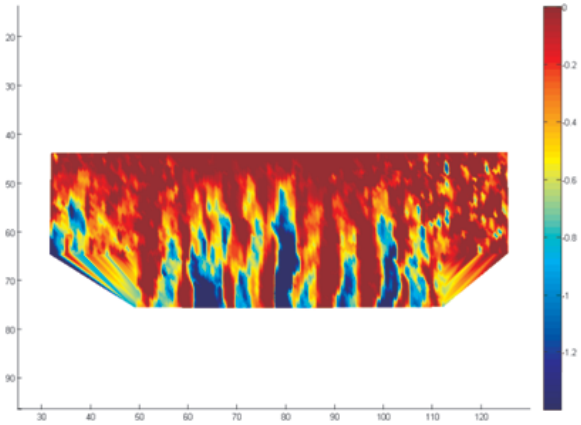

Figure B.31. Longitudinal Strain Field (ε_{xx}) Corresponding to Image 323 (Strain Legend is in %); Axes are in mm).

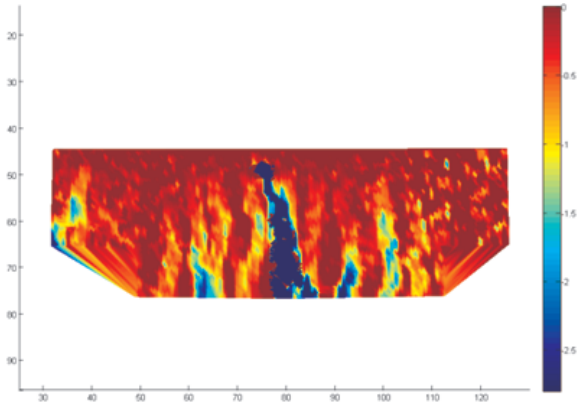

Figure B.32. Longitudinal Strain Field (ε_{xx}) Corresponding to Image 326 (Strain Legend is in %; Axes are in mm).

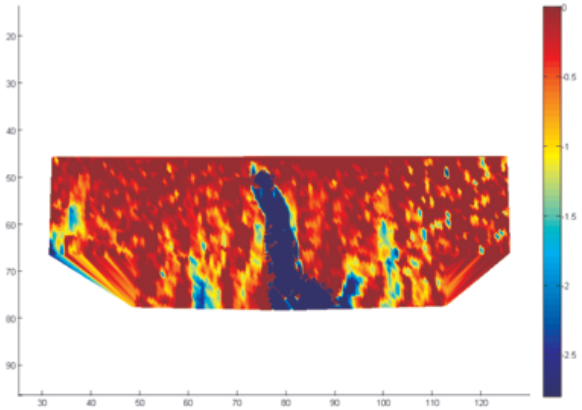

Figure B.33. Longitudinal Strain Field (ε_{xx}) Corresponding to Image 330 (Strain Legend is in %; Axes are in mm

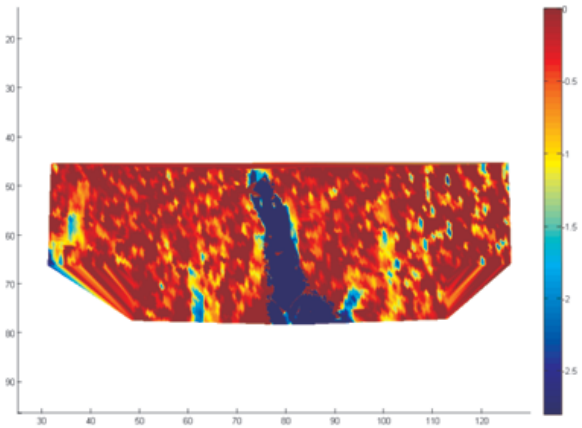

Figure B.34. Longitudinal Strain Field (ε_{xx}) Corresponding to Image 333 (Strain Legend is in %; Axes are in mm.

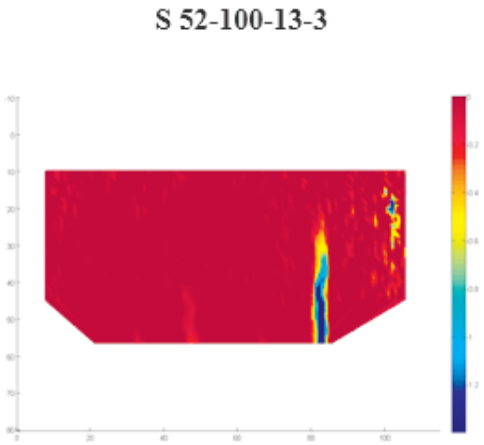

Figure B.35. Longitudinal Strain Field (ε_{xx}) Corresponding to Image 704 (Strain Legend is in %; Axes are in mm).

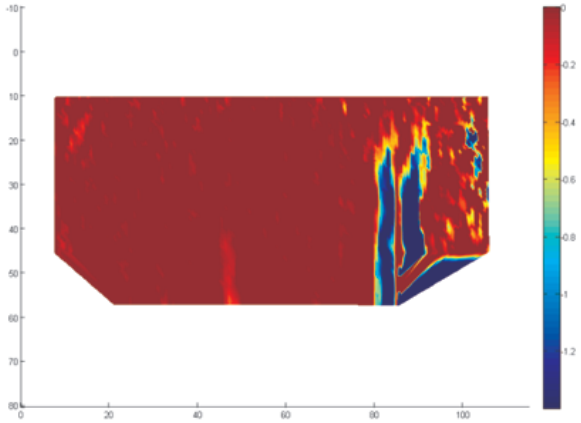

Figure B.36. Longitudinal Strain Field (ε_{xx}) Corresponding to Image 706 (Strain Legend is in %; Axes are in mm).

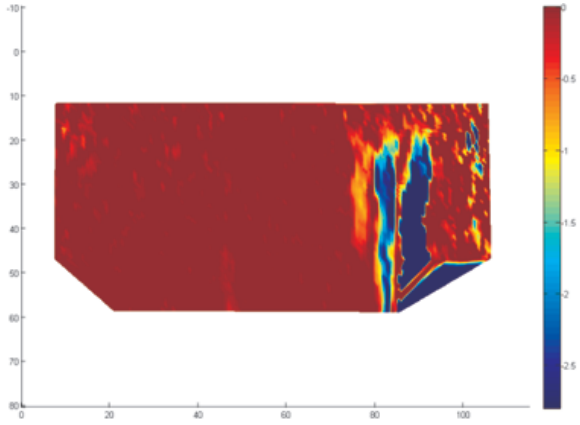

Figure B.37. Longitudinal Strain Field (ε_{xx}) Corresponding to Image 716 (Strain Legend is in %; Axes are in mm).

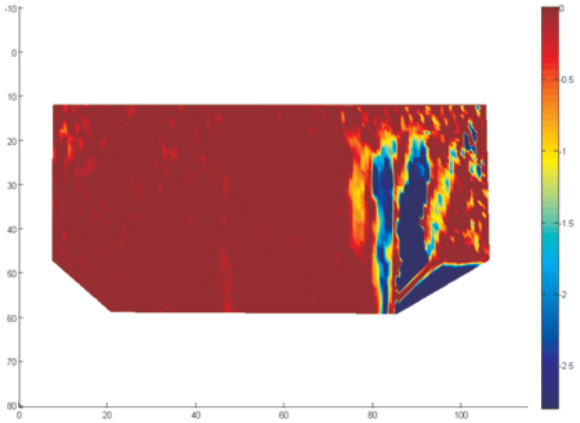

Figure B.38. Longitudinal Strain Field (ε_{xx}) Corresponding to Image 719 (Strain Legend is in %; Axes are in mm).

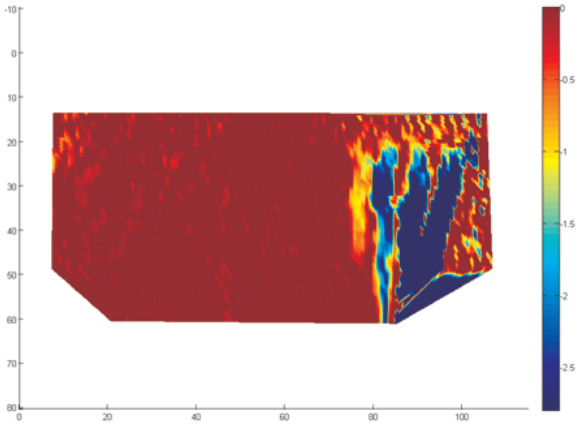

Figure B.39. Longitudinal Strain Field (ε_{xx}) Corresponding to Image 732 (Strain Legend is in %; Axes are in mm).

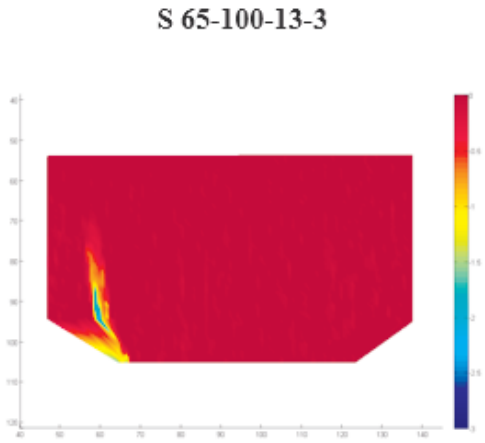

Figure B.40. Longitudinal Strain Field (ε_{xx}) Corresponding to Image DSC-0336 (Strain Legend is in %; Axes are in mm).

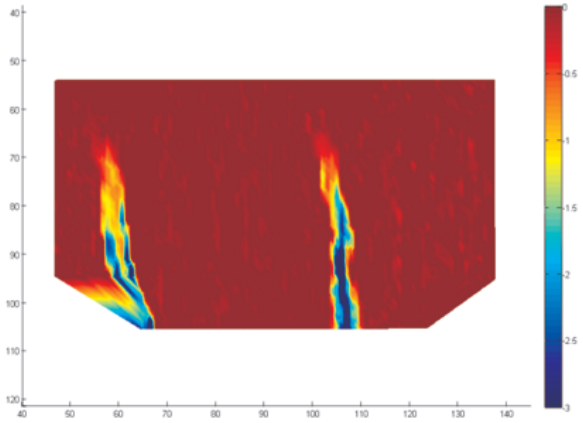

Figure B.41. Longitudinal Strain Field (ε_{xx}) Corresponding to Image DSC-0345 (Strain Legend is in %; Axes are in mm).

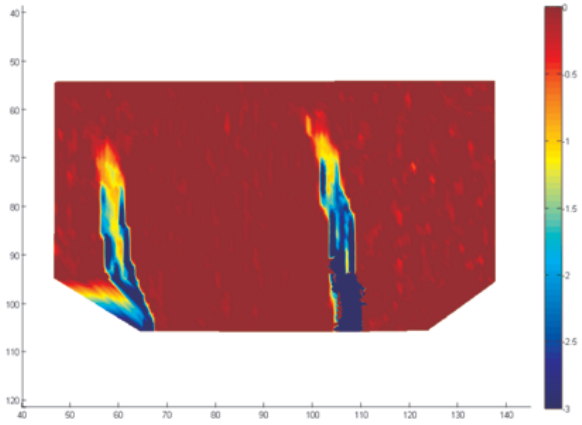

Figure B.42. Longitudinal Strain Field (ε_{xx}) Corresponding to Image DSC-0355 (Strain Legend is in %; Axes are in mm).

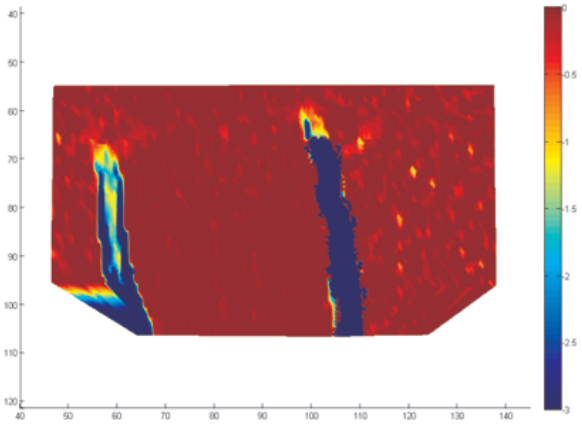

Figure B.43. Longitudinal Strain Field (ε_{xx}) Corresponding to Image DSC-0400 (Strain Legend is in %; Axes are in mm).

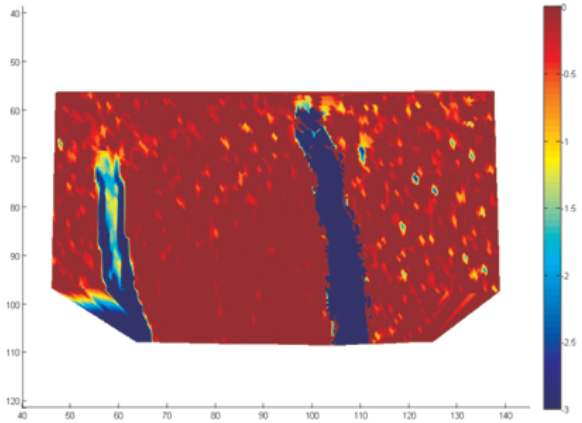

Figure B.44. Longitudinal Strain Field (ε_{xx}) Corresponding to Image DSC-0520 (Strain Legend is in %; Axes are in mm).

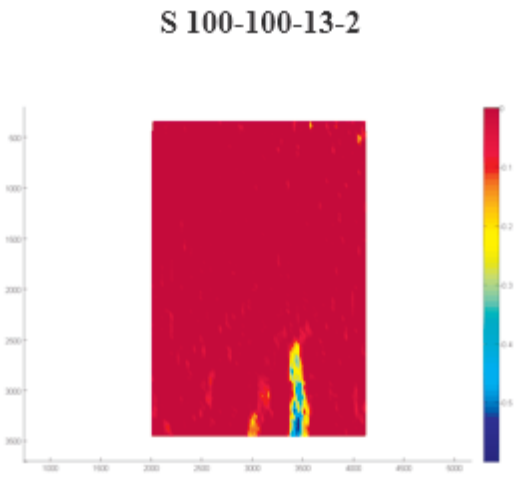

Figure B.45. Longitudinal Strain Field (ε_{xx}) Corresponding to Image 6 (Strain Legend is in %; Axes are in mm).

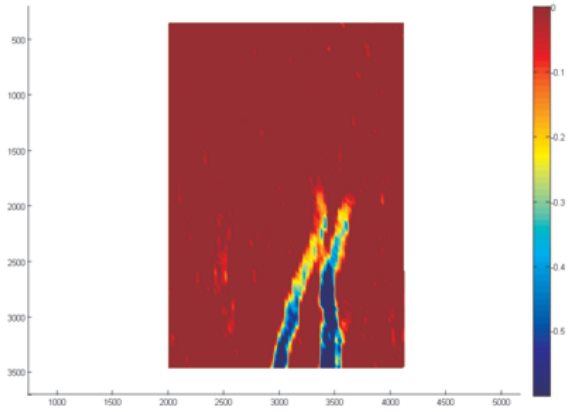

Figure B.46. Longitudinal Strain Field (ε_{xx}) Corresponding to Image 7 (Strain Legend is in %). Comment: There are Signs of one other Crack Which is not Visible in the Captured Image.

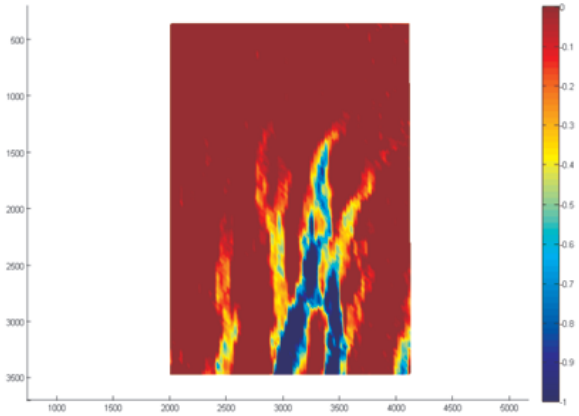

Figure B.47. Longitudinal Strain Field (ε_{xx}) Corresponding to Image 9 (Strain Legend is in %).

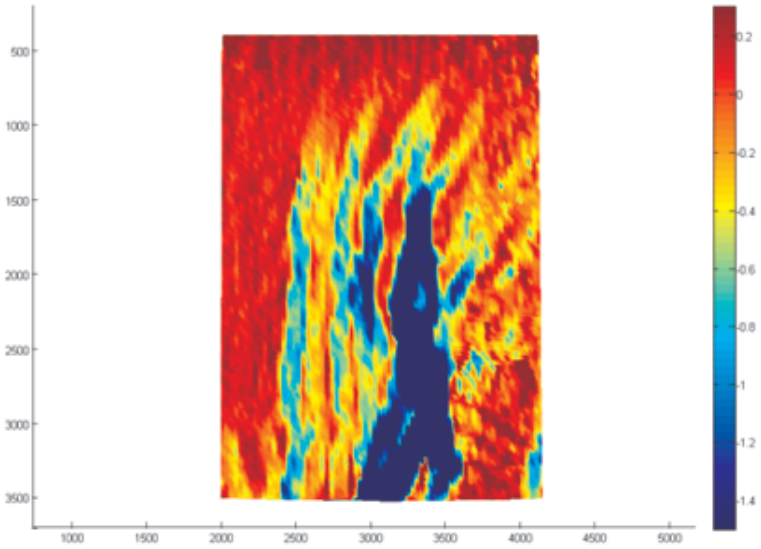

Figure B.48. Longitudinal Strain Field (ε_{xx}) Corresponding to Image 15 (Strain Legend is in %).

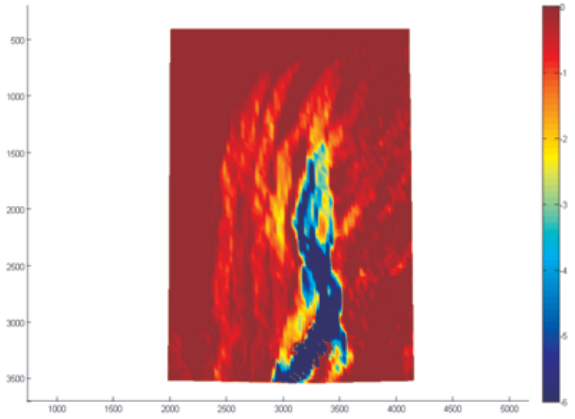

Figure B.49. Longitudinal Strain Field (ε_{xx}) Corresponding to Image 17 (Strain Legend is in %). (Comment: The Maximum Strain in the Legend was Changed to 6.0%).

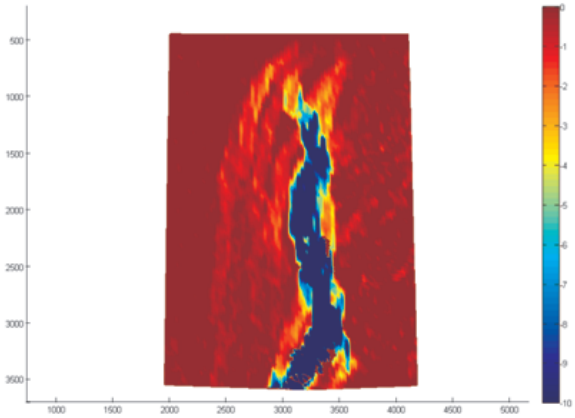

Figure B.50. Longitudinal Strain Field (ε_{xx}) Corresponding to Image 23 (Strain Legend is in %). (Comment: The Maximum Strain in the Legend was Changed to 6.0%)

APPENDIX C: CRACK PROPAGATION IMAGES AND F-D CURVES

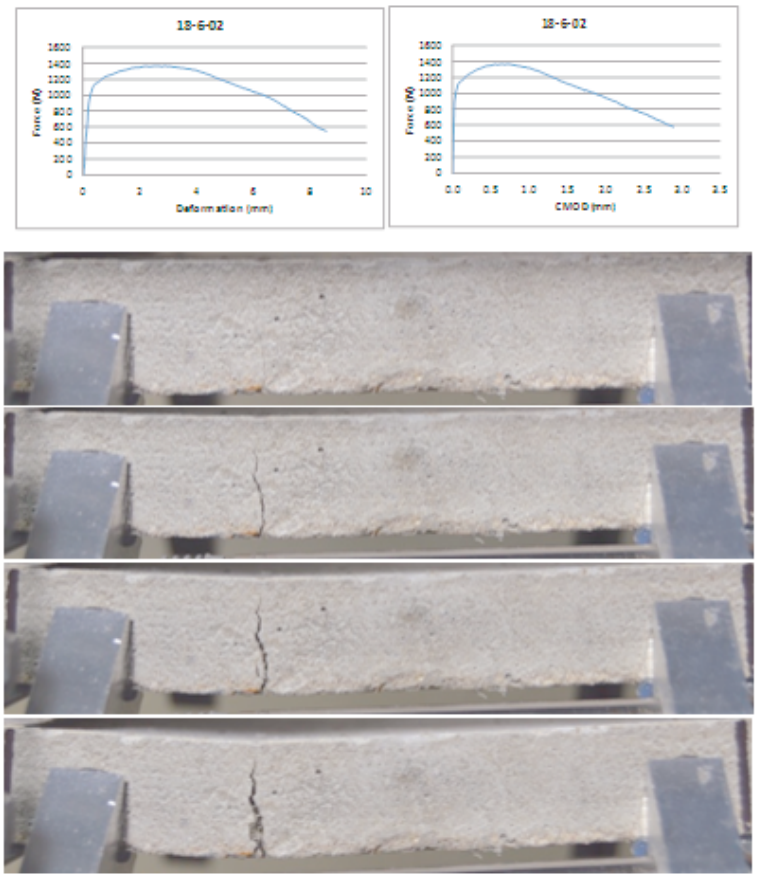

Figure C.1. 18-100-6-2 (a/d=5,56 t/fL=3 A.R=37,5).

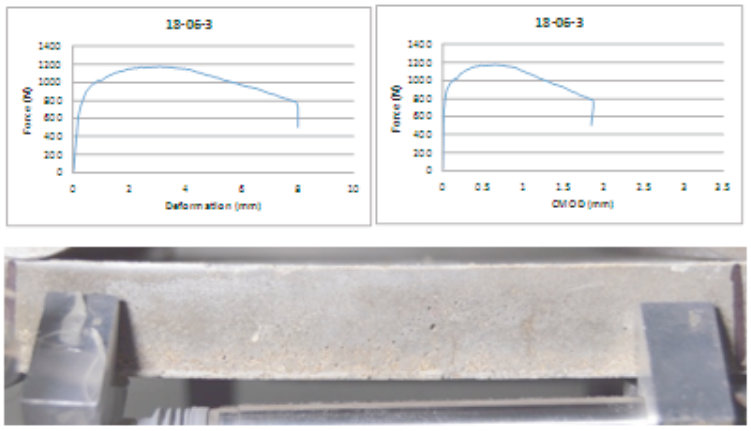

Figure C.2. 18-100-6-3 (a/d=5,56 t/fL=3 A.R=37,5).

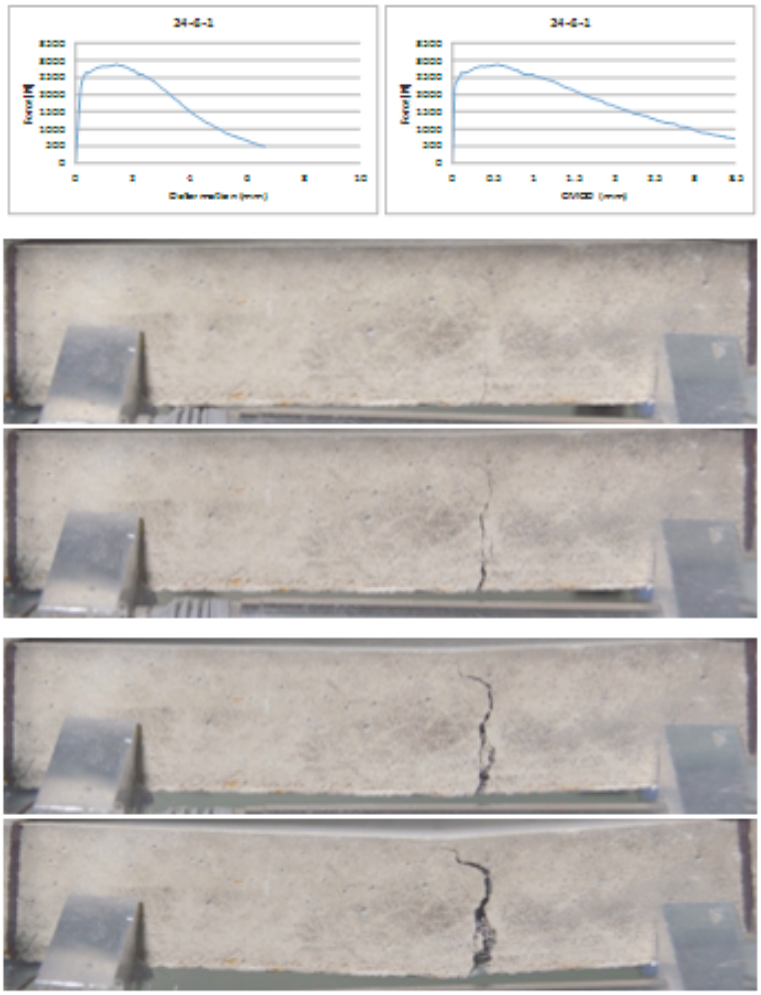

Figure C.3. 24-100-6-1 (a/d=4,17 t/fL=4 A.R=37,5).

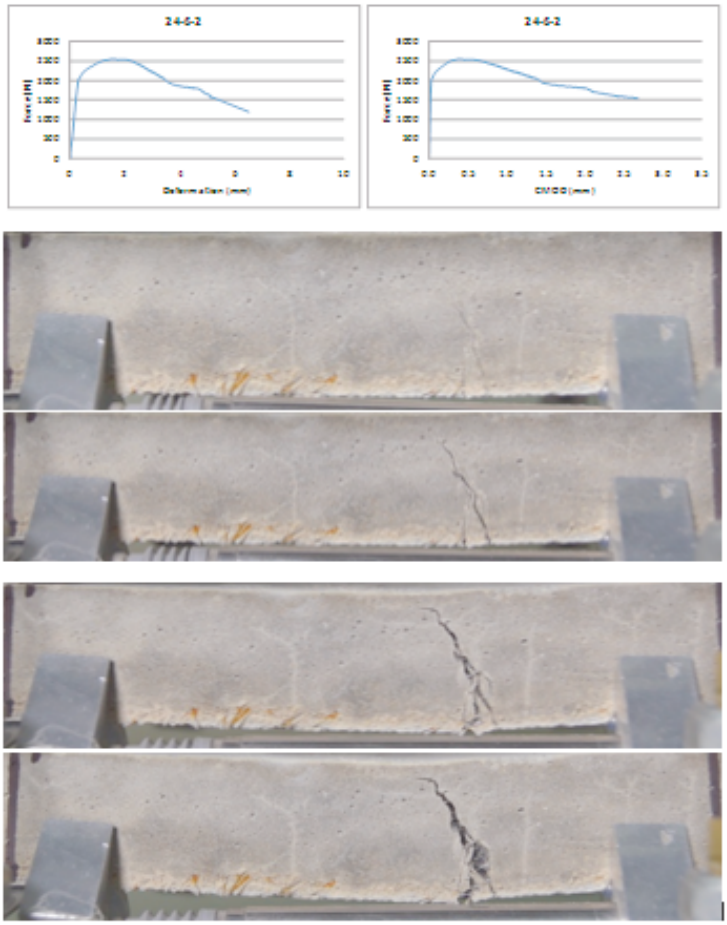

Figure C.4. 24-100-6-2 (a/d=4,17 t/fL=4 A.R=37,5).

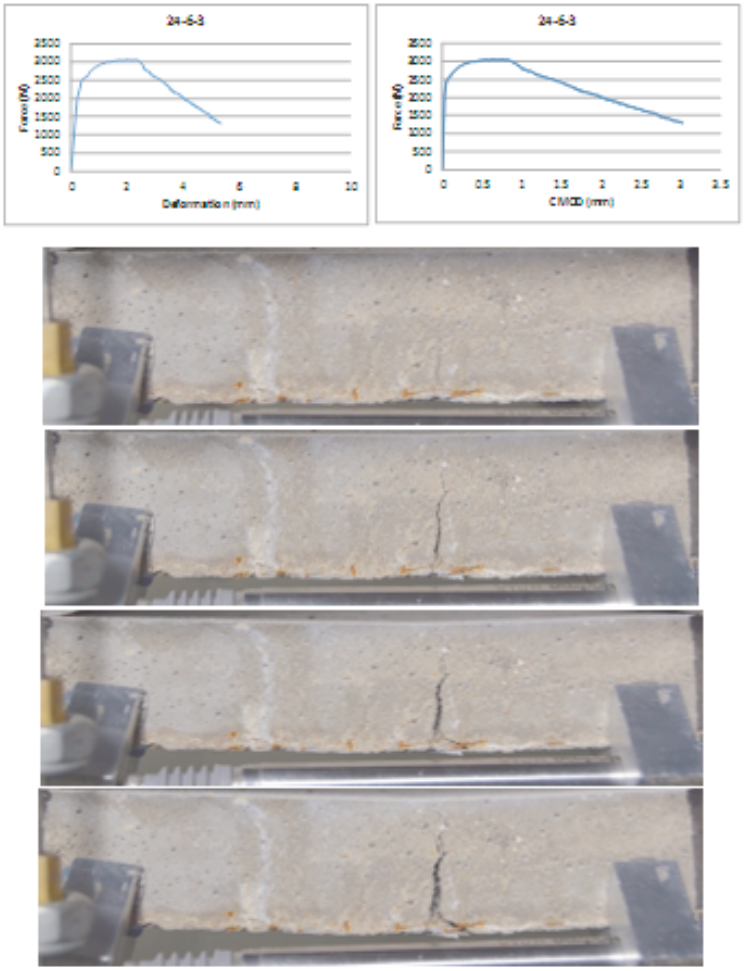

Figure C.5. 24-100-6-3 (a/d=4,17 t/fL=4 A.R=37,5).

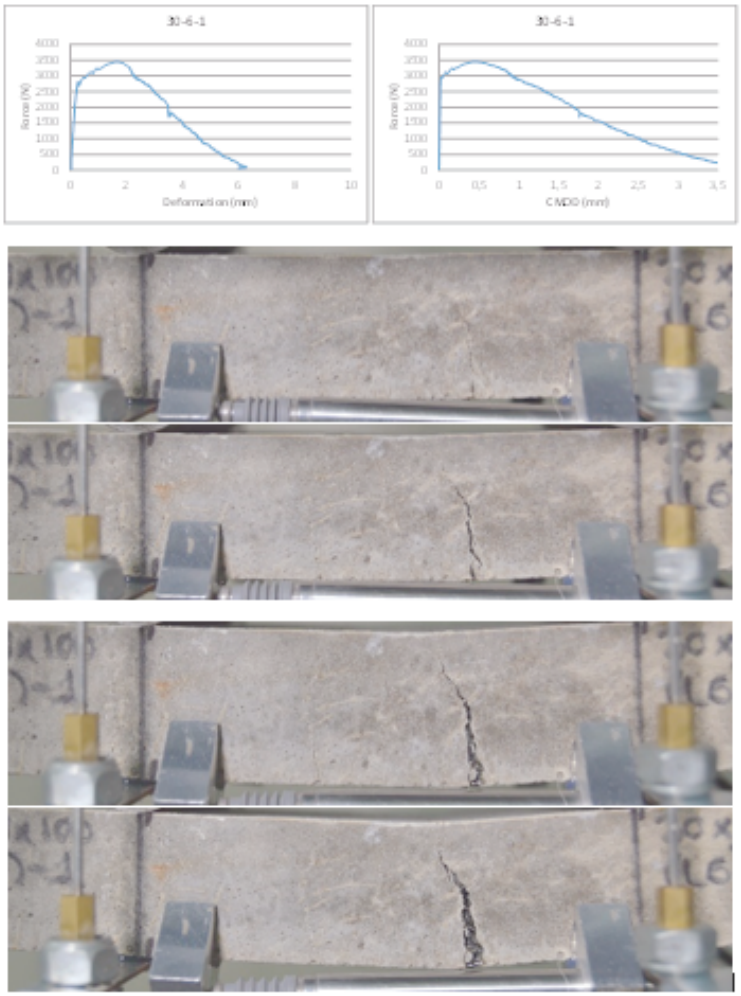

Figure C.6. 30-100-6-1 (a/d=3,33 t/fL=5 A.R=37,5).

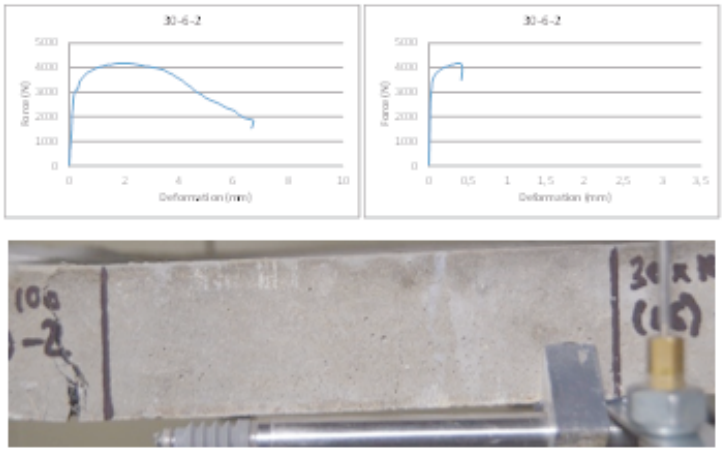

Figure C.7. 30-100-6-2 (a/d=3,33 t/fL=5 A.R=37,5).

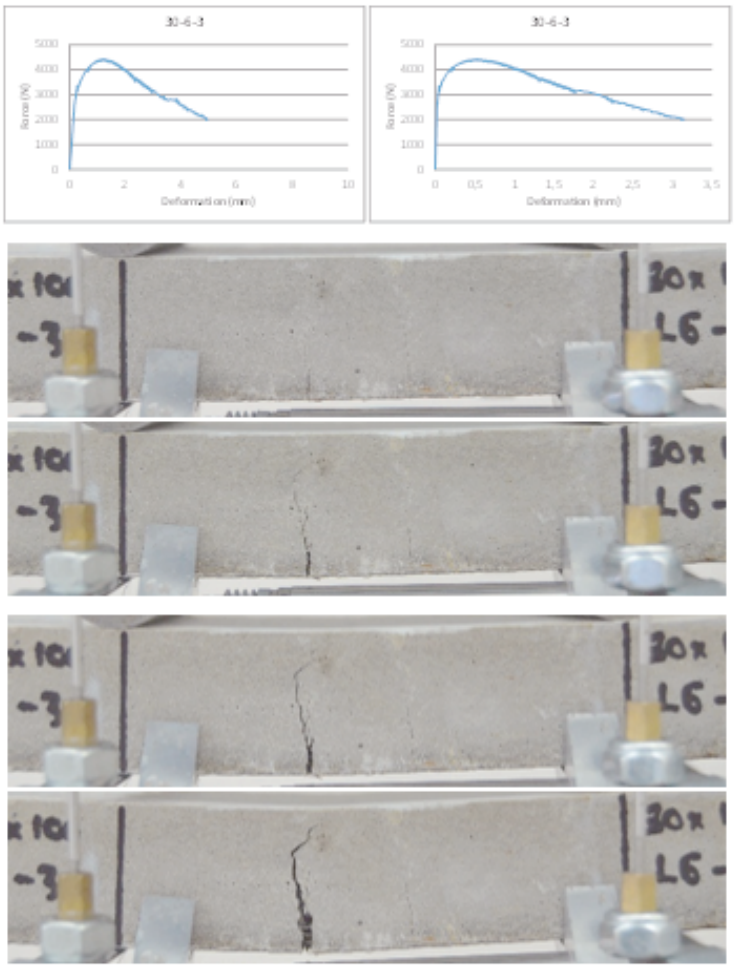

Figure C.8. 48-100-6-1 (a/d=2,08 t/fL=8 A.R=37,5).

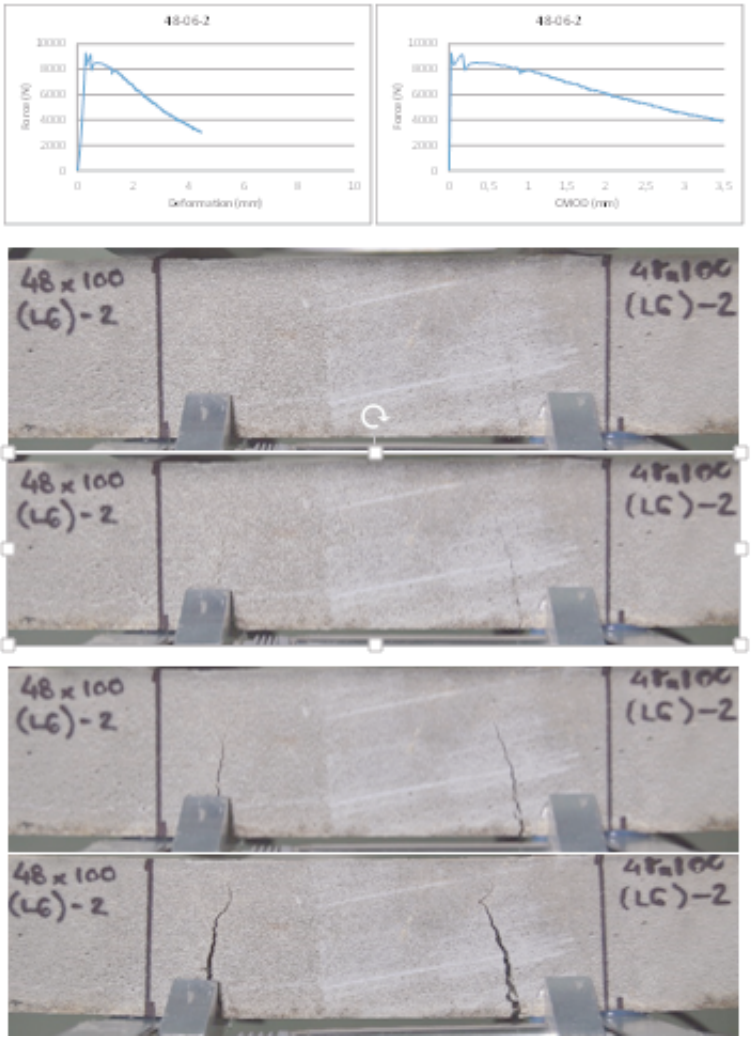

Figure C.9. 48-100-6-2 (a/d=2,08 t/fL=8 A.R=37,5).

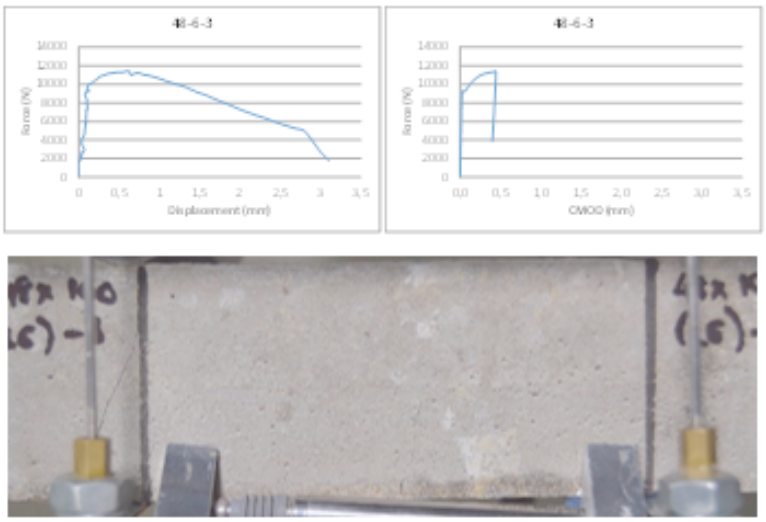

Figure C.10. 48-100-6-3 (a/d=2,08 t/fL=8 A.R=37,5).

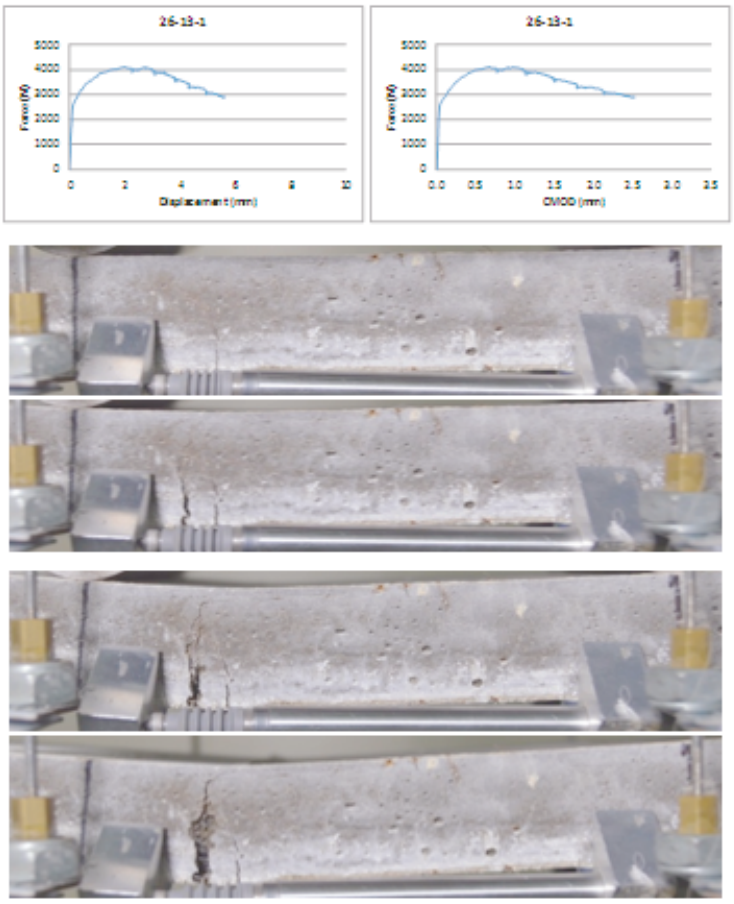

Figure C.11. 26-100-13-1 (a/d=3,85 t/fL=2 A.R=81,3).

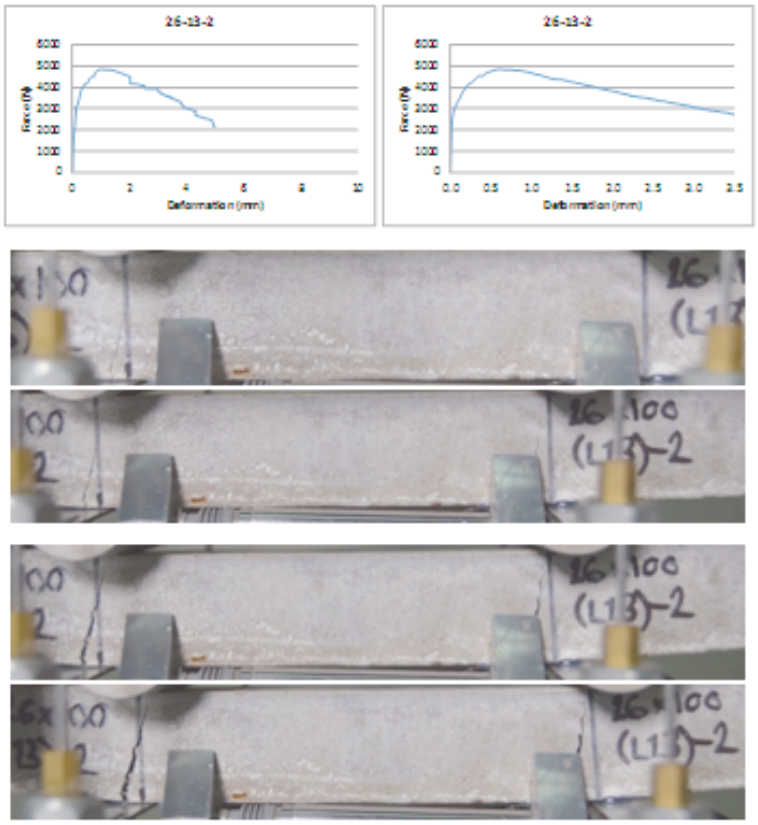

Figure C.12. 26-100-13-2 (a/d=3,85 t/fL=2 A.R=81,3).

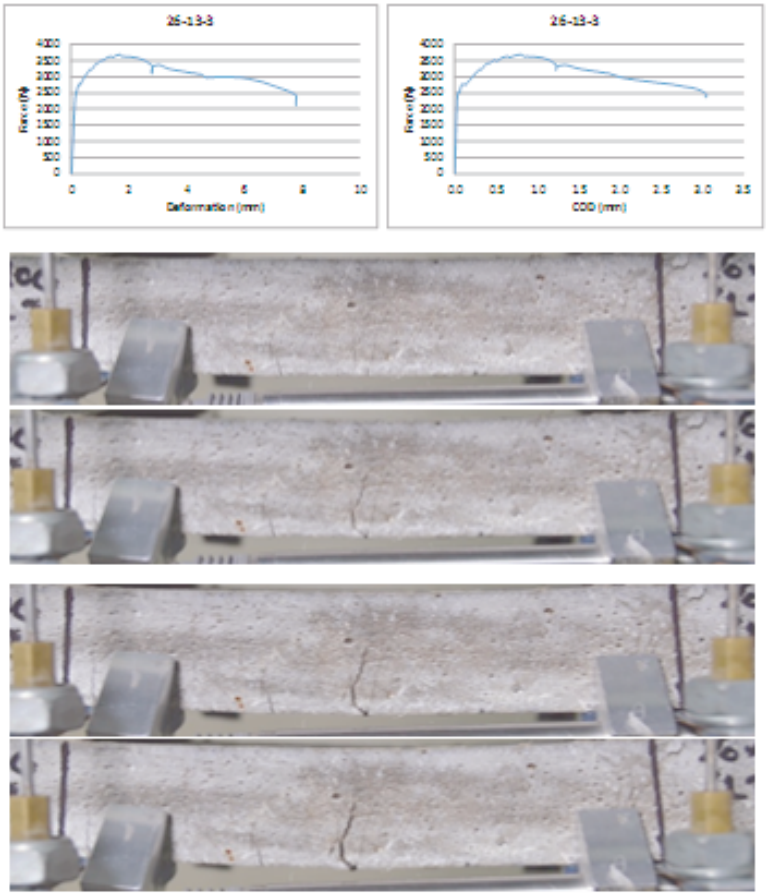

Figure C.13. 26-100-13-3 (a/d=3,85 t/fL=2 A.R=81,3).

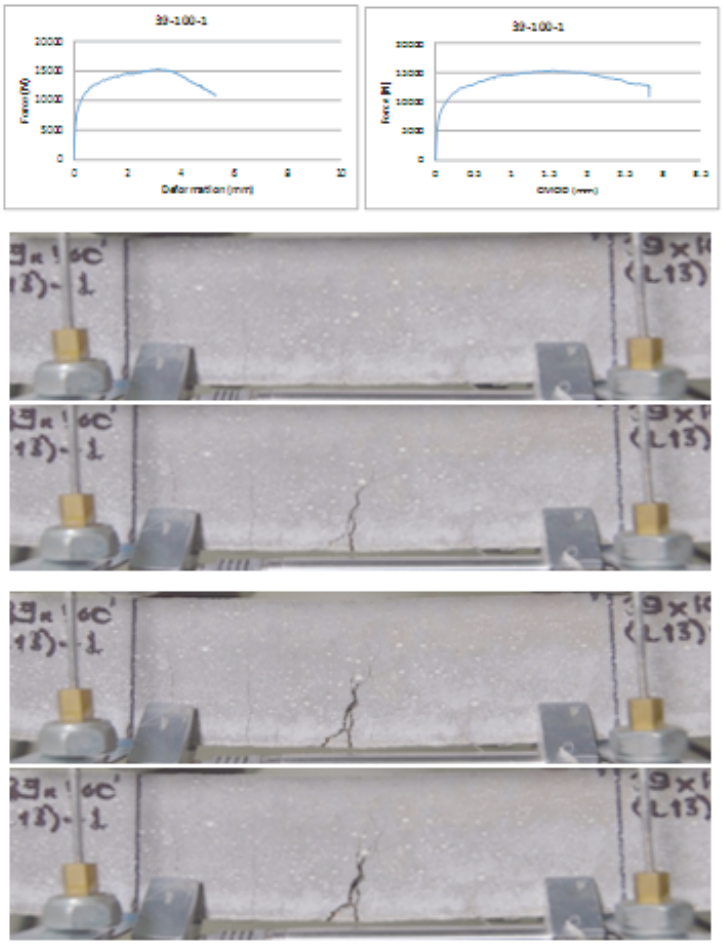

Figure C.14. 39-100-13-1 (a/d=2,56 t/fL=3 A.R=81,3).

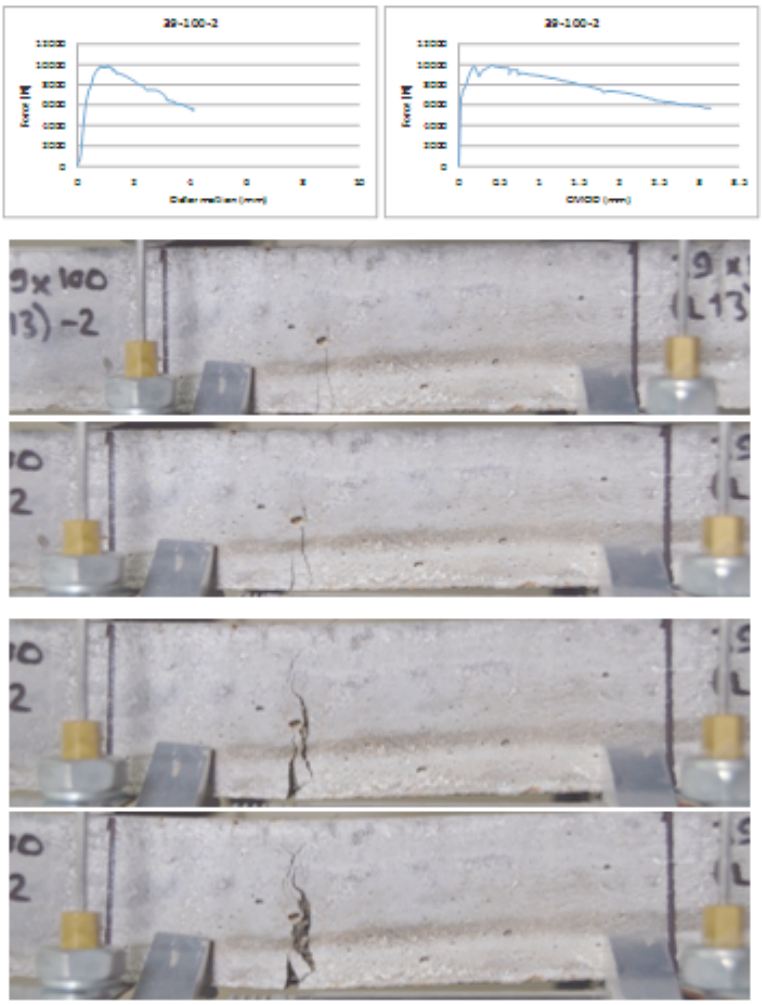

Figure C.15. 39-100-13-2 (a/d=2,56 t/fL=3 A.R=81,3).

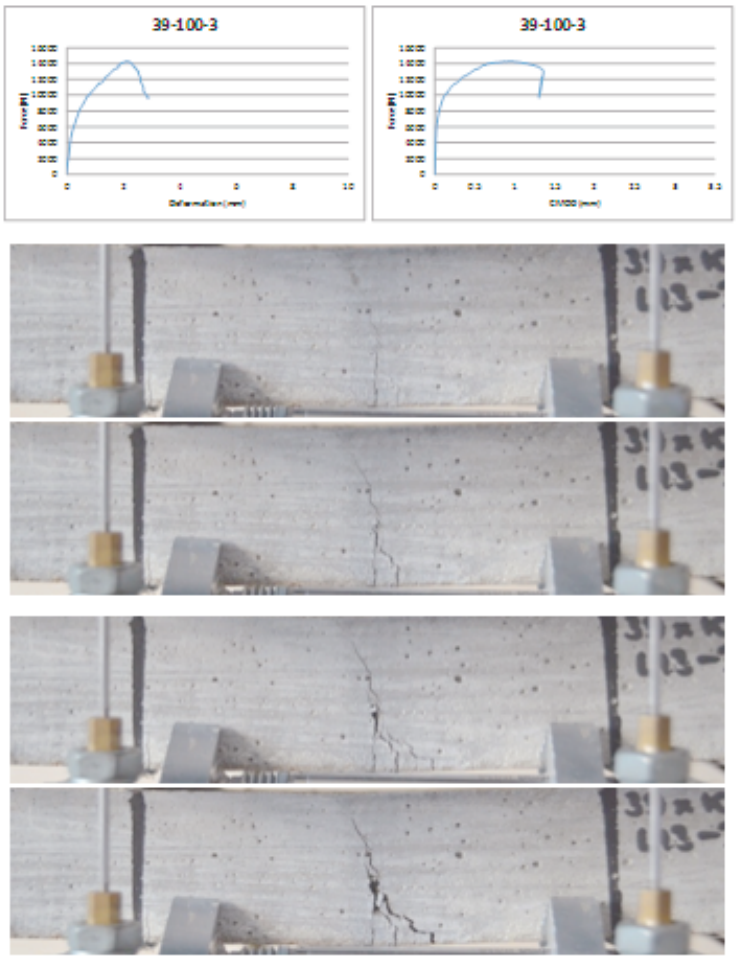

Figure C.16. 39-100-13-3 (a/d=2,56 t/fL=3 A.R=81,3).

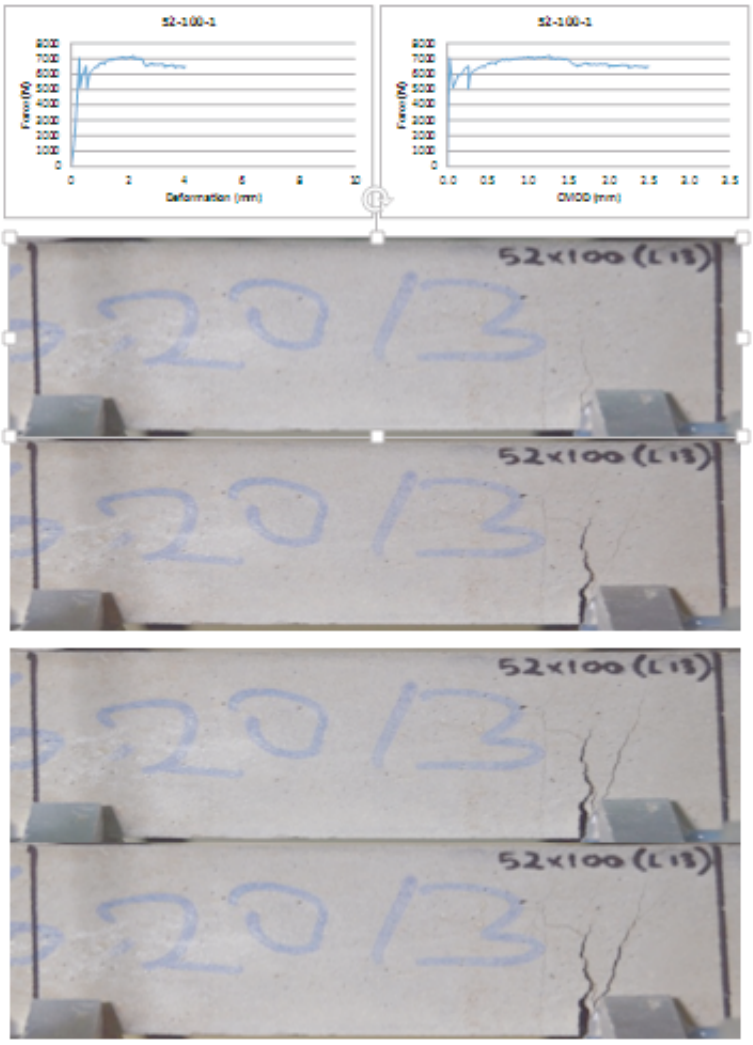

Figure C.17. 52-100-13-1 (a/d=1,92 t/fL=4 A.R=81,3).

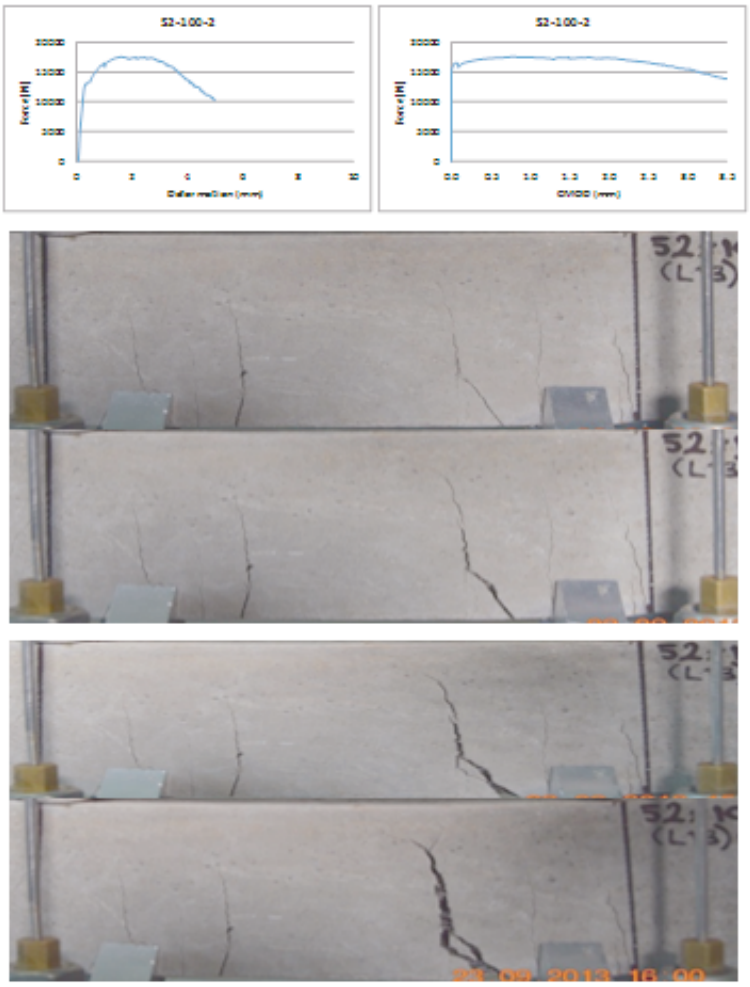

Figure C.18. 52-100-13-2 (a/d=1,92 t/fL=4 A.R=81,3).

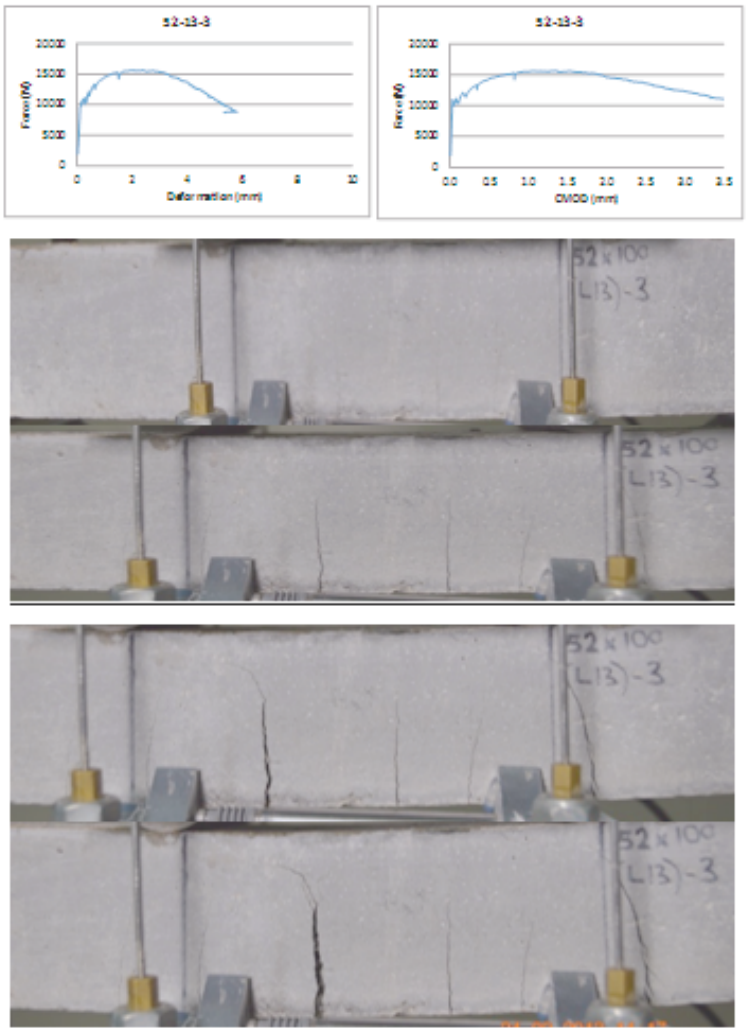

Figure C.19. 52-100-13-3 (a/d=1,92 t/fL=4 A.R=81,3).

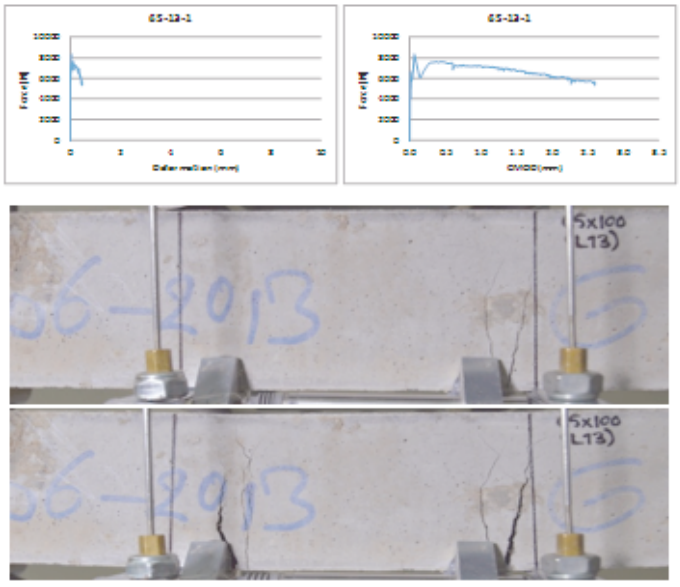

Figure C.20. 52-100-13-3 (a/d=1,92 t/fL=4 A.R=81,3).

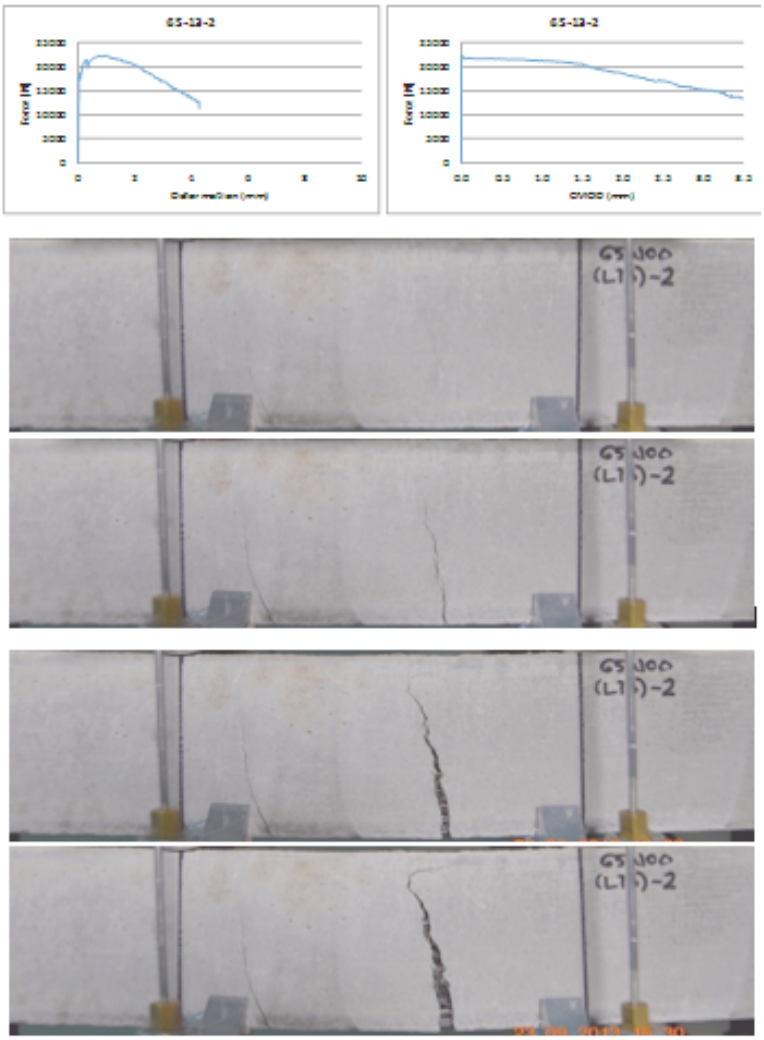

Figure C.21. 65-100-13-2 (a/d=1,54 t/fL=5 A.R=81,3).

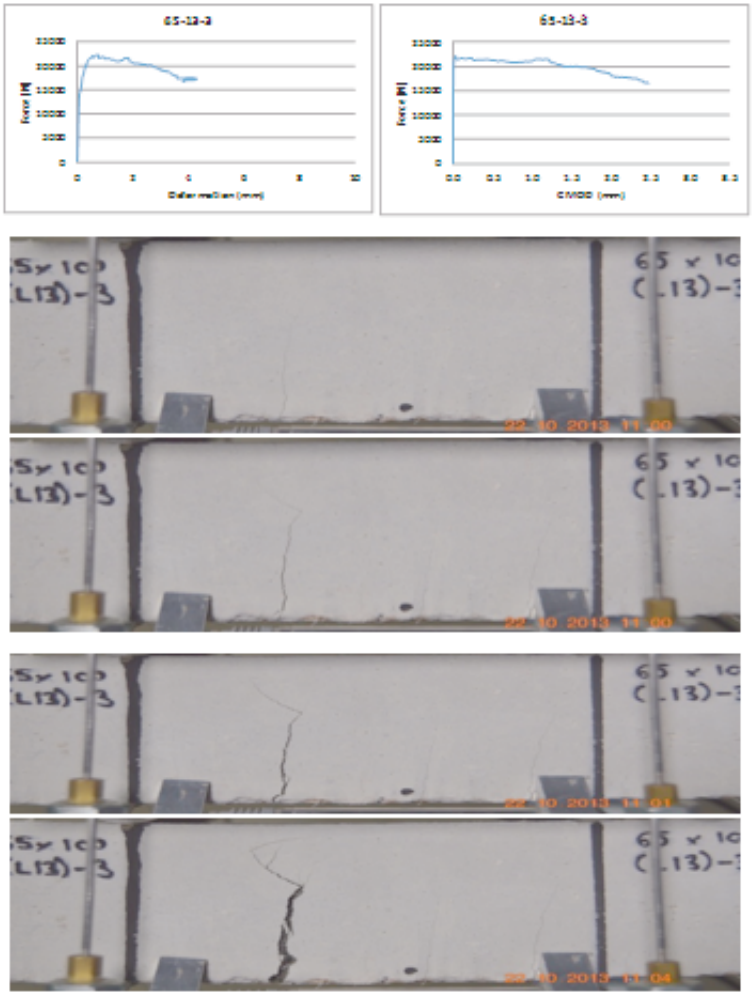

Figure C.22. 65-100-13-3 (a/d=1,54 t/fL=5 A.R=81,3).

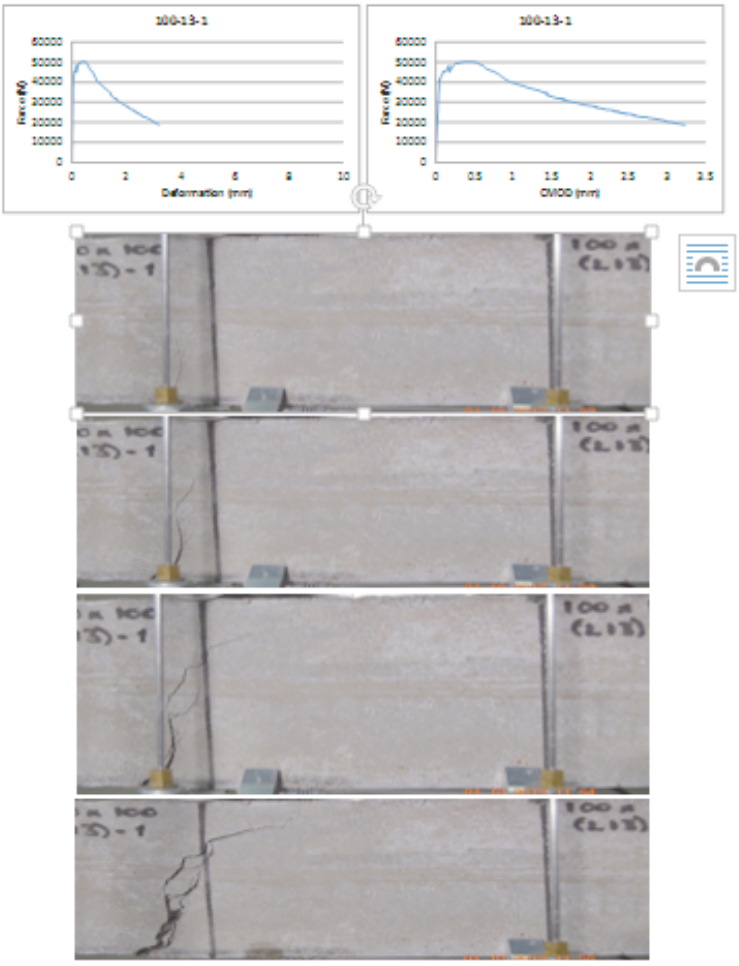

Figure C.23. 100-13-1(a/d=1 t/fL=8 A.R=81,3).

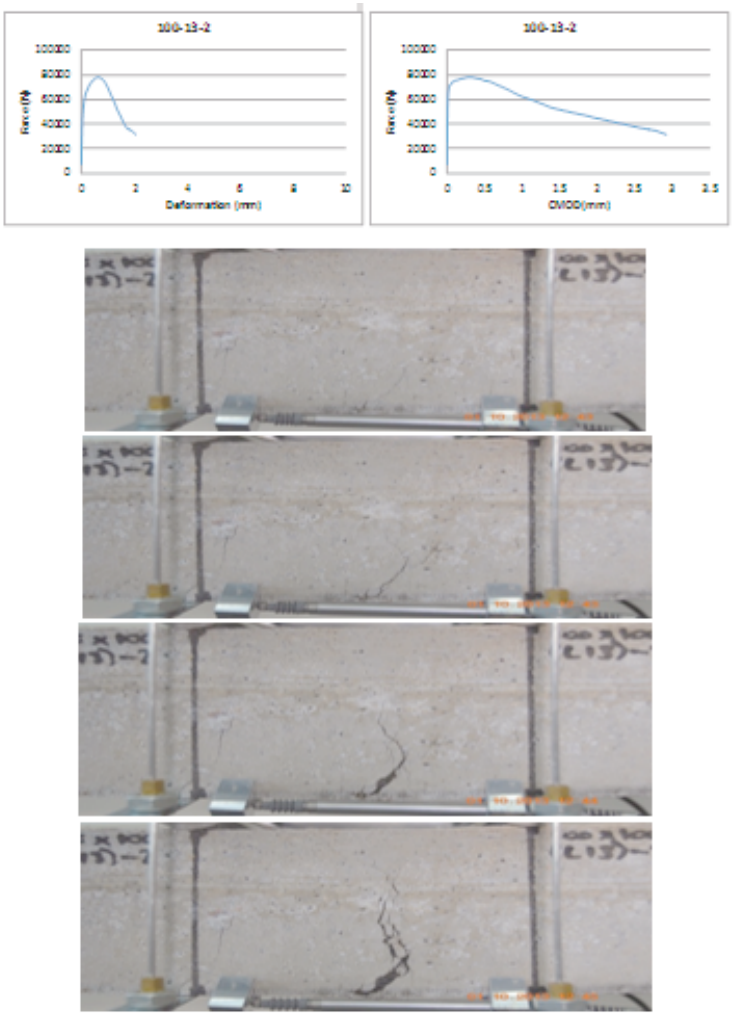

Figure C.24. 100-13-2 (a/d=1 t/fL=8 A.R=81,3).

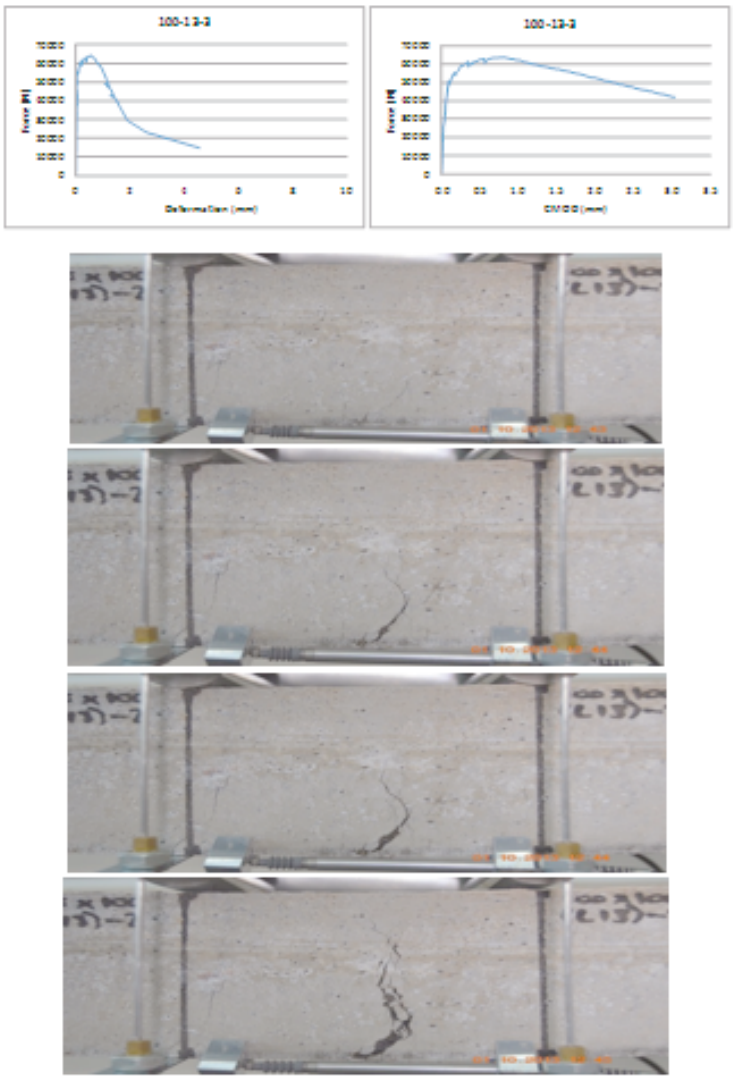

Figure C.25. 100-13-3 (a/d=1 t/fL=8 A.R=81,3).

REFERENCES

1. Oh, BH., "Closure to Flexural Analysis of Reinforced Concrete Beams Containing Steel Fibers", *Journal of Structural Engineering*, Vol. 120, No. 6, 1994.

2. Campione, G. and M.L. Mangiavillano, "Fibrous Reinforced Concrete Beams in Flexure: Experimental Investigation, Analytical Modeling and Design Considerations", *Engineering Structures*, Vol. 30, No. 11, pp. 2970-2980, 2008.

3. Lim, D.H. and B.H. Oh, "Experimental Investigation on the Shear of Steel Fibre Reinforced Concrete Beams", *Engineering Structures*, Vol. 21, No. 10, pp. 937-944, 1999.

4. Chunxiang, Q. and I. Patnaikuni, "Properties of High-Strength Steel Fiber-Reinforced Concrete Beams in Bending", *Cement and Concrete Composites*, Vol. 21, No. 1, pp. 73-81, 1999.

5. Naaman, A.E., Reinhardt H.W., "High Performance Fiber Reinforced Cement Composites-HPFRCC4", In: RILEM Proceedings, PRO 30. RILEM Publications SARL, Bagneaux, France, 2003.

6. Banthia, N. "Fiber Reinforced Cements and Concretes", *Canadian Journal of Civil Engineering*, Vol. 28, No.5, pp. 879-880, 2001.

7. Rossi, P., G. Chanvillard, "Fiber Reinforced Concretes", Bagneux, France. RILEM S.A.R.L. 2000.

8. Kooiman, A.G., "Modelling Steel Fibre Reinforced Concrete for Structural Design", PhD Thesis. *Department of Structural and Building Engineering*, Delft University of Technology, 2000.

9. Shah, S.P. and K.G. Kuder, "Hybrid and High Performance Fiber Reinforced Cemen-

titious Composites", *Proceedings of the International Workshop on Advances in Fiber Reinforced Concrete*, Bergamo, Italy, pp. 83-92.

10. Romualdi J.P. and G.B. Batson, "Mechanics of Crack Arrest in Concrete", *Proceedings of ASCE*, Vol. 89, No. 3, pp. 147-68, 1963.

11. Mobasher B. and C.Y. Li, "Effect of Interfacial Properties on the Crack Propagation in Cementitious Composites", *Advanced Cement Based Materials*, Vol. 4, No. 3-4, pp. 93-105, 1996.

12. Kukreja C.B., S. Chawla, "Flexural Characteristics of Steel fibre reinforced concrete", *The Indian Concrete Journal*, pp. 154., March, 1989.

13. Di Prisco, M., G. Plizzari, L. Vandewalle, "Fiber Reinfroced Concrete: New Design Perspective," *Materials and Structures*, Vol. 42, pp. 1261-81, 2009.

14. ACI Committe 544, Design Considerations for Steel Fiber Reinforced Concrete. In ACI 544.4R-88, Farmington Hills, MI. American Concrete Institute, 1996.

15. Gunavel, M., S.S. Kokila, "Experimental Investigation On Behaviour Of Hybrid Fiber Reinforced Concrete Beams", Integer. J. Engeerign Resistance Techhical, ISSN NO. 2348-6821, 2015.

16. Wegian, F.M., A.A. Alanki, H.M. AlSaeid, F.A. Alotaibi, M. Al-Mitairi, F.A. Kandari, "Influence of Fly Ash on Behavior of Fibres Reinforced Concrete Structures", *Journal of Applied Sciences*, Vol. 11 No. 17, p3185, 2011.

17. Ferrara, L., N. Özyurt and M. di Prisco, "High Mechanical Performance of Fiber-Reinforced Cementitious Composites: the Role of Casting Flow Induced Fiber Orientation", *Materials and Structures, Accepted for Publication*, 2010.

18. Akkaya, Y., J. Picka and S.P. Shah, "Spatial Distribution of Aligned Short Fibers in Cement Composites", *Journal of Materials in Civil Engineering*, Vol. 12, pp. 272, 2000.

19. 19. Blanco, A. *Characterization and Modelling of SFRC Elements*, PhD Thesis, Universitat Politècnica de Catalunya, Departament d'Enginyeria de la Construcció, 2013.

20. Van Zijl, G.P.A.G., W.P. Boshoff, "Verification of Materials Design Formulae for the Structural use of Ductile Fiber Reinforced Cement Composites", *Unpublished Manuscript*, 2006.

21. ASTM C1018-92, "Standard Test Method for Flexural Toughness and First-Crack Strength of Fiber-Reinforced Concrete" *Using Beam with Third Point Loading*, 1992.

22. RILEM TC 162-TDF, "Test and Design Methods for Steel Fibre Reinforced Concrete - re Design Method", *Materials and Structures*, Vol. 35, pp. 262-278, 2002.

23. Naaman A.E., H.W. Reinhardt, "High Performance Fiber Reinforced Cement Composites-HPFRCC4", *In: RILEM Proceedings, PRO 30. RILEM Publications SARL*, Bagneaux, France, 2003.

24. 24. Bazant, Z.P., "Size Effect in Blunt Fracture: Concrete, Rock, Metal" *Journal of Engineering Mechanics*, ASCE, Vol. 110, No. 4, pp. 518-535, 1984.

25. Bazant, Z.P., "Fracture Size Effect: Review of Evidence for concrete structures", *Johurnal Structural Engineering*, Vol. 120, No. 8, pp. 2377-2398, 1994.

26. 26. Erdem, E., "The Flexural Behaviour of SFRC Beams and Slabs: Bending with the $\sigma - \varepsilon$-Method", *Proceedings RILEM TC 162-TDF Workshop: Test and Design Methods for Steel Fibre Reinforced Concrete - Background and Experiences*, 2003.

27. Sener, S., M. Begimgil, C. Belgin, "Size Effect on Failure of Concrete Beams With and Without Steel Fibers", *Journal of Materials in Civil Engineering*, 2002.

28. Ferrara L. and A. Meda, "Relationships Between Fibre Distribution, Workability and the Mechanical Properties of SFRC Applied to Precast Roof Elements", *Materials*

and Structures, Vol. 39, pp. 411-420, 2006.

29. CNR-DT 204/2006, "Guidelines for the Design, Construction and Production Control of Fiber Reinforced Concrete Structures", *Italian National Research Council*, Rome, 2006

30. CEN - European Committee for Standardization, "Steel Fibre Reinforced Concrete Definitions", *Classification and Designation. UNI*, 11039-1, 2003.

31. ACI Committee 544, "Guide for Specifying, Mixing, Placing and Finishing Steel Fiber Reinforced Concrete", *ACI Materials Journal*, Vol. 90, No. 1, pp. 94-101, 1993.

32. Nataraja, M.C., N. Dhang and A.P. Gupta, "Toughness Characterization of Steel Fiber-Reinforced Concrete by JSCE Approach", *Cement and Concrete Research*, Vol. 30, pp. 593-597, 2000.

33. Soroushian, P. and Z. Bayasi, "Fiber Type Effects on the Performance of Steel Fiber Reinforced Concrete", *ACI Materials Journal*, Vol. 88, No. 2, pp. 129-134, 1991.

34. 34. Chen, L., S. Mindess and D.R. Morgan, "Specimen Geometry and Toughness of Steel Fiber Reinforced Concrete", *ASCE Journal of Materials and Civil Engineering*, Vol. 6, No. 4, pp. 529- 541, 1994.

35. ASTM-American Standard of Testing Materials, "Standard Test Method for Flexural Performance of Fiber-Reinforced Concrete (Using Beam With Third-Point Loading)", *ASTM C1609/1609M*, 2010.

36. Boulekbache, B., M. Hamrat, M. Chemrouk and S. Amziane, "Flowability of Fibre-Reinforced Concrete and Its Effect on the Mechanical Properties of the Material", J*ournal of Construction and Building Materials*, Vol. 24, pp. 1664-1671, 2010.

37. Fanella, D.A. and A. Naaman, "Stress-Strain Properties of Fiber Reinforced Mortar in Compression", *ACI Journal*, Vol. 82, No. 4, pp. 475-483, 1985.

38. 38. A. Bentur and S. Mindess, "Fiber Reinforced cementitious Composites", *Elsevier Applied Sciences*, ISBN 0-203-49806-2, 2005.

39. Bencardino F, L. Rizzuti, G. Spadea, "Swamy RN. Experimental evaluation of Fiber Reinforced Concrete", *Fracture Properties Compos Part B: Engeering*; Vol, 41, No. 1, pp. 17-24, 2010.

40. JSCE SF-4, "Method of Test for Flexural Strength and Flexural Toughness for Fiber Reinforced Concrete", *Concrete Library of JSCE*, Vol.3, pp. 58-61, 1984.

41. RILEM Draft Recommendation 50FMC, "Determination of Fracture Energy of Mortars and Concrete by Means of Three-Point Bend Tests on Notched Beams", Matererials Structure Vol. 18, pp. 285-290, 1985.

42. EFNARC , "Specification for Sprayed Concrete", *Final Draft Published by the European Federation of National Associations of Specialist Contractors and Material Suppliers to the Construction Industry (EFNARC)*, Hampshire, UK, pp. 35, 1996.

43. B. Barr, R. Gettu, S.K.A. Al-Oraimi, L.S. Bryars, "Toughness Measurement: the Need to Think Again", *Cement and Concrete Composites*, pp:281-297, 1996.

44. Lianrong, C., "Flexural Toughness of Fibre Reinforced Concrete, Graduate Thesis", University of British Columbia, 2009.

45. Balaguru, P.N., and S.P. Shah, "Fiber-Reinforced Concrete Composites", *McGraw-Hill*, New York, 1992.

46. ACI 544.1R , "State-of-the-Art Report on Fiber Reinforced Concrete", *American Concrete Institute*, Farmington Hills, Michigan, 1996.

47. Walraven, J.C. "High Performance Fiber Reinforced Concrete: Progress in Knowledge and Design Codes", *Materials and Structures*, Vol. 42, No. 9, pp. 1247-1260, 2009.

48. Shah S.P. *et al.*, "Fibre-Reinforced Cement-Based Composites: A Forty Year Odyssey, 6thRILEM Symposium on Fibre-Reinforces Concrete (FRC)",- *BEFIB 2004*, 20-22 September 2004,Varenna, Italy, pp. 3-30, 2004.

49. Nguyen V.C., H.D. Nguyen, "Development of Steel Fibre Reinforced Concrete for Infrastructure Works", National Science Conference "Application of Advanced Concrete Technology"- AACT 2007, V*ietnam Concrete Association, Lao dong Publisher*, pp. 99-106, 2007.

50. Yang, J. and G. Fischer, "Investigation of the Fiber Bridging Stress-Crack Opening Relationship of Fiber Reinforced Cementitious Composites", *International RILEM Workshop on High Performance Fiber Reinforced Cementitious Composites (HPFRCC) in Structural Applications*, Honolulu, Hawai'I, 23-26 May, 2005.

51. Shah, S. P. "Do Fibers Increase the Tensile Strength of Cement-Based Matrixes?" *ACI Material Journal*, Vol. 88, No. 6, pp. 595-602, 1991.

52. Li, V.C. and M. Maalej, "Toughening in Cement Based Composites. Part II: Fiber Reinforced Cementitious Composites", *Cement and Concrete Composites*, Vol. 18, pp. 239-249, 1996.

53. Romualdi, J.P. and G.B. Batson, "Mechanics of crack arrest in concrete", *Proceedings, American Society of Civil Engineers, Journal, Engineering Mechanics Division*, Vol. 89, pp. 147-68, 1963.

54. Johnston, C.D., "Toughness of Steel Fibre Reinforced Concrete. Proceedings of the Steel Fibre Concrete US-Sweden Joint Seminar (NSF-STU)", *Swedish Cement and Concrete Research Institute*, Stockholm / Sweden, pp. 333-360, 1985.

55. Johnston, C.D., and W.R. Zemp, "Flexural Fatigue Performance of Steel Fibre Reinforced Concrete: Influence of Fibre Content, Aspect Ratio, and Type", *American Concrete Institute, Material Journal*, Vol. 88, No. 4, pp. 374-383, 1991.

56. Morgan, D.R. and D.N. Mowat, "A Comparative Evaluation of Plain, Mesh and Steel Fibre Reinforced Concrete", *International Symposium, American Concrete Institute*, Detroit / United States of American, pp. 305-318, 1984.

57. Banthia, N., K. Chokri, and J.F. Trottier, "Impact Tests on Cement-Based Fiber Reinforced Composites", *Publications of the American Concrete Institute*, SP.155-9, Detroit / United States of America, pp. 171-188, 1995.

58. Jindal, R.L., "Shear and Moment Capacities of Steel Fibre Reinforced Concrete Beams", *International Symposium, American Concrete Institute*, Detroit / United States of America. pp. 1-16, 1984.

59. Bekaert, "Steel Fibers for the Pre-cast Industry", *Bekaert NV. Dramix Technical Pamphlet*, 1999.

60. Jansson A. "Analysis and Design Methods for Fibre Reinforced Concrete: a State-of-the-art Rreport", Göteborg, *Department of Civil and Environmental Engineering, Divergence of Structural Engineering/Concrete Structures*, Chalmers University of Technology, 178 pp., 2007.

61. Jansson A., I. Löfgren, K. Gylltoft K. "Design Methods for Fibre - Reinforced Concrete: A State-o-the Art Review", *Nordic Concrete Research*, Vol. 2, No. 38, pp. 31-46, 2008.

62. Naaman A.E. "Strain Hardening and Deflection Hardening Fiber Reinforced Cement Composites", *In: High Performance Fiber Reinforced Cement Composites (HPFRCC4), Proceedings of the 4th International RILEM Workshop*, Ann Arbor, USA, pp. 95-113, 2003.

63. Löfgren, I., "Fibre-Reinforced Concrete for Industrial Construction- A Fracture Mechanics Approach to Material Testing and Structural Analysis", PhD Thesis, Chalmers University Of Technology, Sweden, 2005.

64. Rossi P., P. Acker, and P. Malier, "Effect of Steel Fibres at two Different Stages: The Material and the Structure", *Materials and Structures*, Vol. 20, pp. 436-439, 1987.

65. Betterman, L.R., C. Ouyang, S.P. Shah, "Fiber-Matrix Interaction in Microfiber-Reinforced Mmortar", *Advanced Cement Based Materials*, Vol. 2, pp. 53-61, 1995.

66. Nelson, P.K, V.C. Li, and T. Kamada, "Fracture Toughness of Microfiber Reinforced Cement Composites", *Journal of Materials in Civil Engineering*, pp. 384-391, 2002.

67. Lawler, J.S., T. Wilhelm, D. Zampini, and S.P. Shah, "Fracture Processes of Hybrid Fiberreinforced Mortar", *Materials and Structures*, Vol. 36, pp. 197-208, 2003.

68. J.W. Dally and W.F. Riley, "Experimental Stress Analysis", 3rd edition, *McGraw-Hill Inc.*, Singapore, 1991.

69. P.J. Sevenhuijsen, "The Photonical, Pure Grid Method", *Optics and Lasers in Engineering*, Vol. 18, pp.173-194, 1993.

70. R.C. Gonzalez and R.E. Woods, "Digital Image Processing", *Addison-Wesley Publishing*, London, 1992.

71. E.M. Mikhail, J.C. McGlone and J.S. Bethel, "Introduction to Modern Photogrammetry", *Wiley*, New York, 2001.

72. T.K. Lee and R. Al-Mahaidi, "An Experimental Investigation on Shear Behavior of RCT-beams Strengthened with CFRP Using Photogrammetry", *Composite Structures*, vol. 82, pp. 185-193, 2008.

73. Luna, R., "Digital image analysis techniques for fiber and soilmixtures", LTRC Replection 98-2, *TIRE*, Tulane University, New Orleans, 1999.

74. Seo, Y., Y.R. Kim, M. Witczak, and R. Bonaquist, "Application of Digital Image

Correlation Method to Mechanical Testing of Asphaltaggregate Mixtures", *Transportation Research Record 1789, Transportation Research Board*, Washington, DC, 2002.

75. Yue, Z., S. Chen, and L. Tham, "Finite-Element Modeling of Geomaterials Using Digital Image Processing", Computation Geotechical, Vol. 30, No. 5, pp. 375-397, 2003.

76. Rechenmacher, A.L., and R.J. Finno, "Digital Image Correlation to Evaluate Shear Banding in Dilative Sands", *Journal ASTM Geotech Testing*, Vol. 27, No. 1, pp. 13-22, 2004.

77. Chehab, G.R., Y. Seo, and Y.R. Kim, "Viscoelastoplastic Damage Characterization of Asphalt-Aggregate Mixtures Using Digital Image Correlation", *International Journal Geomechnical*, 10.1061/(ASCE)1532-3641(2007)7: 2(111), 111-118, 2007.

78. Choi, S., and S.P. Shah, "Measurement of Deformations on Concrete Subjected to Compression Using Image Correlation", Exporvement Mechnical, Vol. 37, No. 3, pp. 307-313, 1997.

79. Yoneyama, S., Y. Morimoto, and M. Takashi, "Automatic Evaluation of Mixed-Mode Stress Intensity Factors Utilizing Digital Image Correlation", *Strain*, Vol. 42, No. 1, pp. 21-29, 2006.

80. Kozicki, J., and J. Tejchman, "Experimental Investigations of Strain Localization in Concrete Using Digital Image Correlation (DIC) Technique", *Archnology Hydro-Engineering Environmental Mechanical*, Vol, 54, No. 1, pp. 3-24, 2007.

81. Wu, Z.M., H. Rong, J.J. Zheng, F. Xu, and W. Dong, "An Experimental Investigation on the FPZ Properties in Concrete Using Digital Image Correlation Technique", *Engineering Fraction Mechanical*, Vol. 78, No. 17, pp. 2978-2990, 2011.

82. Huang, Y.H., L. Liu, F.C. Sham, Y.S. Chan, and S.P. Ng, "Optical Strain Gauge

vs. Traditional Strain Ggauges for Concrete Elasticity Modulus Determination", *Optik*, Vol. 121, No. 18, pp. 1635-1641, 2010.

83. Czaderski, C., K. Soudki, and M. Motavalli, "Front and Side View Image Correlation Measurements on FRP to Concrete Pull-off Bond Tests", *Journal Composition Construction*, 10.1061/(ASCE)CC.1943-5614.0000106, pp. 451-463, 2010.

84. Adrian R.J., "Particle-Imaging Techniques for Experimental Fluid Mechanics", *Annual Revience Fluid Mechanical*, Vol. 23, No. 1, pp. 261-304, 1991.

85. White, D.J., W.A. Take, and M.D. Bolton, "Soil Deformation Measurement Using Particle Image Velocimetry (PIV) and Photogrammetry", *Géotechnique*, Vol. 53, No. 7, pp. 619-631, 2003.

86. Slominski, C., M. Niedostatkiewicz, and J. Tejchman, "Application of Particle Image Velocimetry (PIV) for Deformation Measurement During Granular Silo Flow", *Powder Technology*, Vol. 173, No. 1, pp. 1-18, 2007.

87. Hosseini A, D. Mostofinejad, "Experimental Investigation Into Bond Behavior of CFRP Sheets Attached to Concrete Using EBR and EBROG Techniques", *Compos Part B: Engineering*, Vol. 51, pp. 130-9, 2013.

88. Hosseini A, D. Mostofinejad, "Effect of Groove Characteristics on CFRP-Toconcrete Bond Behavior of EBROG Joints: Experimental Study Using Particle Image Velocimetry (PIV)", *Constr Build Materials*, Vol. 49, pp. 364-73, 2013.

89. Hosseini A, D. Mostofinejad "Effective Bond Length of FRP-to-Concrete Adhesively-Bonded Joints: Experimental Evaluation of Existing Models", Int J Adhes Adhes; Vol. 48, pp. 150-8, 2014.

90. Hosseini A., D. Mostofinejad M. Hajialilue-Bonab, "Displacement Measurement of Bending Tests Using Digital Image Analysis Method", International Journal Engineering Technology, Vol. 4, No. 5, pp. 642-4, 2012.

91. Hosseini A., D. Mostofinejad, M. Hajialilue-Bonab "Displacement and Strain Field Measurement in Steel and RC Beams Using Particle Image Velocimetry", ASCE Journal Engineering Mechanical, Vol. 140, No. 11, pp. 150-160, 2014.

92. Barros J.A.O., V.M.C.F. Cunha, A.F. Ribeiro, J.A.B. Antunes, "Post-Cracking Behaviour of Ssteel Fibre Reinforced Concrete", *Mater Struct/Materiaux et Constructions*, Vol. 38, No. 275, pp. 47-56, 2005.

93. Rossi P., "Mechanical Behaviour of Metal-Fibre Reinforced Concretes", Cement Concrete Compos, Vol. 14, No. 1, pp. 3-16, 1992.

94. Soulioti, D., N.M. Barkoula, A. Paipetis, T.E. Matikas, T. Shiotani, D.G. Aggelis, "Acoustic Emission Behavior of Steel Fibre Reinforced Concrete Under Bending", Construct Build Mater, Vol. 23, No. 12, pp. 3532-6, 2009.

95. Soulioti D.V., N.M. Barkoula, A. Paipetis, T.E. Matikas. "Effects of Fibre Geometry and Volume Fraction on the Flexural Behaviour of Steel-Fibre Reinforced Concrete", Vol. 47, No. 1, pp. 535-41, 2011.

96. Bencardino, F., L. Rizzuti, G. Spadea, R.N. Swamy, "Experimental Evaluation of Fiber Rinforced Concrete Fracture Properties", *Compos Part B: Engng*; Vol. 41, No. 1, pp. 17-24, 2010.

97. Reinhardt H-W. "Beton", *Betonkalender*, 2005.

98. Johansen KW. Fibre reinforcement: theoretical and practical investigations of the elasticity and strength of fibre-reinforced materials. Akademisk Forlag; 1964.

99. Özyurt, N., T.Ö. Mason, S.P. Shah, "Correlation of Fiber Dispersion, Rheology and Mechanical Performance of FRCs", *Cement and Concrete Composites*, Vol. 29, No.2, pp. 70-79, 2007.

100. Stahli P., R. Custer, J.G.M. van Mier, "On Flow Properties, Fibre Distribution, Fibre Orientation and Flexural Behavior of FRC", *Mater Struct*, Vol. 41, pp. 189-96,

2008.

101. Şanal I., N. Özyurt Zihnioglu, "To What Extent Does the Fiber Orientation Affect Mechanical Performance?" *Construction Build Materials*, Vol. 44, pp. 671-81, 2013.

102. Şanal, I. "Effects of Formwork Dimensions on The Mechanical Performance of Fiber Reinforced Cement Based Materials", MSc Thesis Bogazici University, 2010.

103. Lin Y.Z. , "Tragverhalten Von Stahlfaserbeton", PhD thesis, Universitat Karlsruhe, 1999.

104. Stahli, P., J.G.M. Van Mier, "Manufacturing, Fibre Anisotropy and Fracture of Hybrid Fibre Concrete", *Engineering Fraction Mechanicay*, Vol. 74, No. 1-2, pp. 223-42, 2007.

105. Kooiman A.G., C. Van Der Veen, J.C. Walraven, "Modelling the Post-Cracking Behaviour of Steel Fibre Reinforced Concrete for Structural Purposes", *HERON*, Vol. 45, No. 4, pp. 275-307, 2000.

106. Schönlin K., "Determination of the Orientation, the Content and the Distribution of the Fibres in Fibre Reinforced Concrete", *Beton- Und Stahlbetonbau*, Vol. 6 pp. 168-171, 1988.

107. Vandewalle, L. and D. Dupont, "Test and Design Methods for Steel Fiber Reinforced Concrete", *In Bending Test and Interpretation.* Bochum, 2003. *RILEM Proceeding 31 of TC 162-TDF Workshop*, 2003.

108. Gettu R., D.R. Gardner, H. Saldı´Var, B.E. Barragan, "Study of the Distribution and Orientation of Fibers in SFRC Specimens", *Journal of Mechanics of Materials and Structures* Vol. 38, No. 1, pp. 31-37, 2005.

109. Grünewald S., "Performance-Based Design of Self-Compacting Fibre Reinforced Concrete", PhD Thesis, Delft University of Technology, 2004.

110. Grünewald, S., F. Laranjeira, J. Walraven, A. Aguado and C. Molins, "Improved Tensile Performance with Fiber Reinforced Selfl Compacting Concrete", *In Proceedings of the 6th International Workshop on High Performance Fiber Reinforced Cement Composites (HPFRCC6)*, Vol. 1, pp. 20-22 2011.

111. Martinie, L., P. Rossi and N. Roussel, "Rheology of Fiber Reinforced Cementitious Materials: Classification and Prediction", *Cement and Concrete Research*, Vol. 40, No. 2, pp. 226-234, 2010.

112. Ferrara, L., Y.-D. Park and S.P. Shah, "Correlation Among Fresh State Behavior, Fiber Dispersion, and Toughness Properties of SFRCs", *Journal of Materials in Civil Engineering*, Vol. 20, No. 7, pp. 493-501, 2008.

113. Robins P.J., S.A. Austin, P.A. Jones, "Spatial Distribution of Steel Fibres in Sprayed and Cast Concrete" Magazine of Concrete Research, Vol. 55, No. 3, pp. 225-235, 2003.

114. Markovic, I., "High-Performance Hybrid-Fiber Reinforced Concrete: Development and Utilisation", Ph.D., Delft University of Technology, Delft, 2006.

115. Torrijos M.C., J.M. Tobes, B.E. Barragán, R.L. Zerbino, "Orientation and Distribution of Steel Fibres in Self-Compacting Concrete", P*roceedings of the 7th RILEM Symposium on Fibre Reinforced Concrete: Design and Applications* (BEFIB 2008), Chennai, India, 729-738, 2008.

116. Lappa, L. "High Strength Fiber Reinforced Concrete: Static and Fatigue Behavior in Bending", PhD Thesis, Delft University of Technology, Delft, 2007.

117. Toujanji H, Z. Bayasi, "Effects of Manufacturing Techniques on the Flexural Behavior of Steel Fiber-Reinforced Concrete", *Cement and Concrete Research*, Vol. 28, No. 1, pp. 115-124, 1998.

118. Roussel N., "Rheology of Fresh Concrete: From Measurements to Predictions of Cast-

ing Processes", *Materials and Structures*, Vol. 40, pp. 1001-1012, 2007.

119. Michels, J., D. Waldmann, S. Maas and A. Zürbes, "Steel Fibers as Only Reinforcement for Flat Slab Construction - Experimental Investigation and Design", *Construction and Building Materials*, Vol. 26, No. 1, pp. 145-155, 2012.

120. Edgington, J. and D.J. Hannant, "Steel Fibre Reinforced Concrete. The Effect on Fibre Orientation of Compaction by Vibration", *Materials Structures*, Vol. 5, No. 25, pp:41-44, 1972.

121. Stroeven, P., "The Analysis of Fibre Distributions in Fibre Reinforced Materials", *Journal Microscopy*, Vol. 111, pp. 283-295, 1977.

122. Stroeven, P., "Morphometry of Fibre Reinforced Cementitiousmaterials, Part II: Inhomogeneity, Segregation and Anisometry of Partially Oriented Fibre Structures", *Materials Structure*, Vol. 12, pp. 9-20, 1979.

123. Soroushian, P. and C.D. Lee, "Distribution and Orientation of Fibers in Steel Fiber Reinforced Concrete", *ACI Materials Journal*, Vol. 87, No. 5, pp.433-439, 1990.

124. Toutanji, H. and Z. Bayasi, "Effect of Manufacturing Techniques on the Flexural Behaviour of Steel Fiber Reinforced Concrete", *Cemontrial Concrete Resistance*, Vol. 28, No. 1, pp. 115-124, 1998.

125. Dupont D., L. Vandewalle, "Distribution of Steel Fibres in Rectangular Sections", *Cemontrial Concrete Compospotion*, Vol. 27, pp. 391-398, 2005.

126. Vandewalle L., G. Heriman, F. Van Rickstal, "Fibre Orientation in Self-Compacting Fibre Reinforced Concrete", In: Proceedings of the 7th RILEM Symposium on Fibre Reinforced Concrete: Design and Applications (BEFIB 2008), *Chennai, India*, pp. 719-728, 2008.

127. Molins C., J. Martinez, N. Arnaiz, "Distribution of Steel Fibers in Prismatic Concrete Samples", *In: CD-ROM from the 4th International Structural Concrete Congress*

(ACHE), Valencia, Spain (in Spanish), 2008.

128. 128. Özyurt, N., T.O. Mason, S.P. Shah, "Non-Destructive Monitoring of Fiber Orientation Using AC-IS: An Industrial Scale Application", *Cement and Concrete Research*, Vol. 36, No. 9, pp. 1653-1660, 2006.

129. Chermant, J.L., L. Chermant, M. Coster, A.S. Dequiedt and C. Redon, "Some Fields of Applications of Automatic Image Analysis in Civil Engineering", *Cement and Concrete Composites*, Vol. 23, pp. 157-169, 2001.

130. Eberhardt, C., and A. Clarke, "Fiber-Orientation Measurements in Short-Glass-Fiber Composites. Part I: Automated, High Angular-Resolution Measurement by Confocal Microscopy", *Composites Science and Technology*, Vol. 61, pp. 1389-1400, 2001.

131. Özyurt, N., L.Y. Woo, T.O. Mason, S.P. Shah, "Monitoring Fiber Dispersion in FRCs: Comparison of AC-Impedance Spectroscopy and Image Analysis", *ACI Materials Journal*, Vol. 103, No.5, pp. 340-347, 1998.

132. Özyurt, N., "Connecting Fiber Dispersion, Rheology and Mechanical Performance for Fiber Reinforced Cement Based Materials", PhD Thesis, Istanbul Technical Institute, 2005.

133. G. Advani and C.L., "Tucker III", *SPE ANTEC Technical*, pp. 31, 1985.

134. S.G. Advani and C.L. Tucker, J. III, "Rheology", pp. 31, 1987.

135. DBV, "Guide to Good Practice Steel Fibre Concrete", *German Society for Concrete and Construction Technology*, Berlin, 2001.

136. CPH, "Instrucción del Hormigón Estructural EHE-08", *Ministerio de Fomento*, Madrid, 2008.

137. FIB, "Model Code 2010", *International Federation for Structural Concrete*, Lausanne,

2010.

138. Blanco A, P. Pujadas, A. De La Fuente, A. Aguado, "Análisis Comparativo De Los Modelos Constitutivos Del Hormigón Reforzado Con Fibras", *Submitted to Hormigóny Acero*, 2010.

139. Tregger N., L. Ferrara, S. Shah, "Identifying Viscosity of Cement Paste from Minislump-Flow Test", *ACI Mater Journal*, Vol. 105, No. 6, pp. 558-66 2008.

140. Roussel N., C. Stefani, R. Leroy, "From Mini-Cone Test to Abrams Cone Test: Measurement of Cement Based Materials Yield Stress Using Slump Tests", *Cem Concrete Resistance*, Vol. 35, No. 5, 817-22, 2005.

141. Martinie L, N. Roussel, "Simple Tools for Fiber Orientation Prediction in Industrial Practice, Cem Concrete Resistance, Vol. 41, No. 10, pp. 993-1000, 2011.

142. White D.J., W.A. Take, "GeoPIV: Particle Image Velocimetry (PIV) Software for Usein Geotechnical Testing", Cambridge University Engineering Department Technical Report, D-SOILS-TR322; 2002.

143. Kuder K., N. Özyurt, B. Mu, S.P. Shah, "Rheology of Fiber-Reinforced Cementitious Materials", *Cem Concrete Resistance* Vol. 37, No. 2, pp. 191-9 2007.

144. BS EN 12390-2, "Making and Curing Specimens for Strength Test", *British Standards*, 2009.

145. Banfill P.F.G., "Rheology of Fresh Cement and Concrete", *Rheol Revitation*, pp. 61-130 2006.

146. Tregger N., A. Gregori, L. Ferrara, S. Shah, "Correlating Dynamic Segregation of Felf-Consolidating Concrete to the Slump-Flow Test", *Construction Build Materials March*, Vol. 28, No. 1, 499-505, 2012.

147. Kang S.T., J.K. Kim, "The Relation Between Fiber Orientation and Tensile Behavior

in an Ultra high Berformance Fiber Reinforced Cementitious Composites (UHPFRCC)", *Cem Concrete Resistance*, Vol. 41, pp. 1001-14, 2011.

148. Naaman, A.E., H.W. Reinhardt, "Proposed Classification of HPFRC Composites Based on Their Tensile Response", *In: Materials and Structures*, Vol. 39, pp. 547-555, 2006.

149. Spasojevic A., D. Redaelli, M. Fernández Ruiz, A. Muttoni, "Influence of Tensile Properties of UHPFRC on size Effect in Bending", *Second International Symposium on Ultra High Performance Concrete*, pp. 303-310, 2008.

150. Wille, K. and J. Gustavo, "Effect of Beam Size, Casting Method and Support Conditions on Flexural Behavior of Ultra-High Performance Fiber-Reinforced Concrete", *ACI Materials Journal*, Vol. 109, No. 3, pp. 379, 2012.

151. Ding, Y., "Investigations Into the Relationship Between Deflection and Crack Mouth Opening Displacement of SFRC Beam", *Construction and Building Materials*, Vol. 25, pp. 2432-2440, 2011.

152. Vandawalle, L., D. Dupont, "Bending test and Interpretation", *International RILEM Workshop on Test and Design Methods for Steelfibre Reinforced Concrete*, 2003.

153. Vikram, J., A. Sivakumar, "Linearity Between Deflection and CMOD in Hybrid Fibre Reinforced Concrete", *Procture of the Second Intlement Conference on Advances in Civil, Structural and Environmental Engineering- ACSEE*, 2014.

154. Farhad, A., B. Morteza, "Relationship Between Deflection and Crack Mouth Opening Displacement of Self-Compacting Concrete Beams with and Without Fibers", J*ournal of Mechanics of Advanced Materials and Structures*, DOI: 10.1080/15376494.2014.9066
2014.

155. Nordstrom E. "Steel Fibre Corrosion in Cracks (Durability of Sprayed Concrete)", Licentiate Thesis, Lulea University of Technology; 2000.

156. Robins, P.J., S.A. Austin and P.A. Jones, "Flexural Strain and Crack width Measurement of Steel-Fibre-Reinforced Concrete by Optical Grid and Electrical Gauge Methods", *Cement and Concrete Research*, Vol. 31, No. 5, pp. 719-729, 2001.

157. Gopalaratnam, V.S., R. Gettu, S. Carmona, D. Jamet, "Characterization of the Toughness of Fiber Reinforced Concretes Using the Load-Cmod Response", *Fracture Mechanics of Concrete Structures*, Proceedings FRAMCOS-2, Freiburg, 1995.

158. Lameiras, R., J.A.O. Barros, M. Azenha, "Effect of Flow-Induced Dispersion and Orientation of Fibres on the Anisotropy of the Fracture Properties of Steel Fibre Reinforced Self-Compacting Concrete (SFRSCC)", *Cement and Concrete Composites*, Manuscript no: CCC-D-14-00459, 2015.